DESIGN OF SHORT DRILLED SHAFT FOUNDATIONS IN HIGH-PLASTICITY CLAY

UNDER INCLINED LOADING

by

THORNCHAYA WEJRUNGSIKUL

Presented to the Faculty of the Graduate School of

The University of Texas at Arlington in Partial Fulfillment

of the Requirements

for the Degree of

DOCTOR OF PHILOSOPHY

THE UNIVERSITY OF TEXAS AT ARLINGTON

May 2011

ABSTRACT

DESIGN OF SHORT DRILLED SHAFT FOUNDATIONS IN HIGH-PLASTICITY CLAY

UNDER INCLINED LOADING

Thornchaya Wejrungsikul, PhD.

The University of Texas at Arlington, 2011

Supervising Professor: Anand J. Puppala

Drilled shaft foundations are primarily used to support structures such as bridge piers, towers, buildings, transmission towers, and roadway median cable barriers. Generally, the main characteristics of drilled shafts are to transfer the loads to the stronger subsoil layers in the vertical direction and also their ability to withstand lateral movements from lateral loads applied. Though the design of shafts is well established with respect to combinations of loads and moments, their behavior under pullout type inclined loading is not well established. The inclined load applied is the combination of lateral and uplift loads applied at the same time and structures such as ends of cable barriers and transmission towers that are supported by the drilled shafts. This dissertation research mainly focuses on the use of drilled shafts supporting at the ends of the cable median barrier systems. These shafts play an important role in protecting the integrity of the cables thereby reducing cross-over collisions at highway medians.

Several foundation problems were recorded in north Texas when drilled shafts were used to connect all the cables of the cable barrier systems. During December 2006 to February 2007, several foundation failures of three cable median barrier were observed in Kaufman County near Dallas without any traffic related vehicular impacts (Heady, 2008). Preliminary

investigation of foundation failures showed that failed drilled shafts were located in a high plasticity clay environment. Causes of failures are attributed to cold temperature induced shrinkage in the cables that might have significantly increased the tensions in them. Other factors consist of soil saturation from prolonged rainfall events and also potential use of smaller size drilled shafts at the site.

In order to fully understand the causes of failures, the present dissertation research was performed. As a part of this research, various sizes of drilled shafts were designed and constructed in a clayey soil environment similar to the one where foundation distress was observed. Geotechnical sampling and laboratory testing were performed and the test results showed different soil layers including high plasticity clayey soil near the ground surface. Soil strength properties for both unsaturated (field condition) and saturated conditions were determined and these results are used in the analysis of field test results to deduce the causes of foundation distress.

A new load test setup for the application of an inclined tensile loading on the drilled shaft was designed to simulate the natural field loading condition exerted by the cables. The capacities of different sizes of drilled shafts from field test were tested and measured with this setup and these results showed that the dimensions of reaction test piers and spacings used between reaction and test piers have yielded results that are not influenced by the boundary effects or reaction shaft movements. All load tests were conducted until the foundations reached failure.

Test results were analyzed with both uplift capacity and lateral capacity analyses models proposed by many researchers as well as Finite Element Method (FEM) based numerical modeling in understanding the behaviors of drilled shafts under the inclined loading. After obtaining good simulation results, the analytical models are further used for various hypothetical foundation dimensions and for different undrained shear strengths of soils. These test results are used to develop foundation design charts for inclined loading conditions. Both

vi

the selection of a specific design chart and its use are explained. Additionally, drilled shaft construction guidelines for cable barrier systems and recommendation for periodic maintenance are provided.

TABLE OF CONTENTS

LIST OF ILLUSTRATIONS

xiv

xvii

xix

LIST OF TABLES

xxv

CHAPTER 1

INTRODUCTION

1.1 Introduction

Drilled shafts and piles are structural members placed in the ground and are predominantly used to transfer loads from a structure to the foundation soil or resist lateral movements of structural objects. Drilled shafts are deep foundations where fluid concrete and steel rebar is placed in the drilled hole whereas precast steel or concrete piles are mostly driven into the ground. In the construction process, drilled shafts can be constructed with or without casing or use slurry to protect the drilled hole walls from soil collapse which is dependent upon the groundwater table and soil conditions. Drilled shaft foundations were originally developed in order to support heavy buildings in many U.S. cities such as Chicago, Cleveland, Detroit, and London (O'Neill and Reese 1999). In Texas, the first use of drilled shafts by the Department of Transportation (TxDOT) was carried out in 1950 to build a bridge in the San Angelo District (McClelland 1996).

Since then, drilled shafts have become one of the design alternatives of foundation systems used throughout the State including the coastal areas of Texas (O'Neill and Reese 1999). The development of drilled shafts in different regions of the world led to different terminologies. "Drilled Shaft" is the term that was first used in Texas, while others call this foundation as a "Drilled Caisson" or "Drilled Pier" (O'Neill and Reese 1999). These terms are referred to the same type of foundation.

Drilled shafts have been used in several civil engineering applications such as foundations for supporting high rise buildings and bridges as well as retaining wall columns.

1

This is because the drilled shafts can support heavy loads and minimize settlement, support uplift loads, and support lateral loads.

The major advantages of drilled shaft construction and usage are summarized and listed below:

1. Drilled shafts provide significantly less noise and ground vibrations and damage to nearby structures;

2. Due to the minimal disturbance by drilling operation, large pore water pressure are not developed resulting in consolidation settlement due to soil remolding is limited;

3. The drilled shafts can be applied for a various soil conditions. For example, it can be drilled into rock;

4. Due to the high load capacity of drilled shafts, it can be used instead of a group driven piles;

5. The bell shaped tip of the drilled shaft can resist the uplift pressures;

6. They have high resistance to both axial and lateral loads; and

7. They are economical by avoiding the usage of heavy pile caps.

Primarily, lateral loads influence drilled shafts from earth pressures in subsoils, current forces from flowing water, wind loads and wave forces in some unusual instances (O'Neil and Reese 1999). Examples of the structures where lateral forces have an effect on the drilled shafts are bridge abutments, offshore platforms, and transmission towers (Reese et al. 1977). Additionally, overhead-sign structures, high mast illumination systems, and median barriers are also required to be supported on or by drilled shaft foundations.

<u>1.2 Problem Statement and Research Objectives</u>

The use of median cable barrier systems within the highway facilities are to eliminate or greatly mitigate cross-over collisions due to high traffic volumes, highway congestion, and driver error. TxDOT extensively used 3-cable type median barriers along many highways including one along Interstate Highway 20 (IH20) and US Highways 80 and 175 (US80 and US175) in

2

Kaufman County, Texas. Construction of these barriers was accomplished from July 2006 to February 2007. The failures of end foundation systems supporting a 3-cable barrier system constructed in an expansive soil area is shown in Figures 1.1 and 1.2. The foundation failure is affecting the safety features of the barrier system.

Figure 1.1 Typical Foundation Failures of 3-cable Median Barriers
Built on Expansive Soils at IH 20 Westbound Sta. 1338+57

Figure 1.2 Typical Foundation Failures of 3-cable Median Barriers
Built on Expansive Soils at US 175 Eastbound Sta. 149+98

From Figures 1.1 and 1.2, it can be demonstrated the foundation used to support cable barrier system showing excessive lateral movements and uprooting of the foundations. A review of the causes of these failures yielded the following observations (Personal communication with Ms. Jan Heady, PE, TxDOT Dallas District, 2008):

- Kaufman County, where the drilled shaft foundation failures were recorded, had experienced low temperatures, including a few ice storms, from December 2006 to February 2007.

- Two of the median barrier systems in which each cable was connected to one 24 inch (0.6 m) diameter by 6 ft (1.8 m) deep drilled shaft.

- Cable barriers in which three cables were connected to one end drilled shaft has experienced the distress in the field as drilled shaft was uprooted from the original position.

4

Median barrier system failures are not acceptable due to the potential liabilities incurred with any failure of these systems. It is imperative to understand the cause(s) of these inclined loaded drilled shaft failures and design practical foundation systems in high PI clays to eliminate future failures. Therefore, in order to understand the possible causes of failures of the drilled shafts and methods to mitigate the failures, the following research objectives and specific tasks are developed:

1. Investigate the mechanisms that cause failure of laterally loaded drilled shafts in highly-plastic clay environments.

2. Design and construct test drilled shafts with various dimensions and subject them to loading similar to the one that might have resulted in the existing failures shown in Figures 1.1 and 1.2 in the actual field environment.

3. Analyze the results of test drilled shaft with various dimension consideration

4. Study behavior of drilled shaft under different seasonal conditions

5. Analyze and investigate the use of analytical and numerical models for predicting the inclined load capacities

6. Compare predictions with the field load test results.

7. Develop foundation design systems based on the analyses of load test results using the models that provided good match the present field load test results.

8. Provide alternative design approaches including modification of soils at shallow depths ($\geq$ 6 ft (1.8 m)) that will lead to no failures of the anchor shafts for the median barrier foundation systems.

<p align="center">1.3 Organization of the Dissertation</p>

This dissertation consists of eight chapters. The detail of each chapter presents below:

Chapter 1 provides an introduction, background history of drilled shafts, problem statements explaining the significance of the project, research objectives, and organization to provide a framework of the completed research.

Chapter 2 presents a literature review on median barriers used in Texas, various factors influencing the failures (i.e. high plasticity clays and temperatures), and lateral load tests on drilled shaft. Several available lateral load tests are discussed.

Chapter 3 provides the site selection and laboratory testing used to determine the soil properties required for the design, construction, and testing of the drilled shaft system. The testing program designed to determine the properties of soil samples from the selected site. The experimental program includes basic soil properties tests and engineering tests on the soils. A summary of the laboratory procedures, equipments used and results are presented in this chapter. In addition, the analysis of the laboratory results is discussed.

Chapter 4 presents design and construction of the drilled shaft test setup under inclined loading including the criteria used in the design and construction technique. Additionally, the instruments used in the loading and capturing load and deformation responses are described.

Chapter 5 presents the results of all the test data in both winter and summer condition. This data consists of the loading process, amount of loading increments, strain gauge result detected in the high tensioned steel bar (Dywidag bar), and the movement of the test shaft from inclinometer, MEMS-SAA, standard elevation survey equipment and dial gauges at each test shaft. Moreover, surrounding soil movement is captured by the inclinometer readings taken in the influence zone between the reaction and test drilled shafts.

Chapter 6 focuses on analysis of the analytical and numerical models used to predict the capacities of test drilled shaft under the different criteria and finding the best-fit model used in generating the design chart. The validation values from each model compared with the field results are evaluated.

Chapter 7 provides the design chart developments, flow charts helping in chart selection, example to illustrate chart usage, construction guideline and recommendation for cable barrier system maintenance.

Chapter 8 presents the all the important conclusions of the experimental results, field results, research studies and future recommendations.

CHAPTER 2

LITERATURE REVIEW

2.1 Introduction

In this chapter, several topics including description of cable barrier systems, factors causing failures of drilled shafts connected to cables, drilled shafts, high Plasticity clays, load testing of shafts, lateral load analysis methods and other related topics are reviewed and covered in the following sections.

2.1.1 Median Barriers Used in Texas

Cable barrier systems are used to prevent cross-over collisions by capturing and maintaining errant vehicles in their direction of travel. A cable barrier system requires appropriate clearance in the lateral direction as it will deflect when struck. This deflection will quickly and effectively reduce the impact forces transmitted to the vehicle occupants greatly increasing their survival chances. In Texas, Texas Department of Transportation (TXDOT) provides a positive median barrier when the distance between the striped edge is 30 ft (10 m.) or less. Cable barrier systems cost $70k + per mile compared to $300k+ per mile for concrete traffic barriers. Hence, they have been increasingly used in a majority of the states (Alberson, 2006). In general, there are six major types of barriers being used in the US as given below and shown in Figure 2.1,

- US Generic Low Tension
- Safence
- Gibraltar (Cable Barrier System)
- Brifen (Wire Rope Safety Fence-WRSF)
- Nucor Marion (U. S. High Tension)
- Trinity (Cable Safety System-CASS)

8

Figure 2.1 Photos of Various Barriers Used in Texas and the US (Alberson, 2006) a) US Low Tension Barrier b) Safence c) Gibraltar Cable Barrier d) Brifen Safety Fence e) Nucor Marion f) Trinity Cable Safety Systems

From the six typical systems shown in Figure 2.1, the other five systems except for the first system (US Low Tension) are classified in the high tension cable barrier group. Each system has a unique post design, cable placement, and end treatment. All of these cable barrier system posts were founded on concrete drill shafts with sockets for ease of repair and maintenance. These barriers were installed for lengths of more than 600 miles (970 km.) (Alberson, 2006).

In this research, 3-cable barrier systems (TL-3) have been focused as they experienced failure. A schematic of the system is presented in the Figure 2.2. The characteristic of this system is three cables connected to single drilled shaft which is used to support the cable barriers at both ends to provide the tension in the cable as per a manufacturer's requirement.

.
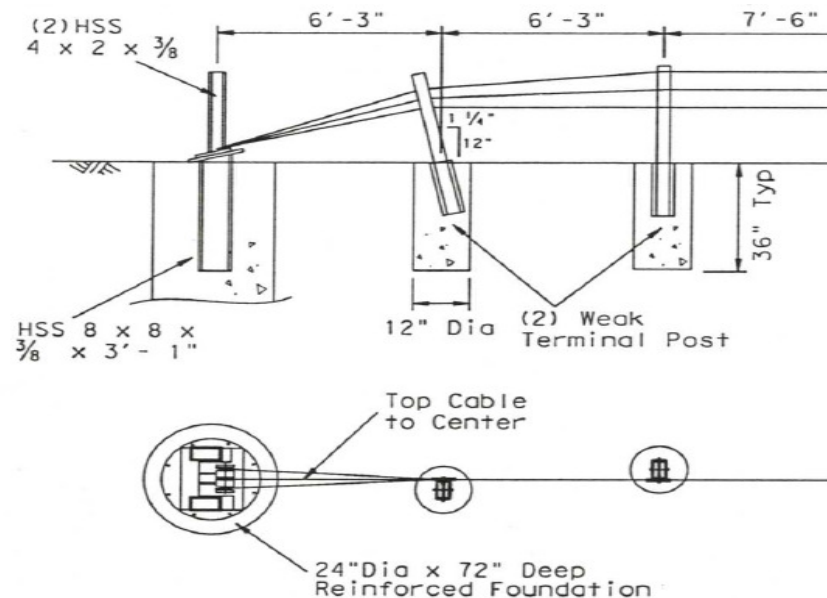
Figure 2.2 Connection Details of Cables to Drilled Shafts for the Gibraltar TL-3 Barrier System

2.2 Overview of Various Factors Influencing the Shaft Failures

Median barriers are used to prevent cross-over collisions due to high traffic volumes, highway congestion, and driver errors (Albin et al., 2001). In the state of Texas, the two types of median barrier systems are currently in use and these are concrete traffic barrier and cable

10

barriers. According to AASHTO's report on cable median barriers, these have been in use in 47 of the 50 US states (Albin et al., 2001). According to AASHTO's technology implementation group, the state of Texas has more than 600 miles of cable median barriers and has invested approximately 157 million dollars on this technology.

With the heavy implementation of these systems across the state in a short amount of time, a vast majority of the installations have relied upon the individual manufacturer recommendations. This research addresses the need for better engineering and design methods to account for all types of cable barrier systems in all soil types across the state.

Many or all of the systems use a drilled shaft for the end treatment to which the three cables are attached. This end treatment provides an anchor on each end of the median barrier runs against which the cables can be tightened to provide the manufacturers' tension requirements. Since drilled shafts are highly resistant against lateral loads in most soil types, drilled shaft foundations have become the primary foundation system for these cable barrier systems (TL-3 and TL-4 types). The drilled shaft foundations function satisfactorily in non-expansive soils; however, same shafts supporting cable barrier systems have some foundation failure issues in expansive soils due to loss of contact between soil and foundation and foundation uplift from the ground. The foundation failures occurred in many places along the highways in the eastern part of Dallas including IH-20, US-175, and US 80 as presented in the Figures 2.3, 2.4, and 2.5, respectively. For the full detail of failure are shown in the Appendix A.

Figure 2.3 Foundation Failures of 3-cable Median Barriers Built on Expansive Soils at IH 20 Westbound Sta. 1069+00

Figure 2.4 Foundation Failures of 3-cable Median Barriers Built on Expansive Soils at US 175 Eastbound Sta. 92+00

Figure 2.5 Foundation Failures of 3-cable Median Barriers Built on Expansive Soils at US 80 Eastbound Sta. 77+37

Therefore, it is hypothesized that these failures are primarily due to a combination of several factors summarized below:

- Foundation soils, where the problems were observed, are high plasticity clays (predominantly CH type) exhibiting an expansive nature. Cyclic movements of the expansive soil also contributed to the lateral load on the drilled shafts. Due to these volumetric movements, the soil around the base of the foundation is softened with time due to moisture changes and lateral forces from the tensioned cables, and ultimately caused the foundation failures.

- Tension developed in the cables due to severe temperature changes observed during this period might have induced higher tensile stresses in the cables. These tensile stresses, along with high vehicular impact forces, would have added risk to the foundation failures.

13

- Another factor contributing to the failure of the foundation could be attributed to the cables connected to a single drilled shaft. Since all three cables were connected to a single drilled shaft, the amount of lateral pull might have exceeded the design value.

- A final possible reason for these failures could be the length of the drill shaft. As mentioned earlier, the drilled shafts were only 3 ft - 6 ft (0.91 m – 1.83 m) deep which is considered as short shafts. The shorter lengths of these foundations could not develop sufficient frictional resistance required to withstand the amount of lateral pull generated as a result of the aforementioned factors.

In summary, the failures of the foundation drill shafts of the 3-cable median barrier systems are influenced by many factors including water availability, high plasticity clays, temperature, and length of the drilled shafts. These contributing factors are further discussed in the following sections.

2.2.1 Moisture Contents in Soil

Water or moisture content changes can greatly affect the engineering behavior of soil. After rainfall, clayey soil becomes soft. This situation shows that fine-grained soils can be weakened in resistance and result in low bearing capacity for the foundations. In this section, examples that influence properties of soil, such as hydrological cycles, groundwater, cutoff water will be mentioned.

2.2.1.1 Hydrological Cycles

Generally, moisture moves from ground surface to the atmosphere and/or vice versa. The movement of water in all forms including solid, liquid or vapor and these are shown in the hydrologic cycle as shown in Figure 2.6. Moisture vapor when condenses will reach the ground surface in the forms of rain, snow, or hail. Most of this precipitation falls on the land and stored in soil, swamps, lakes, reservoirs, river and ocean. Then, water is evaporated from the soil, streams and oceans. In the case of runoff water, it can cause the soil erosion and creates agricultural and engineering problems. For the geotechnical problems, water that soaks into the

14

soil is the main concern. Effect of water to infiltrate soil varies with the soil types. In the present research, since the foundation distress caused during the extreme weather conditions, it is important to understand the movements of moisture and how it impacts expansive soils and their strength and volume changes are important.
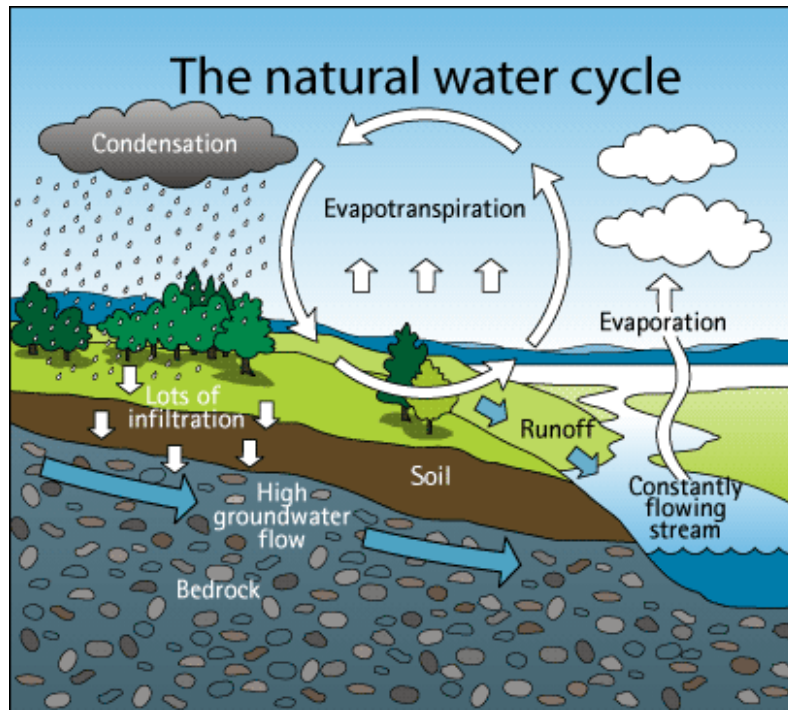
Figure 2.6 The Hydrological Cycle (Source: http://www.crwa.org/projects/sustwater.html)

Water that soaks or infiltrates into the soil can influence the engineering performance of the structure. Generally, the strength of the soil was influenced by the soil grain sizes, moisture content, compaction conditions and angle of contact between the particles. Whenever, the upper layers of soil are saturated with the water, this results in the reduction or weakening of the soil strength and the related bearing capacity. This contributes to the failure of the foundation. Hence it is necessary to understand the moisture migration in the soil. The next section describes the soil types that are influenced by the moisture migration.

2.2.2 High Plasticity Clays

One of the reasons for the failure of these drilled shafts subjected to lateral loading is due to the expansive and high plasticity nature of the clayey soils. According to the Unified Soil Classification System (USCS), particle size of fine-grained soil smaller than 0.002 mm is classified as clay. The cohesion and plasticity of clays are very significant in their engineering behavior. For this research, the focus will be on expansive soils. Expansive soils exhibit swell-shrink characteristics due to moisture fluctuations and have been a problem to civil engineering infrastructures including roads and foundations from ancient times (Nelson and Miller, 1992).

In the United States, expansive soils are abundant in Texas, Colorado, Wyoming, and California (Chen, 1988). Damage from the swell and shrink behavior of these soils costs about 6 to $11 Billion per year (Nuhfer et al., 1993). One of the earlier National Science Foundation (NSF) studies reported that the damage to structures caused by expansive soils, particularly to light buildings and pavements, is more than any other natural disaster, including earthquakes and floods (Jones and Holtz, 1973). Petry and Armstrong (1989) noted that it is always advisable to stabilize expansive clay soils during construction of a facility rather than leaving the soils unstable which would need remediation at a future date. It is more economical to address the problem immediately rather than performing the remedial treatments later.

Many minerals combine naturally to form soils. The type or amount of clay minerals can significantly influence their properties such as swelling, shrinkage, and plasticity. Examples of expansive clays include high plasticity index (high PI) clays, overconsolidated (OC) clays rich with Montmorillonite and Bentonite minerals, and Shales. Soils containing significant quantities of the minerals such as Bentonite, Illite, and Attapulgite are characterized by strong swell or shrinkage properties. Kaolinite is relatively non-expansive (Johnson and Stroman, 1976). The heaving mineral Montmorillonite has an expanding lattice and can undergo large amounts of swelling when hydrated. Soils rich with these minerals can be found in many places all over the

world especially in the arid and semi-arid regions (Hussein, 2001). In this research, North Texas is semiarid region. The plasticity index (PI) and liquid limit (LL) chart was developed to simplify the classification of the type of minerals in the soil as shown in Figure 2.7 (Mitchell (1976) and Holtz and Kovacs (1981)). However, this technique is not accurate enough to satisfactorily identify the soil minerals for this research due to the fact that the soil can consist of many different clay minerals.
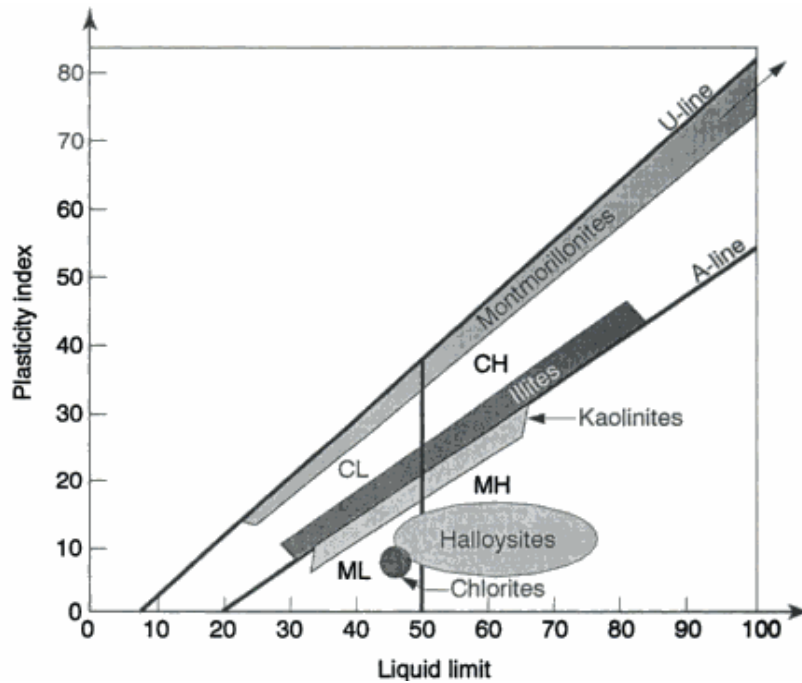
Figure 2.7 Plasticity Chart for Indicating Minerals in Soil (Mitchell, 1976; Holtz and Kovacs, 1981)

According to Wiseman et al. (1985), the following factors can be used to classify a soil as problematic or not:

1) Soil type that exhibits considerable volume change with changes of moisture content.

2) Climatic conditions such as extended wet or dry seasons.

3) Changes in moisture content (climatic, man-made or vegetation).

4) Light structures that are very sensitive to differential movement.

17

A summary of various methods for identifying the expansive nature of soils can be found in Puppala et al. (2004). Expansive soils can be identified by using the following plasticity-based index tests and the magnitudes of their test results are shown in Table 2.1.

Table 2.1 Expansive Soils Identification (from Wiseman et al., 1985)

Index Test	Non- Problematic	Problematic
Plasticity Index	<20	>32
Shrinkage Limit	>13	<10
Free Swell (%)	<50	>100

Foundations to support the civil infrastructure often extend beyond the active depths of these clays. In Texas, active clay depths range from 2 ft (0.61 m) to 15 ft (3.66 m) or more thus creating problematic conditions to the foundations thereby increasing the remedial costs for repairs.

2.2.2.1 Active Zone

When an increase of water content in soil in the upper soil layers, expansive soil problems usually occur. This zone is called as zone of moisture fluctuation or simply active zone. This zone is influenced by the climatic changes between dry and wet seasons. Active zone will vary with the depth as depicted in Figure 2.8. Sometimes, active zone can be 15 to 20 ft (4.5 to 6.0 m) depth from the ground surface. Therefore, any design of structure below the ground or on surface must consider active zone depths in the calculations of soil movements.
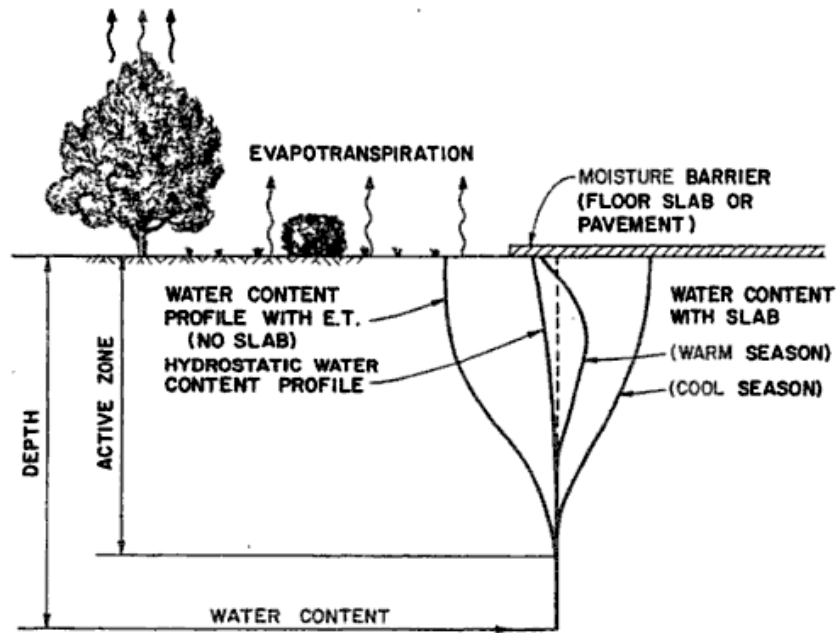
Figure 2.8 Water Content Profile in Active Zone (Nelson and Miller, 1992)

2.2.3 Temperature Effect

In Texas, the temperature varies from -13°F (-25°C) in winters to 120°F (45°C) in summer, and this considered to be a very wide range. As discussed before, failure of the drilled shafts of the 3-cable median barriers occurred during low winter temperatures. Low temperatures cause thermal stresses due to contraction in the steel cables. Therefore, the difference in temperature between the low and high temperatures can have a measurable influence on the barrier systems' performance.

2.2.3.1 Cables

A change in temperature can cause material expansion or contraction. Temperature can significantly influence material properties such as yield strength and modulus of elasticity (Craig 1999). Generally, expansion or contraction of homogeneous materials is linearly related to temperature increase or decrease in all directions (Hibbeler 2008).

Thermal strain can be expressed as the following equation:

$$\epsilon_x = \epsilon_y = \epsilon_z = \alpha \, \Delta T \tag{1}$$

19

where $\epsilon_{x,y,z}$ is thermal strain,

α is coefficient of thermal expansion (COTE), and

ΔT is the change in temperature.

To find the elongation in the member, the following expression can be used:

$$\Delta T_{xT} = (\alpha \, \Delta T)L_x, \; \Delta T_{yT} = (\alpha \, \Delta T)L_y, \Delta T_{zT} = (\alpha \, \Delta T)L_z \tag{2}$$

where $\Delta T_{xT,yT,zT}$ is the elongation in the x, y, and z directions.

The coefficient of thermal expansion, COTE, α, is the thermal property of a material. It can be determined by measuring the change in dimensions of the material when applying a change in temperature. The coefficient of thermal expansion is expressed in strain per degree of temperature unit. For instance, α in the U.S. customary unit is 1/°F (the reciprocal of degree Fahrenheit) with α in 'SI' units as 1/°K (the reciprocal of degree Kelvin) or 1/°C (the reciprocal of degree Celsius). For determining the elongation of materials due to temperature decrease, the change in temperature (ΔT) in Eq. 2 is negative. The elongation is a function of the length of the cable that will be connected to the foundation. In the barrier systems, the lengths of two or three cables that are connected to the drilled shafts are practically close to each other and hence the length of the cable does not influence the failure of the foundation.

2.2.3.2 Soils

In soils, the temperature variation can cause fluctuations in moisture content of the soil. These moisture fluctuations can cause swell-shrink behavior if the given soil is expansive in nature. During summer (high temperatures), soil moisture evaporates leading to shrinkage of the soil. In rainy seasons, the soil moisture increases leading to swelling of these expansive soils. Studies on the effects of frost and heaving, which can cause damage to pavements and foundations, have been studied by many researchers such as Casagrande (1932), Kaplar (1970), Penner and Bern (1970), and Yong and Warkentin (1975). In the expansion of the volume of water when it freezes, there is about a 10 percent increase in volume. Damage from

frost in the soil is due to the formation of ice lens leading to frost heave. Originally, frost heave was considered when freezing of water in the soil occurred. However, the vertical displacement of the frost heaving phenomenon can be greater than the expansion that occurs when ice freezes.

Day (2006) stated that there are many cases where damage or deterioration from the expansion of water is not evidently shown until the frost is melted; therefore, it might be very difficult to summarize damage or deterioration caused from frost heave. For foundations, Penner and Burn (1970) studied movements in the soil resulting from ice lens expansion. The results showed that when soil under a foundation freezes, soil expansion due to ice lens growth can be transmitted to the structure as shown in Figure 2.9 and this process is called "Adfreezing." However, adfreeze strength studies could not provide the exact uplift values for all foundation materials such as concrete, wood, and steel in various soil types. In this research, the probability that frost heave occurred is very low because ice lens expansion needs to occur in very low temperatures for a long period which is atypical in the Dallas area.
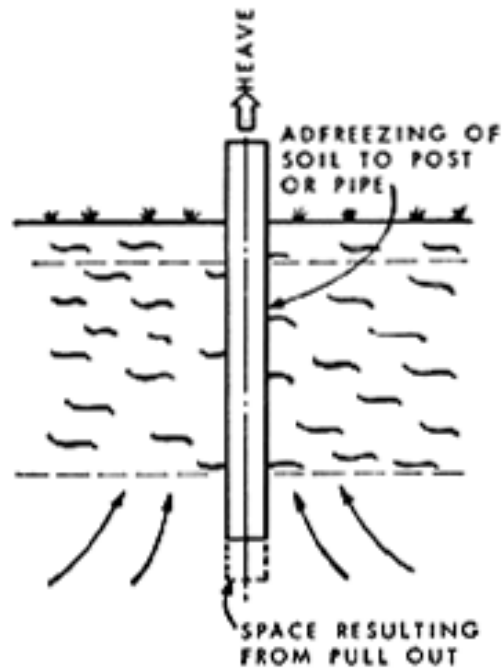
Figure 2.9 Behavior of a Post in Frost Heaving (Penner and Burn, 1970)

2.3 Uplift Capacity of Deep Foundations Subjected to Inclined Loads

The primary function of a deep foundation system is to transfer the axial and lateral loads to the foundation soil. Deep foundations, in particular drilled shafts or piers, are often used to support various structures that are subjected to uplift. In some cases, deep foundations are designed to resist uplift loads, such as foundations for transmission towers and high mast illumination poles in expansive soils. The uplift capacity of a shaft under vertical and inclined anchors was studied by Meyerhof (1973 a, b; 1980). He presented the semi-empirical relationship to estimate the ultimate uplift capacity of rigid shafts in clay under inclined load as shown in Figure 2.10. The behavior of foundations under oblique loads depends, to a considerable extent, on the deformation characteristics of both the foundation and the soil. In addition, the failure mechanism becomes more complicated because of the foundation being unsymmetrical and three-dimensional in nature.
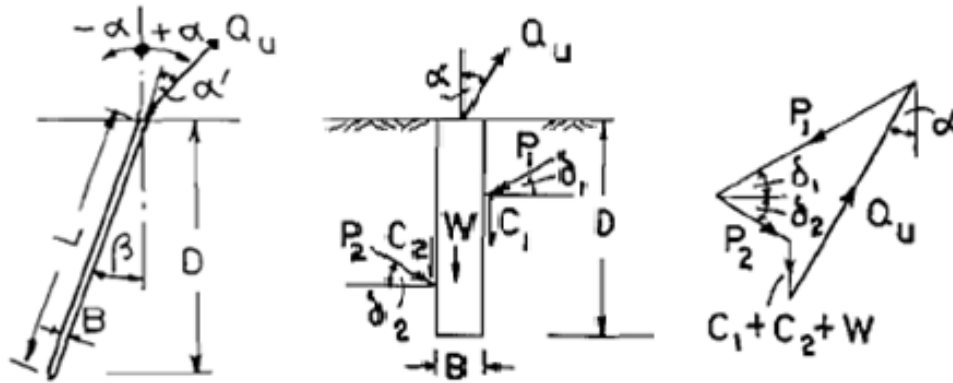
Figure 2.10 Forces of Anchors under Inclined Loads (Meyerhof 1973a; 1980)

From Figure 2.10 above, the ultimate load can be estimated from the force using the semi-empirical equation expressed as:

$$Q_u = \left(cK_c'D + \frac{\gamma D^2 K_b'}{2}\right) B + W\cos\alpha \qquad (3)$$

where Q_u is the net ultimate capacity of the piles,

D is the depth,

K_b' is the uplift coefficient based on the angle of internal friction shown in Figure 2.11,

K_c' is the uplift coefficient given by $K_c' = 1 + 0.08\frac{D}{B}$ with a maximum value of 3 for

horizontal tension (Meyerhof and Adams 1968);

K_c' is π in saturated clay ($\phi = 0°$)

W is the weight of the shafts,

c is the cohesion force,

γ is the unit weight of the soil, and

B is the width (diameter) of the shaft.

23
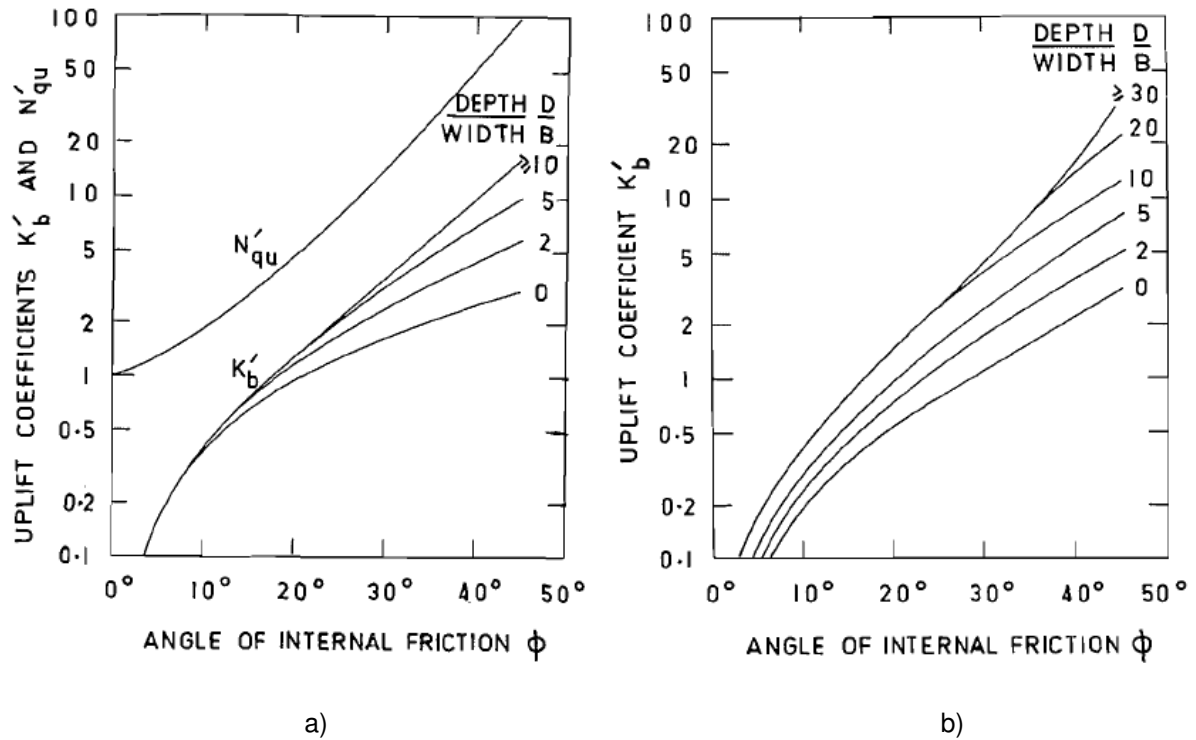
Figure 2.11 Uplift Coefficients for a Rigid Rough Shaft (Meyerhof 1973a) a) Vertical uplift coefficient   and b) Horizontal uplift coefficient

Meyerhof (1973a) developed the relation between vertical and horizontal pulling resistance, Q_v and Q_h, respectively through a series of model tests. The expression for the ultimate bearing capacity (Q_u) due to an obliquely loaded tension is:

$$\left(\frac{Q_{u(\alpha)}\cos\alpha}{Q_v}\right) + \left(\frac{Q_{u(\alpha)}\sin\alpha}{Q_h}\right)^2 = 1 \qquad (4)$$

where Q_h and Q_v are given by Eq. 4 with $\alpha = 90°$ and $\alpha = 0°$ respectively, and

α is the angle of the inclined force with the horizontal axis (°).

In 1985, Ubanyionwu compared his study with Meyerhof's equation by using a laboratory model test in which a 1 in. (25.4 mm) diameter pile was vertically installed in an 18 in x 18 in x 30 in. (457.2 mm x 457.2 mm x 762 mm) box compacted with clay. In these studies, the density of the compacted clay was maintained at 128.81 lb/ft^3 (20.25 kN/m^3) and

24

the degree of saturation was equal to 97.9% which was close to a 100% saturated soil. Also, the piles were pulled out at different angles (0° – 90°). The result of these experiments provided good agreement with the semi-empirical equation developed by Meyerhof (1973a). Figure 2.12 compares the laboratory test data with the theoretical data.
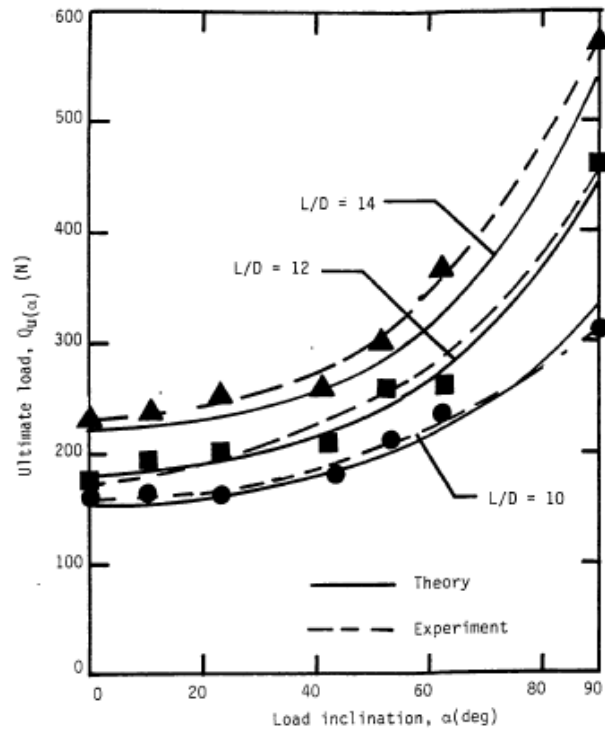
Figure 2.12 Results of $Q_{u(\alpha)}$ with Different Degree of Load Inclinations (α) and L/D
(Ubanyionwu, 1985)

2.4 Uplift Capacity of Deep Foundations in Expansive Soils

Generally, capacity of piles or shafts is the combination of end bearing and skin friction resistance. However, design of deep foundations in expansive soil is different from design in non-expansive soil conditions. If these shafts are not designed and constructed effectively, the damage from the horizontal and vertical soil expansion can be very high. When these movements are excessive, shafts can be uplifted as shown in Figure 2.13. The uplift of shafts occurs when the uplift force is greater from the swelling pressure of the soil than the resistance force of the shaft from the skin friction.

25
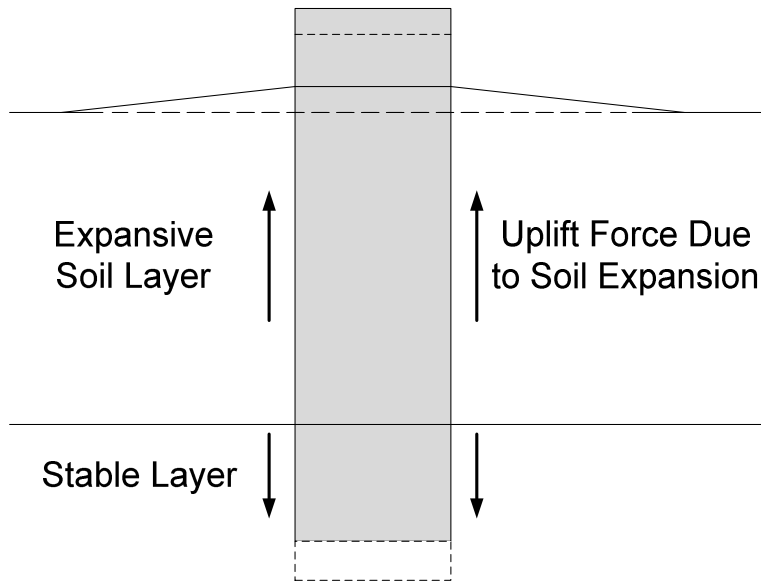
Figure 2.13 Deep Foundation Movements in Expansive Soil

Many researchers have studied the uplift capacity of piles from the viewpoint of temperature, moisture content, and active depth (Westman, 1993). O'Neill and Poormoayed (1980) developed an equation for computing the value of f_{max} in the zone of expansion as presented in Eq. 5.

$$f_{max} = \varphi\, \sigma'_{ho} \tan \delta_r \qquad (5)$$

where φ is a correlation coefficient,

σ'_{ho} is the horizontal swell pressure at the depth where f_{max} is computed, and

δ_r is the effective residual of the interface friction between concrete and

expansive soil.

In the previous equation, it is assumed that the expansion process happens slowly so that excess positive or negative pore water pressures are not developed. Also, they recommended a value of $\varphi = 1.3$; however, the universal value of φ has not been established. Then, Cameron and Walsh (1981) described a study of small diameter timber piles driven to various depths in an expansive soil profile monitored through wet and dry seasons. In the field,

26

the active depth of expansive soil was between 4.92 and 6.56 ft (1.5 and 2.0 m). After monitoring for five years, they observed maximum seasonal ground surface movements of 2.56 in (65 mm). They also observed that the piles driven to the active depth recorded movements between 15 – 32% of the ground surface movement. However, piles installed between the 6.56 and 8.20 ft (2 and 2.5m) depth were effective in resisting the ground movements. Then Duffy and Charania (1984) developed a modified Oedometer-type test to facilitate the design of piled foundations in expansive soils which models the interaction between a pile and a swelling clay as the clay is exposed to water hydration.

Later, numerical simulations of piles in expansive soils were developed by Justo et al. (1984), Mohamedzein et al. (1999), and Sinha and Poulos (1999). Westman (1993) studied different variables that affect pier uplift in expansive soil and formulated the following equation from numerical models to measure the vertical displacement of the pier head where the load applied was calculated:

$$Y = \frac{S^{0.3575} T^{1.61}}{D^{1.17} L^{0.091} f_s^{0.760} C^{1.61}}$$

(6)

Where Y is the vertical displacement of the pier head (ft),

S is the swell pressure of the expansive soil (ksf),

T is the thickness of the expansive soil (ft),

D is the depth to center of the expansive soil (ft),

L is the structural load applied to the pier head (ksf),

f_s is the interface friction between the pier and the soil, and

C is the cohesion of the expansive soil (ksf).

Al-Saoudi and Salim (1998) studied the movements of the heads of the model piles which were embedded in the expansive soils. The results showed that the movements of the heads of the piles were less than the movements at the soil surface. Chapel and Nelson (1998) conducted the test using bored concrete piles and helical screw plate anchors for lightweight

construction in expansive soils and concluded that both the piles and anchors performed satisfactorily when installed below the active depth.

<u>2.5 Lateral Load Analysis Methods</u>

The application of lateral load to a drilled shaft results in lateral deflection which in turn causes a lateral soil reaction. Lateral load which is greater than lateral resistance of the drilled shafts can lead to excessive deformation of the shafts, soil failure around the shafts, and structural failure. The factors such as maximum bending moment and shear force in the embedded drilled shaft are also important depending to a large extent on the reaction provided by the soil. Consequently, the main objectives of designing the shaft are to determine the necessary diameter and penetration depth of the drilled shaft, mechanical properties of the concrete and steel rebar to resist bending and shear, and determine the deformations or stiffness of the drilled shaft in order to assess the performance of the structure.

In the analysis of laterally loaded drilled shafts, there are many common design methods available, such as "Broms' Method", "Equivalent Cantilever Method", "Characteristic Load Method", the "p-y Method" and "Strain Wedge Model." These methods deal with the non-linear system of soil response (Reese et al. 1977) which will be described later.

2.5.1 Broms' Method

The lateral capacity of a shaft had been initially studied by Brinch Hansen (1961). Later, Broms (1964a, 1964b, 1965) developed the test to determine the ultimate lateral capacity of deep foundations in homogeneous deposits which are purely cohesive and cohesionless soils. Broms constituted the analysis by considering the distribution of the shear resistance with the depth, the short-rigid piles, long-flexible piles, and fixed and free-head cases, separately. In addition, he gave the criterion for dividing shafts into two groups which are short-rigid and long-flexible piles, which is the ratio between embedded length of shafts and stiffness factor as given:

28

$$\text{Short-Rigid Pile: } \frac{L}{T} \text{ or } \frac{L}{R} \leq 2$$

$$\text{Long-Flexible Pile: } \frac{L}{T} \geq 4 \text{ or } \frac{L}{R} \geq 3.5$$

where T and R are termed as the stiffness factors which are explained in the following. In the case of NC clays, the stiffness factor, T is used and for OC Clays, R is used in the assessments of short and long piles.

These factors account for the modulus of elasticity (E) and the moment of inertia (I) of the pile and soil modulus (the compressibility of the soil) which depends on the depth of influence area, width of pile, and type of soil. For normally consolidated (NC) clays and cohesionless soils, the modulus of the soil is assumed to increase with the depth linearly, and the stiffness factor can be expressed as:

$$T = \left[\frac{EI}{n_h}\right]^{1/5} \quad \text{in length units} \tag{7}$$

where E is the modulus of elasticity of the pile material,

I is the moment of inertia of the pile section, and

n_h is the coefficient of modulus variation

For normally consolidated clay,

$n_h = 2{,}228 - 4{,}774$ pcf (350 - 750 kN/m^3)

For soft organic silt,

$n_h = 950$ pcf (150 kN/m^3)

For granular soil, n_h can be seen in Table 2.2

Table 2.2 Values of n_h for Cohesionless Soils, kip/ft^3 (kN/m^3) (after Terzaghi 1955)

Type of Sand	Loose	Medium	Dense
Dry or moist sand	15.91 (2500)	47.74 (7500)	127.32 (20000)
Submerged sand	8.91 (1400)	31.83 (5000)	76.39 (12000)

For overconsolidated clays, the modulus is assumed to be constant with the depth, so the stiffness factor is shown as:

$$R = \left[\frac{EI}{KD}\right]^{1/5} \quad \text{in length units} \qquad (8)$$

where D is the diameter or width of pile, and

K is $K_s/1.5$ (where K_s is subgrade modulus reaction (kN/m^3 or (kgf/m^3)), or

K is $n_h \, x/D$ where x is the depth of the soil considered.

According to Terzaghi (1955), K_s values of cohesive soils are listed in Table 2.3 below.

Table 2.3 Values of K_s for Cohesive Soils, kip/ft^3 (kN/m^3)

Consistency	Stiff	Very Stiff	Hard
Unconfined Strength, psf (kN/m^2)	208.85 – 417.71 (10 – 20)	417.71 – 835.42 (20 – 40)	≥835.42 (40)
Recommended K_s	171.88 (27,000)	343.76 (54,000)	687.52 (108,000)

In this case, the short, free-headed piers in the cohesive soils are considered which corresponds with the 3-cable median barriers. Equations 9, 10 and 11 are expressed below. In addition, the schematic of the deflected shape, passive soil reaction, and moment diagram in cohesive soils can be presented in Figure 2.14.

$$f = \frac{H_u}{9c_u D} \qquad (9)$$

where f is the length of pile required to develop the passive soil reaction,

H_u is the ultimate lateral capacity of the pile,

c_u is the undrained cohesion, and

D is the diameter or width of the pile.

$$M = H_u(e + 1.5B + 0.5f) \qquad (10)$$

Where M is the moment in the pile at the point of fixity, and

e is the unsupported length of the pile.

$$2.25Dc_u\left[L - \frac{H_u}{9c_uD}\right]^2 = H_u\left[e + 1.5D + \frac{H_u}{18c_uD}\right] \qquad (11)$$

Where L is the embedded length of the pile.

a) Pile deflection.   b) Soil reaction   c) Bending moment.
                      (force / length).
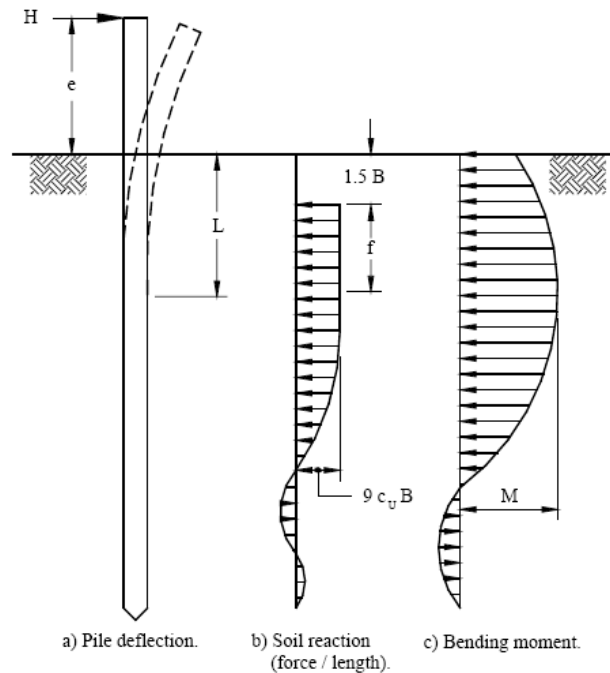
Figure 2.14 Schematic for a Laterally Loaded Pile in a Cohesive Soil (Broms 1964)

Equation (9) can be solved by trial and error for the Q_{hu} value. However, Broms simplified this method by using the graph shown in Figure 2.15 below in order to calculate Q_{hu}.

31
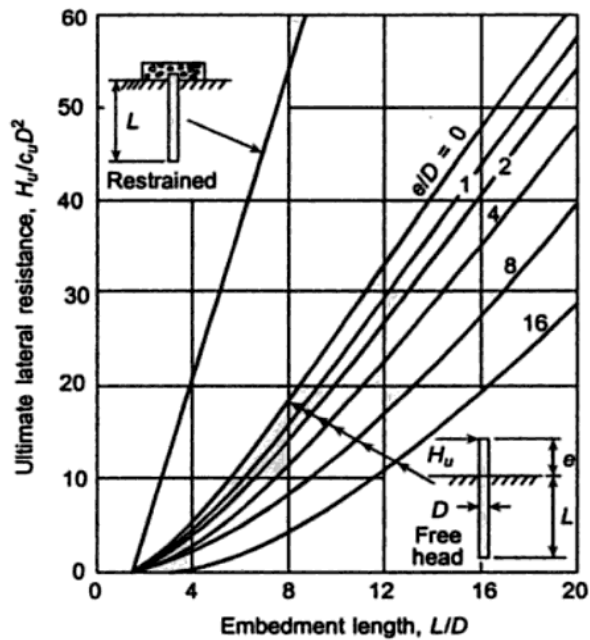
Figure 2.15 Design Chart for Short Piles in Cohesive Soils (Broms, 1964b).

2.5.2 Equivalent Cantilever Method

Davisson and Robinson (1965) determined the elastic forces and moments in piles using the Equivalent Cantilever Method. After that, Greimann et al. (1987) refined this design method based on Rankine's equation for inelastic buckling. Abendroth et al. (1989) evolved this method further for designing piles of integral bridges due to the fact that the previous method provided very conservative results. They idealized the piles through the cantilever model as shown in Figure 2.16. The method was based on analytical and finite element studies. The drilled shaft was replaced by an equivalent cantilever beam in order to simplify the analysis. However, Robinson et al. (2006) observed that the results from the analyses of the cantilevered columns with an "equivalent" length did not match the magnitudes of maximum moments, lateral pile top displacements, or buckling behavior from non-linear lateral analysis.
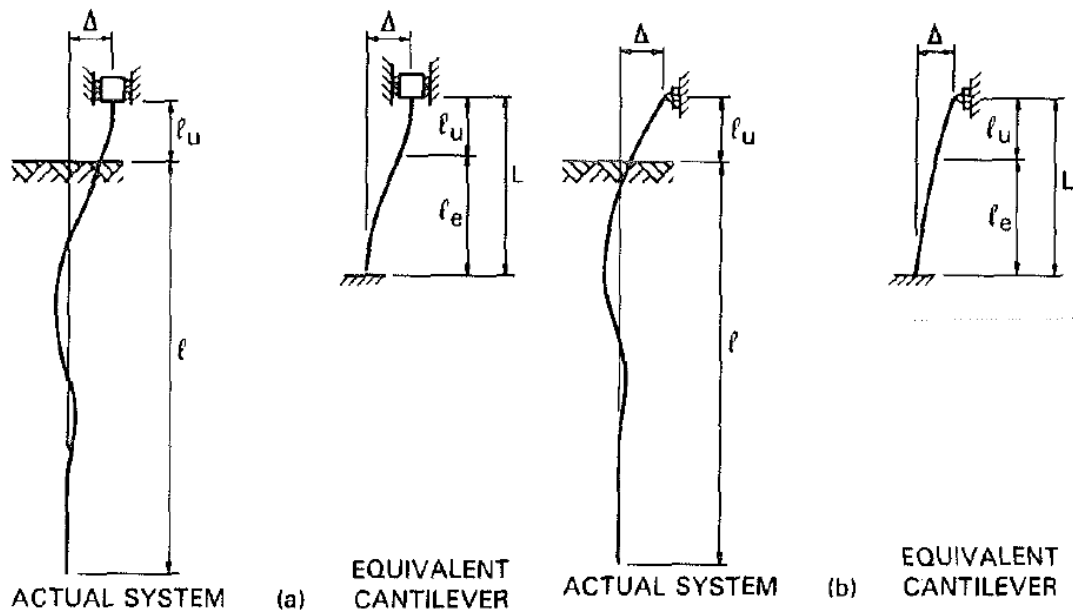
Figure 2.16 Cantilever Idealization of Pile: (a) Fixed Head; *(b)* Pinned Head
(Abendroth et al. 1989)

2.5.3 Characteristic Load Method (CLM)

Duncan et al. (1994) proposed a method based on parametric analysis of numerous p-y curves. The significance of this method over the equivalent cantilever method is that it can deal with non-linearity of the soil behavior. The non-linear behavior of pile foundations subjected to lateral loads is due to two factors. The first factor is non-linearity of the load-deflection behavior of the soil around the pile and the second one is related to load transfer from the upper part of the pile to the greater depths resulting in an increase of the moment from the load at the top of the shaft. In addition, the authors stated that this method can be used to determine:

1.   Ground line deflections due to ground line shears for fixed shaft condition.

2.   Ground line deflections due to moment applied at the ground line.

3.   Maximum bending moment within the shaft.

4.   Position of the maximum moment.

The relationships of the characteristic load method (CLM) were formed by using the dimensionless variables to represent a wide range of real conditions as given below:

For clay,

$$P_c = 7.34 D^2 (E_p R_I) \left[\frac{S_u}{E_p R_I} \right]^{0.68} \qquad (12)$$

$$M_c = 3.86 D^2 (E_p R_I) \left[\frac{S_u}{E_p R_I} \right]^{0.46} \qquad (13)$$

where P_c is the characteristic or normalizing shear load,

M_c is the characteristic or normalizing bending moment,

D is the width or diameter of the pile or drilled shaft,

E_p is the modulus of elasticity of the pile or drilled shaft,

R_I is the ratio of moment of inertia (I_p / I_r) = ratio of moment of inertia of the

pile or drilled shaft (I_p) to the moment of inertia of a solid circular

cross section (I_r), and

S_u is the undrained shear strength of undisturbed samples of clay.

From the above equations, the shear and moment loads are determined at the ground line or ground surface. After determining the variables P_c and M_c, the solution parameters can be obtained with the help of various curves which are ground line shear and ground line moment deflection curves as presented in Figure 2.17.
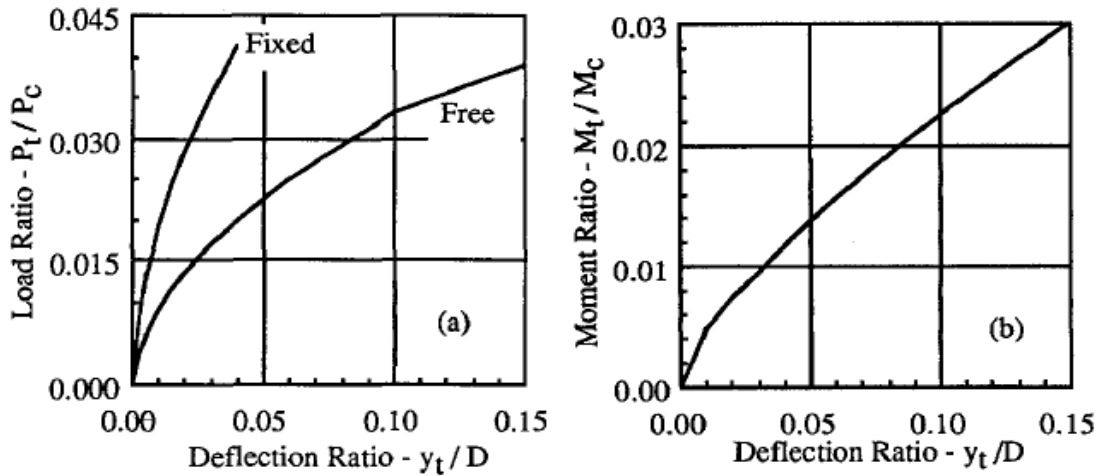
Figure 2.17 Deflection Curves of (a) Ground line Shear and (b) Ground line Moment for Clay
(Duncan et al. 1994)

To compute the ground shear deflection (y_{tpm}) and the ground moment deflection (y_{tmp}) for use in Eq. 14, the following steps are performed:

Step 1 – Divide the ground line load (P_t) by the characteristic shear load (P_c) and the moment (M_t) by the characteristic bending moment (M_c). P_c and M_c are calculated from Eqs. 12 and 13 above.

Step 2- Using the graphs shown in Figure 2.17 (a) and (b) above, determine the deflection ratios for the ground line shear (y_{tp}/D) (Graph a) and for the ground line moment (y_{tm}/D) (Graph b). Multiply the drilled shaft diameter (D) by the shear and moment Deflection Ratios to obtain the ground line deflection (y_t) if only y_t for each property is desired.

Step 3 - Using the same deflection ratio from the ground line moment (y_{tm}/D), determine the ground line shear (P_m) by entering this value on the horizontal axis in Graph a, extend this value vertically to the curve, project a horizontal line from this point to the y-axis, and read the value as P_m/P_c. Using the same deflection ratio from the ground line shear (y_{tp}/D), determine the ground line moment (M_p) in the same manner as described for P_m using Graph b.

35

Step 4 - For the ground line shear, add P_t and P_m, divide by P_c, and enter this value in

Graph a. Project a horizontal line to the curve, and then project a vertical line

down to the x-axis. Read the value and record as y_{tpm}/D. For the ground line

moment, add M_t and M_p, divide by M_c, and enter this value in Graph b. Project

a horizontal line to the curve, and then project a vertical line down to the x-axis.

Read the value and record as y_{tmp}/D. Divide y_{tpm}/D and y_{tmp}/D by D to obtain

y_{tpm} and y_{tmp} respectively.

Step 5 - Finally, compute the lateral deflection ($y_{t\ combined}$) by using the following

equation:

$$y_{t\ (combined)} = 0.5(y_{tpm} + y_{tmp}) \qquad (14)$$

In order to find the maximum moment in this method in a free- or fixed-head drilled shaft

and if the only load applied is a ground line shear, Figure 2.18 can be used.
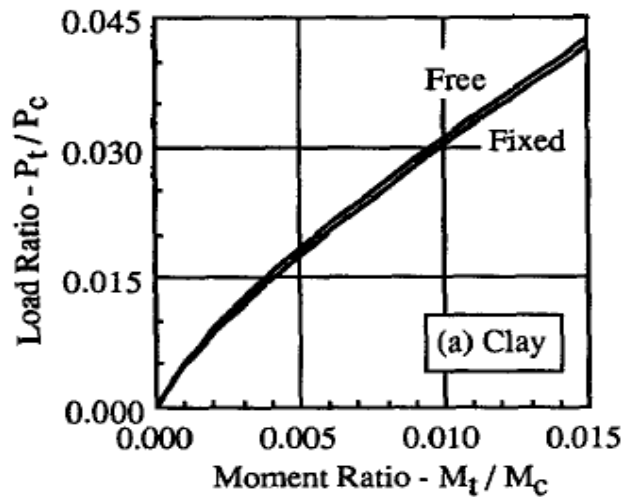
Figure 2.18 Load-Moment Curves (Duncan et al. 1994)

However, if the moment and shear are both applied, the lateral deflection, $y_{t\ (combined)}$, is

determined as mentioned above and then the characteristic length (T) is found from the

following equation:

36

$$y_{t\ (combined)} = \frac{2.43 P_t}{E_p I_p} T^3 + \frac{1.62 M_t}{E_p I_p} T^2 \qquad (15)$$

The next step is to calculate the bending moment of the drilled shaft by using the following equation:

$$M_z = A_m P_t T + B_m M_t \qquad (16)$$

where M_z is the moment at depth z, and

A_m, B_m is the dimensionless moment coefficient which is obtainable from the graph in Figure 2.19 below.
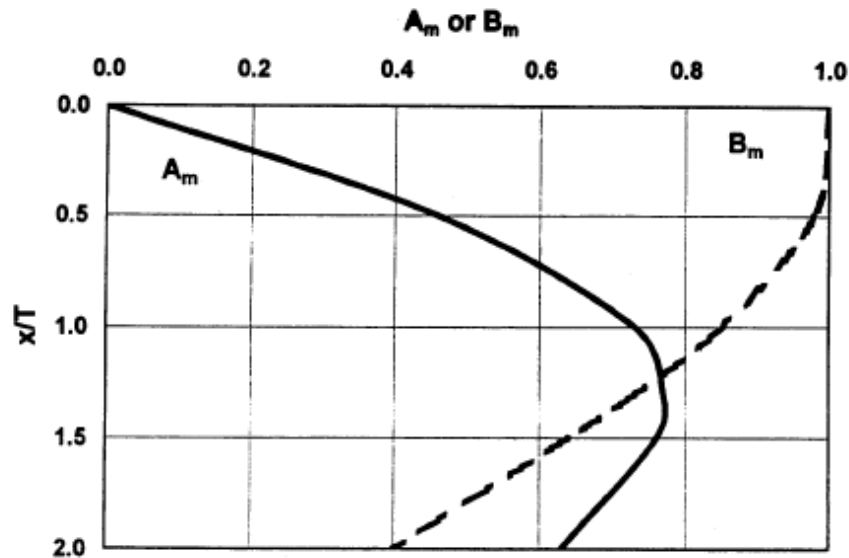
Figure 2.19 Parameters A_m and B_m (Matlock and Reese 1961)

Although the characteristic load method was developed from the p-y method, it is not generally used as the p-y method. There are some limitations of this CLM Method which are outlined below (O'Neil and Reese 1999):

1) Piles and drilled shafts must be long enough so that their behavior is not affected to any significant degree by their length which depends on the relative thickness of the piles or shafts to the stiffness of the soil. Thus, Duncan et al. (1994) provided the minimum drilled shaft penetrations to fit with this method. However, in case that a

37

shaft is shorter than the length mentioned in Table 4, the ground line will be underestimated and the maximum bending moment will be overestimated. In addition, the minimum penetration depth is influenced by the cyclic loading emanating from seismic, environmental (temperature or moisture induced) and other events and the presence of free water.

2) It is founded on generally uniform soil conditions; also, it has not been used when shafts are founded in the rock sockets.

3) The effect of axial loads on the bending moment is not taken into account.

4) The shear could not be analyzed directly.

5) The non-linear bending in the drilled shaft is not considered in this method. Thus, if there are some cracks at the depth of the maximum moment, the ground line deflection will be underestimated.

Table 2.4 Minimum Penetrations for Clay of Drilled Shafts for the Characteristic Load Method (Duncan et al. 1994)

Type of Soil	Criterion	Minimum Length
Clay	$E_p R_l / S_u = 100,000$	6D
Clay	$E_p R_l / S_u = 300,000$	10D
Clay	$E_p R_l / S_u = 1,000,000$	14D
Clay	$E_p R_l / S_u = 3,000,000$	18D

2.5.4 p-y Method (Non-Linear Analysis)

This method is generally used to analyze a drilled shaft subjected to lateral loading due to its' versatility including the distributed load along the shaft caused by flowing water or creeping soil, non-linear bending characteristics, cracked concrete pier sections, layered soils, and non-linear soil response. This method is recommended for use with the most critical foundations. The p-y model was first developed using the response of a single shaft subjected to lateral loads (Reese and Matlock 1956). McClelland and Focht (1958) developed the p-y

model based on the results of a lateral load test on a 24 in. (610 mm) diameter pile embedded to a depth of 75 ft (23 m) in a normally consolidated (NC) clay in the Gulf of Mexico. After that, this method was improved by many researchers including Matlock and Ripperger in 1958, Matlock in 1970, Reese et al. in 1975, Reese and Welch in 1975, and Bhushan et al. in 1979. Later, Reese (1984, 1986) reported comprehensive information on laterally loaded piles and drilled shafts design in a Federal Highway Administration (FHWA) document which has been broadly accepted.

The fundamental aspect of this method is to develop the p-y curves representing the true behavior of soils by considering the non-linearity of the soil modulus. This is based on a numerical solution of a physical model for the laterally loaded, deep foundation based on the soil along the unit length of shafts and replaced with a series of mechanisms surrounding the shaft as shown in Figure 2.20. At different depths of drill shaft, the resisting force per unit length of the shaft (soil reaction) (p) performs as the non-linear function of the lateral deflection (y).
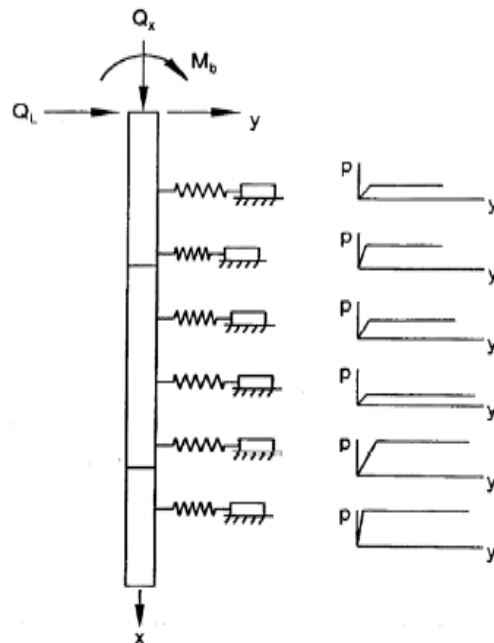
Figure 2.20 Physical Model of a Deep Foundation under a Lateral Load

The methods representing the p-y curves are cited after presenting the governing equations. The drilled shaft is treated as a beam column with lateral soil support. The general behavior of a drilled shaft under a combination of lateral and axial loading can be obtained by solving the differential equation given below (Hetenyi, 1946):

$$EI\frac{d^4y}{dx^4} + Q\frac{d^2y}{dx^2} - p - w = 0 \qquad (17)$$

where Q is the axial load on the shaft,

y is the lateral deflection of the shaft at a point x along the length of the shaft,

p is the lateral soil reaction per unit length,

EI is the flexural rigidity of the drilled shaft, and

w is the distributed load along the length of the shaft.

In addition, the equations that are produced from derivatives are necessary in design as shown below.

For transverse shear (V),

$$EI\frac{d^3y}{dx^3} + Q\frac{dy}{dx} = V \qquad (18)$$

For bending moment in the drilled shaft (M),

$$EI\frac{d^2y}{dx^2} = M \qquad (19)$$

For the slope of the deflection diagram (S),

$$\frac{dy}{dx} = S \qquad (20)$$

For the slope of secant to any p-y curve or soil modulus (E_s)

$$E_s = \frac{p}{y} \qquad (21)$$

After substituting E_s (Eq. 21) into the main equation (Eq. 17), the results show that there are finite difference terms depending on a number of nodes along the drilled shafts, which the p-value at each node is equal to $E_s y$. Thus, y-values are the unknown parameters in this

problem. Generally, y-values depend on soil stiffness. The deeper the embedment depth, the higher the vertical stresses which induce an increase in the soil stiffness. Also, the lateral movement from the piles will additionally increase the stress in the soil.

Even though the bending moment, shear force, and other design aspects of the drilled shafts are computed from the finite difference forms of the equations above, computer generated solutions such as LPILE and other software programs are efficient, time saving, and create an opportunity for investigating the influence of a large number of parameters with minimum difficulty.

In the present research, the researchers propose to analyze the drill shaft load test results using the p-y method-based software such as the 'L-PILE' program. Other methods including the 'Characteristic Load Method' and 'Broms' Method' will also be considered if the soil conditions at the test site location match with the assumptions used in these methods.

2.5.5 Strain Wedge Model

The Strain Wedge (SW) Model, developed in 1996 by Ashour et al. (1998), improved upon Reese's (1977) Beam on Elastic Foundation (BEF) pile response parameters and his realization of limitations of the p-y curves (1983) for soil continuity and pile properties. The SW method added the capability to analyze piles in multiple soil layers to include sand and clay. Additionally, the method allowed the effect of pile head conditions (free- or fixed-head) to be included in the analysis.

The method uses a 3-D passive soil wedge that is formed in front of a laterally loaded pile that accounts for stress-strain-strength parameters. The SW model is interdependent upon the BEF model through the horizontal soil strain, ε, the horizontal soil stress change, $\Delta\sigma_h$, and the non-linear variation in the Young's modulus, E.

A diagram of the soil wedge is shown in Figure 2.21. The deflection pattern of the pile is assumed to be linear and is shown in Figure 2.22. Each layer's soil properties encountered in

41

the field can be applied in this model and used to more accurately determine the effect to the soils from lateral loading on the pile.

(h−x) $\tan \beta_m \tan \varphi_m$

Pile Width (D)

SLICE OF WEDGE AT DEPTH x
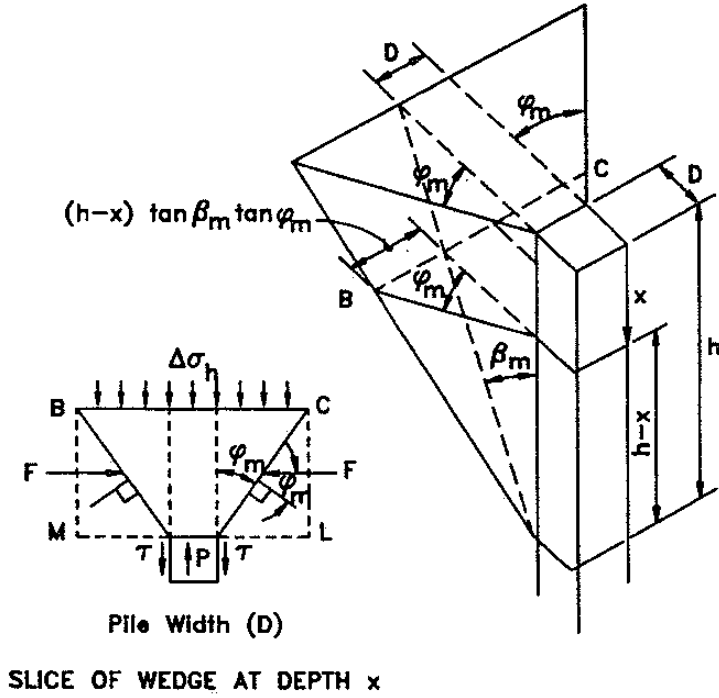
Figure 2.21 Basic Strain Wedge in Uniform Soil (Ashour et. al, 1998)
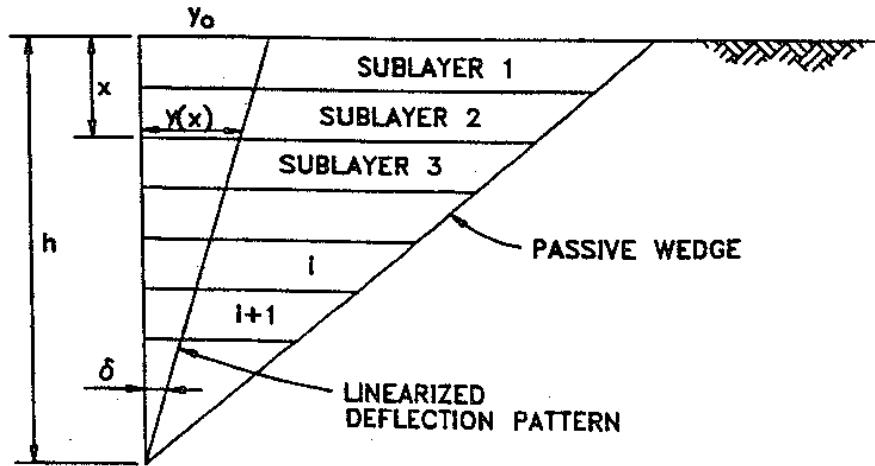
Figure 2.22 Linearized Deflection Pattern (Ashour et al., 1998)

The horizontal strain in the soil is the most influential parameter in the model. In normally consolidated clay, the effective unit weight, the Plasticity Index, effective friction angle,

42

undrained shear strength, and soil strain at 50% stress level are used in the calculation of the modulus of subgrade reaction, E, and representing the secant slope at any point on the p-y curve.

Wedge thicknesses are created based upon soil types. But additional wedges can be created if a soil layer is determined to be too thick and possibly affect the calculations. Additionally, a wedge can be created for a fixed-head pile and included in the calculations. This greatly assists in replacing the conditions in such programs as COM624 and LPILE that consider p-y curves to be unique. Soil and pile variations have a dramatic effect upon the response of soils and their p-y curves as shown by actual field tests in Figure 2.23.
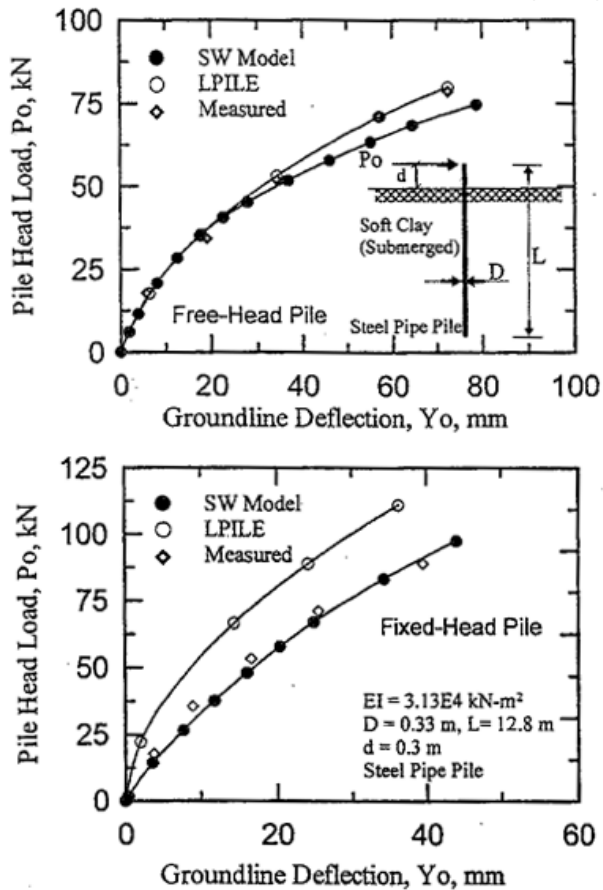
Figure 2.23 Comparison of SW, LPILE, and Field Data for Free- and Fixed-Head Piles in Clays at the Sabine River (Ashour et al., 2002)

2.5.6 Comparison of Lateral Load Analysis (Broms' Method & p-y Method)

Klaiber et al. (2004) compared the results between the Broms' Method and the p-y Method and reported that the p-y Method (the non-linear method) can be used in more complex soil conditions and provides more accurate results of the moment distribution along the depth of piers whereas the Broms' Method (the linear method) does not take into account the redistribution of loads below the point of fixity. They also compared both methods by using different soils, stiff clay (SPT blow count of N = 25), soft clay (SPT blow count of N = 2), and cohesionless soil (SPT blow count of N = 25), with different magnitudes of lateral loads by changing the backwall height. In short, the Broms' Method is more conservative in predicting stiff clays than the p-y Method as shown in Figure 2.24. For soft clays, Broms' Method is less conservative than the p-y Method as shown in Figure 2.25. For cohesionless soils, it is noticed that both methods yield more or less the same results (Figure 2.26).
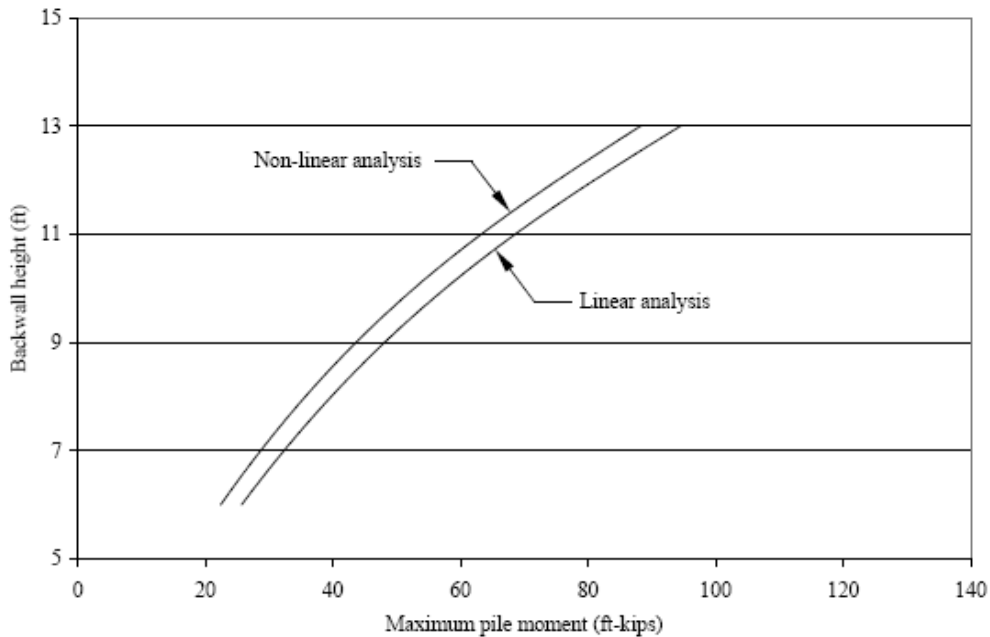
Figure 2.24 Comparison of Lateral Load Analysis in Stiff Clay

44
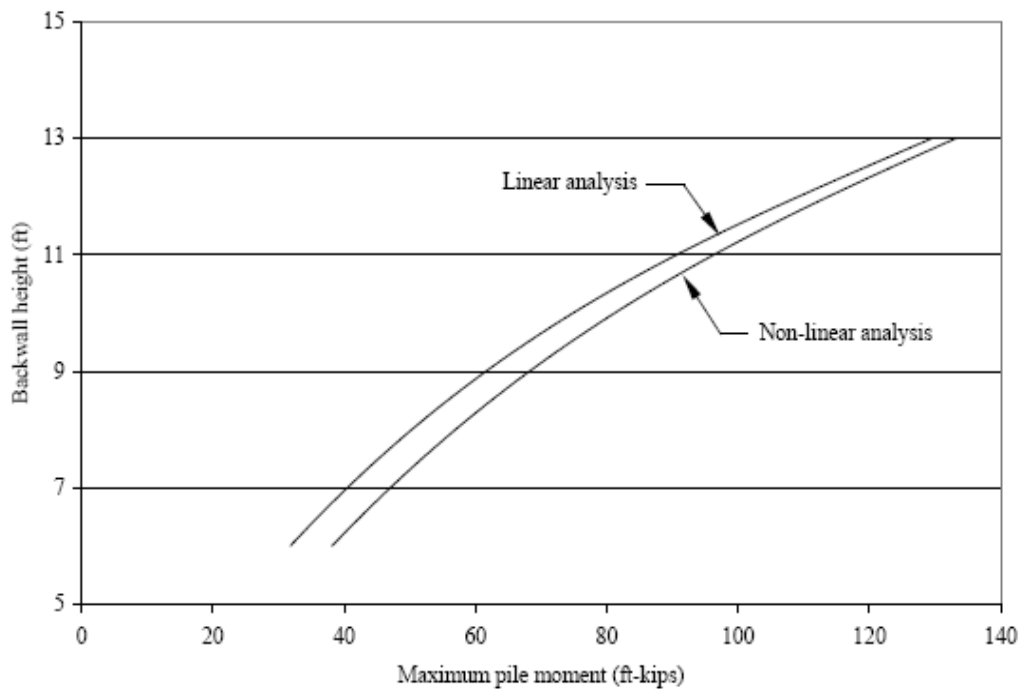
Figure 2.25 Comparison of Lateral Load Analysis in Soft Clay
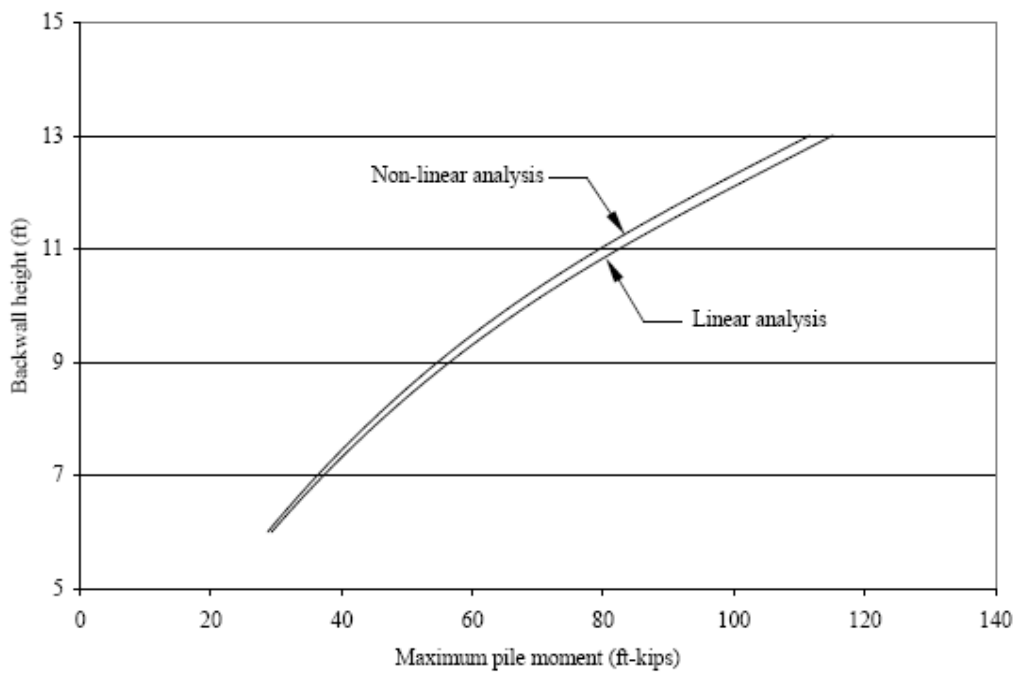
Figure 2.26 Comparison of Lateral Load Analysis in Cohesionless Soil

<u>2.6 Lateral Load Tests on Drilled Shafts</u>

The performance of drilled shafts in different types of soils with the derivation of the p-y curve are able to be evaluated with different types of the tests which leads to more accurate designs of drilled shafts (O'Neil and Reese 1999). Standard lateral load tests for drilled shafts are described in the FHWA IP-84-11 report and ASTM D 3966 (ASTM, 2007). The most common types of lateral load tests that are conducted on drilled shafts are the Conventional Load Test, Osterberg Load Cell Test, and the Statnamic Load Test. A brief description of these test methods is given below.

2.6.1 Conventional Load Test

In the Conventional Load Test, a test shaft of known diameter is placed between two reaction shafts which are mounted with a reaction frame. The load is gradually applied by this reaction frame to the test shaft. Hydraulic jacks are placed on the test shaft on a leveled steel plate. A typical Conventional Load Test setup is shown in Figure 2.27.
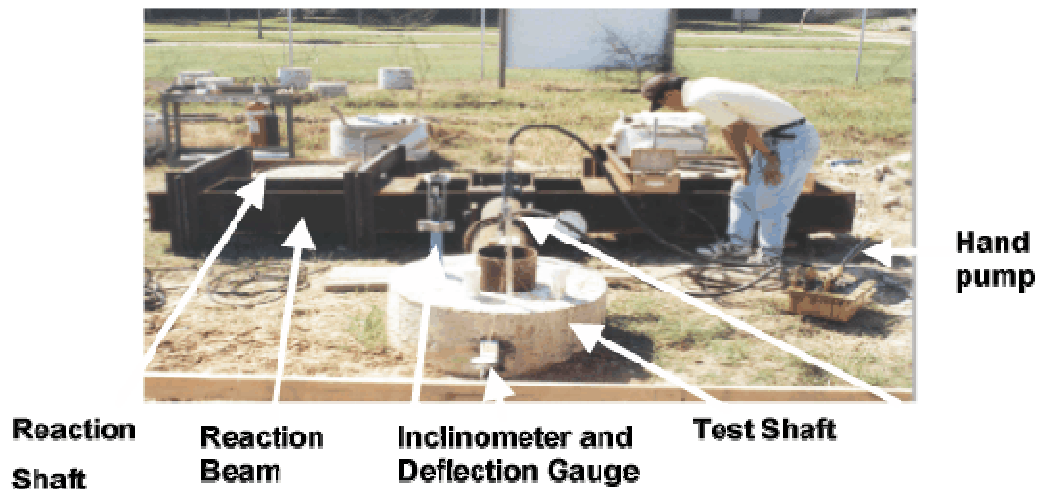
Figure 2.27 Test Setup for a Conventional Load Test (Source:
http://www.fhwa.dot.gov/infrastructure/tccc/tutorial/shafts/fhcha10.htm)

In this test, the test shaft is pulled away from the two reaction shafts and the readings are taken using the dial gauge fitted to the test shaft. From Figure 2.27, the inclinometer which has been cast into the drilled shafts along the centroidal axis is used to measure the deflection

46

of the shafts. As a result, the p-y curves can be obtained from the loading tests directly if the bending moment is considered as a function of the lateral loads and depth (Welch and Reese, 1972; Dunnavant and O'Neill, 1989). The disadvantage of this method is that it is very expensive compared to other testing methods. However, a set number of reaction shafts are installed with an "I" beam framework bolted to the reaction piers. The number of test shafts can be increased since they will be of a smaller magnitude and depth in comparison to the reaction shafts.

2.6.2 Osterberg Load Cell Test

The Osterberg Load Cell, or O-cell, named after its inventor, Dr. Jorj O. Osterberg, has radically changed the way foundation load tests are designed, performed and interpreted. This test can be performed on high capacity shafts at low costs unlike the conventional load testing. Engineers need to rely on the information obtained from the load tests conducted on smaller test shafts. In this method, the Osterberg load cell is installed within the drilled shaft during its construction as shown in Figure 2.28. The cell is mounted on a reaction socket which is made of two sockets and these sockets are jacked apart with the help of hydraulics to duplicate the effect of lateral loading. Lateral displacement is measured by using LVDT's connected between the plates. The lateral load applied can be calculated by dividing the load in the cell by the length of the socket.

Figure 2.28 Osterberg Load Cell for the Lateral Load Test (Source:
http://www.loadtest.co.uk/Loadtest%20Ltd/downloads.htm)

2.6.3 Statnamic Load Test

Drilled shafts are also tested by mounting Statnamic devices horizontally adjacent to the shaft (O'Neill et al., 1990; Rollins et al. 1997). In this test, lateral loads are applied on the shaft with the help of a propellant which is accelerated to generate heavy masses (Figure 2.29). This type of test is more economical when there are no reaction frames. Also, the type of loading that is applied is impact loading. McVay (2003) had conducted a study to collect a database of statnamic tests and conventional tests on drilled shafts and driven piles in different soil and rock conditions and established resistance factors for load and resistance factors design (LRFD) for statnamic tests.

Figure 2.29 Test Setup for a Statnamic Test (Source:
http://www.fhwa.dot.gov/infrastructure/tccc/tutorial/shafts/fhcha10.htm)

Lateral load tests were conducted by several researchers in non-expansive soils and a few of these results are discussed in tasks outlined in the work plan. Houston et al. (2004) conducted lateral load tests to assess the performance of drilled shafts installed in cemented sands. In the case of high plasticity clays, limited test results are available.

<u>2.7 Summary</u>

This chapter provided a comprehensive review of various aspects that are critical for proposed research. Sections describing expansive soils, lateral load analysis and load tests are described in detail. The next Chapter describes few of the earlier tasks including site selection and laboratory tests performed on the site soils.

CHAPTER 3

SITE SELECTION AND LABORATORY STUDIES

3.1 Introduction

The main objective of this research is to perform the load testing on drilled shafts in high plasticity clay environment. It is necessary to find an appropriate site where high plasticity clay is located for considerable depth. Once such a site was located, appropriate laboratory testing program needs to be designed to determine the properties relating to expansive soil behavior of samples taken from site. The experimental program includes basic soil properties tests, and engineering tests on the soils. A summary of the laboratory procedures, equipments used and results are presented in this chapter.

3.2 Site Selection

During the site selection process, two sites were proposed and screened. The first site was along IH 20 near Rose Hill Road exit, and the second one was IH 20 and FM 2578 intersection as presented in Figure 3.1 and 3.2, respectively. Several criteria, such as high plasticity characteristics of the CH soil at Site 1 or cable barrier foundations that experienced distress problems at Site 2, were considered in the selection process but the most important criterion was to see if the area would have enough space to work on the field load tests. Comparing the two sites, the first location met the criteria much better than the second one due to large area for performing testing without obstructing traveling public. Therefore, the test site located on IH 20 and Rose Hill Road located in Kaufman County, Texas was selected.

Figure 3.1 An Alternative Site Located on IH 20 and Rose Hill Road

Figure 3.2 An Alternative Test Site Located on IH 20 and FM 2578

3.3 Soil Sampling and Laboratory Testing

For identifying properties of the soil, field open pit sampling was performed by using a backhoe setup. Nuclear gauge tests were also performed at the site to determine both the density and moisture content of the soil in field conditions, as shown in Figure 3.3

Figure 3.3 Soil Sampling and Density Measurement by Using Nuclear Gauge

The collected soil samples at various elevations were subjected to a variety of laboratory physical tests including specific gravity, Atterberg (ASTM D4318-05), and linear shrinkage bar tests (Tex-107-E, 2002). All the soils are considered as fine-grained soils, as more than 50% of the soils are passing through the sieve No.200. Classification of types of the soils from the field is performed by using Unified Soil Classification System (USCS) method. Detail of each test used is explained in the following sections.

3.3.1 Basic Soil Properties Tests

3.3.1.1 Specific Gravity

Specific gravity is defined as the ratio of the weight of a certain volume of a liquid to the weight of an equal volume of water, which is determined as per TxDOT procedure, Tex-108-E method. In this experiment, temperature must be recorded due to density of water and temperature coefficients are varied with temperatures.

3.3.1.2 Atterberg Limits

Atterberg limits tests are used to reveal properties related to consistency of the soil. Generally, properties of soils consist of liquid limit (LL), plastic limit (PL) and shrinkage limit (SL) ,and these are necessary to correlate the shrink-swell potential of the soils. The states of soil from dry, semisolid, plastic and finally to liquid states depend on amount of mixed water. The water content at the boundaries of these states are well known as shrinkage (SL), plastic (PL) and liquid (LL) limits, respectively (Lambe and Whitman 2000). Therefore, the PL is able to be determined by the amount of water content at which the soil starts crumbling when rolled into a 1/8-inch diameter thread. In addition, LL is measured as the water content at which the soil flows. The difference between LL and PL values is called plasticity index (PI), which characterizes the plasticity nature of the soil. In this test, soil samples from different depths are subjected Atterberg limits tests to determine LL and PL as per Tex-104-E and Tex-105-E, respectively.

3.3.1.3 Standard Proctor Compaction Test

To establish compaction relationships between compaction moisture content and dry unit weights of a soil, standard Proctor compaction test is necessary to perform on the field soil samples. Generally, soil samples that exhibit a high compaction unit weight at low moisture content are good for supporting civil infrastructure due to less void space leading to low settlements. The optimum moisture content (OMC) of the soil is the water content at which the soil is compacted to a maximum dry density condition. Water contents close to 95% of

maximum dry density conditions are dry of OMC and wet of OMC, respectively and these values were determined for soil testing. A typical explanation of a schematic is shown in Figure 3.4 below. The dry density conditions from the Proctor test can be used as the initial stage for determining the volumetric swell and shrinkage strain properties.
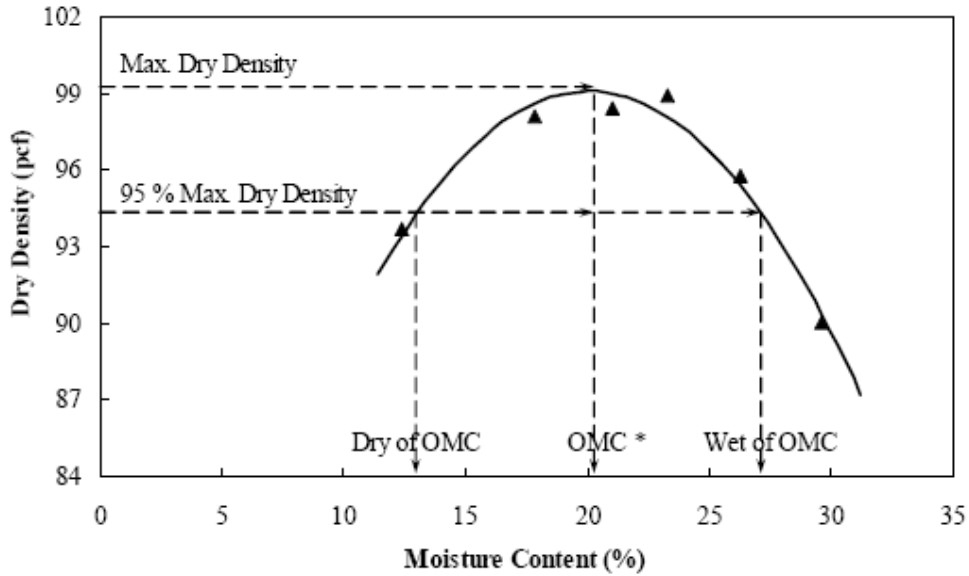
Figure 3.4 Typical Standard Compaction Curve

3.3.2 Engineering Tests

In this research, engineering tests performed were three-dimensional (3-D) free swell strain test, 3-D volumetric shrinkage test, 1-D swell pressure test, total suction measurements and shear strength tests for various soil types.

3.3.2.1 Three Dimensional (3-D) Swell Tests

The three-dimensional free swell test provides a reasonable representation of the maximum volumetric swell potentials of a soil (Punthutaecha, 2006). Soil specimens of 4.0 in. (101.6 mm.) diameter and 4.6 in. (116.8 mm.) height were placed between two porous stones (Figure 3.5), wrapped in a rubber membrane, and was then subjected to soaking by inundating it with water from both ends. The specimen was monitored for the vertical and radial swell movements until there was no considerable movement. The three-dimensional free swell test

54

provides the maximum vertical, diametric and volumetric swell strain potentials of all three soil types. The vertical and radial swell movements are simply measured at specific times by using Dial gauge and PI tapes as presented in Figure 3.5. The three-dimensional free swell test provides a reasonable representation of the maximum volumetric swell potential (Punthutaecha, 2006). All tests were conducted at room temperature conditions and three identical soil specimens were used for each variable condition. Test results are expressed in percentages of swells of original dimensions of the soil samples.

Figure 3.5 Vertical and Radial Measurement for Volumetric Swell Strain

3.3.2.2 Volumetric Shrinkage Test

This test was developed at UTA because of limitations in the linear shrinkage bar test. The cylindrical compacted soil specimens were subjected to a drying process and then measuring the volumetric, axial and radial shrinkage strains. There are several advantages of the volumetric shrinkage test over conventional linear shrinkage bar test and they are reduced interference of boundary conditions on the shrinkage strains, allowance of a larger amount of soil to be tested, and better simulation of the compaction states of the moisture content and dry density conditions. This method was published in an ASTM geotechnical testing journal (Puppala et al., 2004), which signifies the importance of this method being accepted by the researchers and practitioners.

55

Volumetric shrinkage tests were conducted to measure the decrease in the total volume of the soil specimens due to the loss of moisture content from the predetermined initial moisture content to a completely dry state. Three different initial moisture contents (dry of optimum, optimum, and wet of optimum) were used as the initial compaction conditions. Tests were conducted as per the procedure outlined in Puppala et al. (2004). Specimen preparations were performed by mixing the air dried clay with an appropriate amount of water added to achieve the designed water contents, compacting the soil specimens in 2.26 in. (57 mm) diameter by 5 in. (127 mm) high mold, and measuring the initial height of the specimen. The specimens were then cured in the molds at room temperature for 12 hours and then transferred to an oven at a temperature of 220° F (104° C) for 24 hours. Then, the average height and radial of the shrunk soil specimens were manually measured. The typical figure of tested specimen is exhibited in Figure 3.6.

(a)   (b)
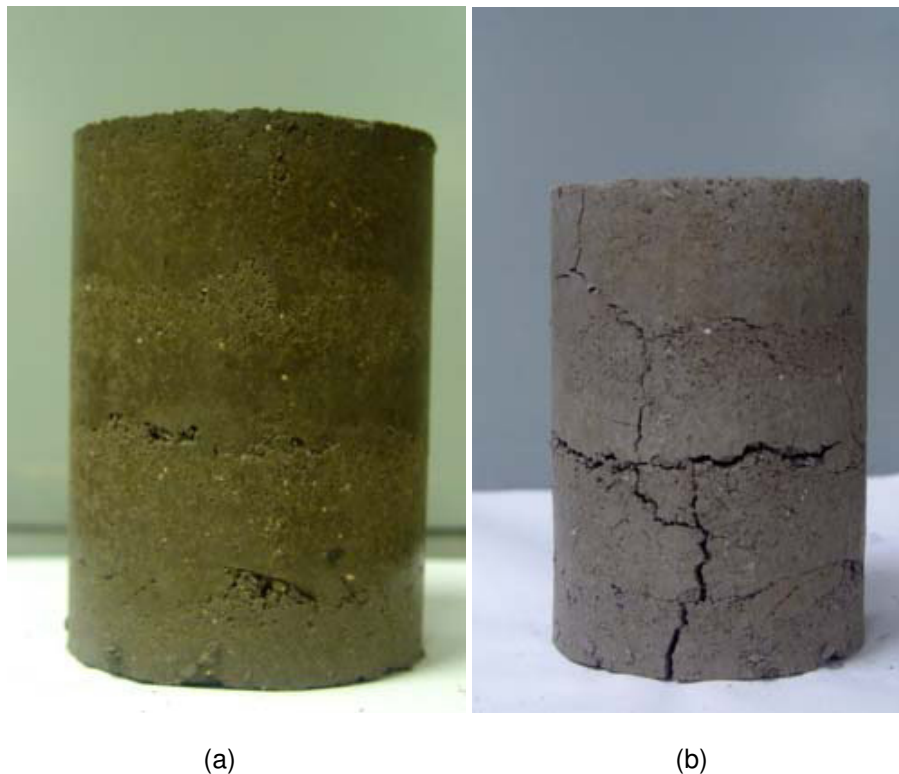
Figure 3.6 Specimen Used in the Test (a) Before Oven Drying   (b) After Oven Drying

3.3.2.3 Swell Pressure Test

Swell pressure tests were also conducted on all soil samples using a 1-D consolidation setup and Test Method ASTM D 4546-96 titled "Standard Test Methods for One-Dimensional Swell or Settlement Potential of Cohesive Soils". These results were used in the estimation of uplift forces. According to Sridharan et al. (1986) and Fredlund and Rahardjo (1993), the swell pressure tests are performed by measuring maximum loads or pressures that soils exhibit the soil specimen still maintains its original volume. Once the sample stops expanding, the pressure at that time is regarded as the maximum swell pressure. In the soil specimen preparation phase, specimens were compacted to have the same density and moisture content conditions in the field. Also, the specimens were kept in the moisture room for at least 24 hours to make the moisture content inside the soil specimens be homogeneous before the tests.

3.3.2.4 Soil Suction Measurement by Pressure Plate and Filter Paper Techniques

Soil suction measurements were made on the soils at different compaction moisture content conditions in order to establish a Soil Water Characteristic Curves (SWCCs) for all soil types. The main reason for considering the SWCCs is to include these results for estimating the shear strength properties at unsaturated soil conditions close to the real field conditions.

The SWCC describes a unique relationship between matric suction and moisture content of soils. In unsaturated soil mechanics, the SWCC is used directly and indirectly to interpret soil strength, permeability and volume change related characteristics (Fredlund et al., 1994). The SWCC curve depends on the size and distribution of the pore structures in the compacted soils, which control the permeability and amount of volume changes expected in the soil (Fredlund et al., 1994). The water content defines as the amount of water contained in the soil pores, which can be expressed as gravimetric water content (w), or volumetric water content (θ), or degree of saturation (S). Methods to measure "Soil Water Characteristic Curves (SWCCs)" of unsaturated soils include filter paper method, Tempe cell and pressure plate

methods. In this research, both pressure plate and filter paper methods were used to generate the SWCC results over a wide range soil suctions expected in the field.

3.3.2.4.1 Pressure Plate Method

A pressure plate consists of a pressure vessel with a saturated high-air entry ceramic disk and this setup can be seen in Figure 3.7. During the test, the applied pressure cannot exceed the air entry value of the ceramic disk. The air will not be able to pass through the saturated high-air entry disk (HAE) which means the matric suction does not go beyond the air entry value of the disk (Aung et al 2001). In applying pressure, air is supplied within the pressure vessel and the lower part of the high-air entry disk which is connected to a burette of water under atmospheric pressure. As shown, a small water reservoir is formed below the plate using an internal screen and a neoprene diaphragm.

The water reservoir is vented to the atmosphere through an outflow tube located on top of the plate, thus allowing the air pressure in the vessel and the water pressure in the reservoir to be separated across the air-water interfaces bridging the saturated pores of the HAE material (Lu and Likos, 2004). Therefore, the applied matric suction can be represented from this test by the applied air pressure subtracted from the atmospheric pressure from the water below the disk. The test was stopped when the outflow of the water connected from the tube ceased. The pressure vessel was opened and the water content of one or more of the specimen was measured generating one point on the soil-water characteristic curve. The current pressure plate device at UTA is limited in that it can only measure matric suction up to 1,000 kPa.
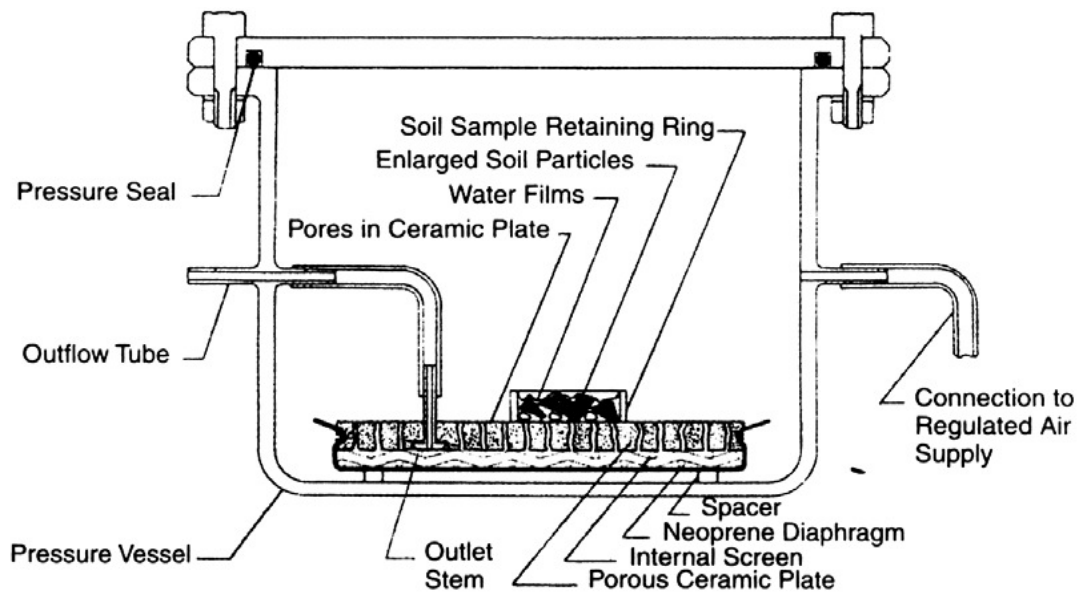
Figure 3.7 Schematic Drawing of Pressure Plate Apparatus
(Soil-Moisture Equipment Corp., 2003)

3.3.2.4.2 Filter Paper Method

The filter paper method is based on the principle that the relative humidity inside the container will be controlled by the soil water content and suction. The filter paper method can evaluate both matric and total suction (total suction is a summation of matric suction and osmotic suction). For total suction, a filter paper (Whatman No. 42) is suspended on a perforated disk in the headspace above the specimen and below the container lid such that the moisture transfer occurs in the vapor phase. The equilibrium amount of water absorbed by the filter paper is a function of the pore-air relative humidity and the corresponding total soil suction. For matric suction, a filter paper (Whatman No. 42) located between two separator papers is contacted directly with water from the soil specimen so that the equilibrium can be achieved by exchanging vapor moisture between the soil and the filter paper as shown in Figure 3.8. The soil sample and filter paper are allowed to equilibrate for a period of at least 7 days at a constant temperature of $25° \pm 1$ °C.

59
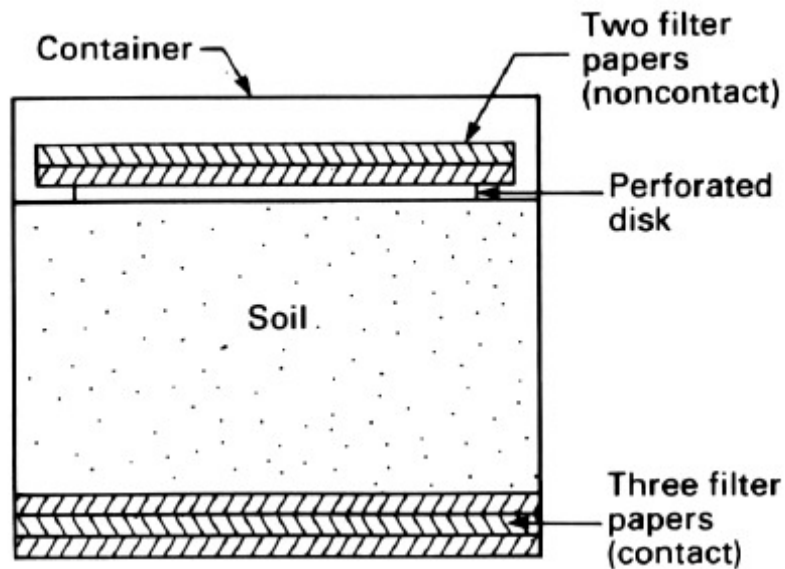
Figure 3.8 Contact and noncontact filter paper methods for measuring matric and total suction, respectively (Al-Khafaf and Hanks, 1974)

After equilibrium has been reached, the suction in the filter paper will be the same value as that in the soil. At the end of the equilibrium period, the filter paper is rapidly removed and it is water content determined by precise weighing (± 0.0001 g) before and after oven drying (Figure 3.9).

Figure 3.9 Weighing Balance used in Measuring the Weight of the Filter Papers

3.3.2.4.2 Calibration of the Filter Paper Test

The filter paper is used as passive sensors to determine the matric and total suctions by absorbing moisture which evaluates the soil suction by using filter paper calibration curves or equations. The calibration curve for this test depends on a specific filter paper (e.g., Whatman No.42 or Schleicher and Schnell, No. 589) which can be found by measuring the water content of the filter paper when it reaches equilibrium with a salt solution having a known osmotic suction (Fredlund and Rahardjo, 1993; Marinho and Oliveira, 2006; Power et al, 2008). Therefore, in order to create SWCCs, several water content points from filter papers (w_f) should be used to determine the corresponding suctions by substituting them into the equations shown below and creating a graph of filter paper water content (%) against their corresponding suction values (kPa). Matric suction equations already developed for the Whatman No. 42 filter paper; and hence this method was used to determine high suction values above 1000 kPa. Based on the ASTM D5298-03 method, the two most commonly used filter papers are the Whatman No. 42 and the Schleicher and Schnell 589. The calibration curves for both types of filters are shown in Figure 3.10
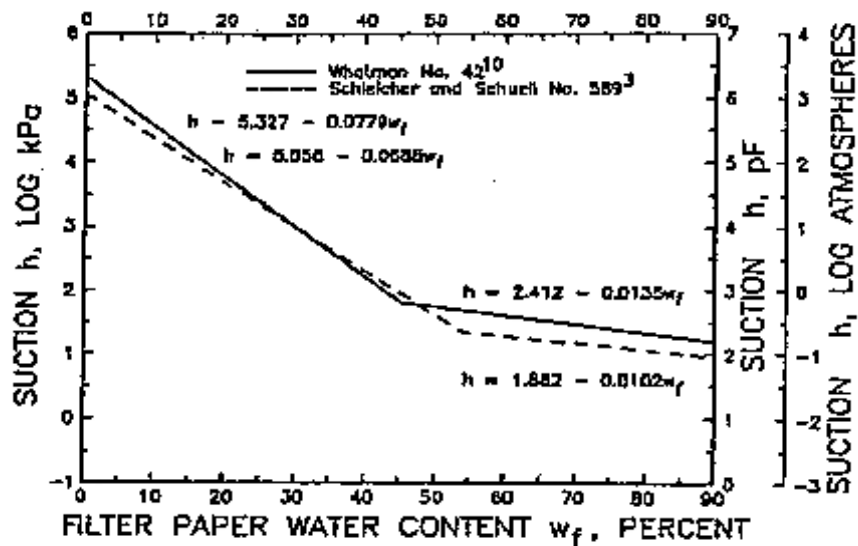
Figure 3.10 Calibration Suction-Water Content Curves for Filter Papers

In this research, the matric suction calibration curve using the Whatman No. 42 filter papers was used. The equations of the matric suction calibration curve for the Whatman No. 42 filter paper are:

$$\log h = 5.327 - 0.0779 \, wf \, , \quad \text{for} \ \ wf < 45.3\% \tag{1}$$

$$\log h = 2.412 - 0.0135 \, wf, \quad \text{for} \ \ wf \geq 45.3\% \tag{2}$$

3.3.2.4.3 Specimen Preparation

All the specimens used in the Filter Paper test were prepared at the same density and moisture content as well as in saturated states. In this research, two specimens were used for establishing the SWCCs. For the saturated specimens, the Pressure Plate test was used as shown Figure 3.11. For the unsaturated field moist compacted specimens, the Filter Paper test was conducted as shown in Figure 3.12. The pattern of specimen preparation developed by Perez (2009) was used in this research. Perez (2009) showed that the advantages of this pattern results in a drastic reduction of specimens required for one SWCC by being able to get the exact moisture of a soil specimen from the drying process, being able to use undisturbed soil samples.

For the filter paper specimen preparation, a soil specimen was extruded from the field sampler and then specimens were cut perpendicular to the field specimen. After that, the specimen was wrapped by plastic paper. Three papers were set into the bottom of the container, the soil specimen placed directly on top of these three papers, a perforated disk was placed on top of the soil specimen, two more papers placed on top of the disk, and the lid screwed onto the container. The lid was then sealed around the interface of the lid and container to minimize water vapor evaporation out of the container. All the steps of the specimen preparation can be seen in Figure 3.12. Soil specimens were cured in the container under constant temperature for 7 to 10 days. After that, the filter papers were rapidly removed from the container and immediately weighed as described above.

Limitations of the current pressure plate device at UTA restrict the measurement of the matric suctions up to only 1,000 kPa. The Filter Paper method can be used over a wider range of suctions up to approximately 1050 MPa (150,000 psi). Hence, the Filter Paper method was used to measure the soil suctions that were over 1,000 kPa. Thus, both the Pressure Plate and the Filter Paper methods were employed in the development of a complete SWCC of the soils used in this study.
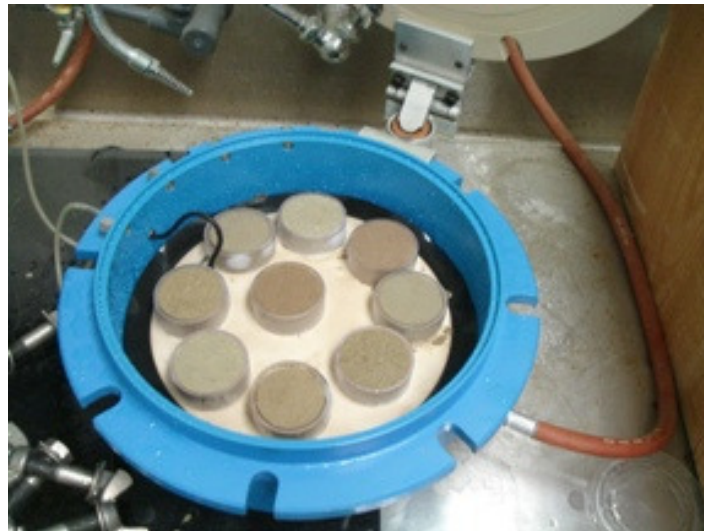
Figure 3.11 Pressure Plate Testing

Figure 3.12 Filter Paper Testing

3.3.2.5 Shear Strength Tests: Direct Shear and Unconsolidated-Undrained or UU Triaxial Tests

Both direct shear and UU triaxial tests were conducted to determine the shear strength and stress-strain relationships of the soils at various moisture content states in the soil. Both Direct Shear and Triaxial UU tests were conducted on both silty sand and clayey soil to determine cohesion, c, and angle of internal friction, ϕ and these methods are summarized here.

3.3.2.5.1 Direct Shear Tests

This test is a simple method for finding shear strength and friction angle of soils and was performed using ASTM D 3080-98 method. Generally, the soil specimen can be cubical or cylindrical and cylindrical specimens were used in this study. Normal stresses used for these tests here were 2000, 4000, and 8000 psf, respectively. Silty sand located in the first layer, 0 –

3 ft (0 – 0.9 m) was first tested. For specimen preparation, all three specimens were prepared at the same density and moisture content condition as measured in the field. The equipment and soil specimen used in the test are shown in the Figure 3.13 below.
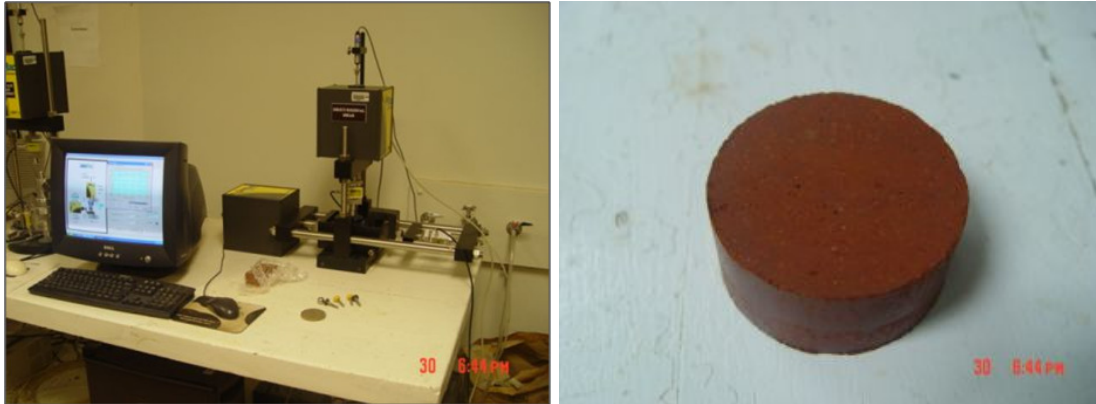
Figure 3.13 Direct shear test setup and compacted silty sand used in the test

3.3.2.5.2 Unconsolidated-Undrained or UU Triaxial Tests

The unconsolidated-undrained test is also used to measure shear strength parameters (c and Ø). This test was performed using ASTM D 2850-95 (2003) titled "Standard Test Method for Unconsolidated-Undrained Triaxial Compression Test on Cohesive Soils." The test procedure requires the placement of a cylindrical soil specimen sealed by the rubber membrane in a triaxial chamber and then applying a confining pressure by not allowing water to dissipate from the soil specimen. After that, the soil specimen was tested by applying deviatoric loading. The failed soil specimen is shown in the Figure 3.14 below.

Tests were performed in two case scenarios. The first one was related to unsaturated case. In this case, all the specimens are prepared at the same density and moisture content as measured in the field at the time of sampling. After the preparation process, the soil specimens were cured in the moisture room for 7 days to make the moisture content inside the soil specimen to be homogeneous.

For the second case, saturated soil specimens were prepared and used. All soil specimens were prepared at the same density and moisture content condition as in the first

case. After compacting the soil specimens, soil specimens were kept in the water for two weeks in order to make them fully saturated.

Figure 3.14 Failed Soil Specimen in the Triaxial Test

3.4 Laboratory Test Results

3.4.1 Basic Soil Properties

All representative soil samples used in this research were collected from the I-20 near Rose Hill Road site located in Kaufman County, Texas and soil samples were subjected to Atterberg limits tests and linear shrinkage tests to determine all basic soil properties. Table 3.1 presents a summary of various physical characteristics of these soils. All these results were compared with the PI properties of Table 3.2 to investigate the swelling potential from each layer.

Table 3.1 Basic Soil Properties

Depth, ft (m)	LL	PL	PI	SL	% Linear Shrinkage	Classification
0.0 – 1.0 (0.0 – 0.3)	N.A.	N.A.	N.A.	N.A.	0.00	Silty Sand
1.0 – 3.0 (0.3 – 0.9)	77	18	59	10	12.07	CH
3.0 – 5.0 (0.9 – 1.5)	47	20	28	14	8.40	CL
5.0 – 10.0 (1.5 – 3.0)	41	20	21	15	2.62	CL
> 10.0 (> 3.0)	33	21	12	17	2.10	CL

Table 3.2 Expansive soil classification based on Plasticity Index (Chen, 1988)

Plasticity Index	Swelling Potential
0 – 15	Low
10 – 35	Medium
20 – 55	High
35 and above	Very High

From the test results presented in the table, it can be concluded that the soil at 1 to 3 ft (0.3 to 0.9 m) depth has the highest plasticity index (PI) value. The second highest PI value is measured for the soil strata located at 5 to 10 ft (1.5 - 3 m) depth interval. The soil encountered in third layer has a PI value equal to 28, and the linear shrinkage strain is 8.4% and this is considered high. Compared with the PI in table 3.2, the soils from layer 2 and 3 have shown to be very high swelling potential and high swelling potential, respectively.

3.4.2 Standard Proctor Compaction Test Results

Standard Proctor compaction tests were also performed to establish compaction relationships of the soils. In this experimental study, soils from layer 2 and 3 were chosen to perform the test because these soils have high swelling potentials, which is able to affect the distress of foundation. The standard compaction for Layers 2 and 3 are shown in the following Figures 3.15 and 3.16. Table 3.3 summarizes the values obtained from the laboratory tests.
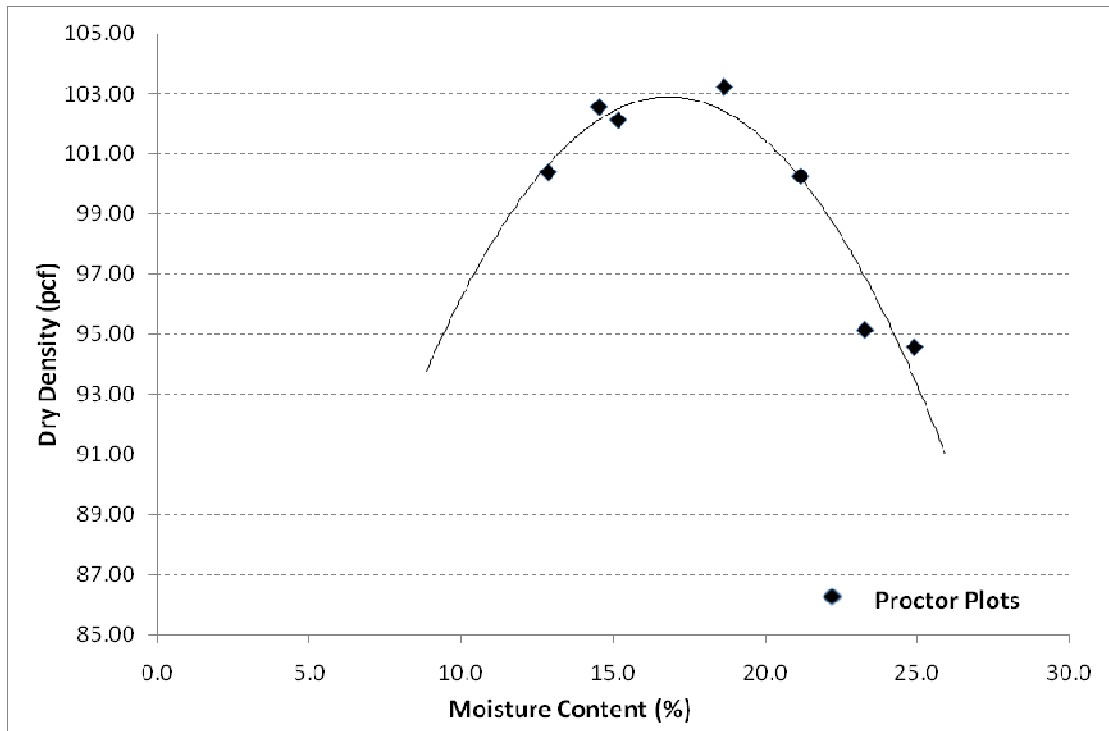
Figure 3.15 Standard Proctor Compaction Curve of Layer 2
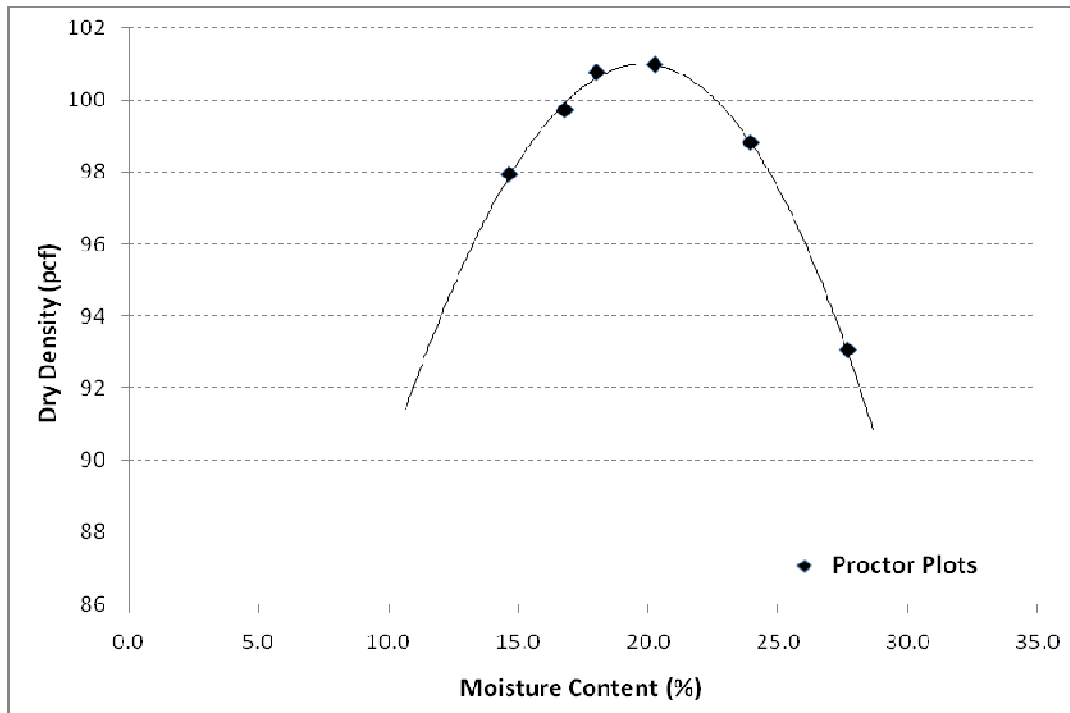
Figure 3.16 Standard Proctor Compaction Curve of Layer 3

Table 3.3 Standard Proctor Compaction Test Results

		Layer 2 1.0 - 3.0 ft (0.3 – 0.9 m)	Layer 3 3.0 - 5.0 ft (0.9 – 1.5 m)
	Wet OMC	22.80	26.05
Moisture Content (%)	OMC	16.80	19.80
	Dry OMC	10.91	13.02
	Wet OMC	97.76	95.95
Dry Density (pcf)	OMC	102.90	101.0
	Dry OMC	97.76	95.95

Note: OMC – Optimum Moisture Content in %

From Table 3.3, both second and third soil layers exhibit high dry density values equal to 102.9 and 101.0 pcf, respectively. It is noted that all three compaction moisture contents conditions, wet of OMC, OMC and dry of OMC, are used as reference moisture contents for the

69

engineering tests performed in this research. Soils in the field undergo moisture content fluctuations during the seasonal changes and hence it is important to determine the properties of soils over a wider range of moisture contents expected in the field. Such properties will be needed for numerical modeling of the field load tests on drilled shafts as a part of the analysis task.

3.4.3 Three-dimensional (3-D) Free Swell Test Results

In this research, soil specimens were prepared at three different moisture content conditions, dry of optimum, optimum and wet of optimum moisture content conditions as well as at field moisture content condition (Figure 3.17). The 3D swell test results can be seen in Figures 3.18 to 3.23 and in Table 3.4.

Figure 3.17 Three Dimensional Swell Test of Dry OMC, OMC and Wet OMC Conditions
(Left to Right)
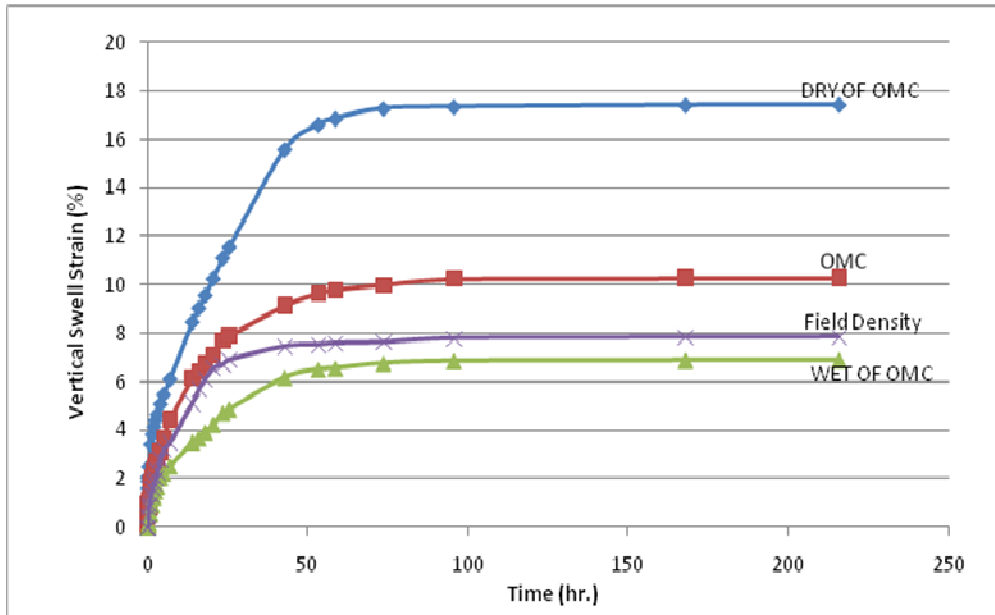
Figure 3.18 Vertical Swell Strain Results for Soil Layer 2 at Three Different Moisture Contents and Field Density Conditions
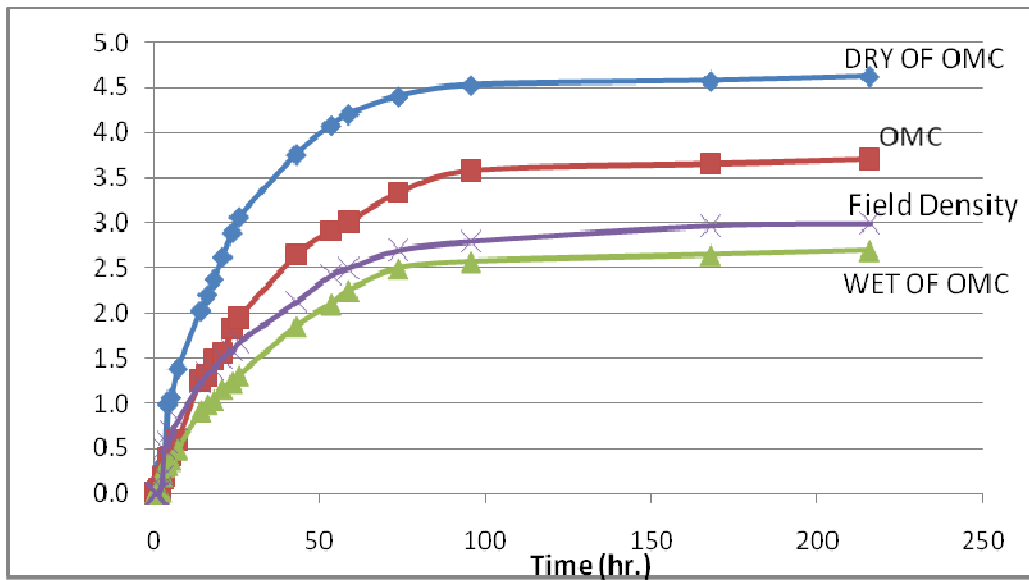
Figure 3.19 Radial Swell Strain Results for Soil Layer 2 at Three Different Moisture Contents and Field Density Conditions

71
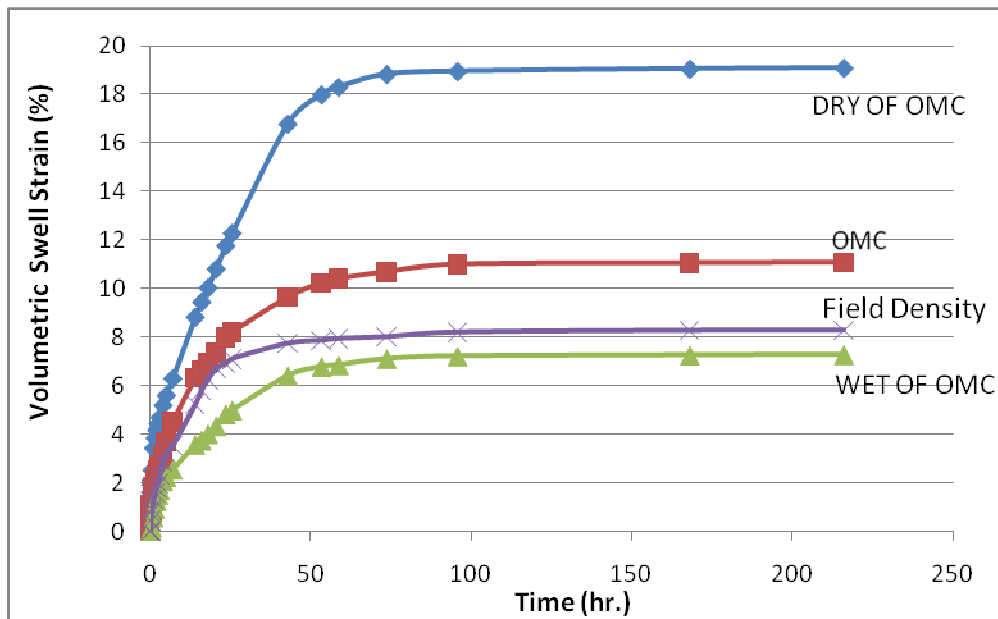
Figure 3.20 Volumetric Swell Strain Results for Soil Layer 2 at Three Different Moisture Contents and Field Density Conditions
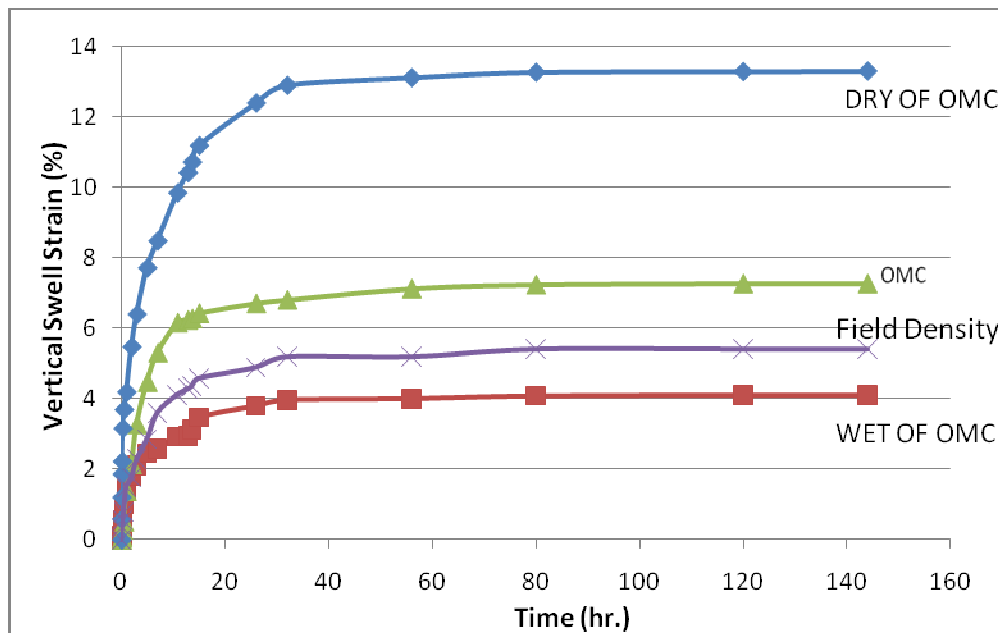
Figure 3.21 Vertical Swell Strain Results for Soil Layer 3 at Three Different Moisture and Field Density Conditions
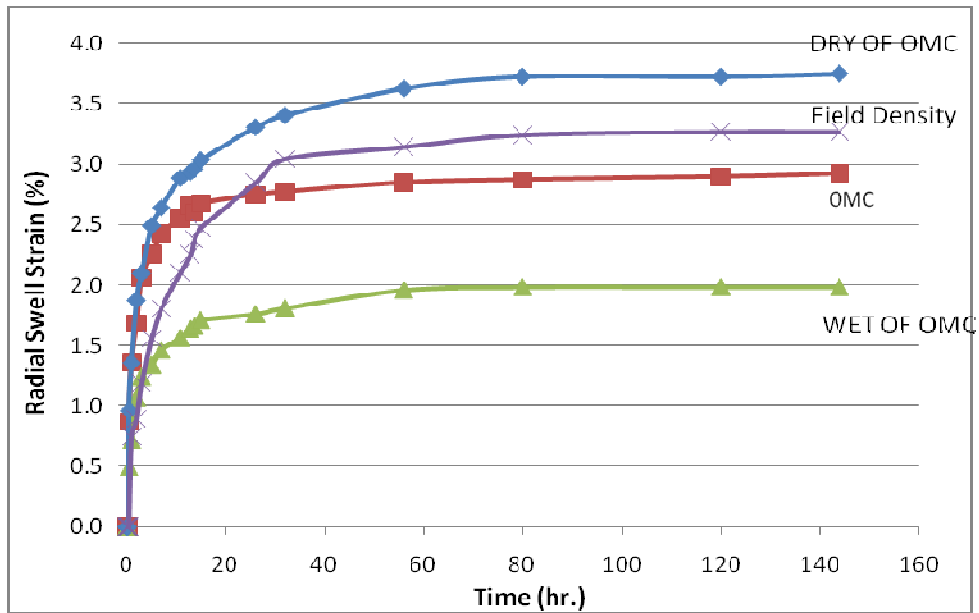
Figure 3.22 Radial Swell Strain Results for Soil Layer 3 at Three Different Moisture Contents and Field Density Conditions
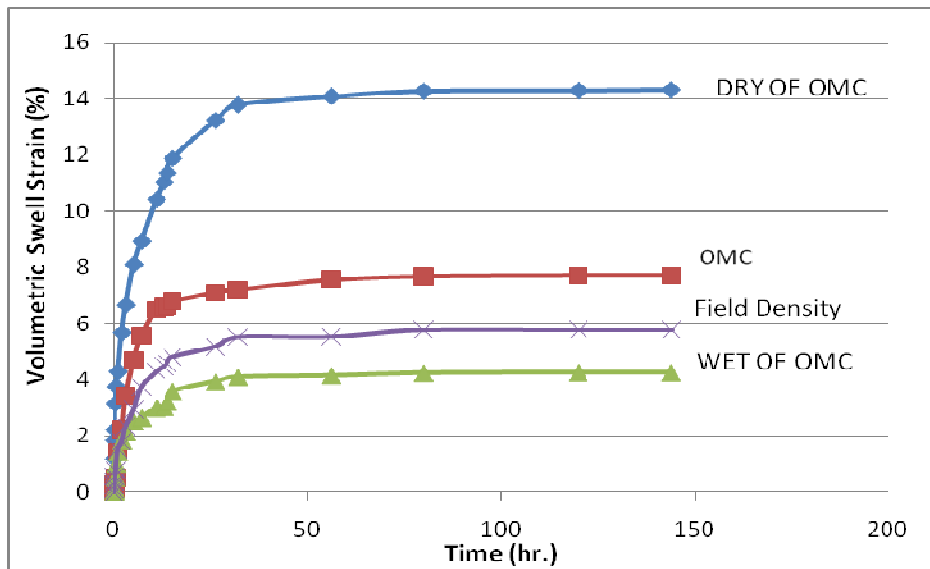
Figure 3.23 Volumetric Swell Strain Results for Soil Layer 3 at Three Different Moisture Contents and Field Density Conditions

Table 3.4 Three-Dimensional Volumetric Swell Strain Test Results

Moisture Condition	Swell Strain (%)	
	Soil Layer 2 1.0 – 3.0 ft (0.9 - 1.5 m)	Soil Layer 3 3.0 – 5.0 ft (1.5 - 3.0 m)
95 % Dry of OMC		
Vertical	17.44	13.30
Radial	4.63	3.73
Volumetric	19.09	14.32
OMC		
Vertical	10.29	7.28
Radial	3.71	2.87
Volumetric	11.07	7.71
95 % Dry of OMC		
Vertical	6.90	4.10
Radial	2.69	1.98
Volumetric	7.28	4.26
Field Density		
Vertical	7.83	7.28
Radial	3.00	3.24
Volumetric	8.28	5.77

Based on these results and those shown in Table 3.4 and 3.1, it can be concluded that both second and third layers have the highest swelling potential. Layer 2 soil sampled from 1.0 and 3.0 ft (0.9 - 1.5 m) depth interval has a volumetric swell strain value larger than 10% at the OMC condition and this value indicates a high degree of expansion potential as per the problematic volumetric swell characterizations mentioned by Chen (1988). In addition, the soils encountered between 3.0 and 5.0 ft (1.5 to 3.0 m) depth interval (i.e. Layer 3) exhibited a plasticity index (PI) value of 28, a linear shrinkage strain of 8.4%, and a volumetric swell strain of 7.7%. Again, these values indicate that this soil layer is a problematic expansive soil layer as per the soil characterizations mentioned by Chen (1988).

3.4.4 Volumetric Shrinkage Strain Results

Test results are expressed in term of percent of volume shrinkage strain compared with the original volume. Volumetric shrinkage strain test is the new development test which provides a better result than linear shrinkage strain test since this test was evaluates on tests on a considerable volume of soil samples. These test results are shown in Table 3.5

Table 3.5 Volumetric Shrinkage Strain Results

Moisture Content Condition	Shrinkage Strain (%)	
	Soil Layer 2 1.0 – 3.0 ft (0.9 - 1.5 m)	Soil Layer 3 3.0 – 5.0 ft (1.5 - 3.0 m)
95 % Dry of OMC		
Vertical	1.93	1.34
Radial	1.70	1.19
Volumetric	5.24	3.68
OMC		
Vertical	3.01	1.87
Radial	1.97	1.73
Volumetric	6.79	5.22
95 % Wet of OMC		
Vertical	4.37	2.91
Radial	2.19	2.58
Volumetric	8.51	7.85

Overall, these test results indicate that the present soils undergo large volumetric shrinkage strains when subjected to drying. Such strains are expected to induce problematic soil conditions in the field during drought type situations.

3.4.5 Swell Pressure Test

This test was conducted to measure maximum swell pressures that soils exhibit in order to maintain original volume. Swell pressure test results are presented in terms of ksf (kilopounds per square foot) values. Table 3.6 presents the test results of two soils from layer 2 and 3 by controlling the density and moisture content same as field condition.

Table 3.6 Swell Pressure Test Results

Soil Sample	Swell Pressure, ksf (kPa)
Soil Layer 2 (1 - 3 ft.)	1.28 (61.2)
Soil Layer 3 (3- 5 ft.)	0.49 (23.3)

As expected, the swelling pressures of Layer 2 are higher than those of Layer 3. This is in agreement with the Plasticity Index of these clays. Overall, the swell pressure values measured for Layers 2 and 3 are considerable to potentially pose an uplift problem in the field.

3.4.6 Suction Measurement by Pressure Plate and Filter Paper Method

The combined test results from the Pressure Plate and Filter Paper methods are presented in the form of SWCCs as shown in Figures 3.24 - 3.28 for all five soils.
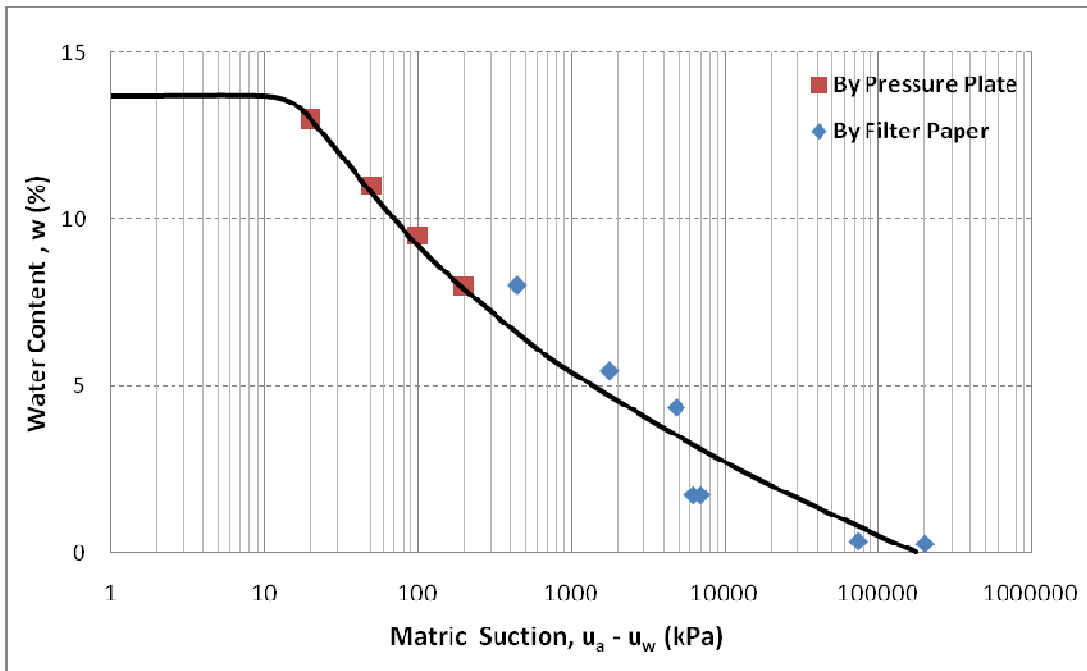
Figure 3.24 SWCC for Soil in Layer 1
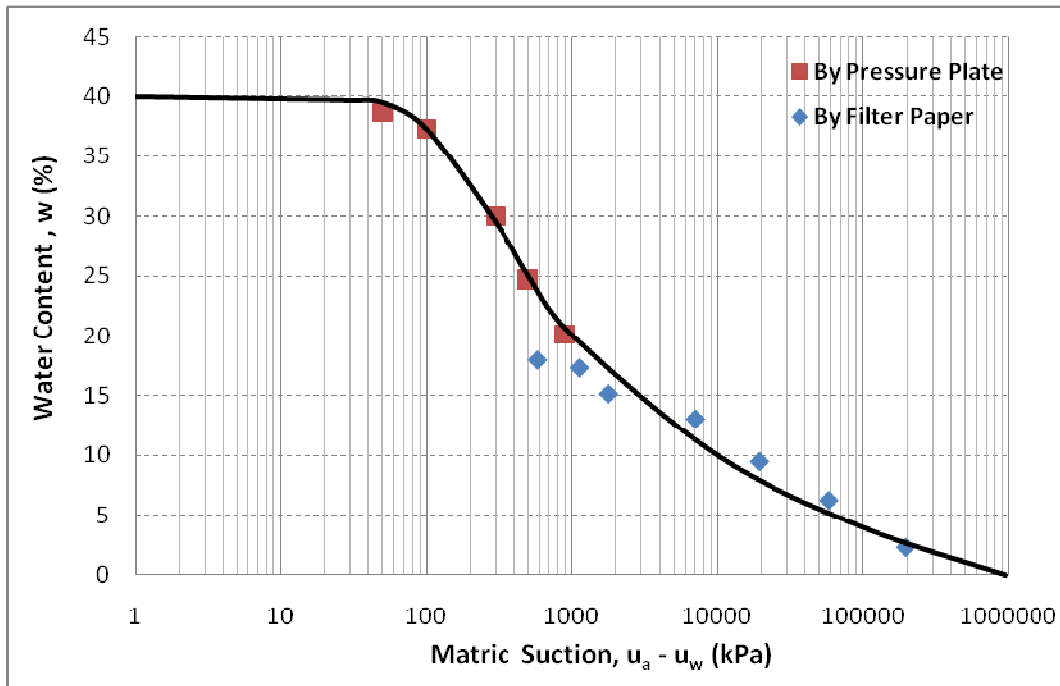
Figure 3.25 SWCC for Soil in Layer 2
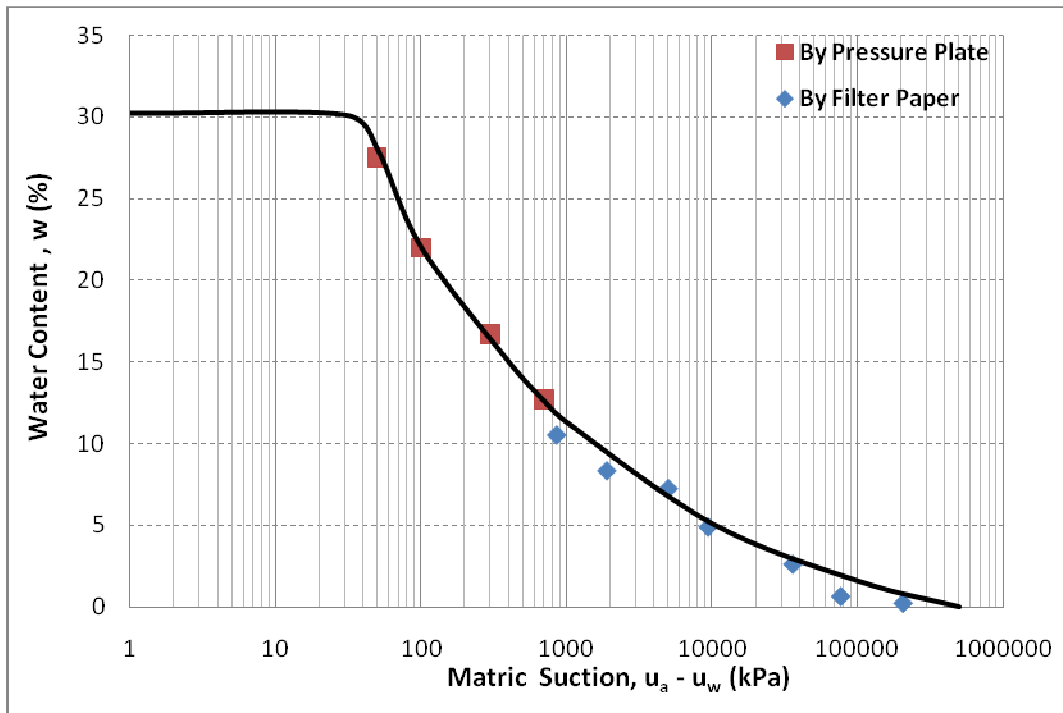
Figure 3.26 SWCC for Soil in Layer 3
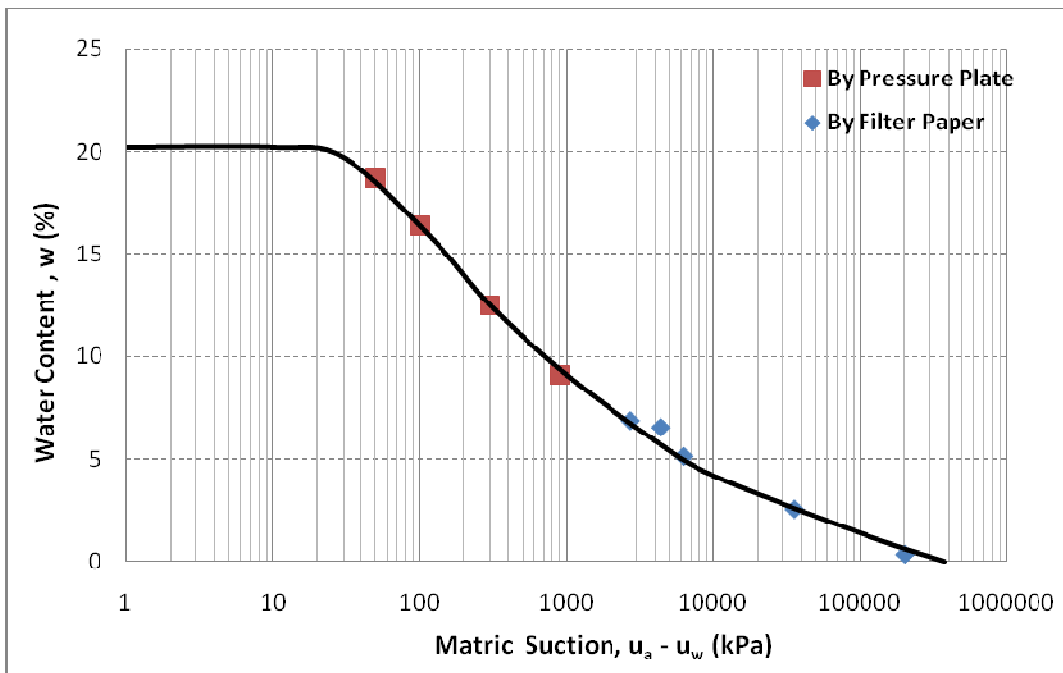
Figure 3.27 SWCC for Soil in Layer 4

78
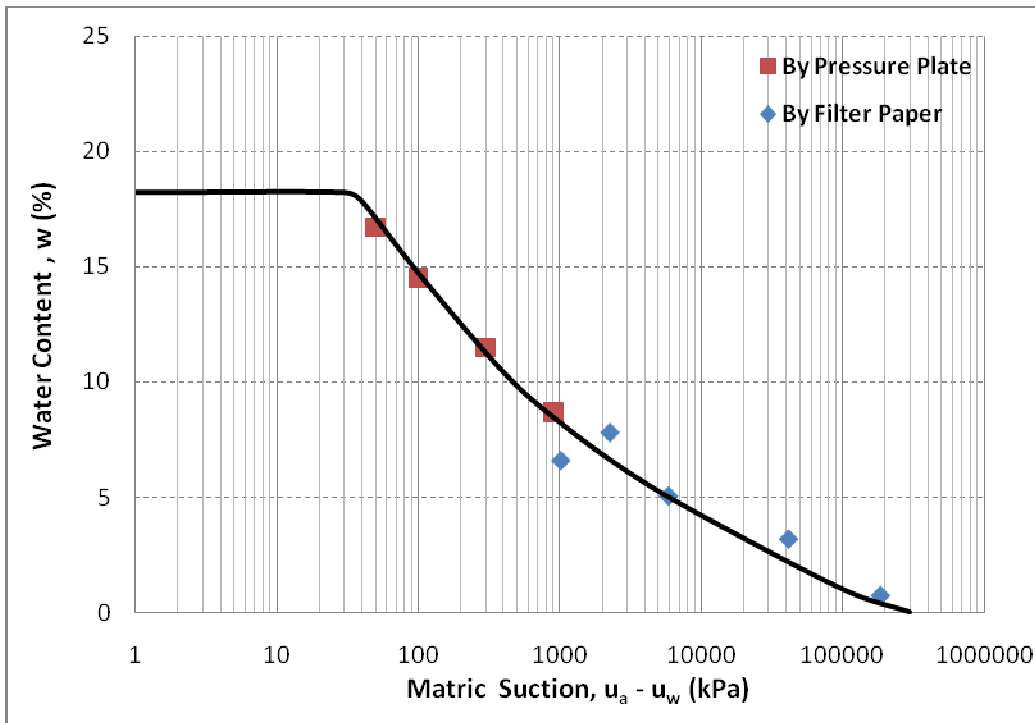
Figure 3.28 SWCC for Soil in Layer 5

SWCCs of all five types of soils exhibited similar shapes. The only noticeable difference is the saturated moisture content (at zero suction) between CL and CH types from layers 3, 4, and 5 versus layer 2. CL soils have saturated moisture contents much lower than the CH soil. This lower value indicates less ability to hold up water or moisture, which means that these soils do not undergo large swelling when hydrated.

3.4.7 Shear Strength Parameters (Direct Shear and Unconsolidated-Undrained Triaxial Tests)

From all five soil layers, the first soil layer type is a silty sand. Only direct shear strength tests were performed on this soil. Test results of this soil are presented in Figures 3.29 and 3.30. From the results, the friction angle of this sand is around 26.2 degree. For soils from layers 2 to 5, unconsolidated-undrained tests (UU) were conducted. Tests were conducted on soils at both unsaturated and saturated conditions. These results are presented in sections 3.4.7.1 and 3.4.7.2 and summary of these results is shown in Table 3.7 and 3.8 for unsaturated and saturated conditions, respectively.

79
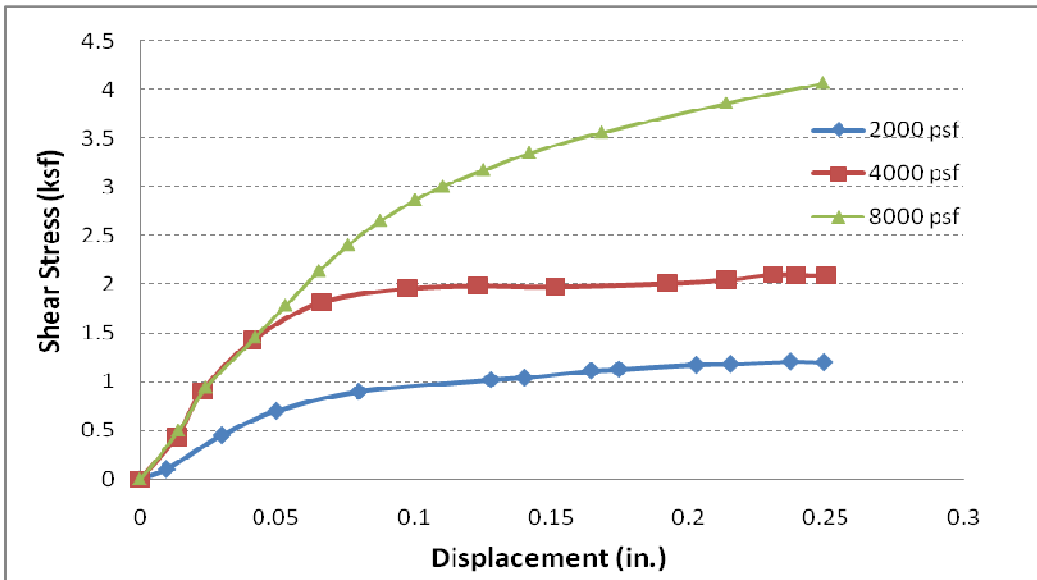
Figure 3.29 Shear Stress versus Horizontal Displacement for the Silty Sand from 1st layer
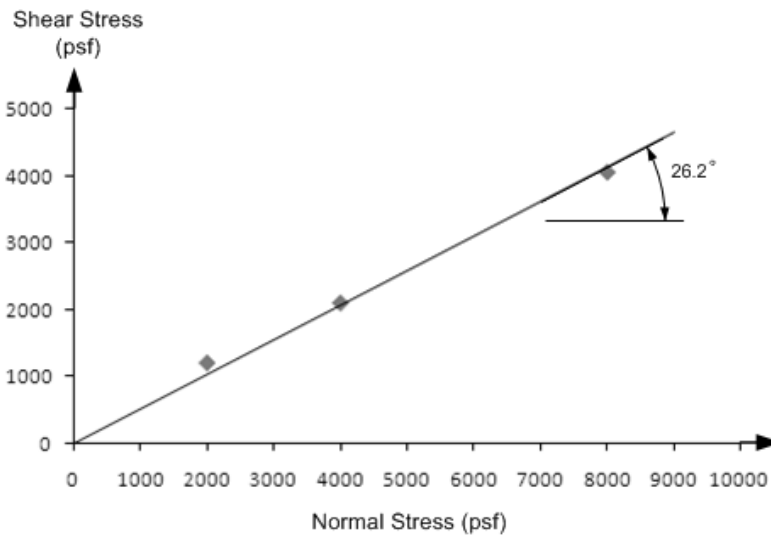
Figure 3.30 Shear Strength versus Effective Normal Stress for the Silty Sand

3.4.7.1 Unsaturated Condition Test Results

Table 3.7 summarizes the shear strength test results from the Direct Shear and Unconsolidated-Undrained Triaxial tests conducted on soils prepared at unsaturated soil conditions. Test results are expressed in terms of psi (pounds per square inch) for cohesion and degrees for internal friction angle (°). Figures 3.31 to 3.38 show both stress-strain plots and Mohr circles depicting shear strength parameters.
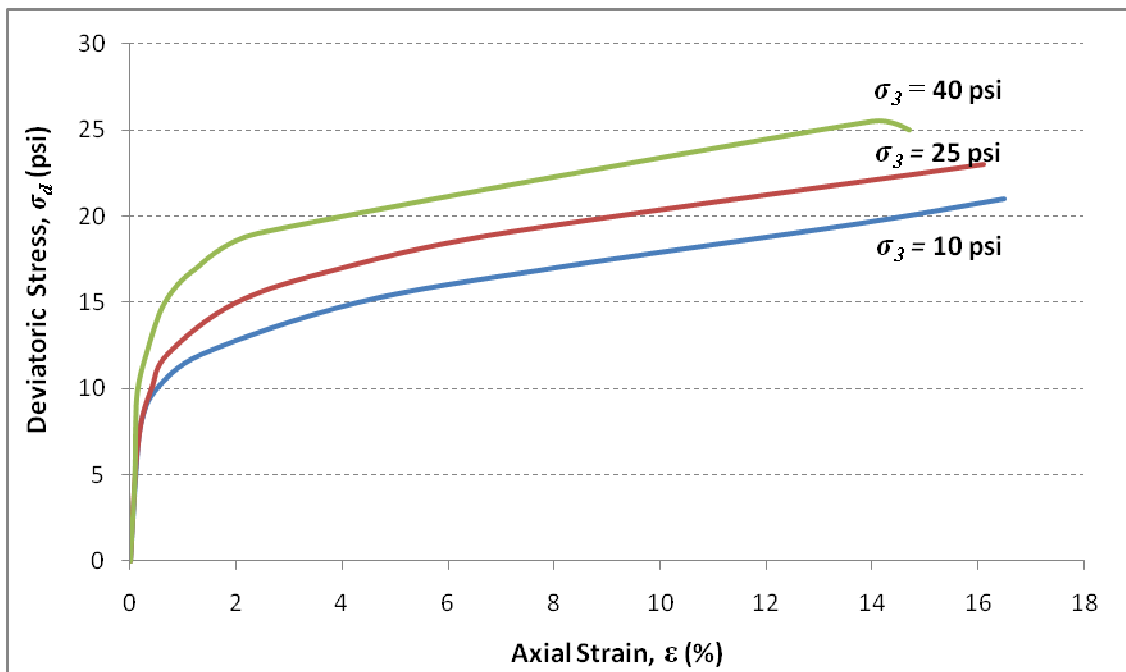
Figure 3.31 Triaxial Test Plot for 10, 25, and 40 psi Confining Pressure of Soil Layer 2
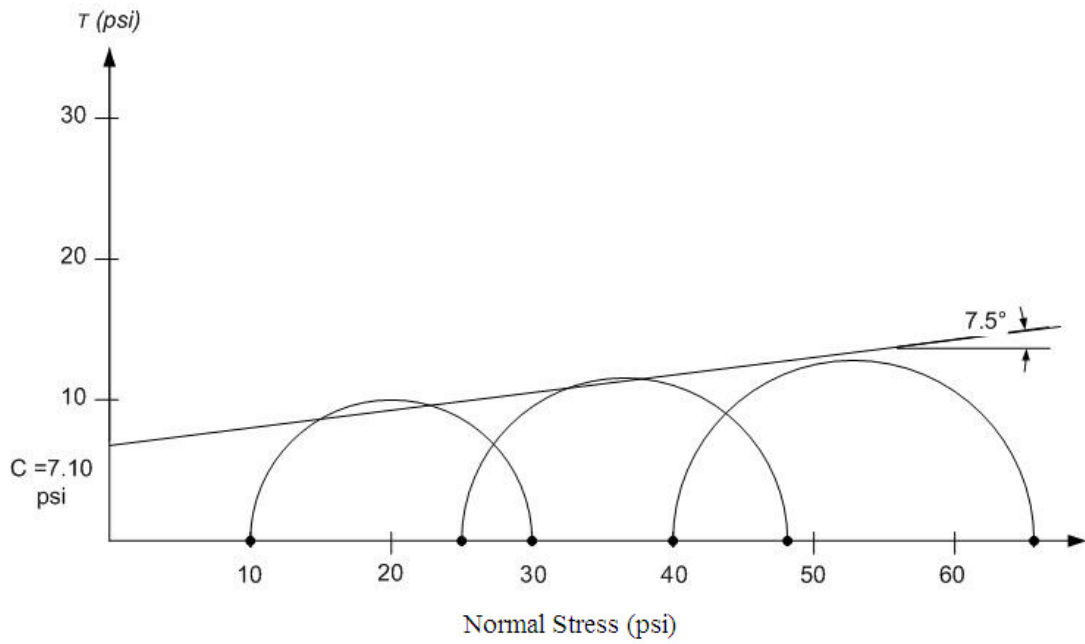
Figure 3.32 Mohr's Circle at Failure for 10, 25, and 40 psi Confining Pressure of Soil Layer 2
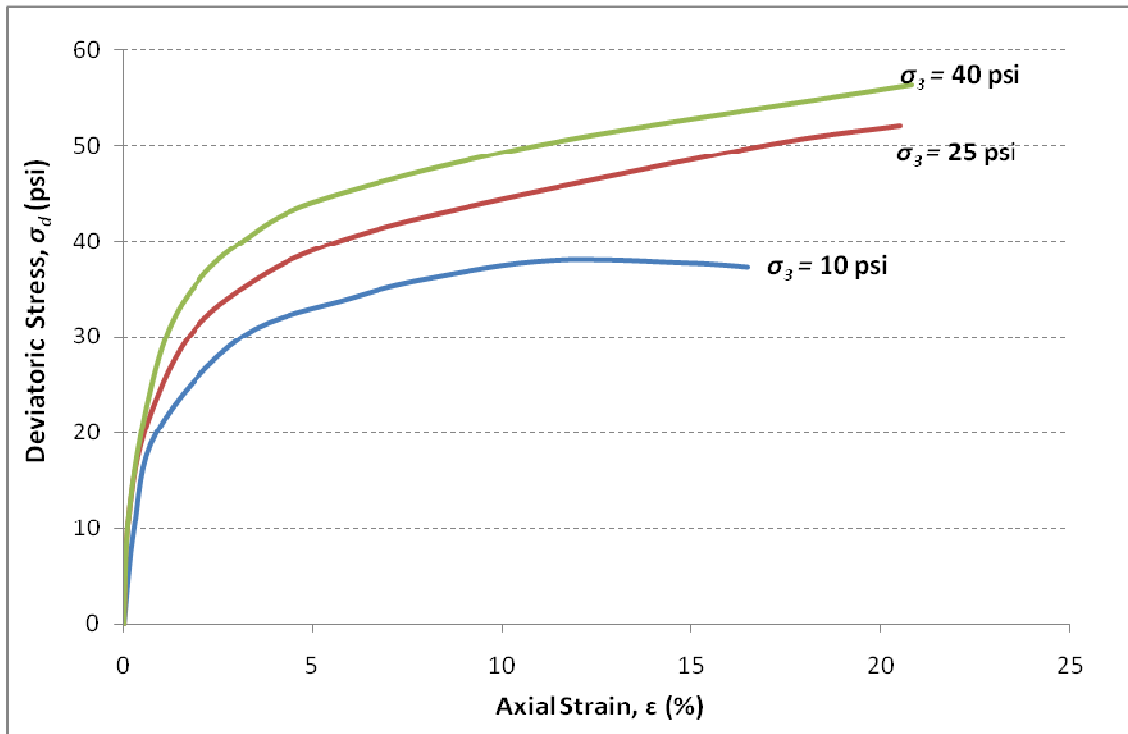
Figure 3.33 Triaxial Test Plot for 10, 25, and 40 psi Confining Pressure of Soil Layer 3
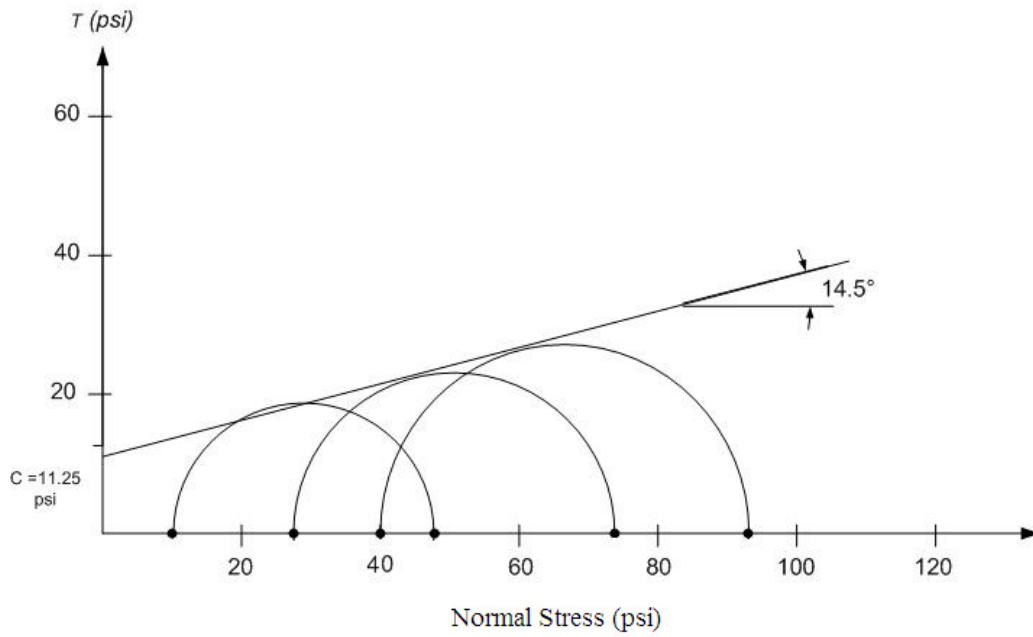
Figure 3.34 Mohr's Circle at Failure for 10, 25, and 40 psi Confining Pressure of Soil Layer 3
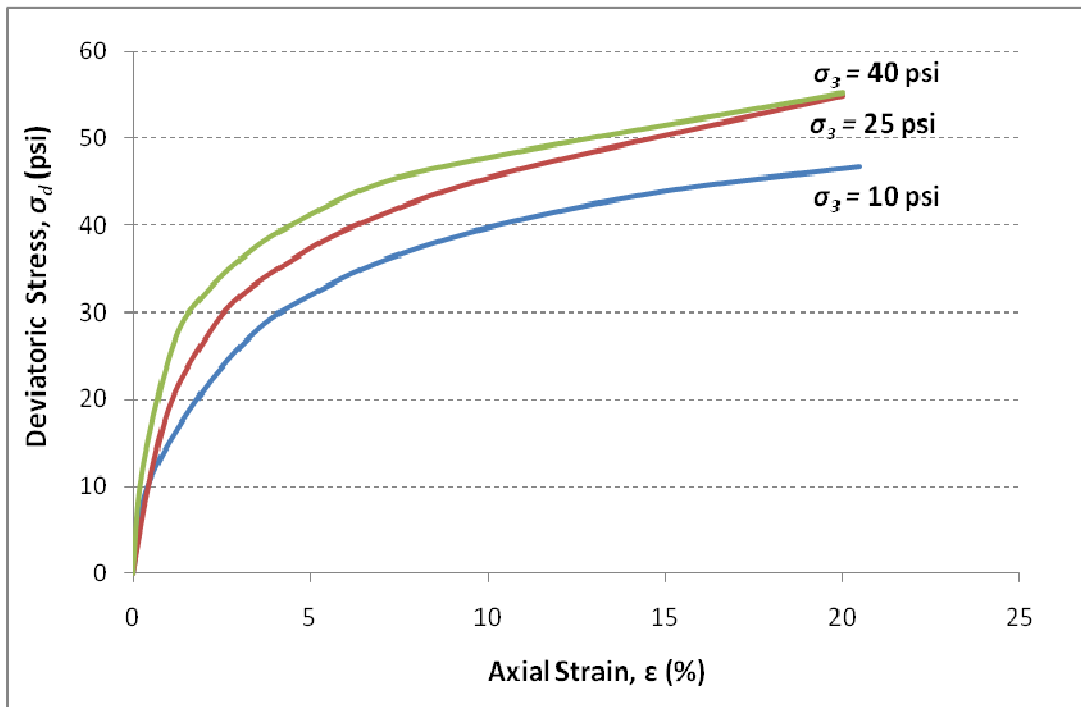
Figure 3.35 Triaxial Test Plot for 10, 25, and 40 psi Confining Pressure of Soil Layer 4
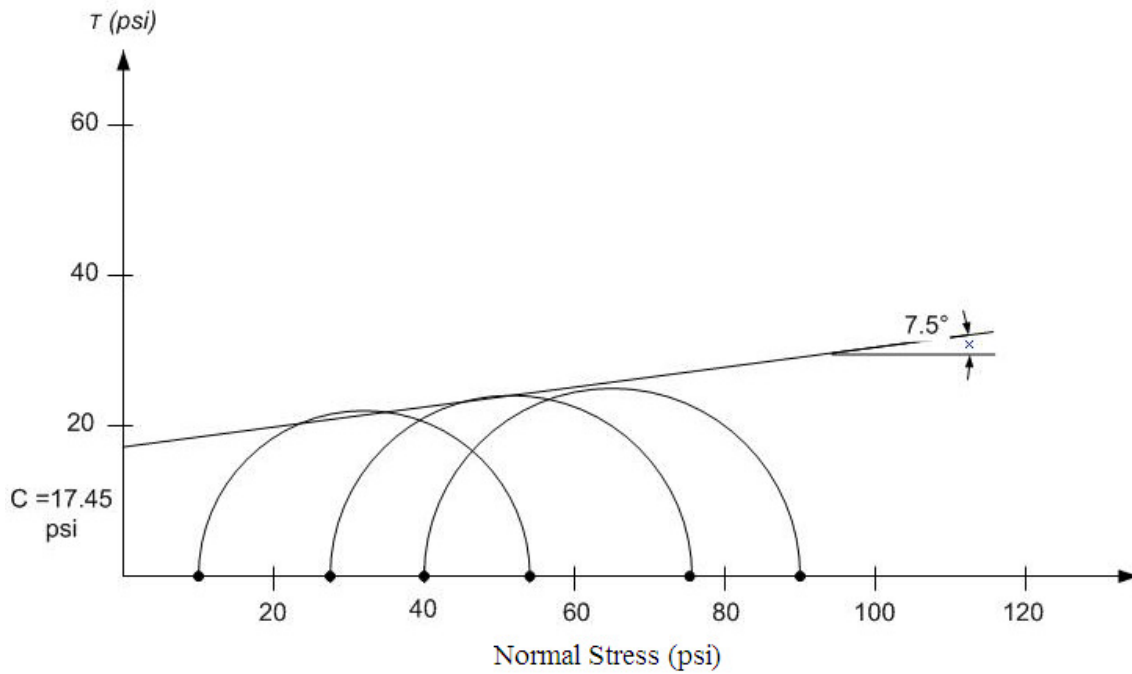
Figure 3.36 Mohr's Circle at Failure for 10, 25, and 40 psi Confining Pressure of Soil Layer 4
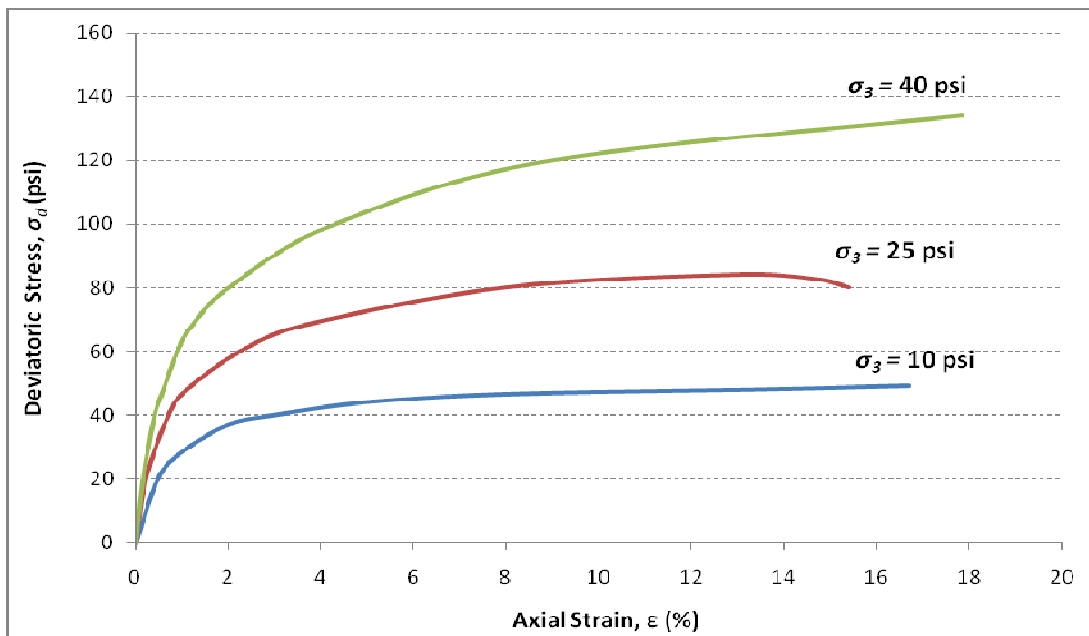
Figure 3.37 Triaxial Test Plot for 10, 25, and 40 psi Confining Pressure of Soil Layer 5
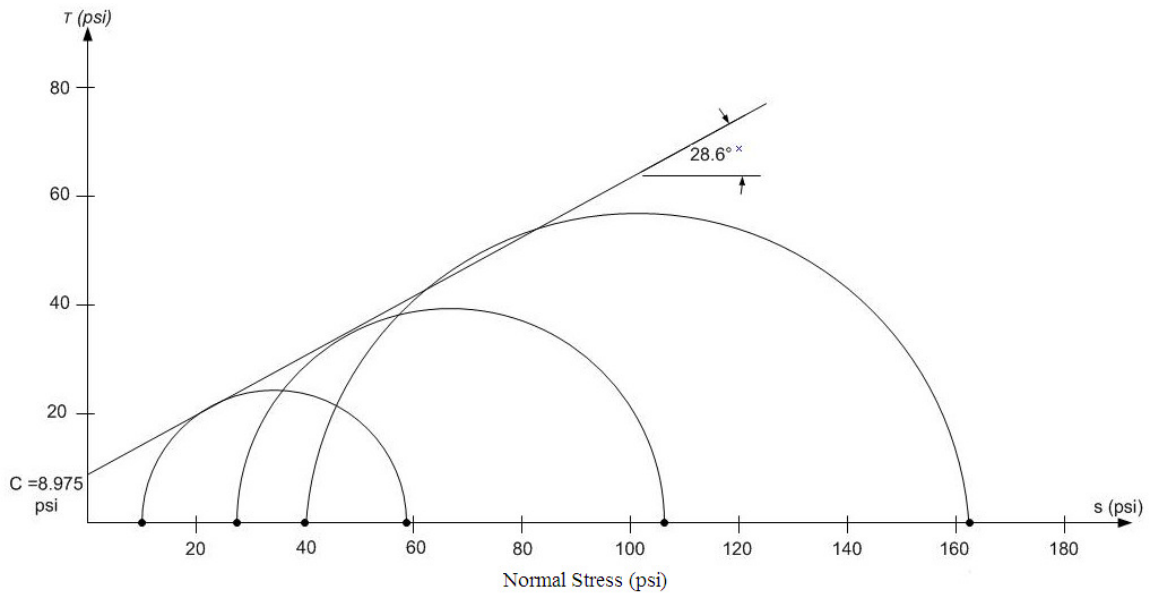
Figure 3.38 Mohr's Circle at Failure for 10, 25, and 40 psi Confining Pressure of Soil Layer 5

Table 3.7 Direct Shear and Unconsolidated-Undrained Triaxial Test Results for Unsaturated Cases

Depth (ft)	Total Density (pcf)	Moisture Content (%)	Cohesion, c (psi)	Friction, ϕ, (°)
0 – 1.0 (DS)	110.38	18.7	0	26.2
1.0 – 3.0 (TX)	119.54	21.2	7.10	7.5
3.0 – 5.0 (TX)	124.57	16.9	11.25	14.5
5.0 – 10.0 (TX)	137.87	15.7	17.45	7.5
> 10.0 (TX)	125.27	12.9	8.98	28.6

Note: DS – Direct Shear; TX- Triaxial

3.4.7.2 Saturated Soil Condition Test Results

Table 3.8 summarizes the shear strength test results from the Direct Shear and Unconsolidated-Undrained Triaxial tests conducted on soils prepared at saturated soil conditions. Test results are expressed in terms of psi (pounds per square inch) for cohesion and

degrees for which internal friction angle is zero since soils are saturated and undrained. Figures 3.39 to 3.46 show both stress-strain plots and Mohr circles depicting shear strength parameters.
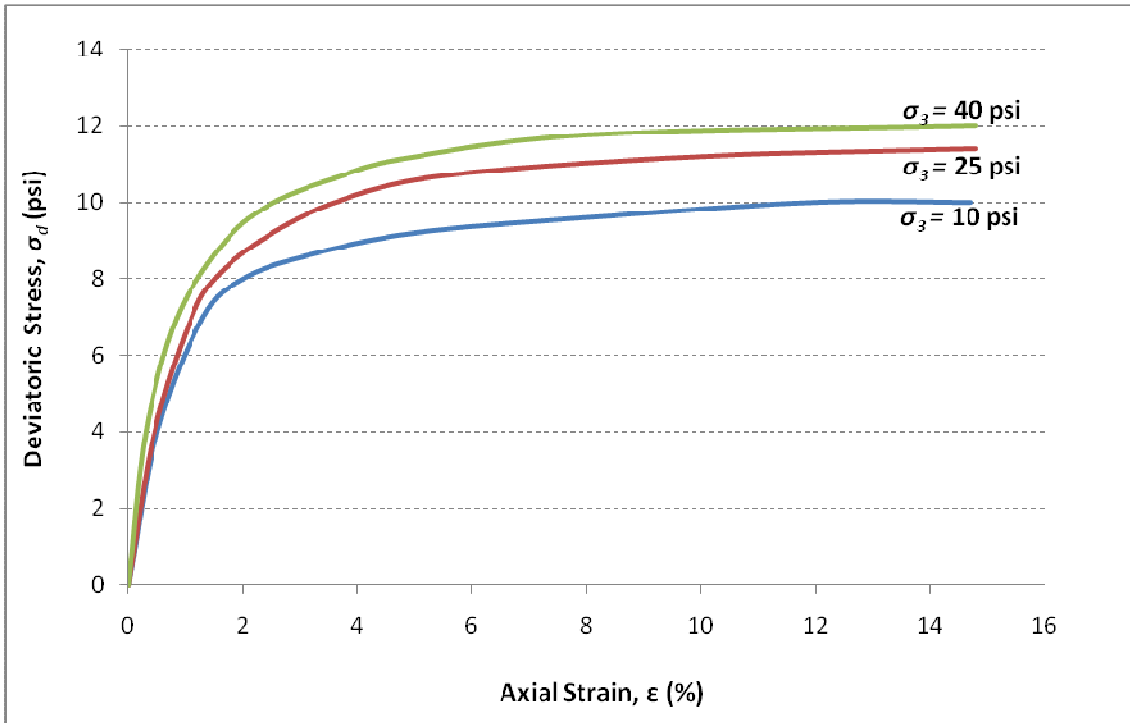
Figure 3.39 Triaxial Test Plot for 10, 25, and 40 psi Confining Pressure of Soil Layer 2 in Saturated Case
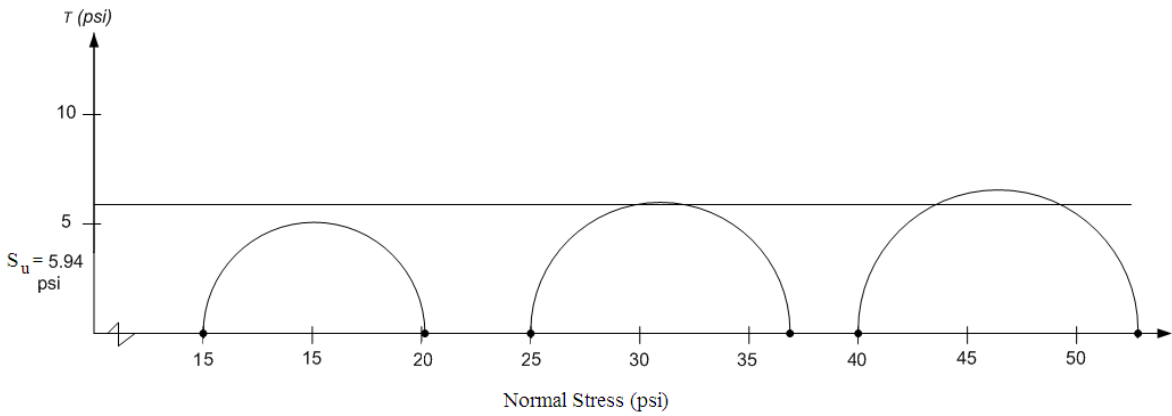
Figure 3.40 Mohr's circle at Failure for 10, 25, and 40 psi Confining Pressure of Soil Layer 2 in Saturated Case
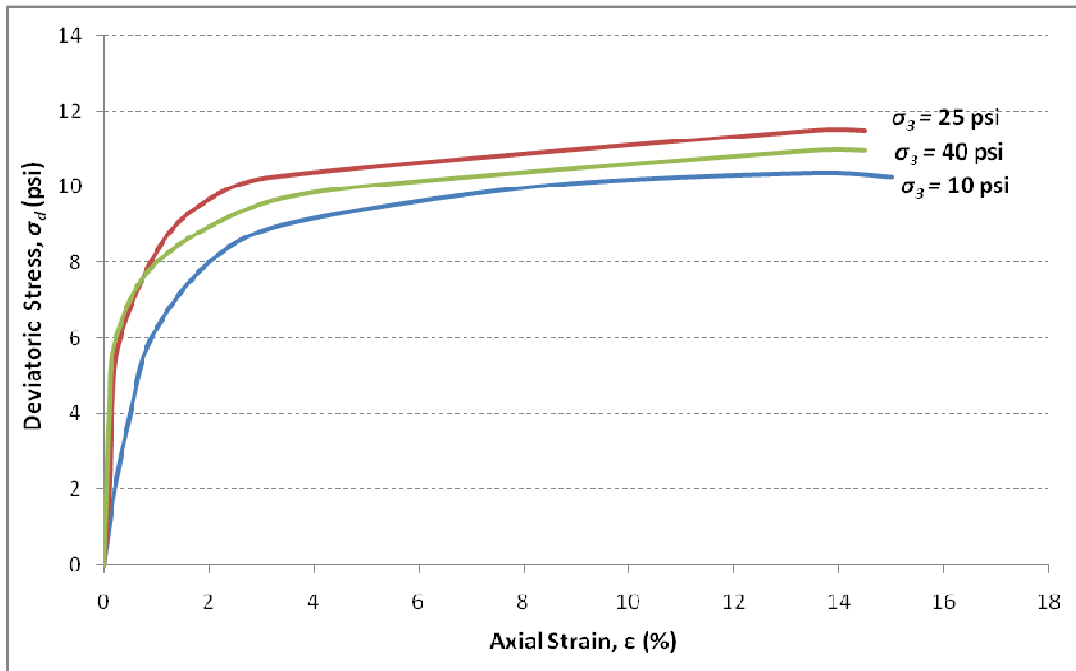
Figure 3.41 Triaxial Test Plot for 10, 25, and 40 psi Confining Pressure of Soil Layer 3 in Saturated Case
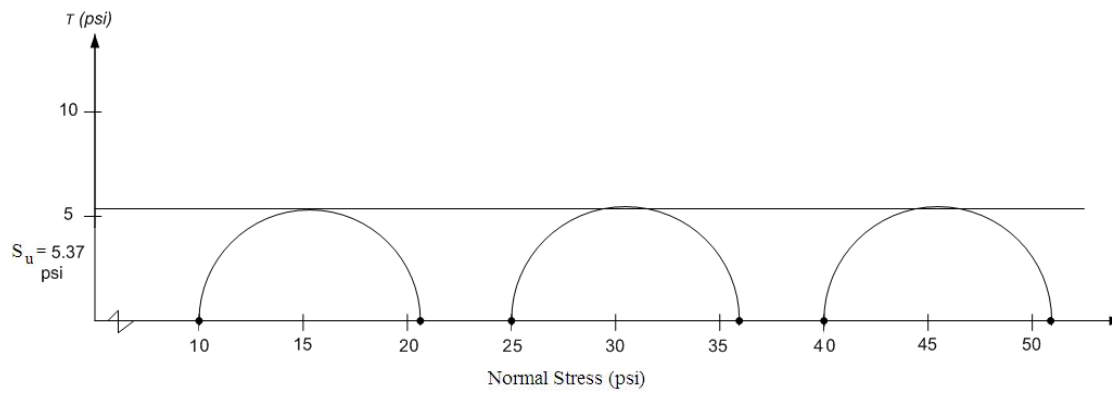
Figure 3.42 Mohr's Circle at Failure for 10, 25, and 40 psi Confining Pressures of Soil Layer 3 in Saturated Case
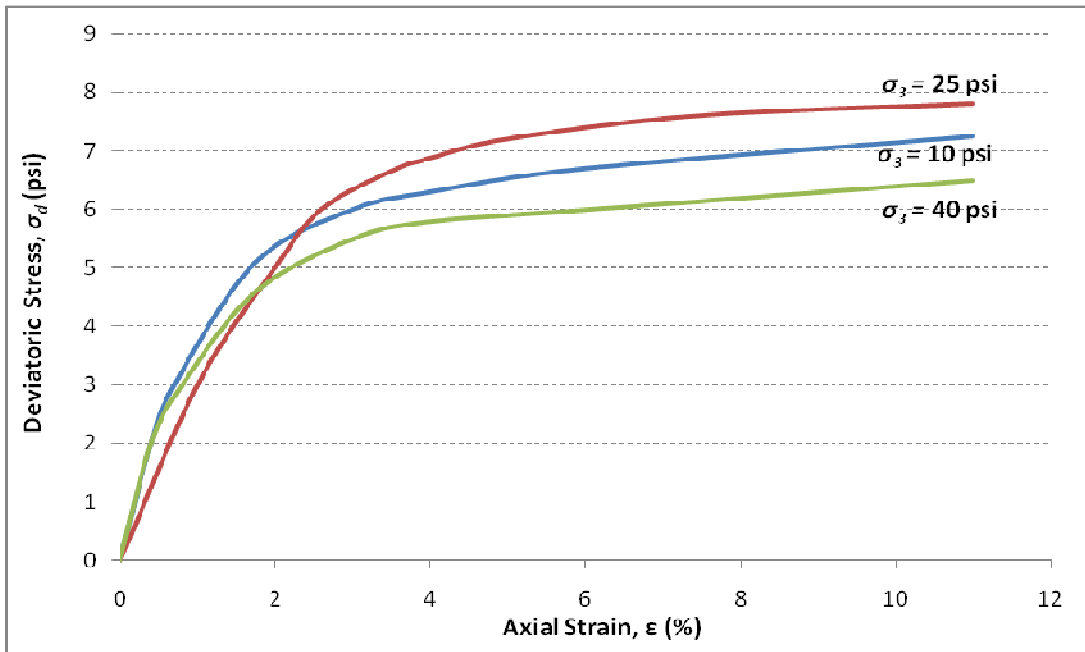
Figure 3.43 Triaxial Test Plot for 10, 25, and 40 psi Confining Pressure of Soil Layer 4 in Saturated Case
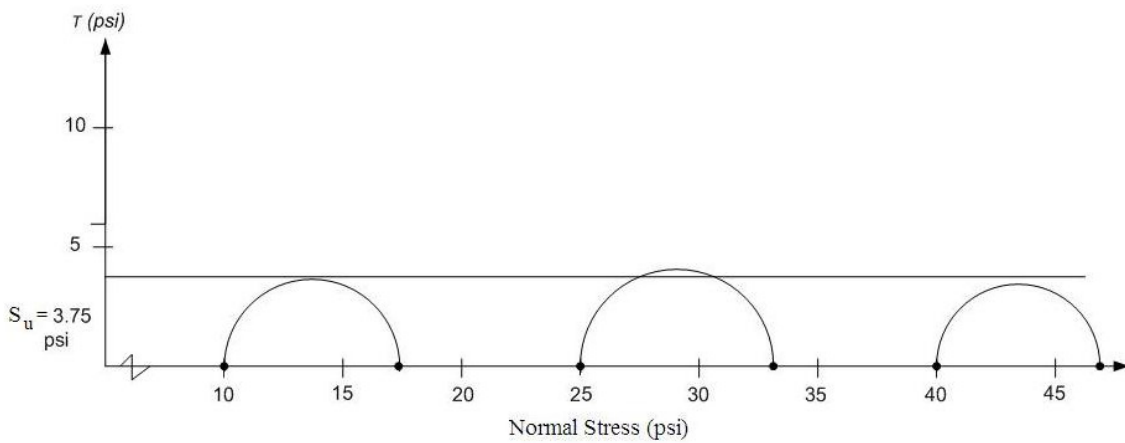
Figure 3.44 Mohr's Circle at Failure for 10, 25, and 40 psi Confining Pressure of Soil Layer 4 in Saturated Case

88
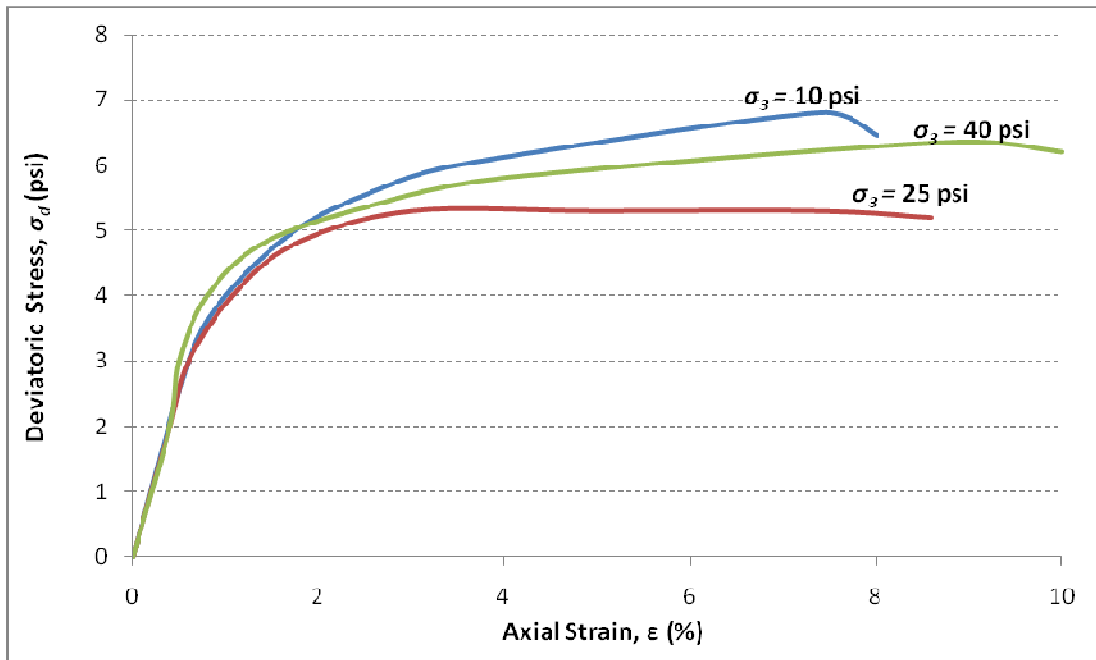
Figure 3.45 Triaxial Test Plot for 10, 25, and 40 psi Confining Pressures of Soil Layer 5 in Saturated Case
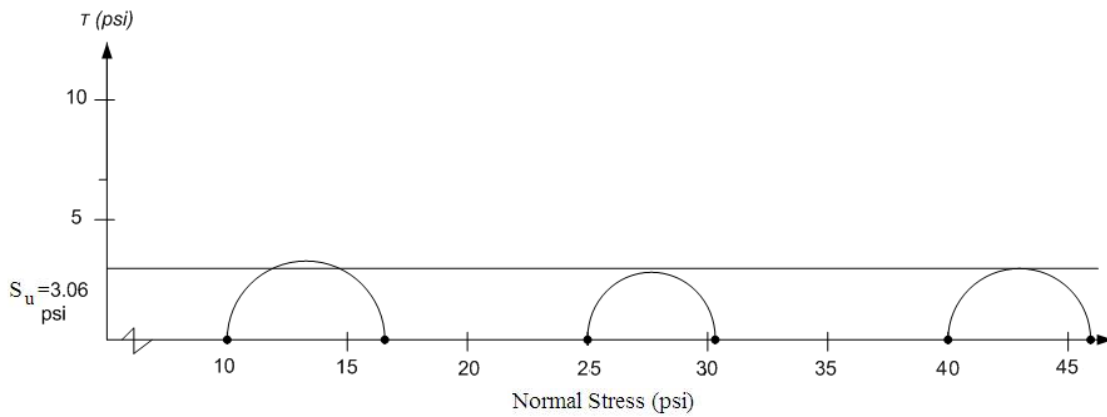
Figure 3.46 Mohr's Circle at Failure for 10, 25, and 40 psi Confining Pressure of Soil Layer 5 in Saturated Case

89

Table 3.8 Unconsolidated-Undrained Triaxial Test Results for Saturated Case

Depth (ft)	Water Content, w (%) at complete saturation	Total Density (pcf)	Undrained Shear Strength, S_u (psi)
1.0 – 3.0	32.3	119.54	5.97
3.0 – 5.0	26.3	124.57	5.37
5.0 – 10.0	19.2	137.87	3.75
> 10.0	17.1	125.27	3.06

3.5 Summary

This chapter describes the test site details, soil sampling and laboratory testing program. A summary of soil sampling details from the field site, laboratory methods and test results on site soils are also presented in this Chapter. The soils from second and third layers showed that they exhibit large volumetric swell strains more than 10% at OMC condition. These results are considered as a very high degree of soil expansion. UU triaxial tests were also performed to determine the shear strength properties of soils at both unsaturated and full saturated conditions. The next chapter describes construction of field load test setup and instrumentation details used in the load testing.

CHAPTER 4

DESIGN AND CONSTRUCTION OF DRILLED SHAFTS

UNDER INCLINED LOAD TESTING

4.1 Introduction

This chapter presents the design of the reaction pier system to induce inclined load testing on the test shafts. Both design and construction details are presented. In addition, the instrument details used for inclined loading and capturing load-deformation responses are described.

4.2 Design of Field Test Setup

Two types of field load testing designs are originally considered and formulated here for simulating the inclined load testing on the drilled shafts. These are termed here as 'push' and 'pull' type loading test setups and schematics are shown in Figures 4.1 a and b, with one designed to apply load behind the test shaft and the other designed to apply the load as a tensile or pull load in front of the drilled shaft. Loading mechanism in both setups is at an oblique angle similar to the angles at which the cables are connected to the drilled shaft. Both approaches have advantages and disadvantages; the 'push' type setup does not require spacing requirements between the reaction and the test shafts whereas the pull type setup must be designed such that the reaction shaft does not move or yield during tensile loading on the test shafts.
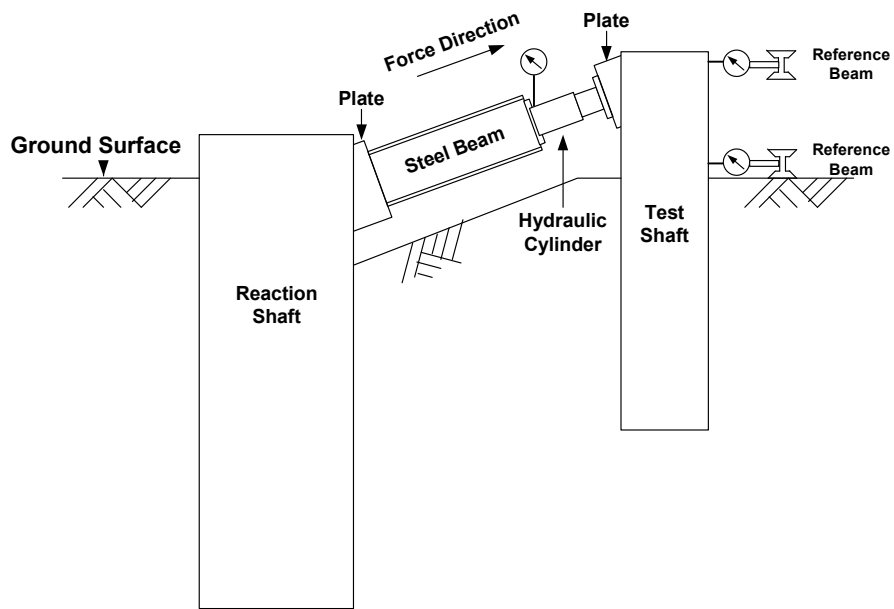
(a)
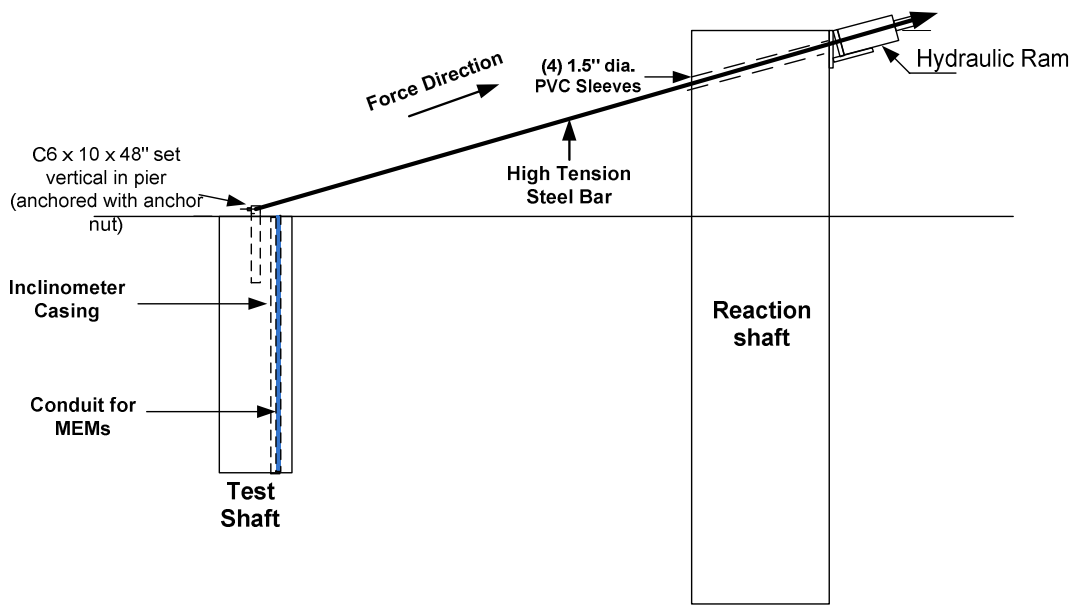
(b)

Figure 4.1 Schematic Diagrams of the Inclined Load Testing System: a) Cross Section View of Inclined 'Push' Setup and b) Cross Section View of 'Pull' System of the Reaction and Test Shafts

One major disadvantage of the push setup requires excavation of the soil around the reaction shaft and it also requires projection of the test shaft above the ground in order to accommodate the same cable connection mechanism. The projection of the test shaft above the ground will influence the uplift forces due to an increase in self weight of the foundation from the part above the ground. As a result, the push type test setup was discarded and the pull type load test was considered here. The design plan layout, as shown in Figure 4.2, was designed to have the three test sets completely separated from each other to eliminate any chance of influence from any of the tests performed at an adjoining set.
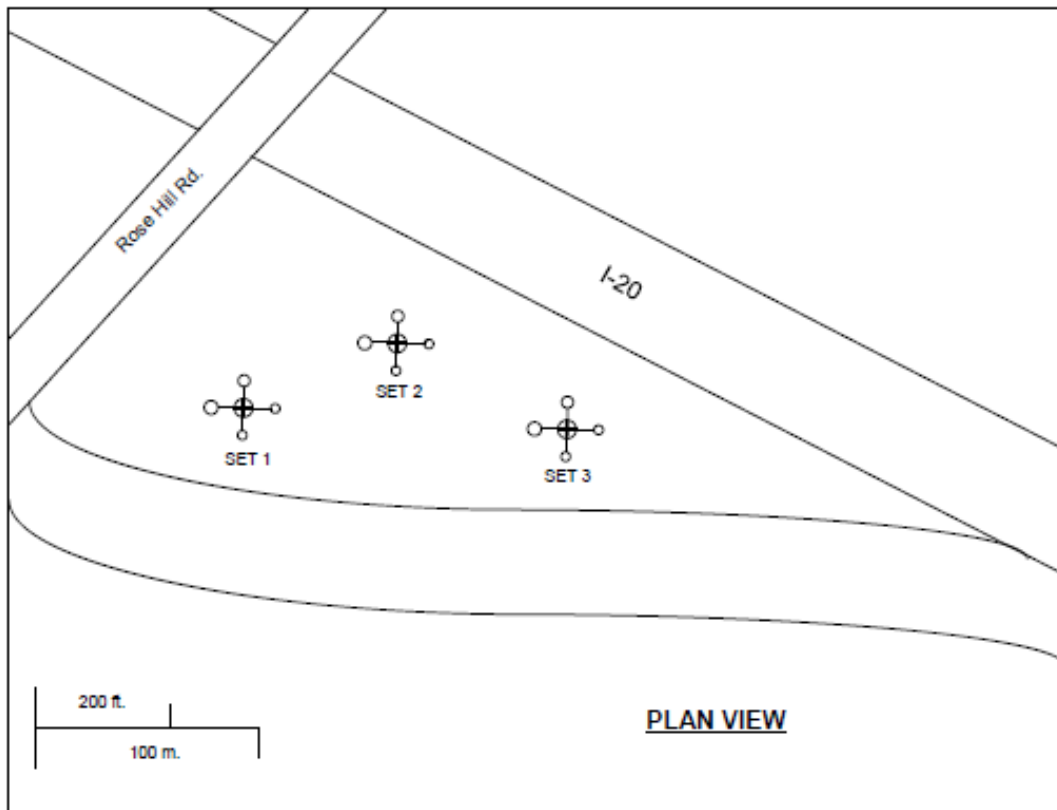
Figure 4.2 Plan View of Test Setups with Three Reaction Piers and Twelve Test Piers

One full test set system was comprised of one reaction shaft and four test shafts with the clear distance between the reaction shaft and the test shafts at 20 ft (6.1 m) based on ASTM 3966. The angle of force acting toward the test shafts was set at 16.1 degrees to copy

93

the angle of the currently installed cable barrier systems. These tests represent one of the fewest number of Inclined Load field tests performed in the USA based upon the Literature Review.

4.2.1 Design of Test and Reaction Drilled Shafts

Originally, the dimensions of the drilled shafts that failed in the field were 2 ft (0.6 m) in diameter and 6 ft (1.8 m) depth. In order to determine the most effective size(s) of drilled shafts to be required in research plans for expansive soil environments, three different test shaft diameter sizes of 1 ft (0.3 m), 2 ft (0.6 m), and 3 ft (0.9 m), and three different lengths of 6 ft (1.8 m), 10 ft (3.0 m) and 14 ft (4.3 m) were designed. Additionally, the three reaction shafts were designed and the dimensions were 3 ft (0.9 m) and 4 ft (1.2 m) in diameters and 35 ft (10.7 m) long.

The reaction shafts were used as foundations to subject the tensile loads to the long high tensioned steel bar (Dywidag bar) which in turn simulates the tension mobilized in the three-cable barrier system on the test shaft. To reiterate, the angle of force acting toward the test shafts was set at 16.1 degrees by facilitating the bar at the same angle.

During the lateral load testing, the distance between the test shafts and the reaction shaft is an important parameter. Stress created in the soil around the reaction shaft during the testing can influence the results of the test shafts. A clear distance between each test shaft and the reaction shaft of 20 ft (6.1 m) was hence selected based on Test Method ASTM D 3966 - 90, 'Standard Test Method for Piles under Lateral Loads'. In this research, one of the important steps for this testing was to design each reaction shaft such that the loading sequence followed in the procedure would not influence test results of the test shafts.

The reaction drilled shaft must be rigid enough to resist significant movements during load testing, which in turn would mean that the reaction shafts have not affected the test shaft reactions. To check this, the L-PILE software analysis for probable deformation pattern under hypothetical loading conditions was attempted to compare the deformations in the drilled shafts.

Table 4.1 presents the predicted deflection results of all test shafts using the forces calculated from tension forces that may act on cable barrier systems in winter and summer conditions. The saturated soil conditions in winter scenario were used for the analysis. Based on the analyzed lateral displacements of all test shafts, the percent differences in surface lateral movements are determined and are included in Table 4.2.

Table 4.1 Predicted Lateral Deflection of Drilled Shafts at the Ground Surface

Shaft Number (Diameter x Length)	Deflection at ground surface (in.) (Winter Time)	Deflection at ground surface (in.) (Summer Time)
1 (1 ft x 6 ft)	N.A.	1.26
2 (1 ft x 10 ft)	1.03	0.30
3 (1 ft x 14 ft)	0.91	0.32
4 (2 ft x 6 ft)	N.A.	0.79
5 (2 ft x 10 ft)	0.51	0.15
6 (2 ft x 14 ft)	0.28	0.09
7 (3 ft x 6 ft)	N.A.	0.75
8 (3 ft x 14 ft)	0.22	0.06
Reaction Shafts (Diameter x Length)	Deflection at ground surface (in) (Winter Time)	Deflection at ground surface (in) (Summer Time)
3 ft x 35 ft depth	0.10	0.04
4 ft x 35 ft depth	0.05	0.02

Note: N.A. means the deflection of the pile head was high due to the computed deflection being larger than the allowable deflection limit.

From Table 4.1, it was concluded that the first reaction shaft, 3 ft (0.9 m) diameter and 35 ft (10.7 m) deep, can be used with the test shafts of 6 ft (1.8 m) depths. This becomes possible due to the high computed lateral deflections of the short test shafts when compared with small lateral deflection experienced by the reaction shaft. Hence, it was concluded that

while performing the lateral load tests, all the test shafts would not be influenced by the movements of the reaction shafts.

Table 4.2 Predicted Percent Differences in Lateral Movements of Reaction Shaft and Test Shaft

Shaft Number	Percent difference of lateral movement (%) in Winter		Percent difference of lateral movement (%) in Summer	
(Diameter x Depth)	Reaction Shaft 1	Reaction Shaft 2	Reaction Shaft 1	Reaction Shaft 2
1 (1 ft x 6 ft)	N.A.	N.A.	2.8	1.6
2 (1 ft x 10 ft)	9.3	5.1	11.7	6.5
3 (1 ft x 14 ft)	10.5	5.7	11.1	6.2
4 (2 ft x 6 ft)	N.A.	N.A.	4.5	2.5
5 (2 ft x 10 ft)	18.8	10.2	24.3	13.5
6 (2 ft x 14 ft)	33.6	18.3	39.1	21.7
7 (3 ft x 6 ft)	N.A.	N.A.	4.7	2.6
8 (3 ft x 14 ft)	44.0	24.0	56.3	31.3

Note: N.A. means the deflection of the pile head could not be analyzed due to the computed deflection being larger than the allowable deflection limit.

For the larger reaction shaft, 4 ft (1.2 m) diameter and 35 ft (10.7 m) deep, it was also concluded that the load tests could be conducted on test shafts of 10 ft (3.0 m) and 14 ft (4.3 m) depth. This is determined from the predicted percent differences in the lateral deflections which varied from a low of 5% to 24%, with the high value computed for the winter test condition. For the Test Shaft 8 (3 ft (0.9 m) x 14 ft (4.3 m)), the percent difference is slightly high for summer test conditions. Hence, load tests need to be interpreted by considering the influence of the reaction test set movements on the test results.

From the analyzed predictions above, test shafts in the winter condition have higher lateral deflections and bending moments than for the summer condition. Cable tensions in the

summer conditions are lower than the winter conditions and the uplift force in the summer season (dry season) are also low resulting in less deflection values than predicted for the winter conditions.

The field load test system included a means of applying the inclined load plus measuring the lateral load and deflections of the drilled shafts. The overall system is presented in Figures 4.3 and 4.4 which show the schematics of plan and elevation views of the three test sets and how each one is different from the other two. The steel rebar reinforcement plans for the test and reaction shafts that were used are shown in Appendix A.
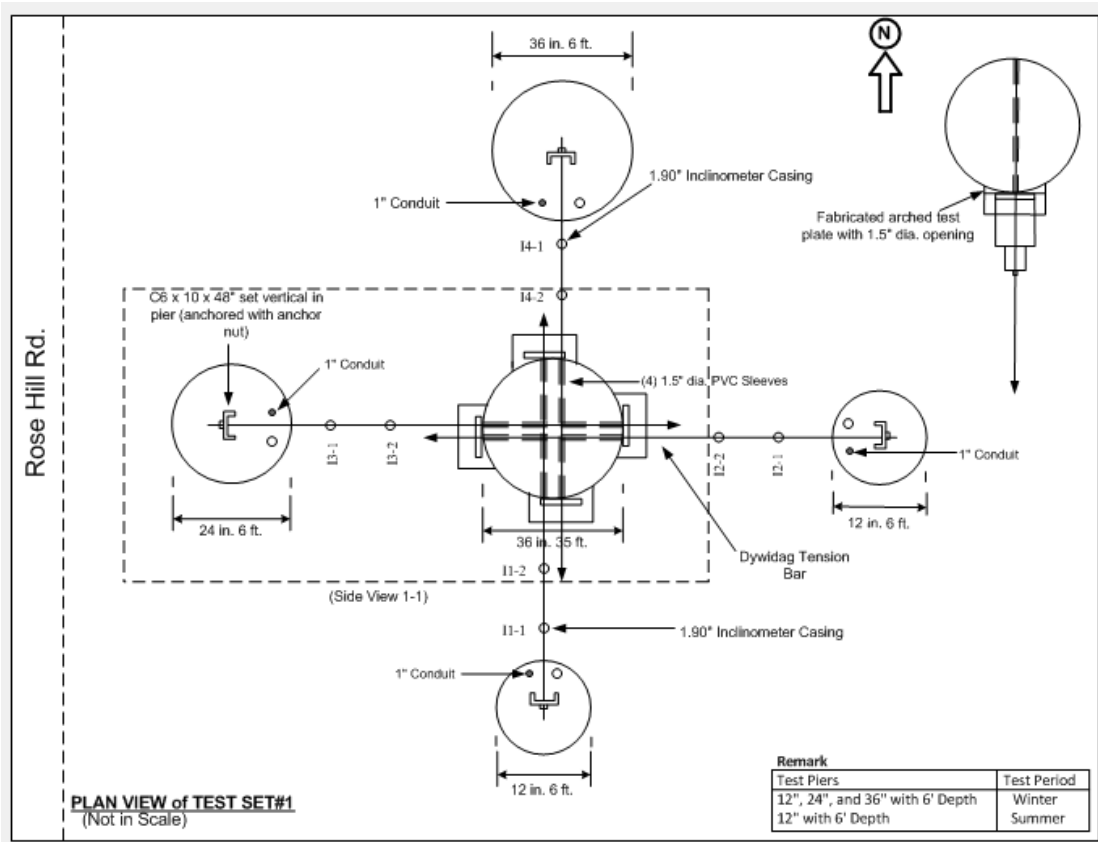
Figure 4.3 Typical Plan Views of Test Setup
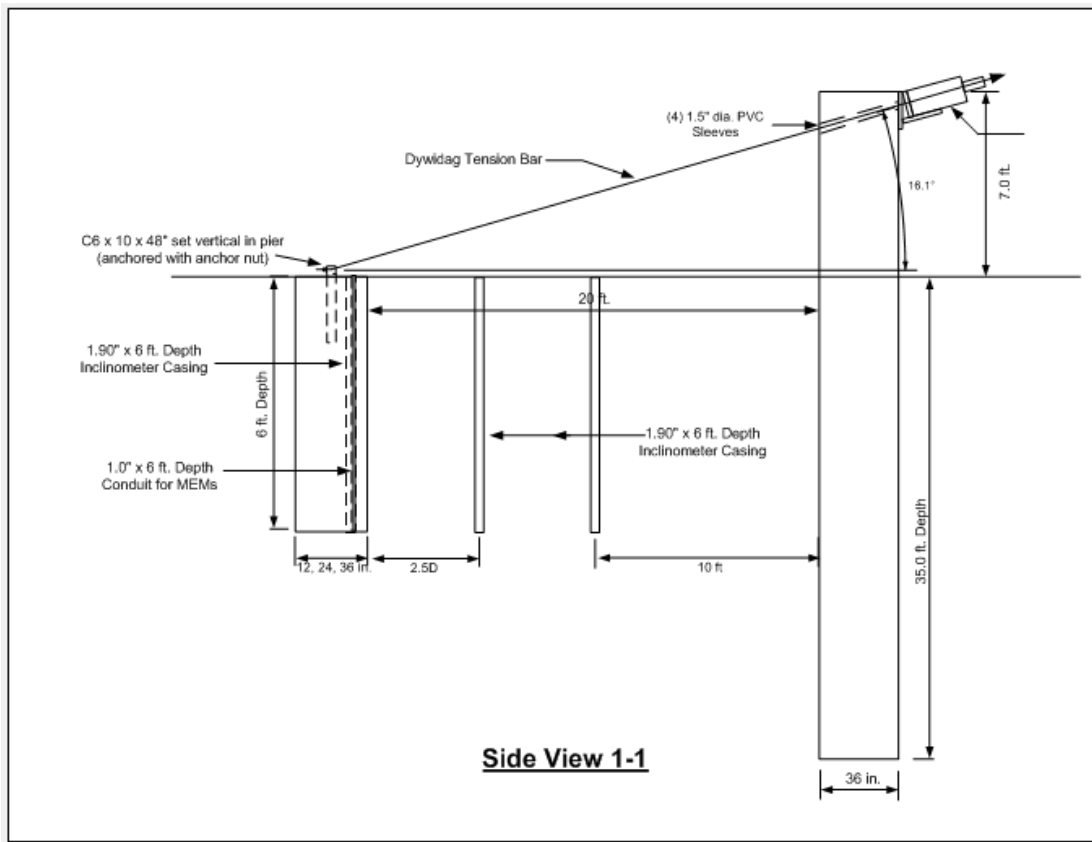
Figure 4.4 Typical Elevation Views of Test Setup

4.3 Construction of Test Setup

The drilled shaft installation plan was not constructed according to design but was modified in the field to accommodate the speed of construction with the available equipment. The final test sets that were constructed are shown in Figure 4.5 The required spacing between the test and reaction shafts were still retained per the design requirements and were not expected to influence the loading and the final results.

98
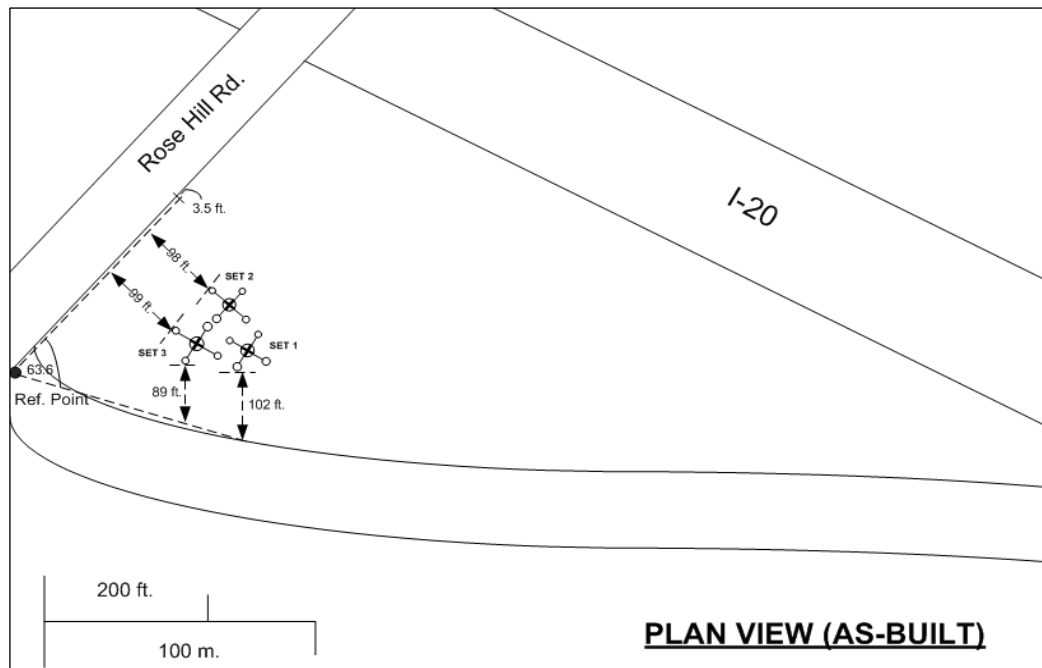
Figure 4.5 Plan View of As-Built Test Setups

4.3.1 Construction Process

Construction commenced at the test site on Monday, June 8, 2009. The first task was to tie the steel rebar into the circular shapes used in typical drill shaft construction. Two separate crews began tying the steel; one crew built and tied the three (3) reaction shafts (Figure 4.6) while a second crew built and tied the twelve (12) test shafts (Figure 4.7). Different size vertical rebar was used as well as spiral rebar to hold the cages together. This was accomplished on June 8 and 9, 2009.

99

a)

b)

Figure 4.6 Construction of the First Reaction Shaft Rebar Cage: a) Frame Used for Rebar Cage Construction and b) Arrangement of Main Rebars in the Cage

Figure 4.7 Construction of a Test Shaft Rebar Cage

Inclinometer casing (2.75 in. (70 mm) dia.) was measured, cut, and tied onto the steel cages prior to installation for use by Slope Indicator's DigiTilt Measurement System. Additionally, 1.25 in. (32 mm) PVC pipe was measured, cut, and tied to the steel cages for use by the MEMS sensor system for in-place deformation data collection during the loading application. These can be seen in Figure 4.8

Figure 4.8 Construction of Casings of Drilled Shafts

The drilling for reaction shaft holes was started on June 9th. The first drilled hole encountered slight sloughing or caving of the in-situ soil at about the 18-20 ft (5.0 – 6.1 m) depth (Figure 4.9). Extra care was taken by slowing the drilling operations at those depths and as a result soil caving did not occur in the other two reaction shafts.

Figure 4.9 Drilling of Reaction Shaft Holes

While drilling operations were on-going, steel rebar cages were prepared and both inclinometer (blue casings) and MEMS instrumentation (white casings) were attached to these

cages. Also, steel channels were connected into the test shaft cages (Figure 4.10) which were used to attach the Dywidag bars to the reaction shaft to perform the load testing.

Figure 4.10 Channel Steel Tied to Steel Rebar Cage

Each steel rebar cage was carefully lifted into a vertical position (refer to Figure 4.11), moved into position over each drilled hole, and then carefully lowered into the hole until they were approximately 3 in. (76 mm) above the bottom of the hole. A gravel concrete mix was then poured into each hole until the drilled hole was completely filled to the groundline (Figure 4.12). Concrete materials supplied by Texas Industries Inc. (TXI) and the mix design details were Self-Consolidating Concrete or SCC. It is a highly flowable, non-segregating concrete mix that can spread into place and fill the formwork without using mechanical vibration. The code used to order the concrete was P40PSIN. In the concrete design, the Water/Cement Ratio was 0.459 with a slump of 6 inches (150 mm) or more. Concrete materials and the mix design details are shown in the next page:

The material proportions per one cubic yard of concrete mix are:

Water	30 gal.
Cement	451 lbs.
Pea Gravel	1800 lbs.

Sand   1479 lbs.

Flyash   113 lbs.

Admixtures:

Water Reducing Admixtures (Type A) – MIRA 85   16.9 oz.
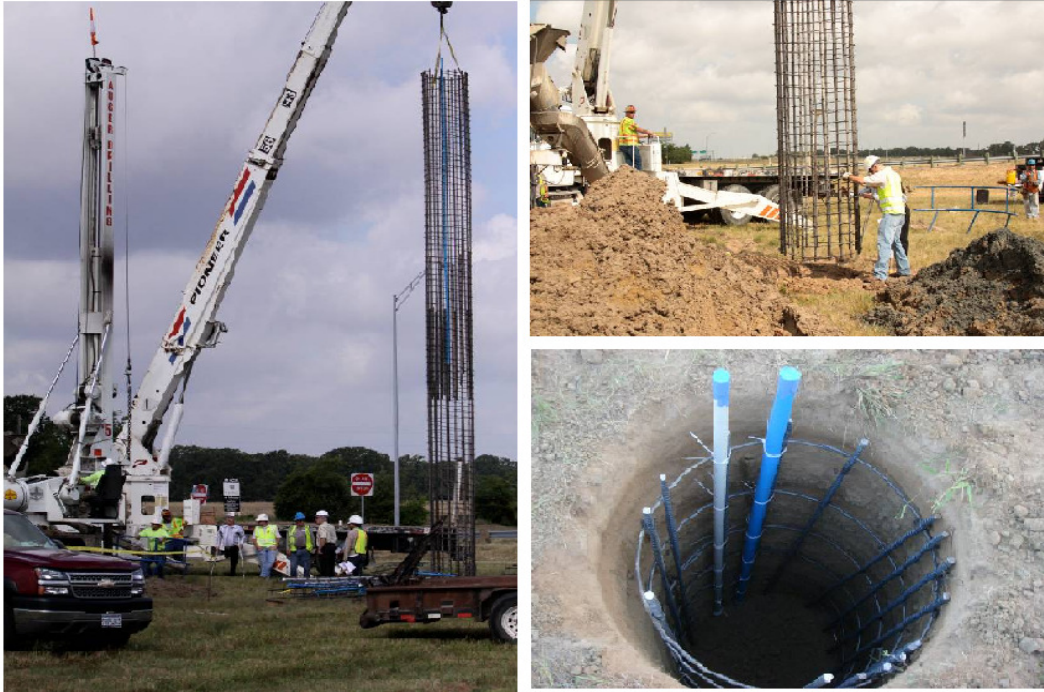
Figure 4.11 Setting the Steel Rebar Cages

Figure 4.12 Pouring Concrete and Final Shaft

For the three reaction shafts, the steel rebar cages were extended above the groundline to their designed height prior to the application of a cardboard sonotube and concrete. Cardboard sonotube was used to extend the concrete reaction shafts 7 ft (2.1 m) and 7.5 ft (2.3 m) above the groundline (Figure 4.13) to provide the proper angles and lengths of the Dywidag bars in direct proportion to those used by the median cable barrier system manufacturers.

<center>(a)</center>

<center>(b)</center>

Figure 4.13 Construction of Reaction Shafts: (a) Sonotube Casing for Reaction Shaft and (b) 7.0 and 7.5 ft (2.1 and 2.3 m) Tall Sonotube Casing for Reaction Shaft

PVC pipes measuring 2 in. (50 mm) in diameter were cut and placed through the sonotube walls at the proper angles (Figure 4.14) to allow the future tensioning of the Dywidag system by connecting it to the test shafts. The angle of placement (16.1 degrees) of the PVC pipes matches the angles of the cables connected to the drilled shafts in the field. The same concrete mix supplied by the local vendor was also used to fill in around the steel rebar up to the top of each piece of sonotube to create the reaction shafts (Figure 4.15).

(a)   (b)

Figure 4.14 Dywidag Construction: (a) Installing the PVC Pipe   and (b) Check of Angle for
Dywidag Bars

(a)   (b)

Figure 4.15 Sonotube Installations: (a) Pouring Concrete in Sonotubes and (b) Final View of
Test Setup Area

Initial inclinometer data was collected on Monday, June 15, six (6) days after installation

of all the reaction and test shafts (Figure 4.16).

Figure 4.16 Taking Initial Inclinometer Readings

Twelve (12) additional inclinometers were installed between the reaction and test shafts on August 14, 2009. The holes were drilled with a 3.5 in. (90 mm) auger powered by a small generator and turned with a hydraulic-driven chuck as shown in Figure 4.17

(a)   (b)

Figure 4.17 Test Shaft Inclinometer Installation: (a) Auger and Drill Stem   (b) Drilling Operation

Thirteen (13) days were allowed to elapse before any inclinometer readings were taken. Initial inclinometer readings of these new inclinometer setups were taken on August 27, 2009. Additionally, the sonotube casing for the easternmost reaction shaft was removed exposing the concrete and effectually stopping the cement hydration process and the strength gain. The sonotube on the other two reaction shafts was removed on September 5, 2009.

4.3.2 Field Quality Control Checks – Concrete Material

In construction, it is necessary to have quality control of the material used in order to ensure that the structures in the field are built as per the design and construction specifications. For this research, the quality of the concrete material used was investigated by randomly collecting samples from different concrete trucks that provided the concrete material for both reaction and test shafts. A total of five cylinder specimens were fabricated and tested. Three samples were from each of three reaction shafts and two samples were randomly prepared from the test shafts. The dimensions of the cylindrical specimens prepared was 6 in (150 mm) in diameter and 12 in (300 mm) in length as specified by the ASTM C31/C31M–09 method, Standard Practice for Making and Curing Concrete Test Specimens in the Field.

All five specimens were cured in water for an additional 26 days. After completion of the standard curing time frame of 28 days, the specimens were taken out of the water. All specimens were capped on the top and bottom with sulfur compound prior to breaking. This provided a 100 percent contact between the base and loading plates and the surfaces of the concrete cylinders as required by Test Method ASTM C617 - 09a, Standard Practice for Capping Cylindrical Concrete Specimens and as shown in Figure 4.18.

Figure 4.18 Concrete Cylinder Specimens with Capping Compound

A Tinius Olsen compression tester was used to break the specimens in compression as required by Test Method ASTM C39 / C39M - 05e2, "Standard Test Method for Compressive Strength of Cylindrical Concrete Specimens". The testing machine primarily performs compressive strength testing and has a capacity of about 400 kips for both compression and tension (Figure 4.19). The target compressive strength of the concrete based on the mix design was 4000 psi. In providing the load to the specimens, they were individually placed between the base and the loading plates and the loading was applied and manually controlled at a rate of 300 lb/sec until the specimens failed as shown in Figure 4.20
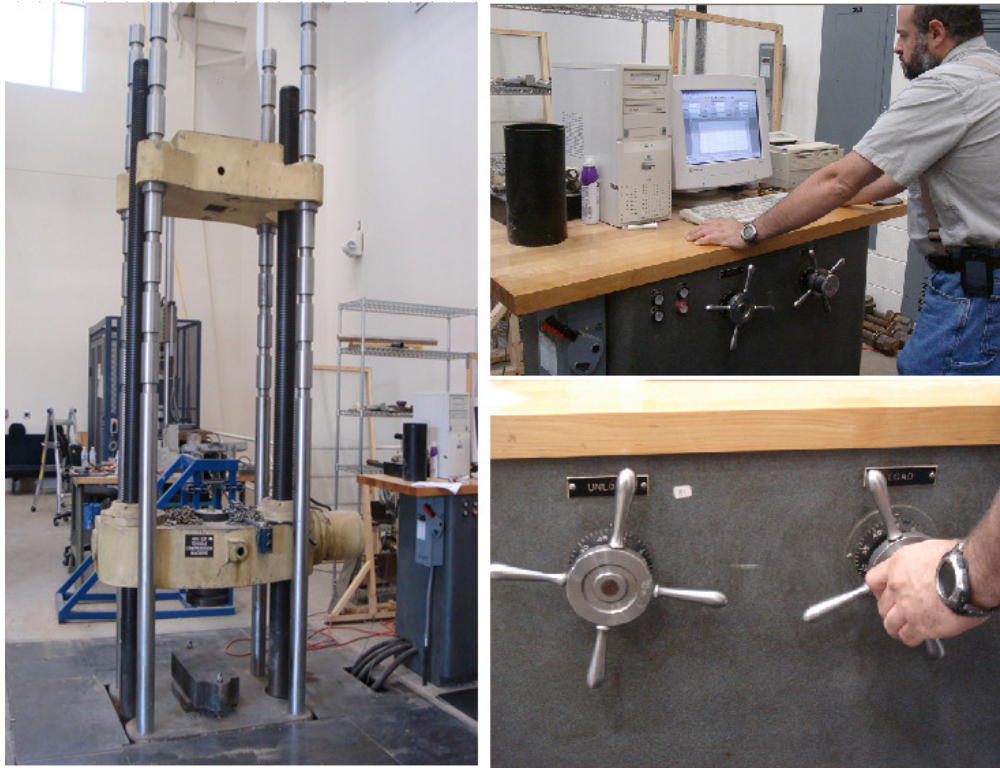
Figure 4.19 The 400 kip Tinius Olsen Tensile and Compression Machine used for Testing

Figure 4.20 Compressive Strength Test Setup and Failed Concrete Specimen

The results and interpretations are automatically collected by the testing machine which all of the results are summarized and shown in Table 4.3.

Table 4.3 Compressiion Strength Test Results on the Concrete

Specimen No.	Peak Stress (psi) at 28 days
1	4075
2	4037
3	3972
4	4116
5	4033

From the results, the average compressive strength of all five specimens is equal to 4046.6 psi with a Standard Deviation (SD) equal to 53.54 psi. Although one specimen broke at a compressive strength lower than 4000 psi, it was more than 90% of the design concrete strength of 3600 psi and was deemed acceptable.

<u>4.4 Instrumentation and Field Load Testing</u>

4.4.1 Displacement Monitoring Instrumentation

It is possible that part of the inclined load applied by the hydraulic system on the reaction shaft may have been lost due to both the length of the Dywidag bar used and friction developed within the PVC tubing. To account for this loss and provide actual load data for analysis, strain gages were attached to the bar close to each test shaft to measure the actual loads transmitted to the test shaft. The strain gage was attached on the smooth area of Dywidag bar and within 0.60 m (2 ft) from the top of the test shafts (connection between C-Channel at top of the drilled shaft and Dywidag bar). In order to determine the forces acting on the drilled shafts, strain results recorded are multiplied by elastic modulus and cross-section area of Dywidag bar.

For the lateral and vertical displacement measurements of the shafts during load testing, several methods were used which included vertical inclinometer probing placed inside the test shaft, Micro-Electro-Mechanical System (MEMS-SAA) probes placed inside the shaft for continuous displacement monitoring, dial gauges placed at top of the drilled shafts on the ground, and survey equipment monitoring of the a few points selected on top of the test drilled shafts. The following sections describe in detail about the inclinometer and MEMS-SAA measurement systems used in the lateral deformation monitoring during field load tests.

4.4.1.1 Vertical Inclinometer Surveys

A Digitilt vertical inclinometer system was used here and this probe consists of one accelerometer measuring tilt in the plane of the inclinometer wheels which track in the longitudinal grooves of the casing. The other accelerometer measures tilt in the plane perpendicular to the wheels. At each load increments applied during the load tests, the inclinometer probe was inserted into the casing to record and monitor the lateral deformation of the shaft.

4.4.1.2 MEMS-SAA Readings

The Micro-Electro-Mechanical System – Shape Acceleration Array (MEMS-SAA) is innovative equipment capable of providing continuous displacement data for geotechnical tasks and is shown in Figure 4.21a. This sensor consists of 30 cm (1 ft) long rigid segments connected by composite joints that are designed to prevent torsion but allow flexibility with a diametral array close to 25 mm (1 in.). These rigid segments and flexible joints are combined as a set of sensor arrays called a Shape Acceleration Array (SAA) capable of measuring three-dimensional (3D) ground deformations at 30 cm (1 ft) intervals to any required depth. It can also be used for two-dimensional (2D) deformation monitoring of the system. For measurements taken with this unit, 32 mm (1.25 in.) diameter PVC pipe was installed along the longitudinal reinforcement of each test shaft.

113

Due to the flexibility of the sensors, the MEMS-SAA probe was rolled up on a reel for shipping and storage. Prior to actual field use, a few preliminary tests were conducted on the probe by inducing known displacements which were then monitored. Monitored readings showed an excellent match with the calibrated test data. The MEMS-SAA system provided continuous and real-time test results. Thus, using the MEMS-SAA system, continuous data was collected which included critical displacement data for each time period during incremental load application and close to the shaft failure.

For horizontal movements of reaction and test shafts, the dial gauges were also placed at the top of the test shafts and at the reaction shafts near the ground surface. In order to measure the vertical movements of test shafts, dial gauges were placed close to the center of the shafts. A photograph showing various dial gauge positions on the test shafts is shown in Figure 4.21 b. Table 4 provides a list of these deformation monitoring systems used along with their measurement accuracy details.

Field testing along with data collection from inclinometer and MEMS as well as strain gauges was performed on September 30, 2009. One test shaft for each reaction shaft was used. Inclinometer and MEMS probe data was acquired during the incremental load testing. In addition, elevation surveys were also performed under each incremental load to measure surface elevation changes of the drilled shaft.

Table 4.4 Summary of the Resolution and Accuracy of the Monitoring Equipment

Type of Equipment	Resolution	Accuracy
Vertical Inclinometer[1]	0.002 mm per 500 mm	±0.25 mm per reading and ±6 mm per 50 readings
MEM-SAA[2]	-	±0.5 mm per 32 m

Note: [1] Manufacturer: Durham Geo Slope Indicator (DGS); Model Number: N/A

[2] Manufacturer: Measurand Inc. ; Model Number: SAAF
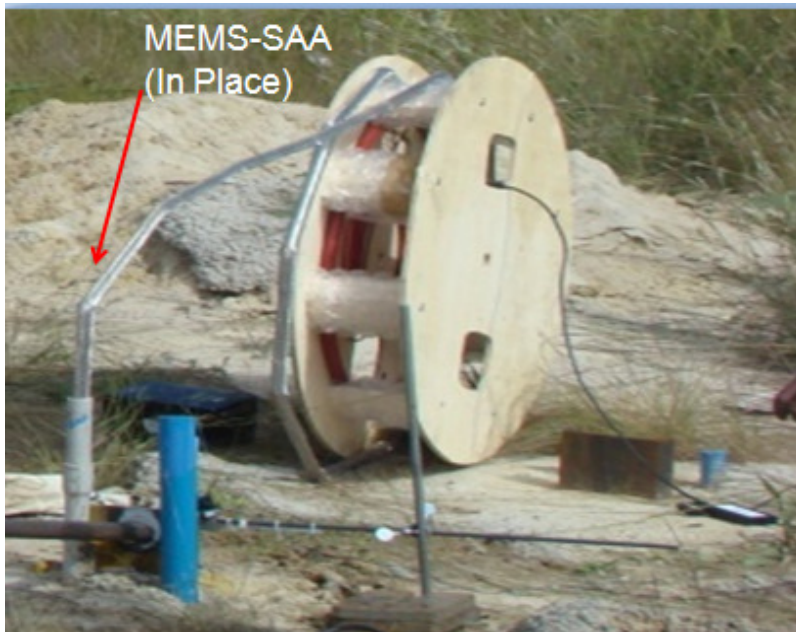
a)

b)

Figure 4.21 Equipments for Lateral and Vertical Measurements a) MEMS-SAA and b) Dial Gauges used for Horizontal and Vertical Measurement

4.4.2 Temperature and Moisture Content Monitoring

Moisture probes along with a buried data logger system was placed adjacent to the test shafts at various depths to continuously record the moisture content and temperatures around the test shafts. Two moisture probes were placed at 0.6 m (2 ft) and 1.2 m (4 ft) depths and one temperature probe was also placed at 0.3 m depth from the ground surface (Figures 4.22 and 4.23). The moisture sensor works on the principle of 'Time Domain Transmissivity' (TDT) technology and provides volumetric moisture content data which was later converted to gravimetric moisture contents. The data was recorded at hourly interval, and was downloaded to a computer periodically during site visits.
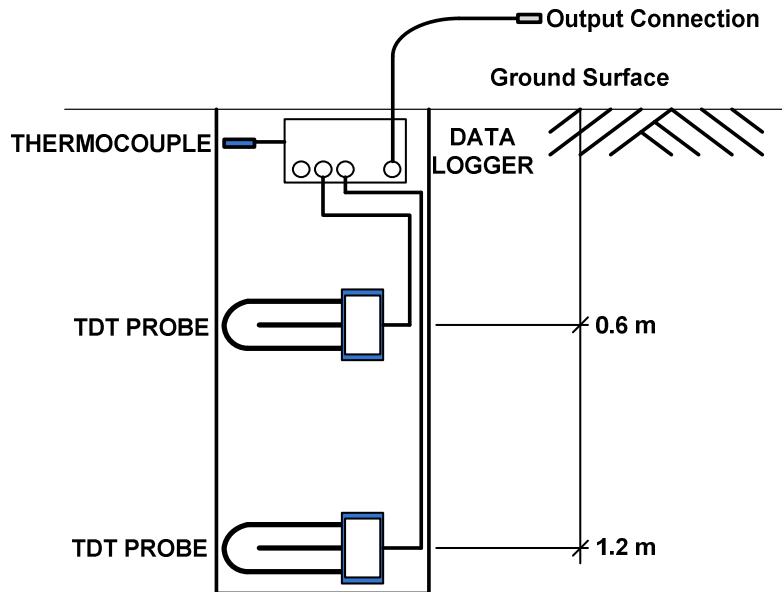
Figure 4.22 Schematic of Moisture Sensors Installation
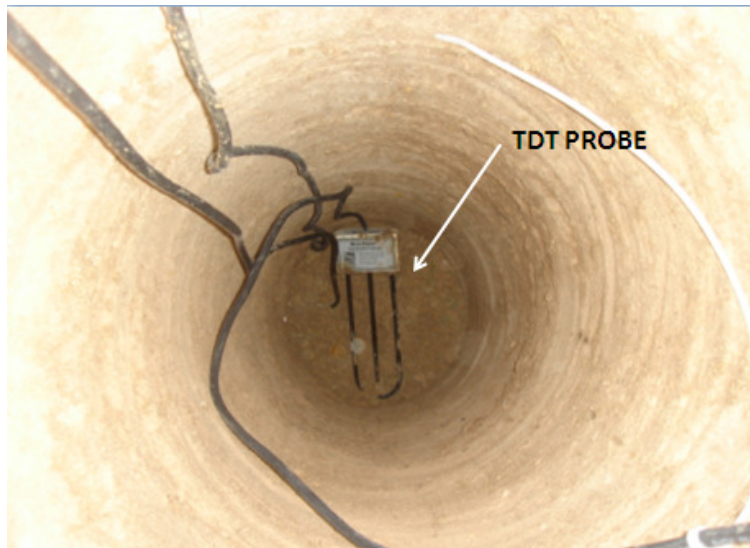
Figure 4.23 Moisture Sensors Installed in the Field at 0.6 and 1.20 m Depth

4.4.3 Field Load Testing

Once all the equipments and instruments were set in the field, one test was performed on each drilled shaft with an inclined reaction load applied using a hydraulic system placed against the reaction shaft. The actual loads acting on the test shaft were detected by strain gage attached to the Dywidag bar close to the head of test drilled shaft. For the test shafts, the lateral movements were measured by both inclinometer and MEMS-SAA sensors. In addition, the final vertical movements of the reaction shafts were measured at the center both before and after the start of each test by using both dial gage and standard survey sensors. Overall, it took 3 to 5 hours to complete load testing on one shaft. The following figures provide details of the field testing for the summer and winter condition.

(a)   (b)

Figure 4.24 Dywidag System Parts: a) Dywidag Bars and (b) Dywidag Bar Retaining Nut

(a)   (b)

Figure 4.25 Dywidag Tensioning System: (a) Hydraulic Piston Shelf and (b) Hydraulic Piston and Pump

(a)   (b)

Figure 4.26 Dywidag Bar System: (a) Dywidag Bar in Place for Testing (b) Retaining Nut
Attached to Test Shaft Steel Channel
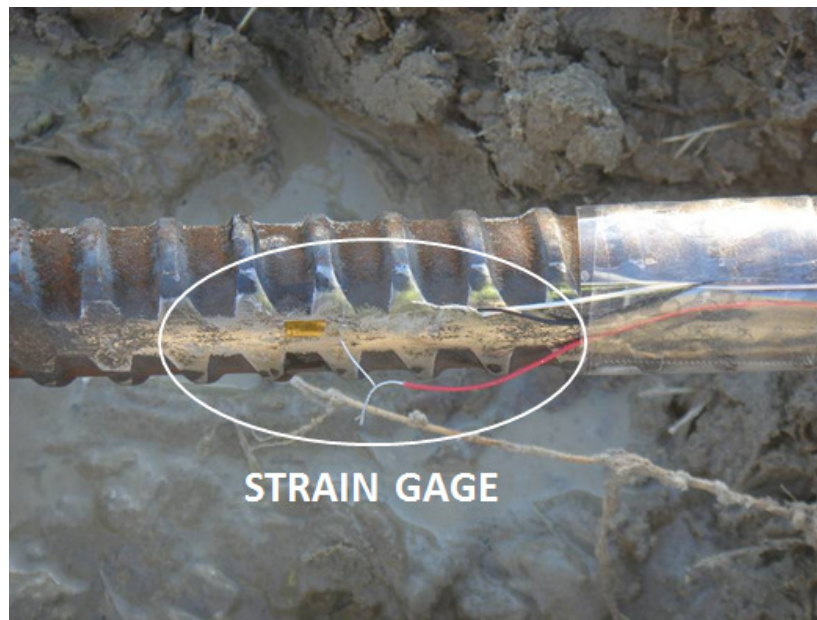
Figure 4.27 Strain Gage Attached to Dywidag Bar

<center>
(a)   (b)

Figure 4.28 Hydraulic Piston Setup for Tensioning: (a) Installing the Hydraulic Piston
(b) Hydraulic Piston and Retaining Nut
</center>
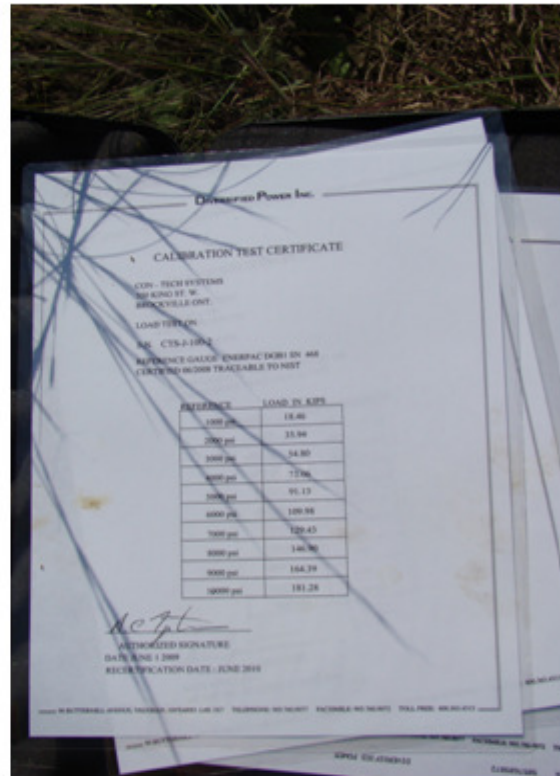
<center>
(a)   (b)

Figure 4.29 Hydraulic Tensioning System: (a) Tensioning System Setup (b) Hydraulic Pump
Calibration Records
</center>

<center>120</center>

(a)   (b)

Figure 4.30 Test Shaft Loading: (a) Applying Tensioning Loads and (b) Test Shaft Deflection due to Loading

(a)   (b)

Figure 4.31 Collecting Inclinometer Readings: (a) Test Shaft and (b) Mid-Point

Figure 4.32 Collecting MEMS Probe and Elevation Survey Readings

4.5 Summary

This chapter describes the design of load test setups and the final selection of the reaction pier setup for inclined load testing. In order to mimic the drilled shaft failure patterns recorded in the field and ease of operations, the pull type hydraulic loading system was chosen and designed. The construction of the system was also described in detail in this chapter. In addition, instrumentation details for capturing load-deformation responses of the test drilled shafts and testing processes are mentioned.

CHAPTER 5

INCLINED LOAD TESTING AND RESULTS

5.1 Introduction

A total of twelve (12) test shafts were subjected to inclined load tests with three (3) of them tested in the summer condition and the other nine (9) piers were tested in the winter condition. The summer condition load testing was conducted in early September, 2009 in dry soils and with daytime temperatures close to 104˚F (40˚C). The winter condition load testing was conducted in early February, 2010 between a high rainfall amounts and a 24 hr record 12 in. snow storm producing totally saturated soil conditions similar to those created in the Winter of 2006 to 2007 in which the original shafts were distressed and the average temperature at testing period was 39˚F (4˚C).

5.2 Load Test Procedure

The following procedure was used to apply load testing on the shafts. As noted earlier, various displacement measurements were monitored during load testing in the field. The steps followed are:

1. Take initial inclinometer and MEM-SAA readings as the reference readings

2. Apply an initial load of 25 psi from hydraulic pump for ensuring that the fabricated plate is in full contact with the outer concrete surface of reaction drilled shaft and also making the high tensioned steel bar (Dywidag Bar) straightened in the PVC slot.

3. Start applying the first load increment with the hydraulic system. Load is applied to Dywidag bar which is connected to the test shaft. Load was increased at 100 psi increments until the test shaft experienced the failure. Failure is defined as large movements of the test shaft or breaking of the drilled shaft which can be observed as a loss of load applied.

4. Record the drilled shaft vertical movements using both dial gage and survey equipment (total station)

5. Perform inclinometer readings for under each load increment

6. Repeat these steps until the failure of the drilled shaft was reached.

5.3 Field Temperature and Moisture Content Monitoring

In order to measure the moisture contents and temperatures in the subsoil, moisture probes along with a data logger system were placed along the depth of the test shafts to continuously record the moisture content and temperatures around the shafts. Two moisture probes were placed at 0.6 m (2 ft) and 1.2 m (4 ft) depths and the temperature probe was also placed at 1 ft (0.3 m) depth from the ground surface. The moisture sensor works on the principle of 'Time Domain Transmissivity' (TDT) technology and provides volumetric moisture content which was later converted to gravimetric moisture content using the mass density of the field soil. The data was recorded at hourly interval, and was downloaded to a computer periodically during the site visits.
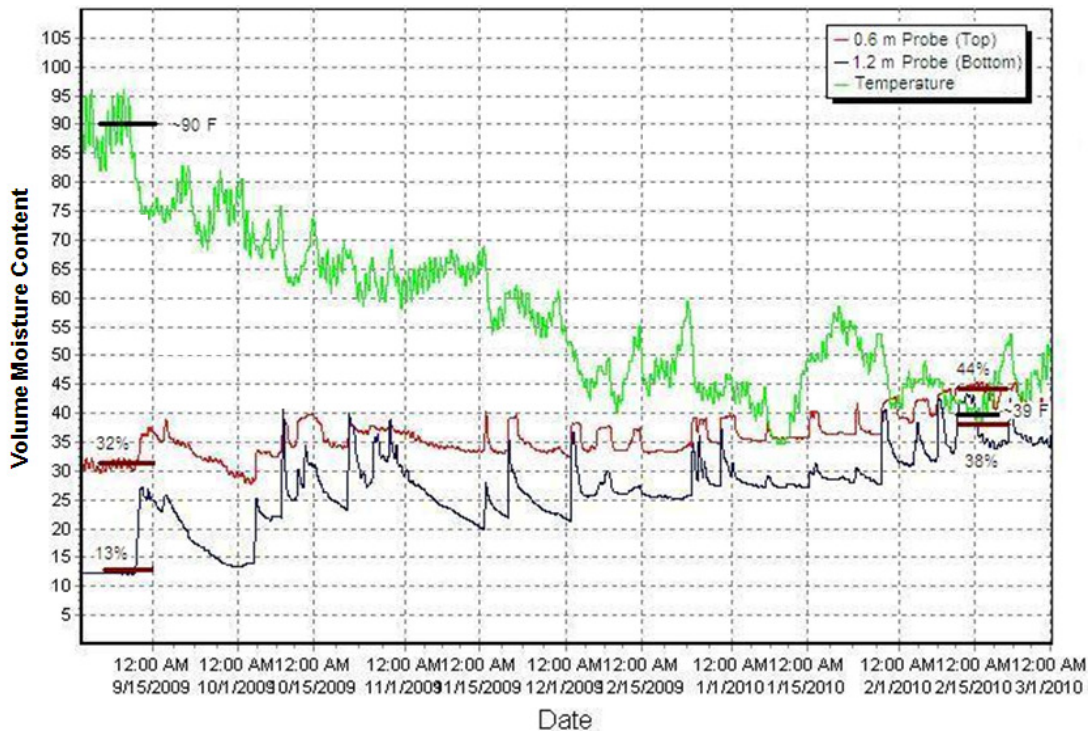
Figure 5.1 Temperature and Moisture Probe Data at 2ft and 4 ft Depths at the Ground

Both temperature and volumetric moisture content data shown in Figure 5.1 indicate that during summer load tests, the temperature sensor embedded at 1 ft (0.3 m) depth showed readings close to 90°F (32°C) and during winter load tests, the same sensor readings were close to 39°F (3.9°C).

In summer load tests, volumetric moisture contents recorded at 2 ft (0.6 m) and 4 ft (1.2 m) were 32 and 13%, respectively, and in the winter load tests, these readings were close to 44 and 38%, respectively. From the temperature and moisture data results, it can be mentioned that field load test environmental conditions are close to conditions expected for load tests in summer and winter environment. It should also be noted that soil strata was not frozen during winter testing, but was close to saturation during winter load testing.

5.4 Drilled Shaft Failure Observations

5.4.1 Summer Condition Tests

Several different failure mechanisms were observed during field load testing. As shown in Figure 5.2, the concrete at the ground surface was cracked in one test. Figures 5.3 and 5.4 show the separation of the test shaft from the adjoining soil. This indicates movement of the test shaft toward the reaction shaft along the direction of the inclined loading.

Figure 5.2 Cracking in Concrete Material

a)

b)

Figure 5.3 Drilled Shaft Separation from the Soil: a) Soil-Test Shaft Separation (Distance) and b) Soil-Test Shaft Separation (Depth)

Figure 5.4a shows yielding and the failure of the steel channel in a test shaft. This was of great concern to the safety of researchers and was hence corrected immediately for the subsequent load tests with the addition of a steel plate to reinforce the steel channel allowing the shaft to fail rather than the channel as shown in Figure 5.4b.
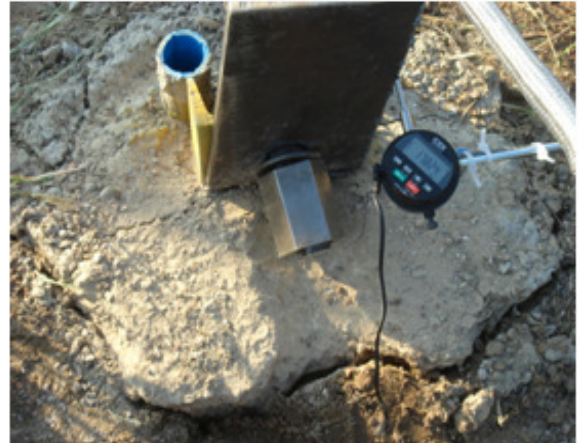
| (a) | (b) |

Figure 5.4 Field Adjustments to Eliminate Yielding of Steel Channels: (a) Steel Channel Yielding and (b) Extra Plate Added

5.4.2 Winter Condition Tests

Before performing the load tests in the winter, thin ice plates were observed due to low temperature in the night before testing can be noticed at the top of test drilled shaft and below ice plate, there was some water retained at the head of drilled shaft due to long rainfall events as shown in Figure 5.5. Failure of surrounding soil and drilled shaft in the form of large movements were observed during testing. As shown in Figures 5.6 and 5.7, the separation of the soil and concrete for the test shaft was clearly noticeable.

Figure 5.5 Ice Plate Captured in the Morning of Testing day

Figure 5.6 Soil and Drilled Shaft Separation in Top View

Figure 5.7 Soil and Drilled Shaft Separation in Angle of View

In short, it can be noticed that test drilled shafts in winter time have experienced larger movements than those tested in summer conditions. Softening of the surrounding soil was attributed to these large movements. In addition, cracking of the concrete at the top of the drilled shaft was not observed during the winter load tests.

5.5 Inclined Load Test Results

5.5.1 Comparisons between Measured and Actual Applied Loads

Transfer of the load from the appropriate reaction shaft to each test shaft was accomplished thru a Dywidag high tension steel bar. The load data was recorded using two (2) different methods; hydraulic applied load gauge and strain gage based load calculation. It was necessary to measure the load during and after each test to measure any losses from friction or other factors of the bar passed through a PVC pipe in each reaction shaft. Strain gage instrumentation, explained in an earlier section, was used to collect the applied tensile stresses at the top of each test shaft. The actual results were calculated using the modulus of elasticity of the Dywidag bar steel. Figure 5.8 presents the applied tensile load by the hydraulic system and the measured tensile load from the strain gage on the bar of three tested shafts of different

diameters. In all three cases, the loads at the top of the test shaft are about 92% to 93% of the applied load, thus indicating no major loss of loads applied by the hydraulic system. This loss was also applied to the load acting on the test drilled shaft in summer condition as only hydraulic load gauge was used to apply the loads.
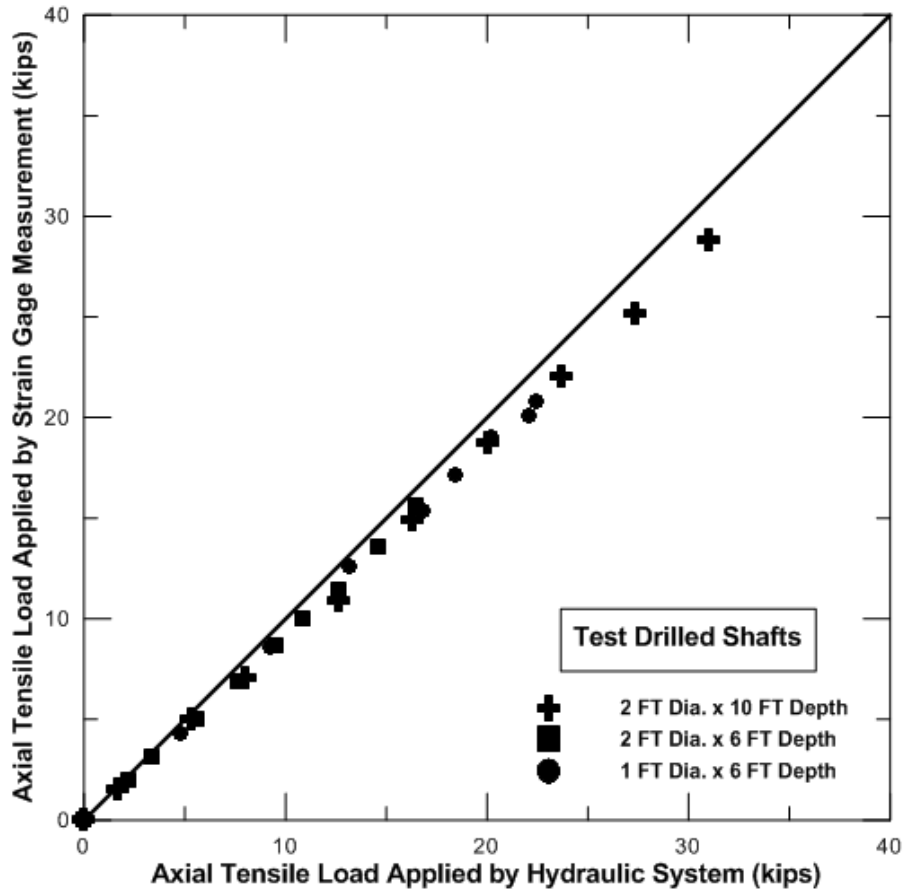
Figure 5.8 Comparisons between Measured and Actual Applied Loads

5.5.2 Applied Load Results

The maximum capacity values were computed by recording the values read directly from the strain gage and applying the calibration curve conversion. The actual loads applied to the Dywidag bars versus the time of application for each load are shown in Figures 5.9 to 5.17, which are the full set of actual forces of all test shafts in winter condition. The extended horizontal portions of the graphs are the loads at which the inclinometer readings were taken.
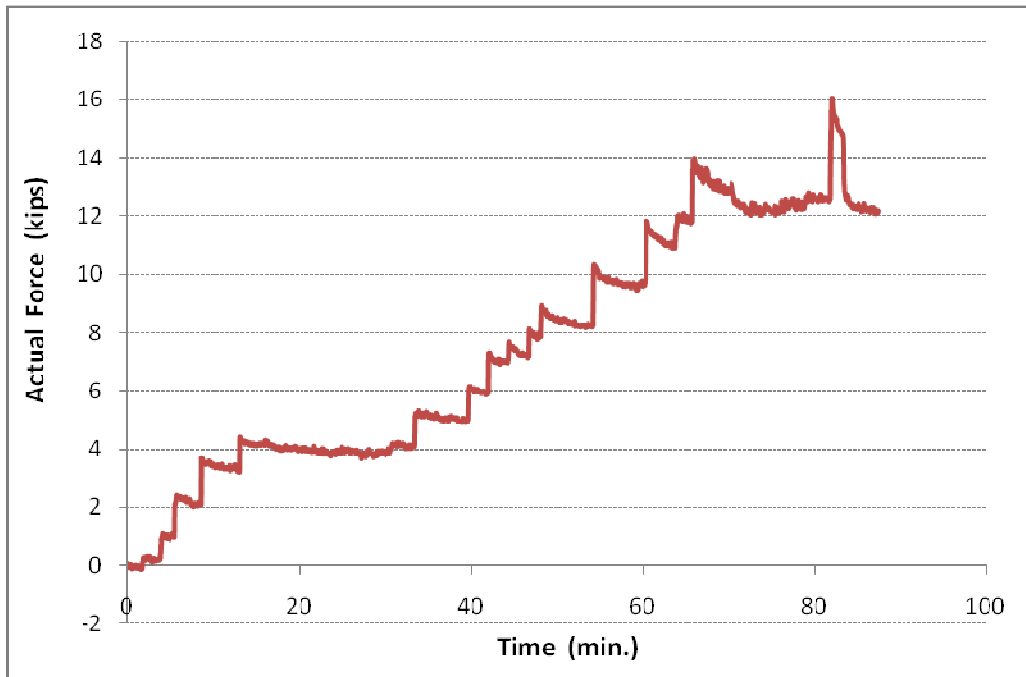
Figure 5.9 Applied Load Versus Elapsed Time of 1 ft diameter x 6 ft depth shaft
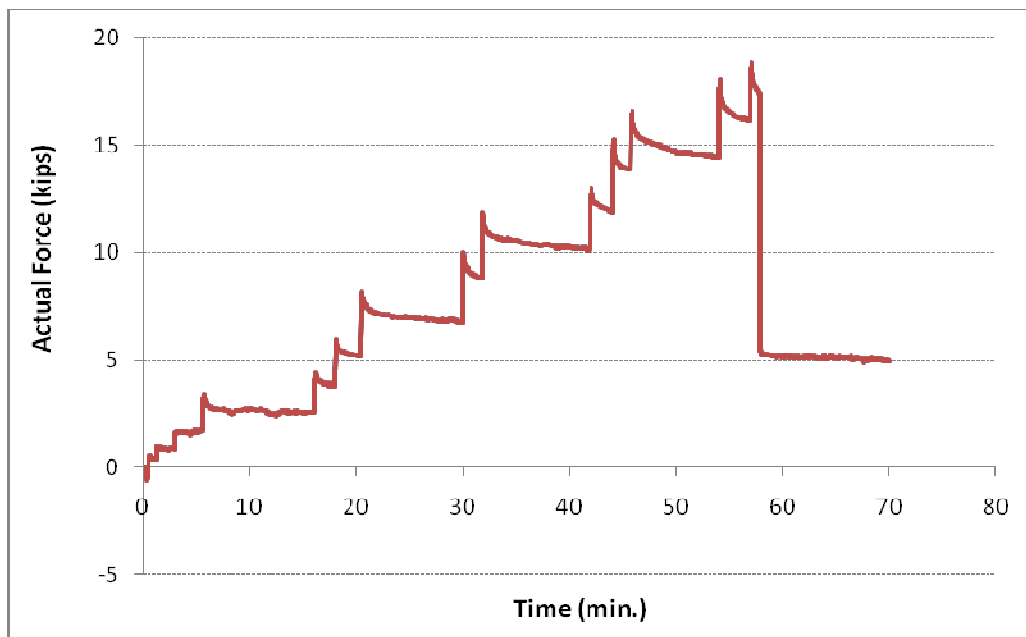
Figure 5.10 Applied Load Versus Elapsed Time of 1 ft diameter x 10 ft depth shaft

132
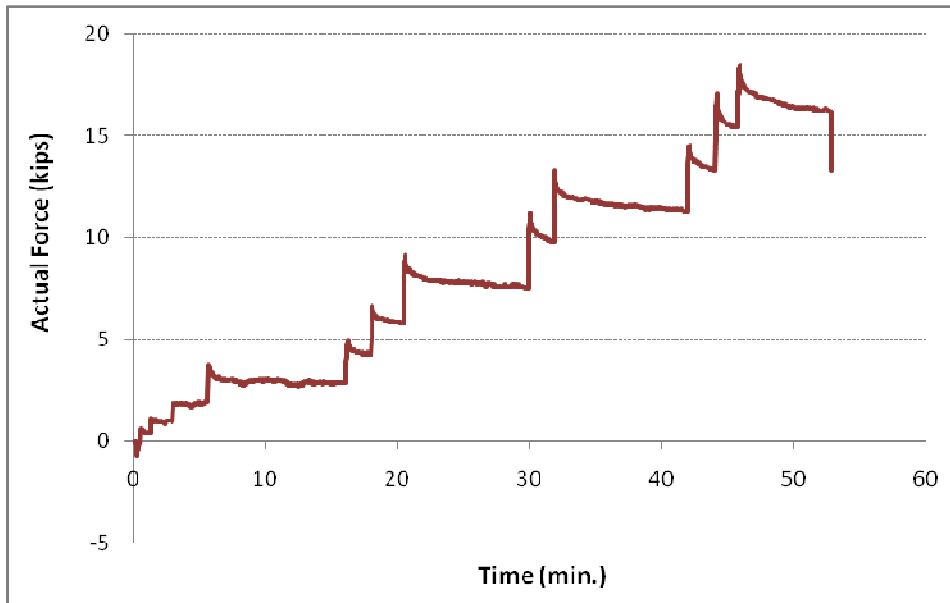
Figure 5.11 Applied Load Versus Elapsed Time of 1 ft diameter x 14 ft depth shaft
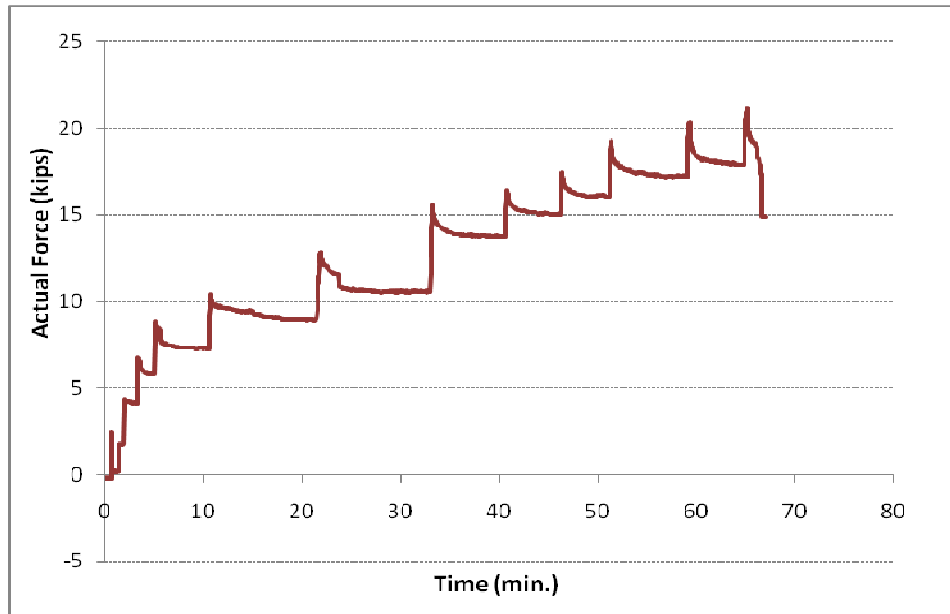
Figure 5.12 Applied Load Versus Elapsed Time of 2ft diameter x 6 ft depth shaft
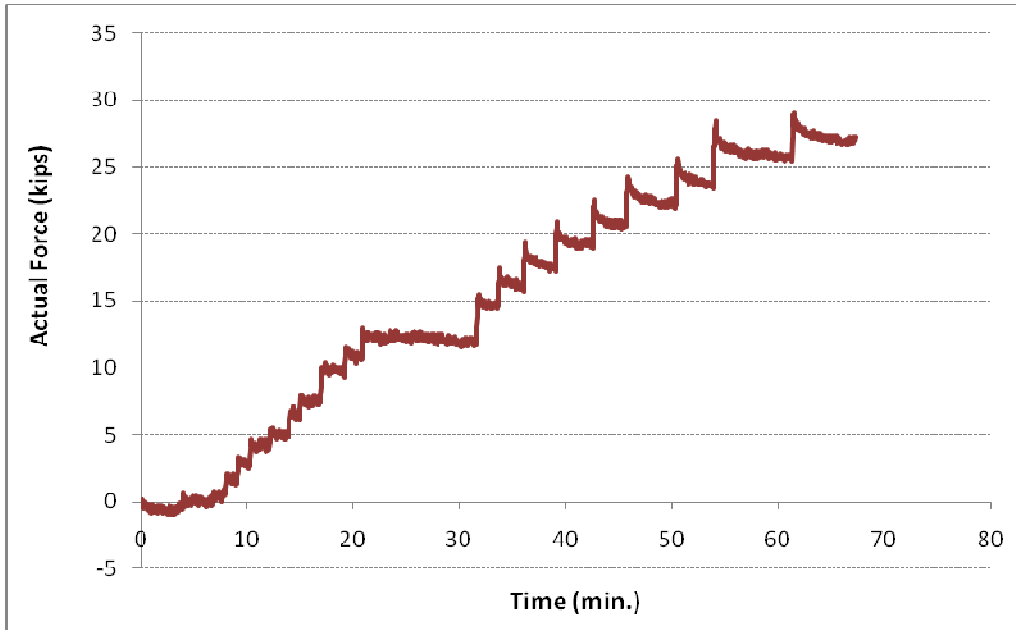
Figure 5.13 Applied Load Versus Elapsed Time of 2 ft diameter x 10 ft depth (1) shaft
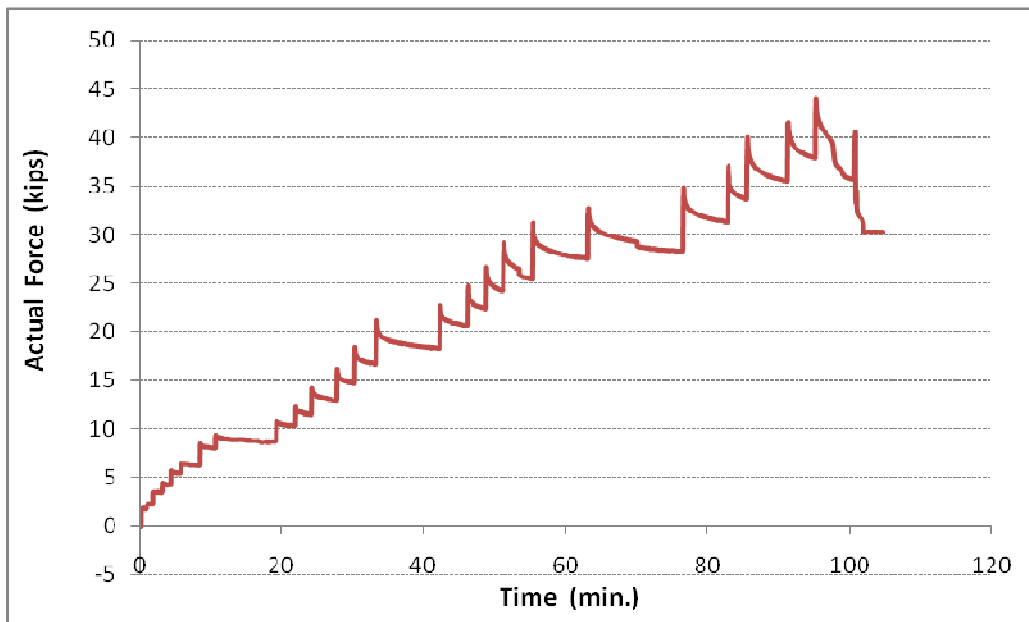
Figure 5.14 Applied Load Versus Elapsed Time of 2 ft diameter x 10ft depth (2) shaft
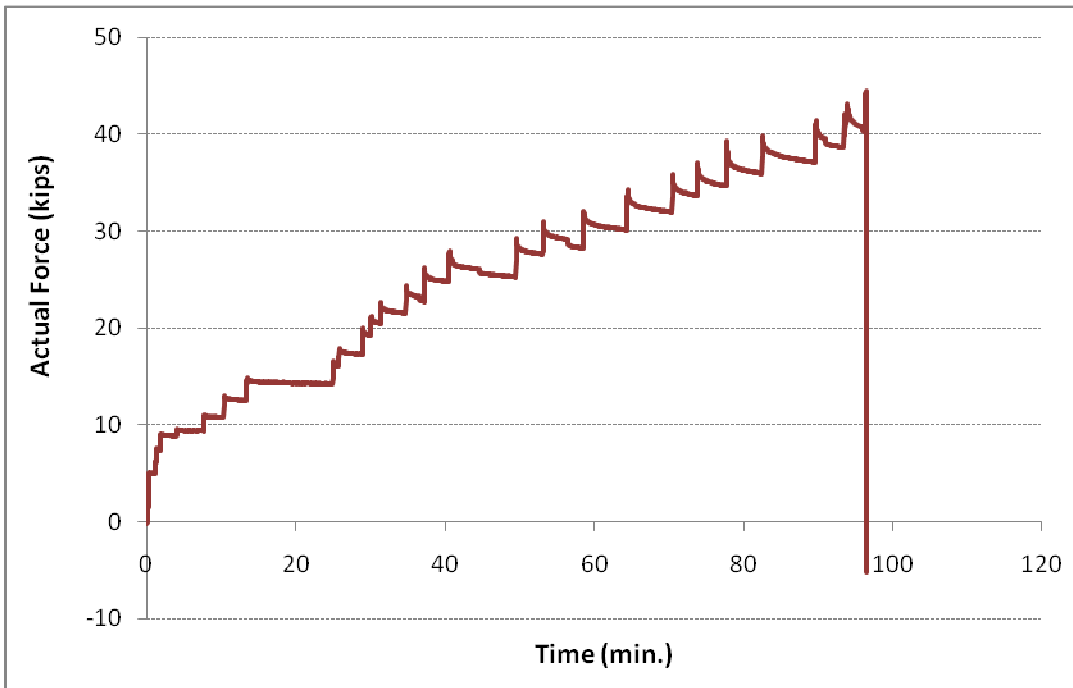
Figure 5.15 Applied Load Versus Elapsed Time of 2 ft diameter x 14 ft depth shaft
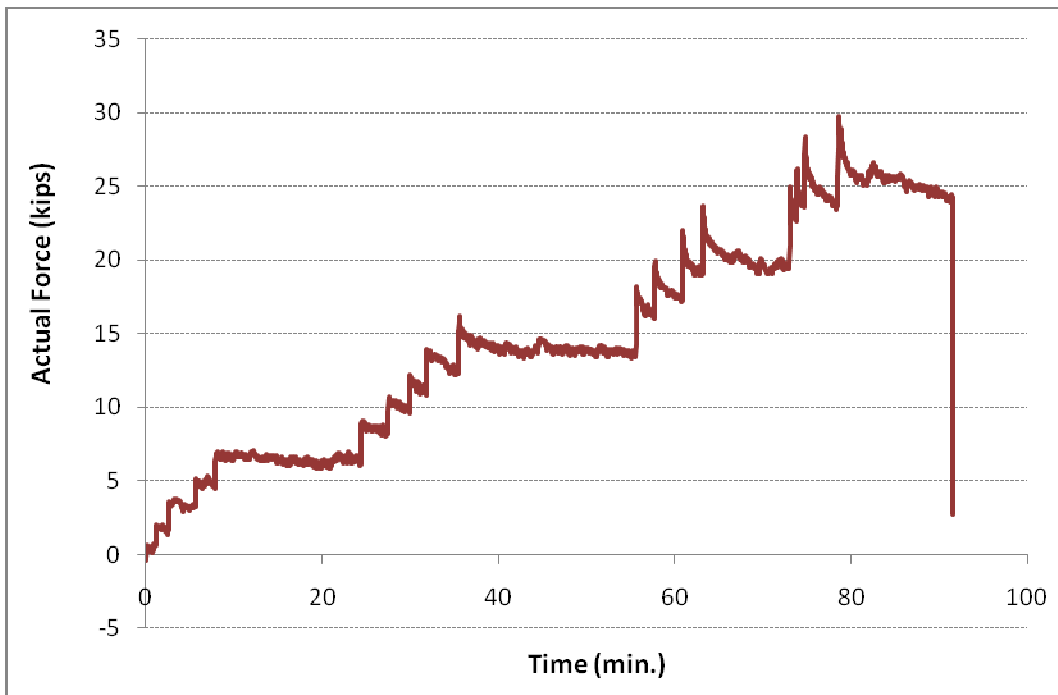
Figure 5.16 Applied Load Versus Elapsed Time of 3 ft diameter x 6 ft depth shaft

135
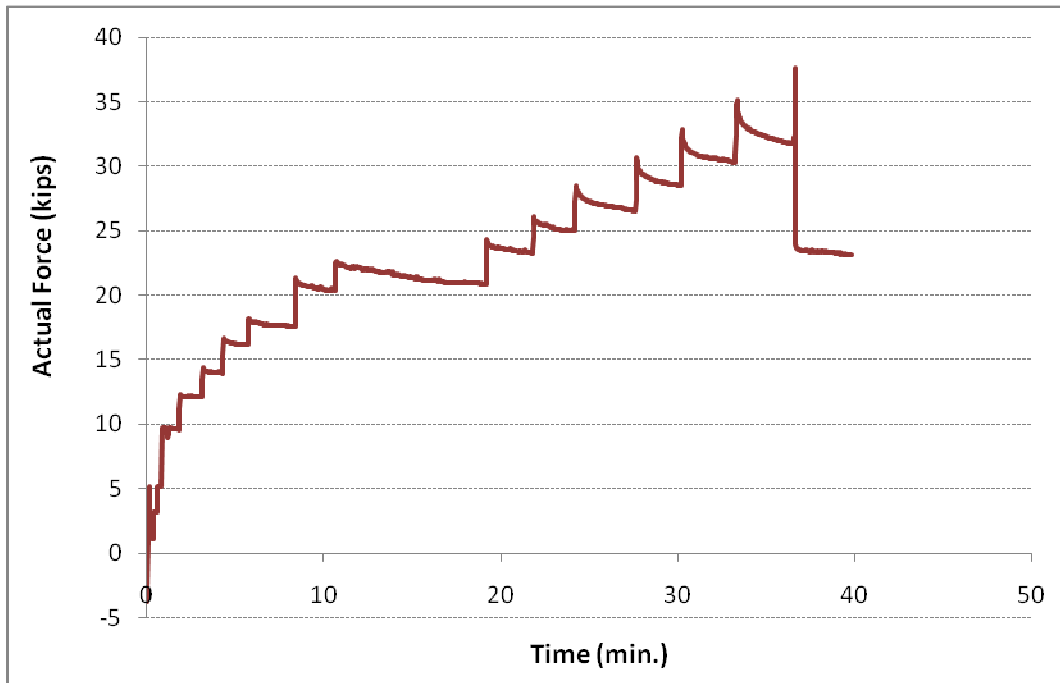
Figure 5.17 Applied Load Versus Elapsed Time of 3 ft diameter x 14 ft depth Shaft

5.5.3 Lateral Displacement Data

5.5.3.1 Inclinometer and MEMS-SAA Displacement Plots for Test Drilled Shafts

Both inclinometer data and MEMS-SAA readings were collected during testing on each test shaft. The inclinometer displacement data was collected at certain incremental loads while the MEMS-SAA data was continuously recorded and stored through a laptop computer used onsite. The plots created from the field collected data for both the inclinometer and MEMS-SAA systems are shown in Figure 5.18.
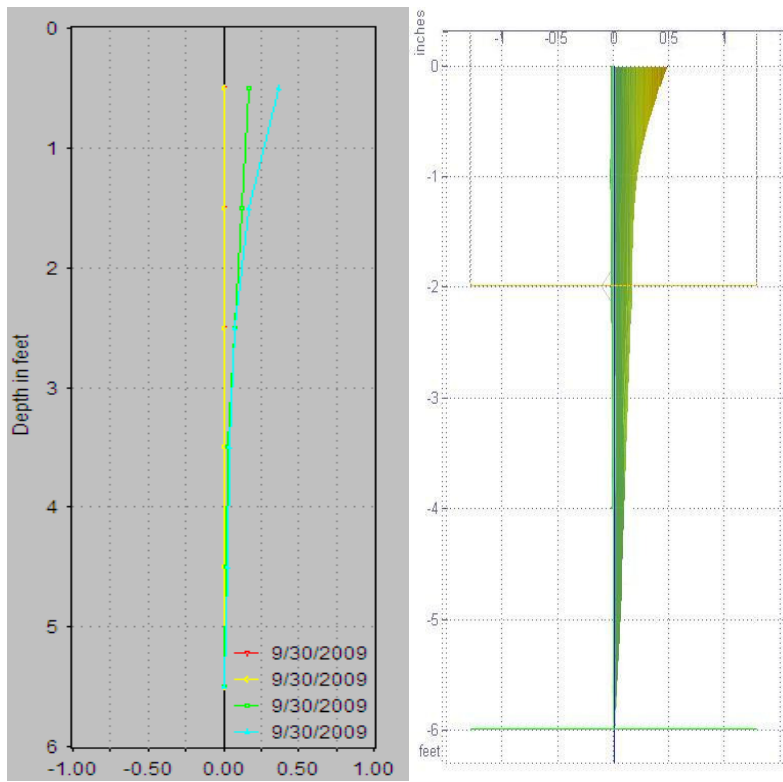
(a)   (b)
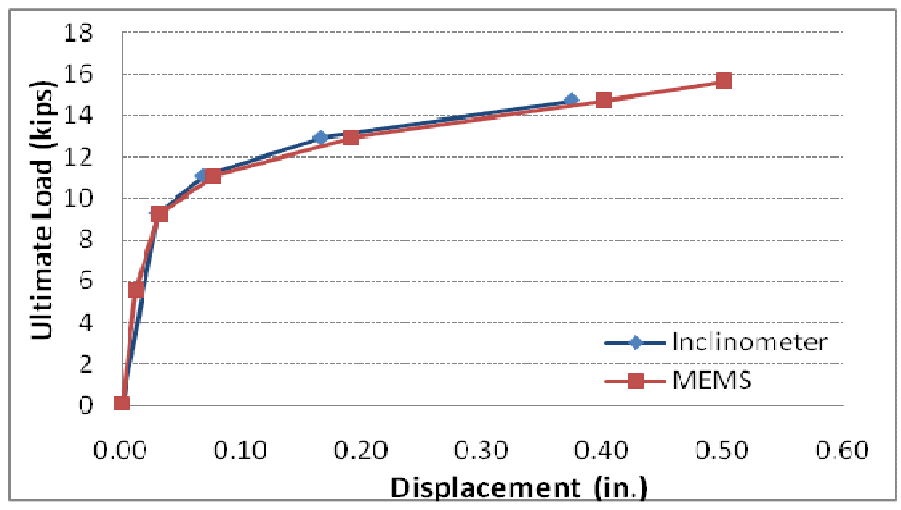
(c)

Figure 5.18 Load Test Results of Test Shaft (1 ft (0.3 m) diameter x 6 ft (1.8 m) depth) in Summer Condition: (a) Inclinometer Data (b) MEMS-SAA Data and (c) Ultimate Load versus Displacement Comparison Plots

The graphs illustrate that the MEMS-SAA data is close to the inclinometer displacement data. Additionally, the MEMS-SAA provided continuous real time data showing the continuous increase in the lateral displacements under each load increment. Another benefit of using the MEMS-SAA system was realized in the final loading increment. The MEMS-SAA probe, with its' flexibility, was able to capture the ultimate load and displacement profile whereas the inclinometer was not able to do so since the probe was not able to be inserted into the failed test shaft due to the casing being distorted. This is a significant advantage between the inclinometer and the MEMS-SAA when the load tests were conducted from the start of initial loading until the final failure of the deep foundation system. This provides very valuable information to allow future research and investigations to use the MEMS-SAA system. Therefore, for the rest of this analysis, displacement results will be reviewed using the MEMS-SAA data, where applicable, in lieu of the inclinometer data. All the graph results can be seen in the Figure 5.19 – 5.30.
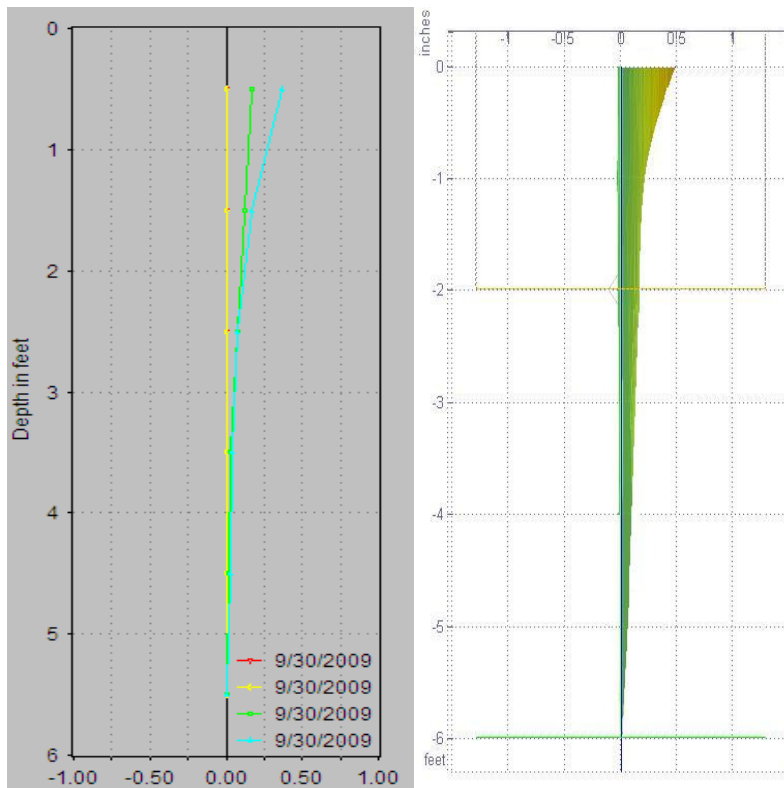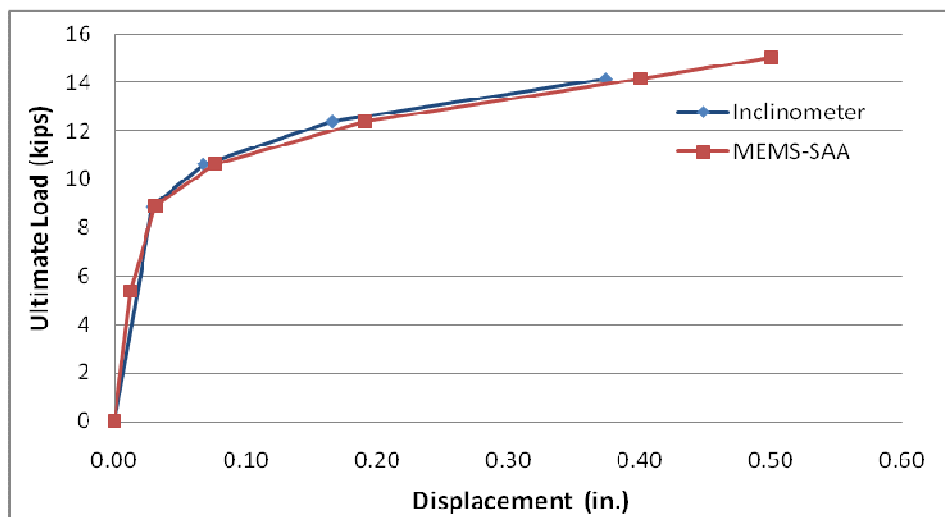
Figure 5.19 Test Shaft (1 ft diameter x 6 ft depth) Displacement Data:
(a) Inclinometer Data, (b) MEMS-SAA Readings, and (c) Ultimate Load versus Displacement
Comparison Plots (Summer Condition)
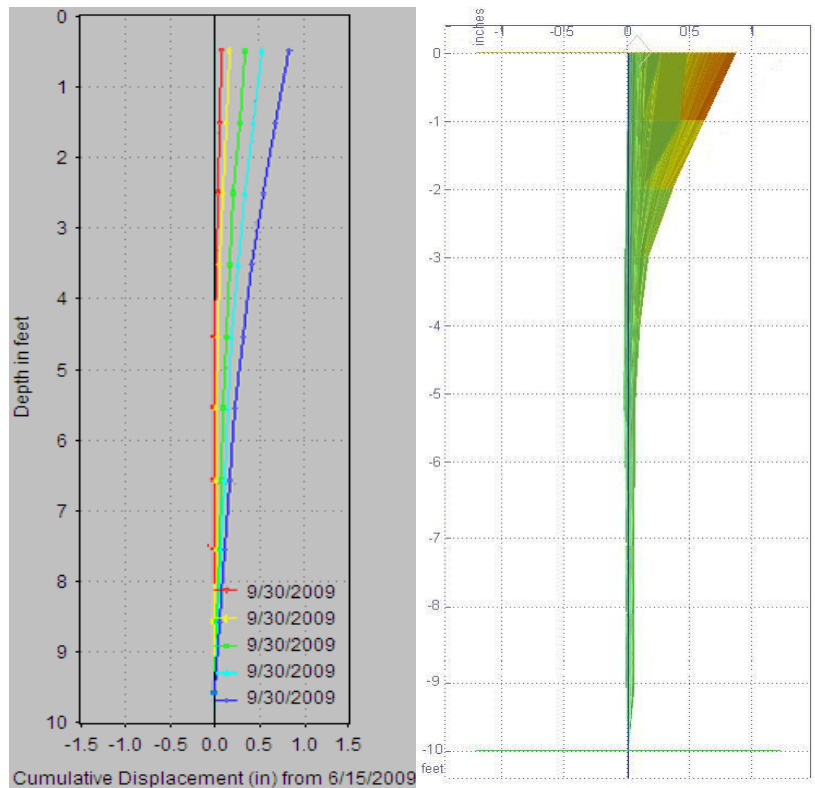
(a)

(b)
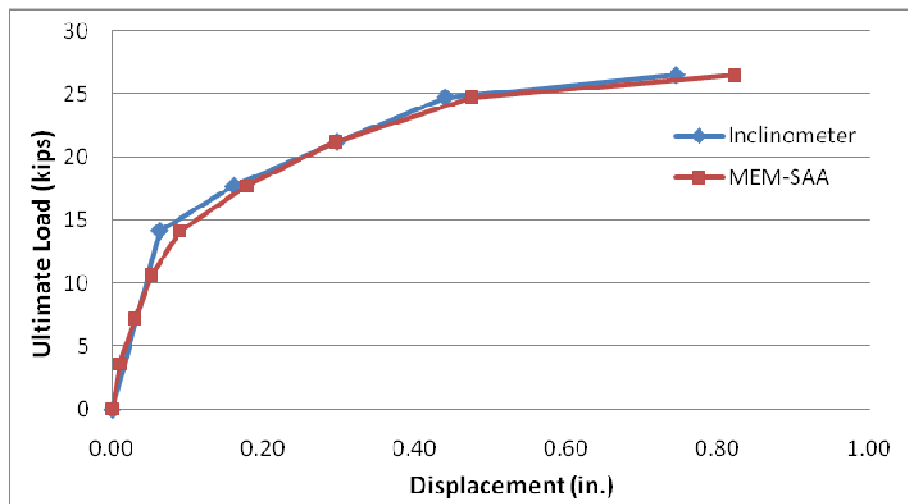
(c)

Figure 5.20 Test Shaft (1 ft diameter x 10 ft depth) Displacement Data:
(a) Inclinometer Data (b) MEMS-SAA Readings, and (c) Ultimate Load versus Displacement
Comparison (Summer Condition)
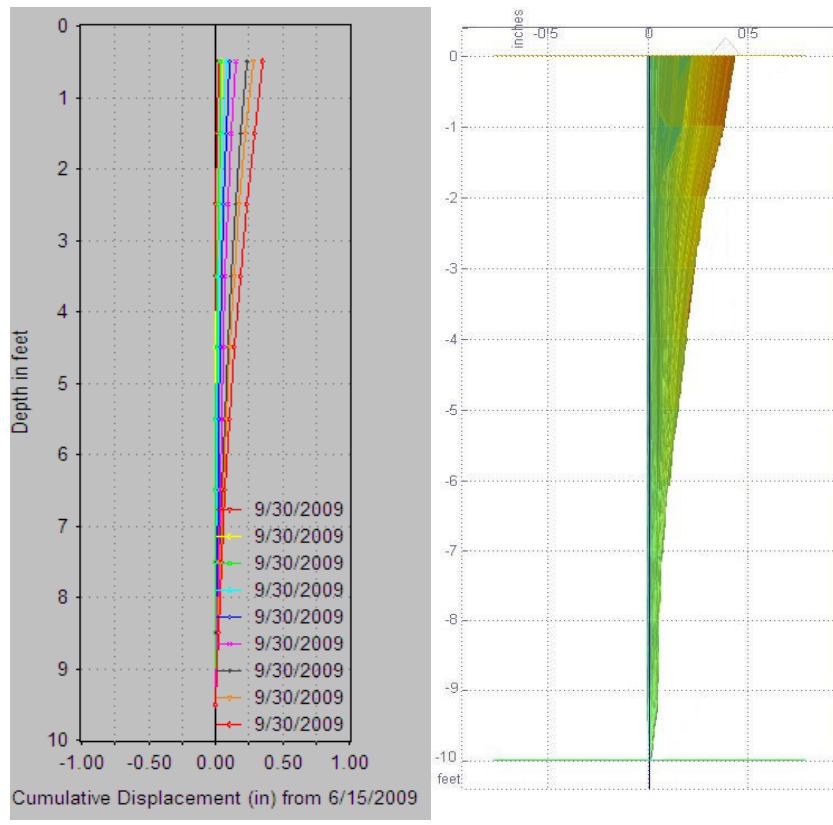
(a)

(b)
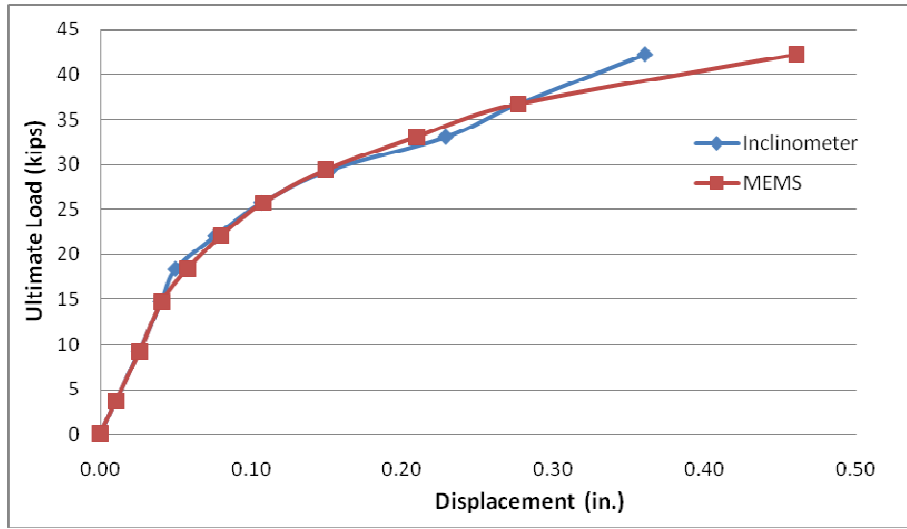
(c)

Figure 5.21 Test Shaft (2 ft diameter x 10 ft depth) Displacement Data:
(a) Inclinometer Data (b) MEMS-SAA Readings and (c) Ultimate Load versus Displacement
Comparison Plots (Summer Condition)

141

(a)

(b)

(c)
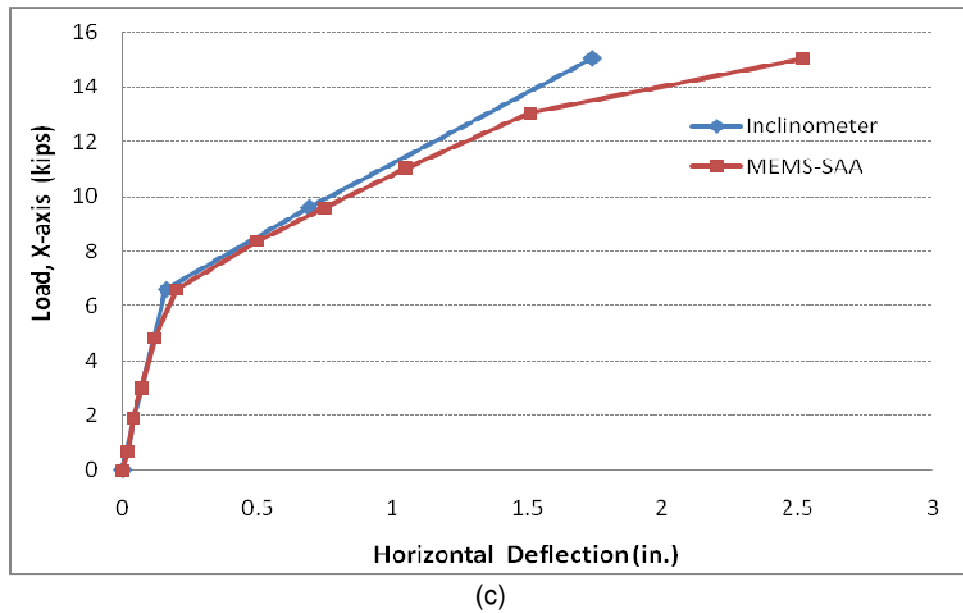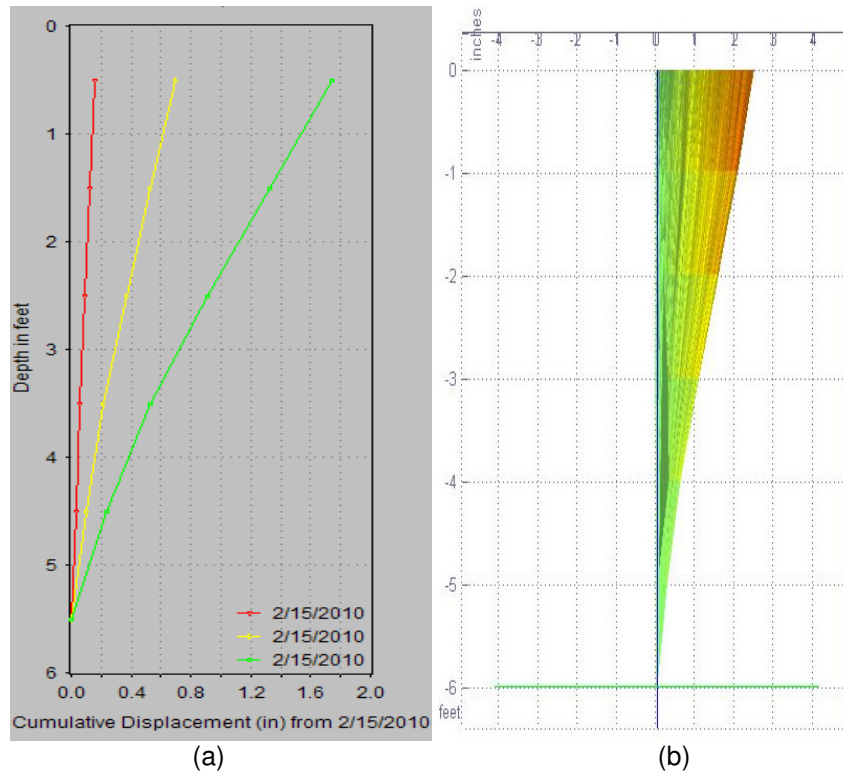
Figure 5.22 Test Shaft (1 ft diameter x 6 ft depth) Displacement Data:
(a) Inclinometer Data (b) MEMS-SAA Readings (c) Ultimate Load versus Displacement
Comparison Plots(Winter Condition)
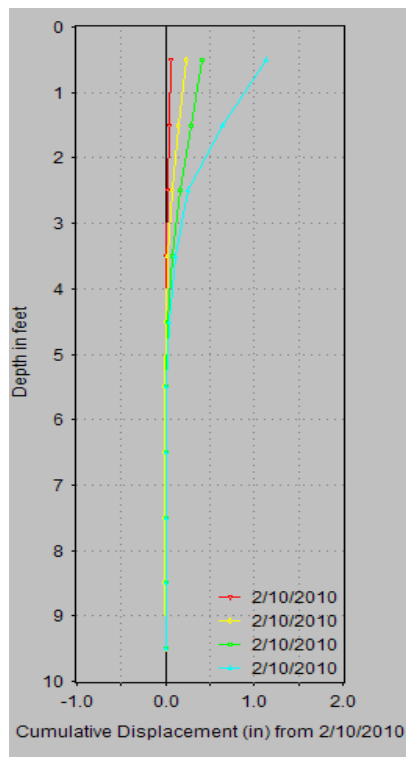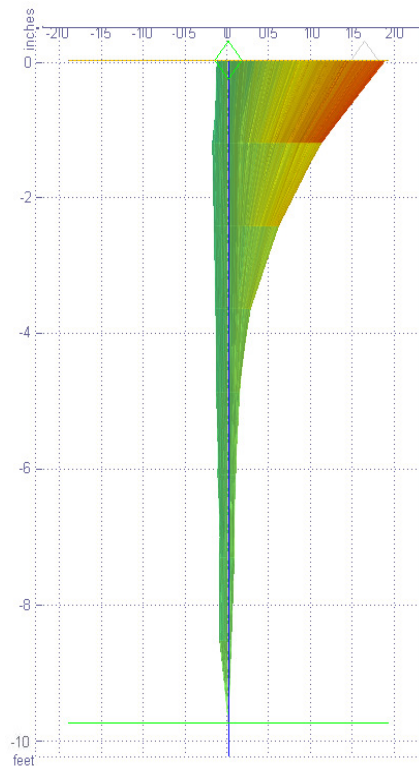
(a)   (b)
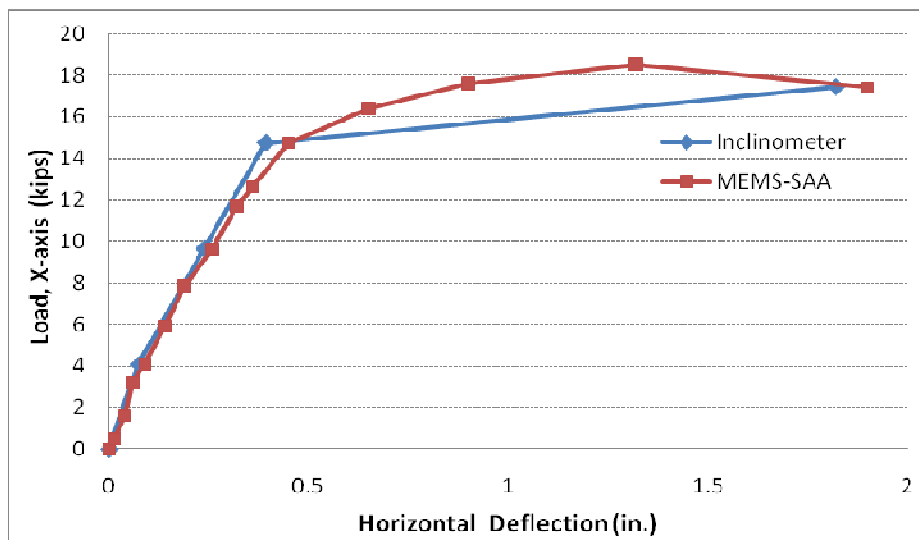
(c)

Figure 5.23 Test Shaft (1 ft diameter x 10 ft depth) Displacement Data:
(a) Inclinometer Data (b) MEMS-SAA Reading, (c) Ultimate Load versus Displacement
Comparison Plots (Winter Condition)
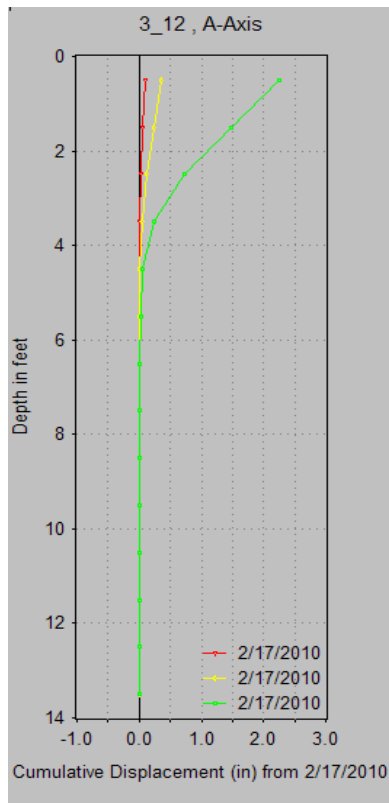
(a)
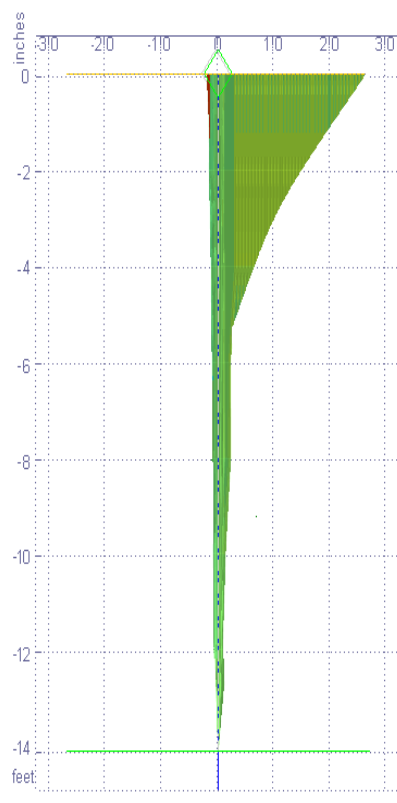
(b)
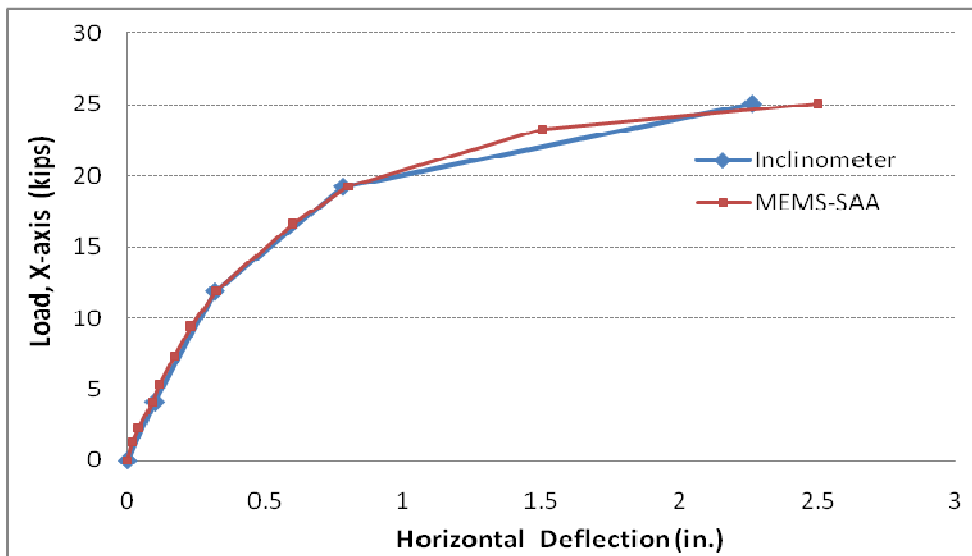
(c)

Figure 5.24 Test Shaft (1 ft diameter x 14 ft depth) Displacement Data:
(a) Inclinometer Data (b) MEMS-SAA Readings (c) Ultimate Load versus Displacement
Comparison Plots(Winter Condition)
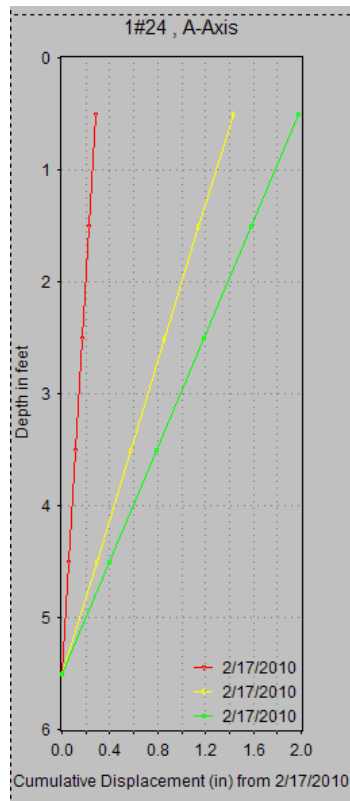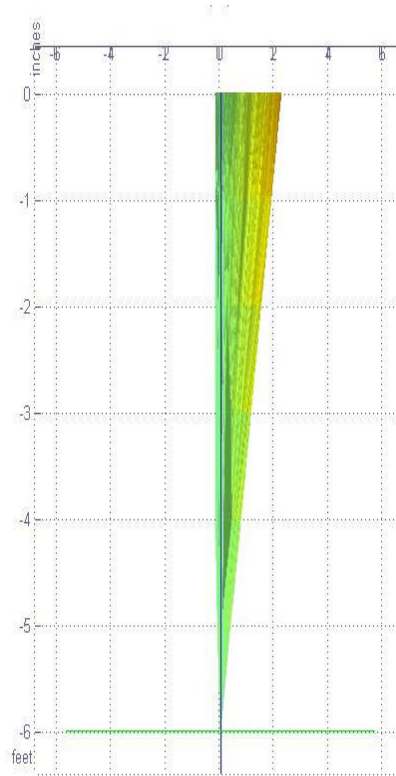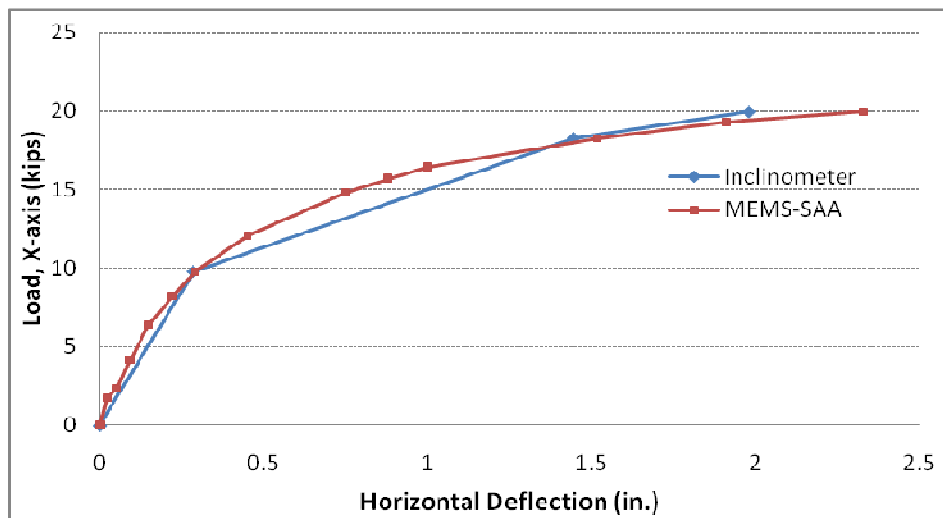
Figure 5.25 Test Shaft (2 ft diameter x 6 ft depth) Displacement Data:
(a) Inclinometer Data (b) MEMS-SAA Readings and (c) Ultimate Load versus Displacement
Comparison Plots (Winter Condition)

(a)

(b)

(c)
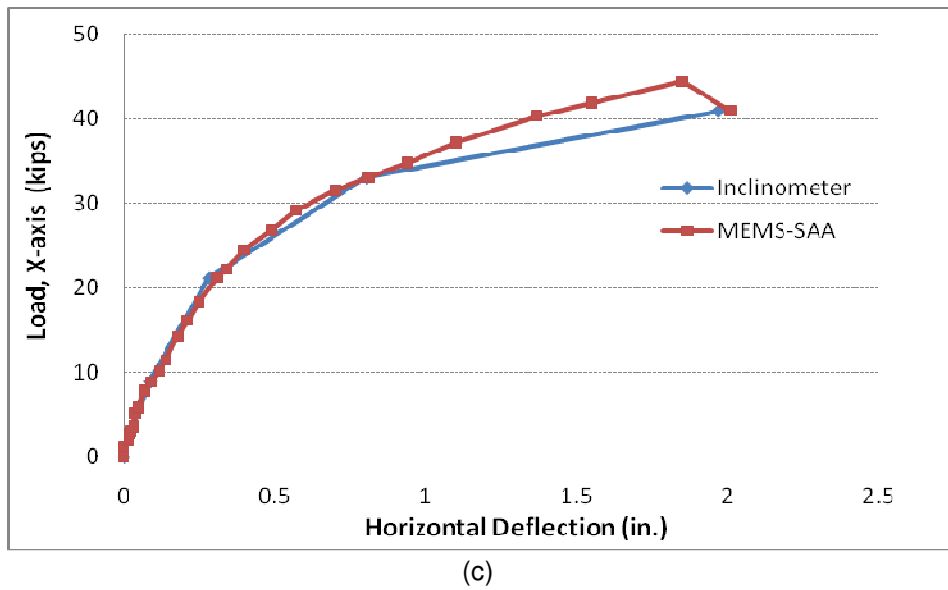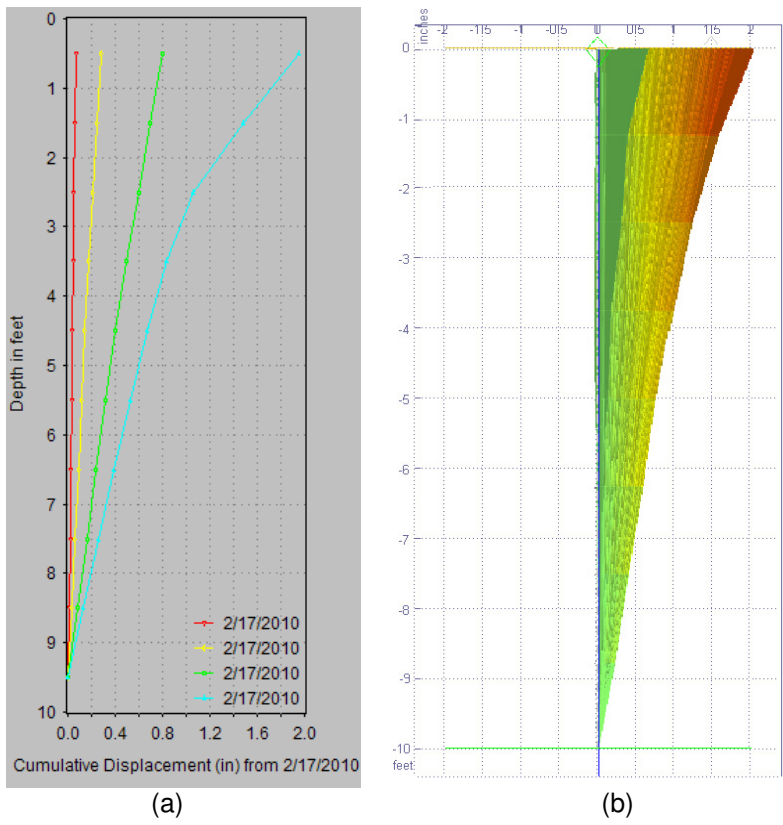
Figure 5.26 Test Shaft (2 ft diameter x 10 ft depth) Displacement Data:
(a) Inclinometer, (b) MEMS-SAA, and (c) Ultimate Load versus Displacement Comparison
(Winter Condition)

146
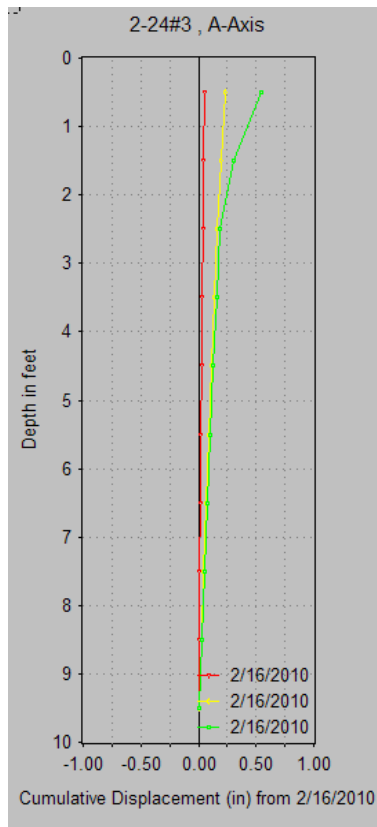
(a)
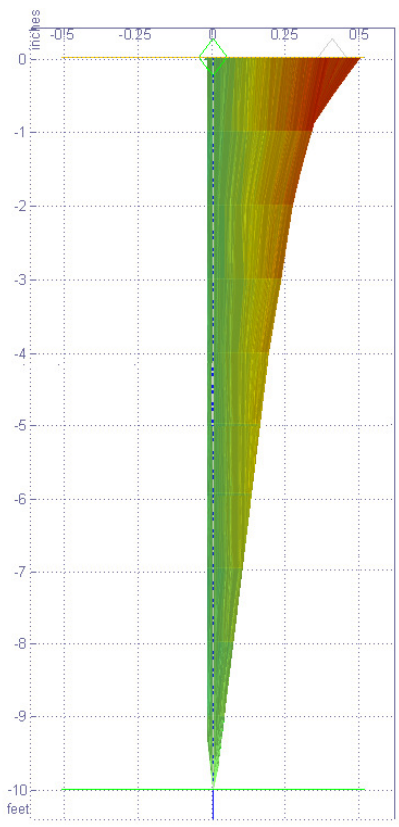
(b)
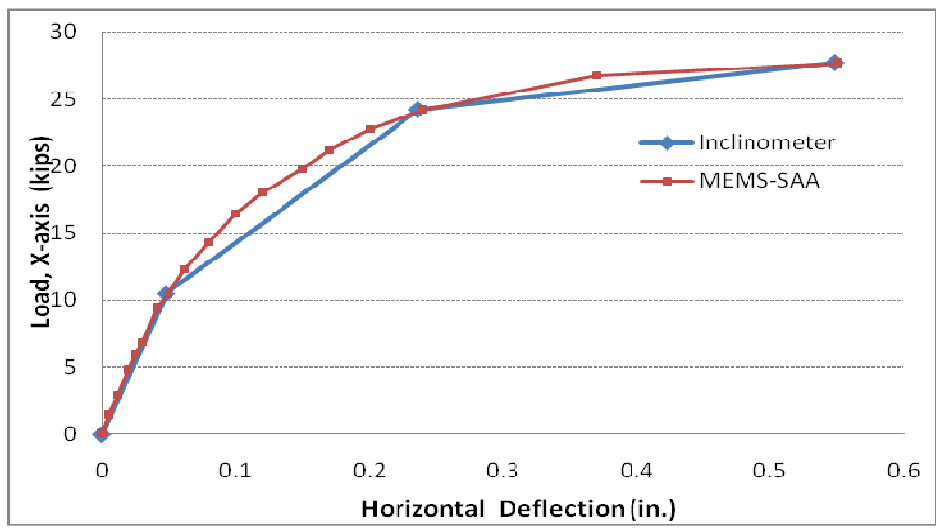
(c)

Figure 5.27 Test Shaft (2 ft diameter x 10 ft depth) Displacement Data:
(a) Inclinometer Data (b) MEMS-SAA Readings, and (c) Ultimate Load versus Displacement
Comparison Plots(Winter Condition)

(a)

(b)

(c)
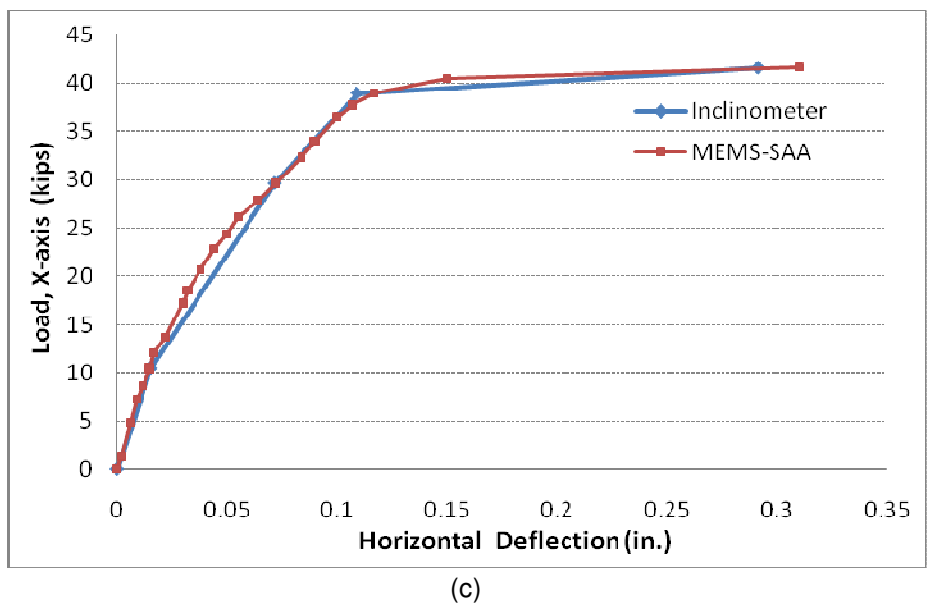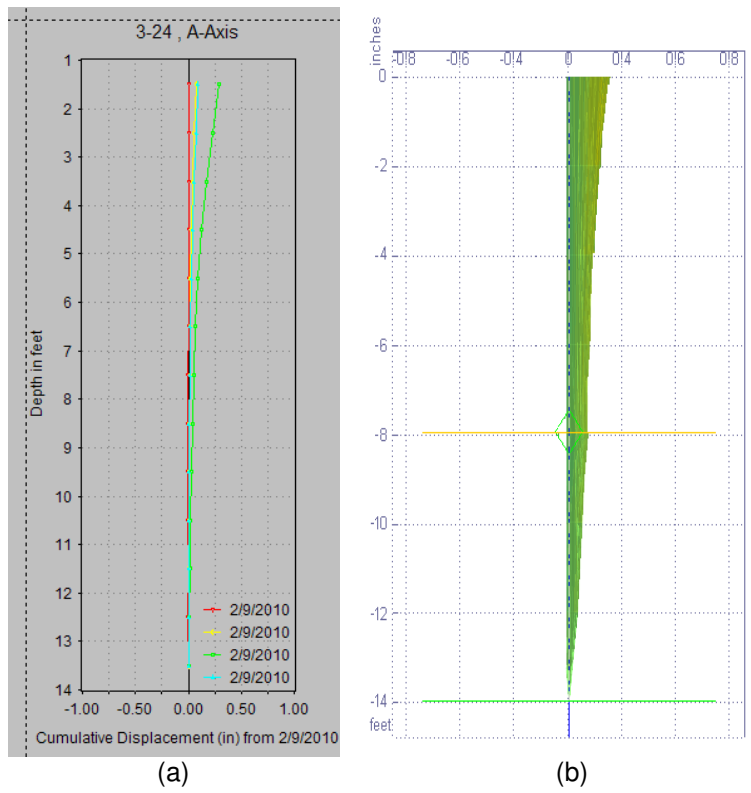
Figure 5.28 Test Shaft (2 ft diameter x 14 ft depth) Displacement Data:
(a) Inclinometer Data (b) MEMS-SAA Readings and (c) Ultimate Load versus Displacement
Comparison Plots(Winter Condition)
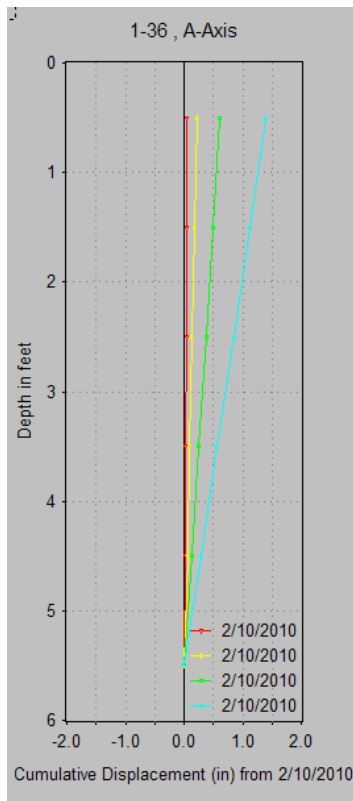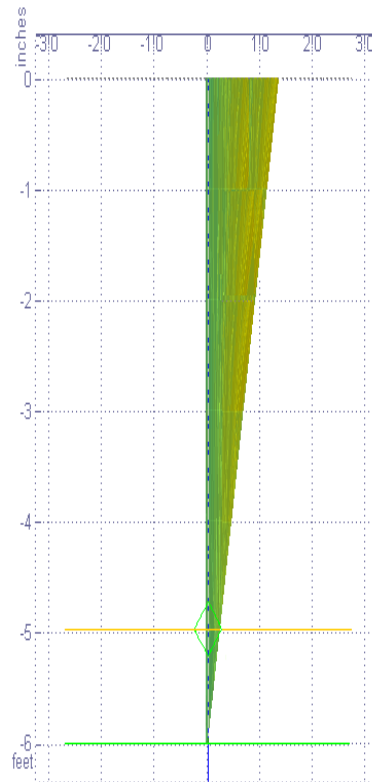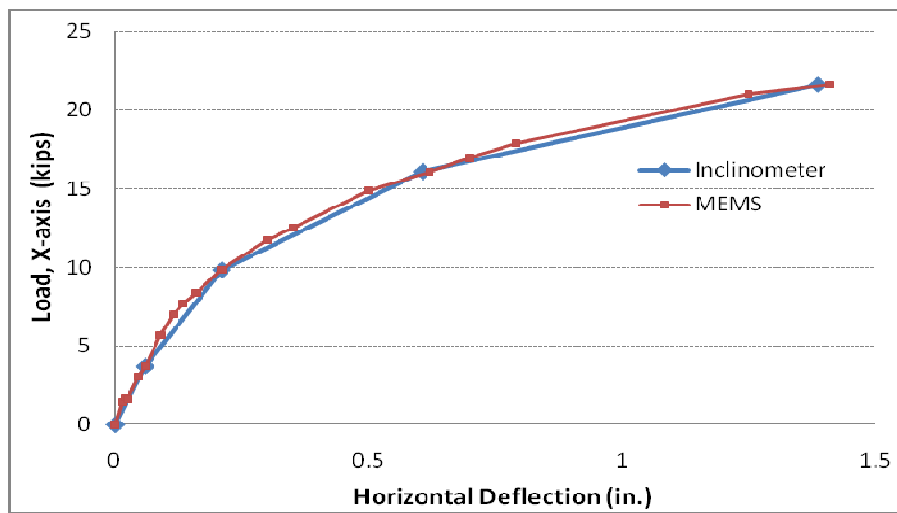
Figure 5.29 Test Shaft (3 ft diameter x 6 ft depth) Displacement Data:
(a) Inclinometer Data (b) MEMS-SAA Readings and (c) Ultimate Load versus Displacement
Comparison Plots(Winter Condition)
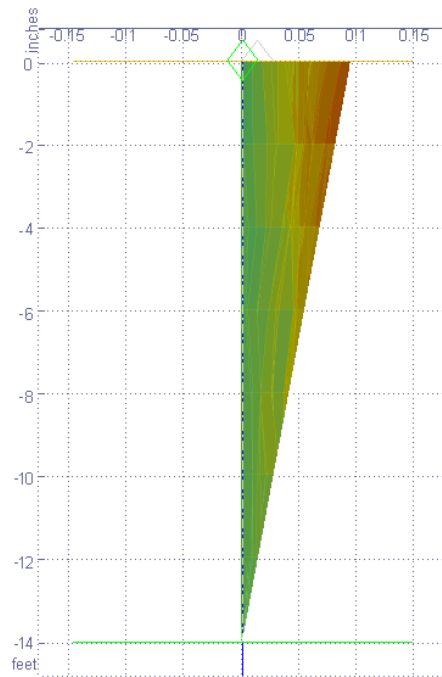
(a)
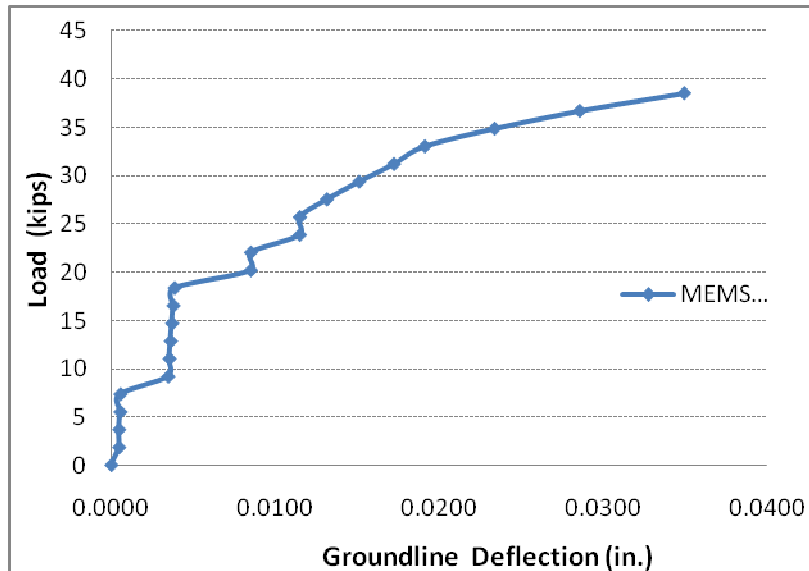
(b)

Figure 5.30 Test Shaft (3 ft diameter x 14 ft depth) Displacement Data:
(a) MEMS-SAA Readings (b) Ultimate Load versus Displacement Comparison
(Winter Condition)
Note: OnlyMEMS-SAA data can be provided.

150

Table 5.1 summarizes the ultimate inclined load results at failure and inclined loads at the specific displacements; 0.5 in. (12.5 mm) or 0.75 in (19.0 mm) for both the summer and winter conditions. These test results are analyzed for the development of design charts and tables for drilled shafts subjected to inclined load conditions.

Table 5.1 Summary of Loads at Lateral Movements of 0.50 in., 0.75 in. and at Failure

	Shaft No.	Diameter ft (m)	Depth ft (m)	Measured Load in kips (kN)		
				@0.50 in (12.5 mm)	@0.75 in (19.0 mm)	@ Failure (Ultimate Load)
Winter	1	1 (0.3)	6 (1.8)	8.4 (37.2)	9.6 (42.6)	15.0 (66.9)
	2	1 (0.3)	10 (3.0)	15.1 (67.2)	16.9 (75.2)	17.4 (77.5)
	3	1 (0.3)	14 (4.2)	15.0 (47.6)	18.5 (61.8)	26.0 (84.7)
	4	2 (0.6)	6 (1.8)	12.6 (56.1)	14.8 (65.8)	19.9 (88.5)
	5[A]	2 (0.6)	10 (3.0)	-	-	27.7 (123.2)
	6	2 (0.6)	10 (3.0)	26.9 (119.7)	32.1 (142.6)	41.0 (182.2)
	7	2 (0.6)	14 (4.2)	41.6 (185.0)	Failed Already	41.6 (185.0)
	8	3 (0.9)	6 (1.8)	14.9 (66.1)	17.8 (79.0)	22.5 (100.0)
	9[B]	3 (0.9)	14 (4.2)	-	-	35.6 (158.2)
Summer	1	1 (0.3)	6 (1.8)	15.0 (66.9)	-	15.0 (66.9)
	2	1 (0.3)	10 (3.0)	25.0 (111.2)	26.1 (116.1)	26.5 (117.7)
	3	2 (0.6)	10 (3.0)	40.5 (180.3)	-	40.5 (180.3)

Note: [A] denotes concrete material failure and [B] denotes excessive channel section yielding

5.5.3.2 Inclinometer Displacement Plots for Influence Zone from Test Shafts

To evaluate the influence of the reaction shaft movements, if any, on the load test results of test shafts, inclinometer casings located between the reaction and test shafts were used to record soil movements during selected load applications. In these measurements, the movements of the surrounding soil in winter condition were focused because the stiffness of soil

in winter condition will be soft, and this may have more influence on the results of test drilled shafts. Additional inclinometer survey readings were taken at the middle point and twice the diameter point from the test shaft. These results are shown in Figures 5.31 – 5.38 depicting all the movement of test shafts. Table 5.1 summarizes the maximum lateral movement in the influence zone between the reaction and test shafts due to the load applied.
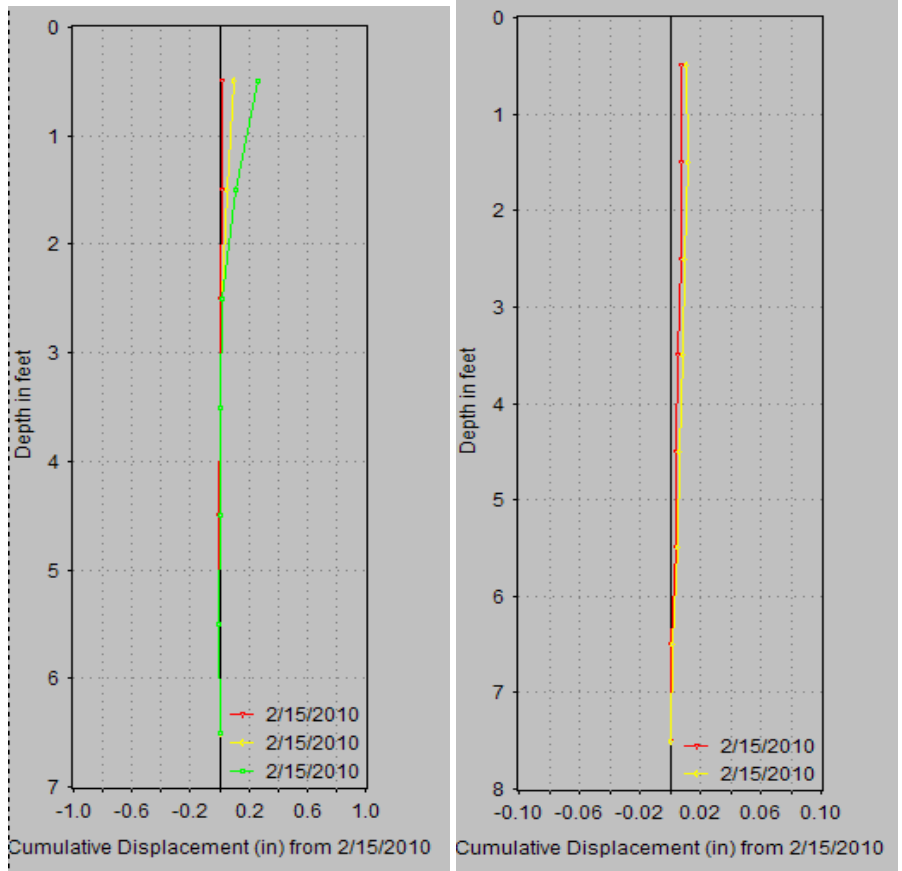
(a)   (b)

Figure 5.31 Displacement Data of Surrounding Soil of Test Shaft (1 ft diameter x 6 ft depth)
(a) Inclinometer Data at 2D Location from Test Shaft
(b) Inclinometer Data at the Middle of Test Shaft and Reaction Shaft

152
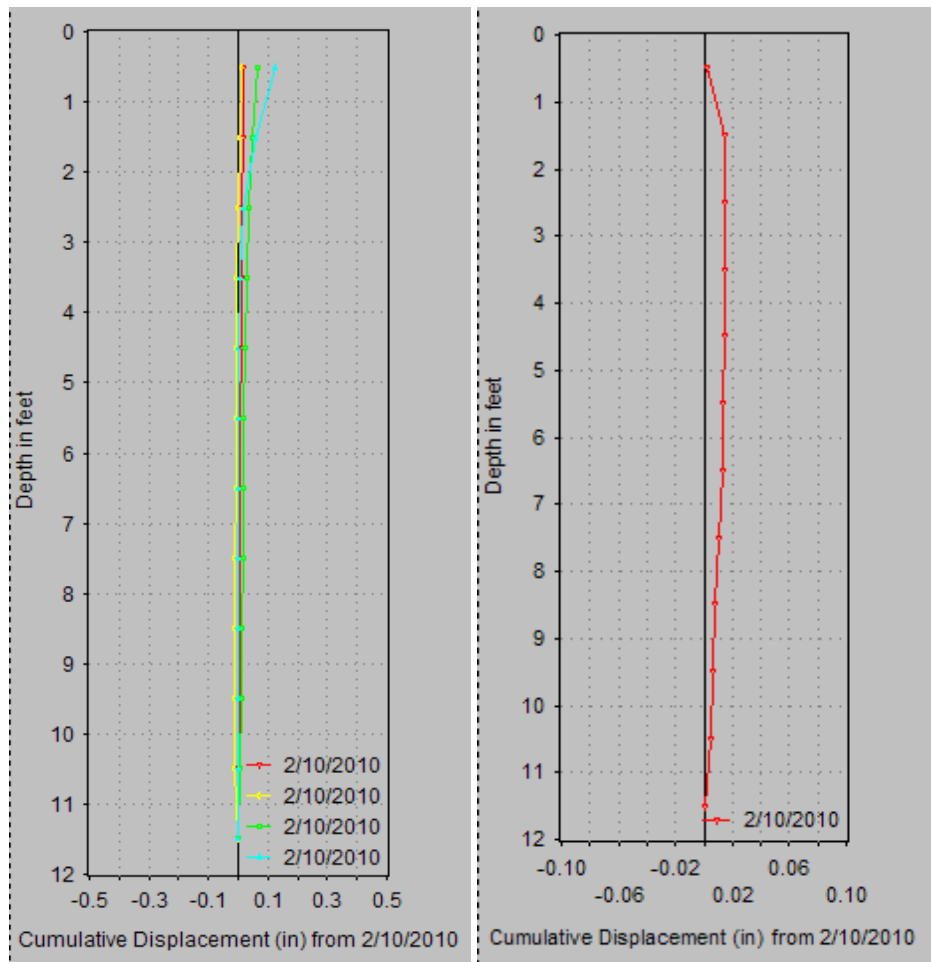
(a)   (b)

Figure 5.32 Displacement Data of Surrounding Soil of Test Shaft (1 ft diameter x 10 ft depth):
(a) Inclinometer Data at 2D Location from Test Shaft
(b) Inclinometer Data at the Middle of Test Shaft and Reaction Shaft

153
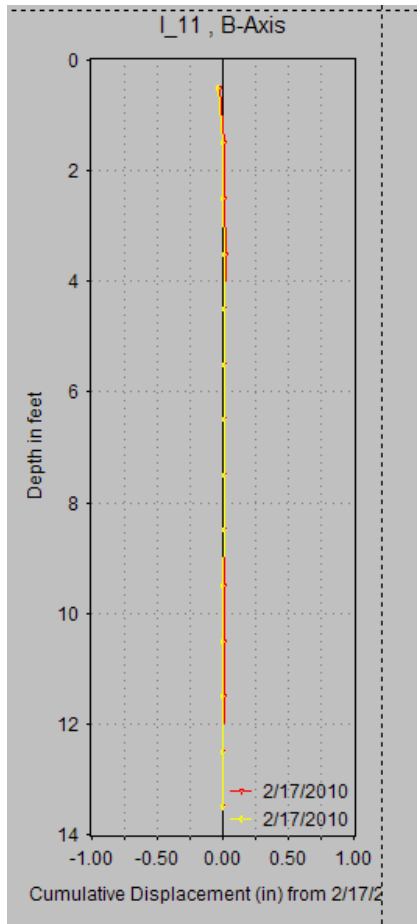
Figure 5.33 Displacement Data from Inclinometer Surveys of Surrounding Soil of Test Shaft
(1 ft diameter x 14 ft depth) at the Middle of Test and Reaction Shafts

154
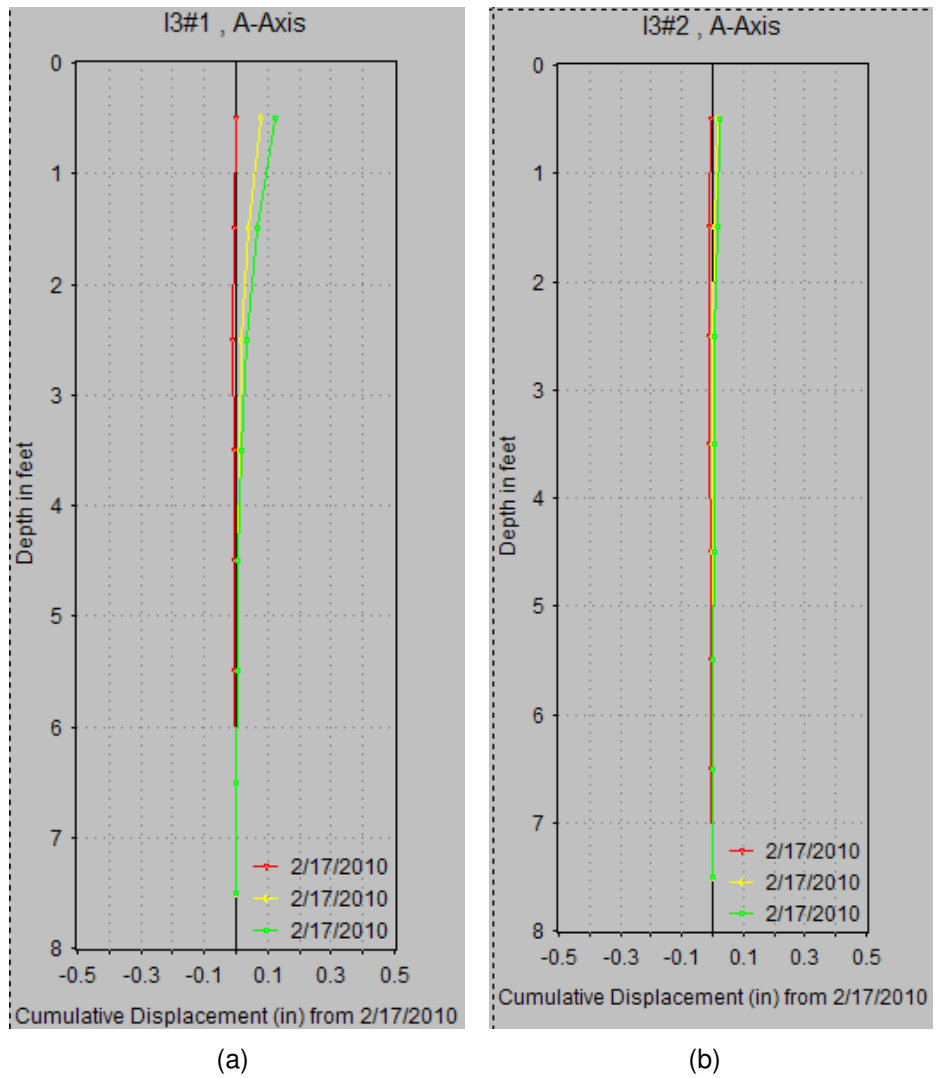
Figure 5.34 Displacement Data of Surrounding Soil of Test Shaft (2 ft diameter x 6 ft depth):
(a) Inclinometer at 2D of Test Shaft
(b) Inclinometer at the Middle of Test Shaft and Reaction Shaft
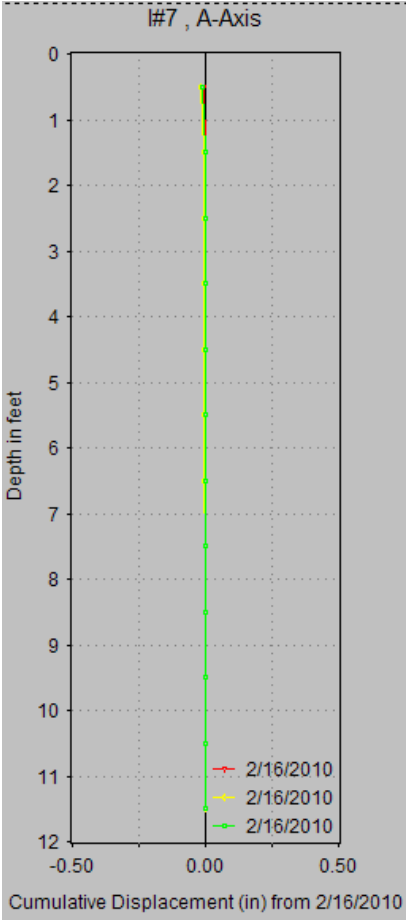
Figure 5.36 Displacement Data from Inclinometer of Surrounding Soil of Test Shaft#1 (2 ft diameter x 10 ft depth) at the Middle of Test Shaft and Reaction Shaft
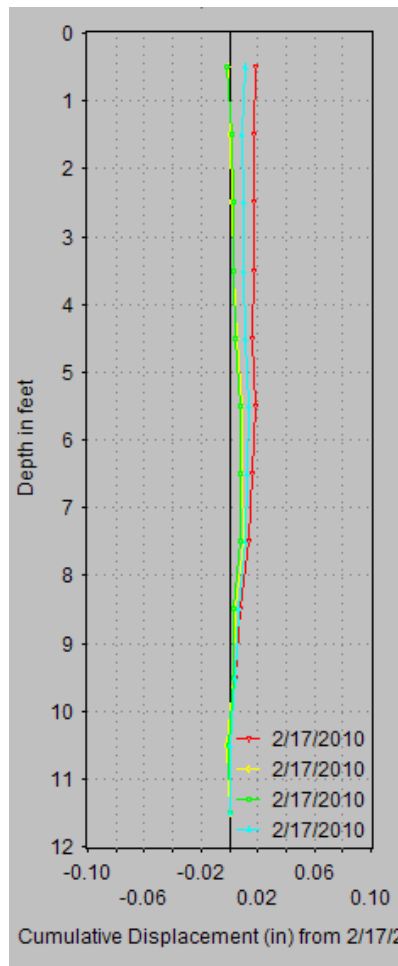
Figure 5.35 Displacement Data from Inclinometer of Surrounding Soil of Test Shaft#2
(2 ft diameter x 10 ft depth) at 2 times Diameter of Test Shaft
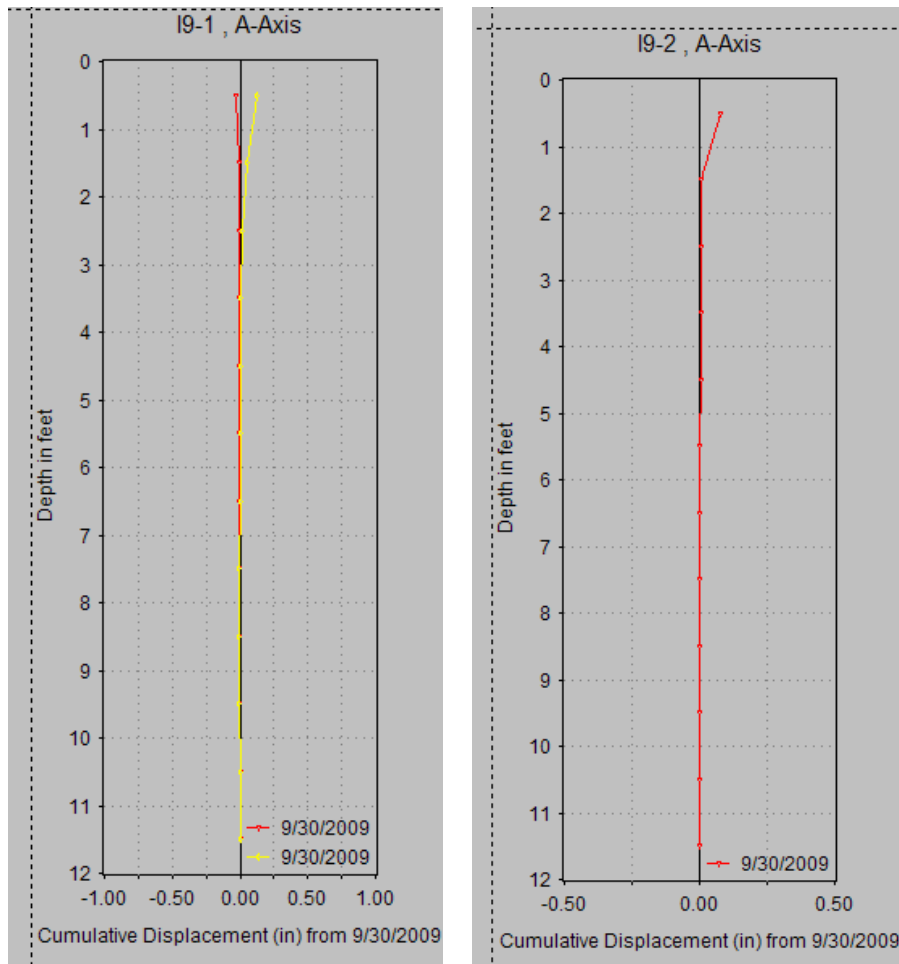
Figure 5.37 Displacement Data of Surrounding Soil of Test Shaft (2 ft diameter x 14 ft depth): (a) Inclinometer at 2D of Test Shaft and (b) Inclinometer at the Middle of Test Shaft and Reaction Shaft
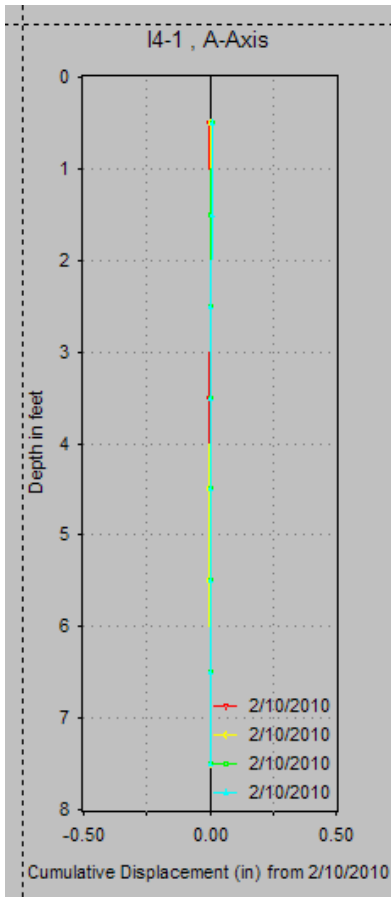
Figure 5.38 Displacement Data from Inclinomter of Surrounding Soil of Test Shaft
(3 ft diameter x 6 ft depth) at the Middle of Test Shaft and Reaction Shaft

Table 5.2 Examples of Maximum Lateral Movement in the Influence Zone
Due to the Load Applied to the Shafts in Winter Condition

Dimension Diameter x Depth ft x ft (m x m)	Lateral Movement at 2 Times Diameters from Test Shaft in. (mm)	Lateral Movement at Midpoint between Reaction and Test Shaft in. (mm)
1 x 6 (0.3 x 1.8)	0.27 (6.86)	0.016 (0.40)
1 x 10 (0.3 x 3)	0.12 (3.05)	0.017 (0.43)
1x 14 (0.3 x 4.2)	N.A.	0.020 (0.51)
2 x 6 (0.6 x 1.8)	0.12 (3.05)	0.017 (0.43)
#1_2 x 10 (0.6 x 3)	N.A.	0.010 (0.25)
#2_2 x 10 (0.6 x 3)[A]	N.A.	0.018 (0.46)
2 x14 (0.6 x 4.2)	0.11 (2.79)	0.010 (0.25)
3 x 6 (0.9 x 1.8)	N.A.	0.016 (0.40)
3 x 14 (0.9 x 4.2)	N.A.	N.A.

Note: [A] denotes concrete material failure and N.A. means no construction of inclinometer at that point

In summary, the inclinometer results showed larger lateral movements close to test shaft location. For the inclinometer results recorded at the middle point between reaction and test drilled shafts showed small movements. Thus, it can be concluded that the movement are small and hence no influence of movements between test and reaction shafts.

5.5.3.3 MEMS-SAA Comparison Plots (Summer versus Winter)

From the continuous data recorded by the MEMS-SAA system, the data collected during the summer (dry season) and the winter condition (wet season) for the three (3) test shafts are plotted in Figures 5.39 through 5.41.
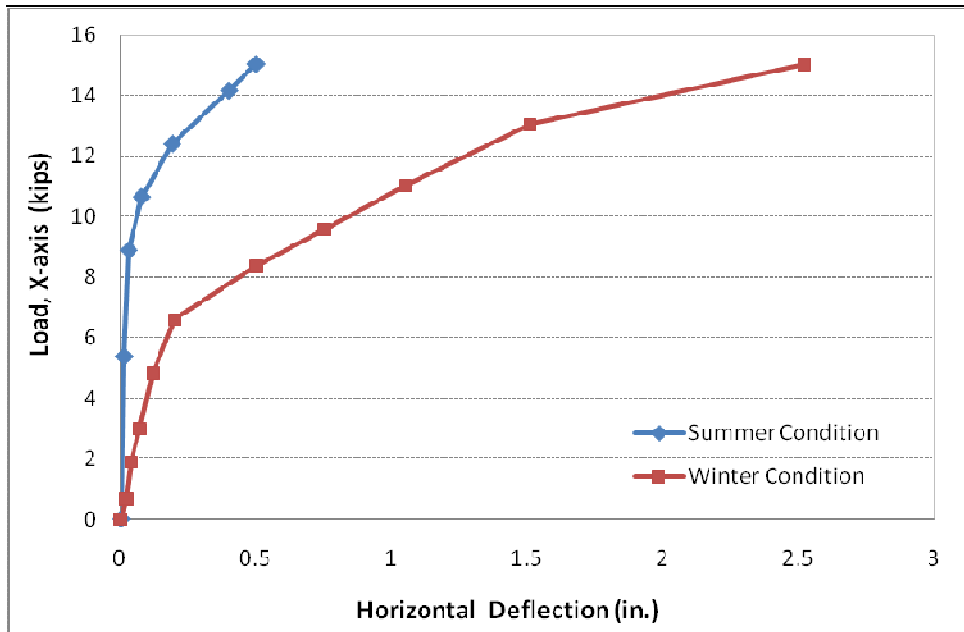
Figure 5.39 MEMS-SAA Plots for Summer and Winter Condition of 1 ft (0.3 m) diameter x 6 ft (1.8 m) depth
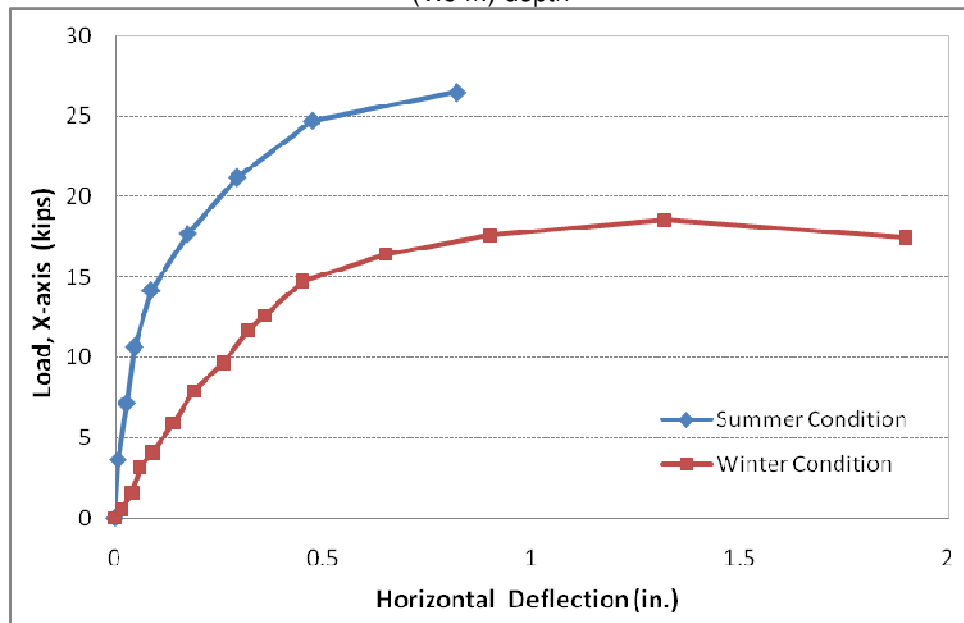
Figure 5.40 MEMS-SAA Plots for Summer and Winter Condition of 1 ft (0.3 m) diameter x 10 ft (3.0 m) depth

161
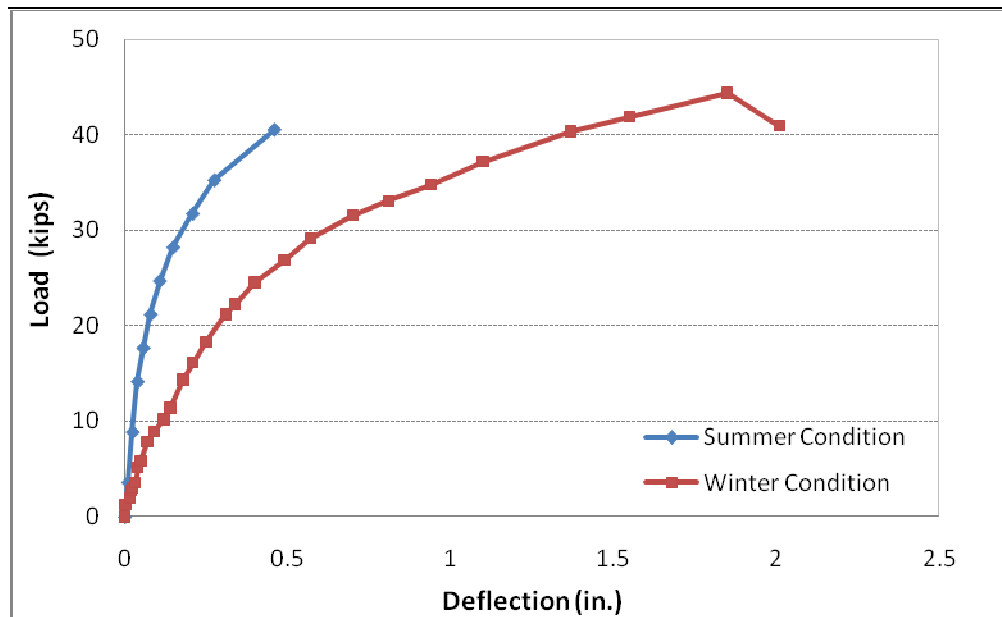
Figure 5.41 MEMS-SAA Plots for Summer and Winter Condition of 2 ft (0.6 m) diameter x 10 ft (3.0 m) depth

In the above figures, the results show that there was larger deflection (along the axis of the shaft) of the test shafts in the winter condition than in the summer condition. Also, the failure results of the test shafts (Figures 5.37 – 5.39) showed a brittle failure mode in the summer condition while the test shafts in the winter condition showed a semi-flexible failure mode. From Figures 5.37 – 5.39, for the same lateral deflections, the drilled shafts tested in the summer condition provided higher capacities.

Figures 5.42 and 5.43 show the photos of the distressed drilled shafts following load testing. Majority of the drilled shafts experienced large lateral deformation as seen by the gaps between shaft and the adjacent soil. In one case the foundation cracking due to concrete material failure was observed. Hence it can be mentioned that the failures of drilled shafts are governed by the large movements of soils around the shaft.

Figure 5.42 Test Shaft Displacements in Summer Condition

Figure 5.43 Test Shaft Displacement in Winter Condition

5.5.3.4 Vertical Movement from Dial Gage and Standard Survey Equipment

Due to the applied inclined loading on the test shaft, vertical movement of the same shaft was recorded. Table 6 presents the summary of vertical deflection results at ultimate loads for winter and summer conditions. The vertical deflection was measured at the center of test drilled shaft compared with a reference level established at the ground surface by using dial gage and standard survey equipments.

Table 5.3 Summary of Vertical Movements at Failure Loads (Measured from Ground Surface)

	Shaft No.	Diameter, ft (m.)	Depth, ft (m.)	Vertical Load Component, kips (kN)	Vertical Movement, in (mm)
Winter	1	1 (0.3)	6 (1.8)	4.34 (19.3)	0.29 (7.37)
	2	1 (0.3)	10 (3.0)	5.11 (22.7)	0.16 (4.00)
	3	1 (0.3)	14 (4.2)	7.22 (32.1)	0.15 (3.76)
	4	2 (0.6)	6 (1.8)	5.76 (25.6)	0.23 (5.84)
	5[A]	2 (0.6)	10 (3.0)	8.01 (35.6)	0.00 (0.05)
	6	2 (0.6)	10 (3.0)	11.84 (52.6)	0.09 (2.34)
	7	2 (0.6)	14 (4.2)	12.02 (53.4)	0.03 (0.65)
	8	3 (0.9)	6 (1.8)	6.23 (27.7)	0.19 (4.88)
	9[B]	3 (0.9)	14 (4.2)	10.69 (47.5)	0.00 (0.002)
Summer	1	1 (0.3)	6 (1.8)	4.34 (19.3)	0.11 (2.91)
	2	1 (0.3)	10 (3.0)	7.65 (34.0)	0.05 (1.27)
	3	2 (0.6)	10 (3.0)	11.70 (52.0)	0.00 (0.09)

Note: [A] denotes concrete material failure and [B] denotes excessive channel section yielding

These results indicate that the size of the drilled shaft has a direct influence on the vertical movements of test shafts. Figure 5.44 present vertical components of load-deflections of three different shafts for and these results indicate that the larger diameter shaft has experienced smallest vertical movement which is attributed to higher uplift capacity of the large shafts due to high self weight of the shaft. Figure 5.45 compares the vertical movements of same sized shafts tested in summer and winter and it indicates that the test shaft experienced higher movement in winter than in summer. Also, the vertical movements were recorded only when the vertical component of the inclined loads reached 1.12 kips (5 kN) or above, which suggest that the overall deflections of the test shafts are contributed by the lateral movements.
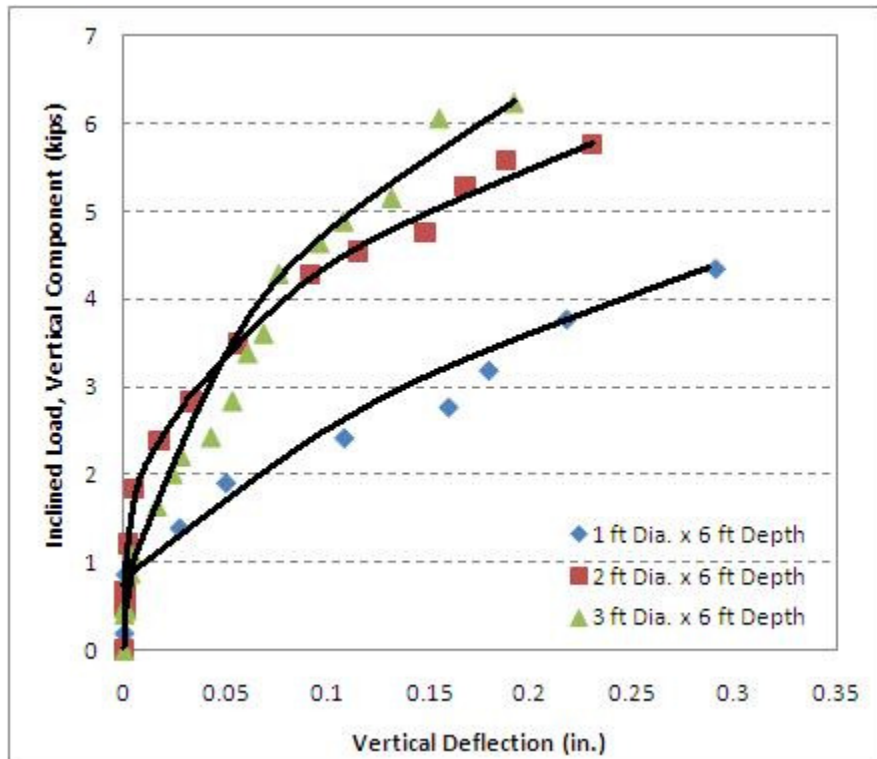
Figure 5.44 Load Test Results of Test Shafts of Three Different-Size Diameters for Vertical Deflection (Winter)

165
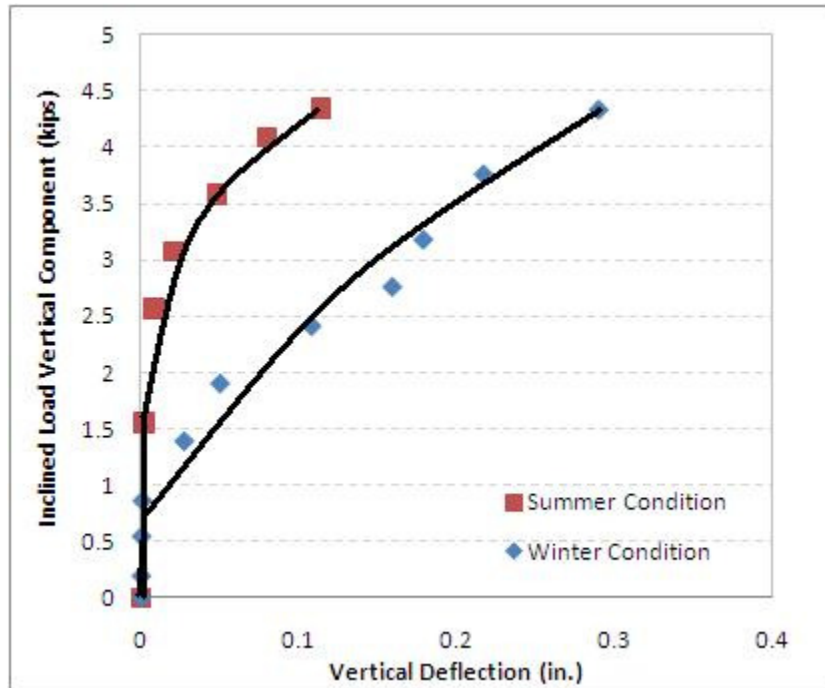
Figure 5.45 Vertical Deflection Comparison for Summer and Winter Conditions of 1 ft (0.3 m)
Diameter x 6 ft (1.8 m) Depth Shaft

5.6 Summary of Test Results

As shown in Figure 5.46, the test drilled shafts experienced various failure patterns with most of them showing the large movements of the shafts away from the adjacent soil. Overall, the load test results show that the test setup and field tests conducted were able to capture the failure patterns that were transpired in the original drilled shaft foundations built to support the cable barrier systems.

(a)

(b)

Figure 5.46 Failures of Test Shafts from Inclined Loading Tests: a) Vertical Movement of Test Shaft and b) Overview of The Failure

All drilled shafts were tested under static inclined loading and the data recorded was fully analyzed to formulate acceptable design methods for drilled shafts under the inclined tensile loads. The conclusions based on the lateral load results and analyses are shown in the following:

1. The designed test setup was successfully constructed and used to apply inclined load tests on various sized drilled shafts. Tests provided results that are well within the trends expected for test shafts of different dimensions. Test results and inclinometer data showed no effects of yielding or lateral movement from reaction shaft recorded during field load tests on large sized drilled shafts. This indicates that the current standard approach of using a twenty times the diameter of smaller shafts is acceptable in the design of reaction and test drilled shaft system in the field.

2. The drilled shafts tested in the summer and winter conditions showed major variations in their load versus displacement behaviors. The test shafts in the winter condition experienced larger lateral and vertical movements. The major contributor to differences in the summer (dry) and winter (wet) test conditions was the softening of soil response to loading due to moisture ingress in the shallow soil layers. Also, the nature of the high-plasticity clay in undergoing larger vertical movements in Winter due to soil expansion from the elevated moisture content levels. Overall, the load-lateral displacement pattern of drilled shafts in the winter condition showed semi-brittle response (displacements reaching plateau conditions) whereas the same displacements of the test shafts in the summer condition is close to rigid brittle or abrupt failure pattern. The variation was attributed to stiffness of the soils at these winter and summer conditions.

3. The percent loss of the tensile loads applied at the reaction shafts and the loads experienced at the test shafts is less than 10%, indicating that there was no major friction loss during load testing of the test shafts. The recorded failures of all test shafts matched with the original distressed shafts visually observed in the Winter of 2006-2007. This indicated that this field inclined load testing was successful in simulating the loading mechanisms that transpired in the original distressed shafts.

4. The load-deformation patterns of test shafts were recorded by the MEMS-SAA probe, and these results showed very good agreement with those recorded with the inclinometer system embedded in the test shafts. The major advantage of the MEMS-SAA system was realized when it provided a complete load-displacement data collection process including the final inclined load and lateral displacement near failure conditions. This is possible due to the use of the in-place and flexible MEMS-SAA probe which was able to capture the complete loading profile at the same time allowing users to retrieve back the probe after the test.

5. The recorded failures of all test shafts matched with the original distressed shafts visually observed in the winter of 2006-2007. This indicated that this field inclined load testing was successful in simulating the loading mechanisms that transpired in the original distressed shafts.

The next chapter presents numerical and analytical modeling of the present test results.

CHAPTER 6

ANALYSIS OF TEST RESULTS

6.1 Introduction

This chapter presents the analyses of field load test results which can be separated into two parts, analytical and numerical analysis. For the analytical analysis using lateral load and uplift models, the measured inclined loads are separated into horizontal and vertical components. These forces are then compared with the predicted uplift and lateral capacities and based on these comparisons, necessary correction factors are introduced. For numerical analysis, finite element modeling (FEM) based ABAQUS software is used to model the field load testing conditions on the test shafts. Results are analyzed to evaluate the behaviors of drilled shafts under this unique loading.

6.2 Analysis of Load Test Results

In order to generate the design charts, it is necessary to analyze the present test results with existing analytical and numerical models and find the appropriate models. Since the applied load has both lateral and vertical uplift type force components, the present test results are separated into two force components. Then the loads are simulated with the available lateral and vertical uplift load analyses methods to predict the lateral load and uplift loads for the same test shafts. Saturated soil layer properties are used in this analysis. The load predictions are compared with the field load test results. Necessary modifications to the analyses are developed as a part of this analysis.

Later, the modified models for uplift capacity and lateral load predictions are used to determine the inclined loads for various drilled shaft dimensions and soil conditions. These results are used to develop the design charts that can be used to design the foundations to support the median cable barrier systems. Designs are developed for worst case scenarios i.e.

simulating below freezing temperatures in the environment and full saturation in soils, included all of the soil properties and load results acquired in the winter condition.

The measured inclined loads were first split into lateral and vertical uplift components and then analyses are done using the following methods.

1. Vertical uplift load models using Das and Seely (1982) and O'Neill and Poormoayde (1980), were analyzed and comparisons with the measured ultimate vertical uplift load component was made.

2. Based on the comparisons, the calibration factor for the vertical uplift load analysis was established.

3. Three lateral load analyses using Broms' Method (1965), Characteristic Load Methods (CLM) (1994) and p-y Method (LPILE), were performed and then comparisons with measured lateral load were attempted.

4. Calibration factor for the lateral load analysis was then established such that the modeling analysis provides the best-fit trends with the measured lateral load test results.

5. A design chart for the inclined load at the 16.1° angle is then developed based on calibration factors from the horizontal and lateral load analyses for various foundation dimensions.

6.2.1 Uplift Force Models

When drilled shafts need to resist the pulling force in the vertical axis or in the inclined directions, they need to be designed against pullout or uplift considerations. In general two models can be used to determine the uplift capacities. This study presents two models developed by Das and Seeley (1982) and O'Neill and Poormoayed (1980). In general, the total ultimate uplift capacity of a single shaft or pile can be expressed as shown in the following Eq.6.1:

171

$$P_u = P_0 + W \qquad\qquad (6.1)$$

Where P_u = Total Ultimate Uplift Capacity,

P_0 = Net Uplift Capacity, and

W = Self-Weight of the Drilled Shaft

Das and Seeley (1982) presented the following Equation for uplift force predictions. This equation was originally developed from pipe piles located in saturated clay environment. The net ultimate capacity for vertical uplifting load can be given:

$$P_0 = L \times p \times \alpha' \times c_u \qquad\qquad (6.2)$$

Where L = Depth of Shaft below the Ground,

p = Perimeter of the Shaft,

α' = Adhesion Factor, and

c_u = Undrained Shear Strength Parameter

The prediction results from the Das and Seeley model for the present test shafts are shown in Table 6.1. However, this model was developed by not considering the swell pressure data of the surrounding soils, and hence it is necessary to find a model in which swell pressure was only considered. O'Neill and Poormoayed (1980) proposed the following Equation 6.3 based on swell induced pressure. They also suggested a value of φ = 1.3 and δ_r, = 9.0° which are recommended for Texas soils.

$$f_{max} = \varphi \times \sigma'_{ho} \times Tan\,(\delta_r) \qquad\qquad (6.3)$$

Where φ = Correlation Coefficient,

σ'_{ho} = Horizontal Swell Pressure, and

δ_r = The Effective Angle of Internal Friction between Soil and Concrete

A summary of the test results between the aforementioned models compared with the actual vertical uplift components of the field load test results and these can be seen in Table 6.1.

172

Table 6.1 Summary of Ultimate Uplift Load Results Compared with the Models

Shaft No.	Diameter (ft.)	Depth (ft.)	Actual Vertical Uplift Force (kips)	Prediction of Uplift Force (kips)	
				Das and Seely (1982)	O'Neill and Poormoayed (1980)
1	1	6	4.17	6.77	1.85
2	1	10	4.83	13.98	2.30
3	1	14	7.22	19.10	2.76
4	2	6	5.52	14.90	5.06
5	2[A]	10	-	30.23	6.88
6	2	10	11.36	30.23	6.88
7	2	14	11.53	41.38	8.71
8	3	6	7.72	24.40	9.64
9	3[B]	14	-	66.85	17.84
Average Ratio (Measured/Predicted)				0.37	1.67

Note: [A] denotes concrete material failure and [B] denotes excessive channel section yielding

From Table 6.1, it can be seen that the model developed by Das and Seely (1982) has provided predictions that are different, but followed the similar trends as the actual field test results. The variations in comparisons can be attributed to the fact the field load tests were conducted at an angle and hence they are somewhat different from the true uplift conditions. Hence some variation should be expected in these comparisons. An attempt is made to introduce a correction factor by determining the average of the ratios between actual results and the predicted values. The average ratio is around 0.37 for Das and Seely model. This means that the model provides overestimated results when compared with the actual field test results.

O'neill and Poormoayed (1980) model based on swell pressures under predicted the uplift capacities and this variation is attributed to lack of complete simulation of swell pressure simulation or under prediction of true side shear component that acts on the drilled shaft

foundation. Also, it should be noted the soil saturation during winter events may not have reached larger depths.

The first model with side friction was chosen since most of the uplift was due to the tension mobilized in the cables of the barrier due to low temperature conditions which has resulted in the uplifting of the drilled shaft. This mechanical uplifting is hence suspected as one of the contributors to the distressing mechanism in the field. Otherwise, the shafts would have failed during rainfall events under normal temperature conditions which were not observed in the field. Cold temperature conditions triggered the failures more than the uplift being fully mobilized by the swelling pressures of the soils at the site. Hence, the first model that uses the side friction based analysis to estimate the total vertical force was hence considered for the design chart development.

6.2.2 Lateral Deflection and Lateral Capacity Models Consideration

6.2.2.1 Lateral Deflection Criteria

In order to analyze the lateral load component results and the use of the load to develop design charts, an appropriate criterion for lateral allowable deflection should be selected at which the loads are construed as ultimate loads. Many researchers and organizations, such as Broms, Czerniak, Kinney, Ivey and Hawkins, International Building Code (IBC) and local DOTs use different deflection values for defining the ultimate loads on the drilled shafts. Generally, deflections vary with the types of civil structures. For example, 0.25 in. deflection at the top of the shaft is used to estimate loads for foundations supporting high-rise structures whereas, for structures such as transmission towers, sign posts, and noise barriers, 0.5 in or larger deflection (can be several inches) criterion are typically followed to define ultimate loads in load tests (Chen, 2000).

Broms (1964), Czerniak (1958), Kinney (1959), Ivey and Hawkins (1966) assumed that 0.5 in. lateral deflection at ground surface is the deflection limitation for several conditions and structures. Based on the 2003 International Building Code (IBC) requirements, the ultimate

174

inclined load at 0.5 in. (12.5 mm) or 0.75 in. (19.0 mm) is considered as a failure load. For DOTs, Colorado Department of Transportation (CDOT) (2004) presented study of permissible lateral deflections, 0.6 in., 1.0 in., and 1.5 in., relating to various factor of safety values. The results show that all proposed deflections are safe and provide factor of safety values ranging from 1.20 to 4.70. However, in some cases, 1.5 in. deflection may not be able to work for wall constructions because the top of the wall may exceed the deflection requirement. Thus, they concluded that 1 in. permissible deflection at the drilled shaft head is an appropriate criterion for such walls.

As aforementioned, the criterion of lateral movement varies from 0.25 – 1.5 in. depending on the structures. In this section, both importance of the structure and efficiency of the cable barrier systems located in expansive soil area are considered in evaluating the ultimate load criteria. Maximum deflections of 0.5 and 1.0 in are considered for defining the ultimate loads for drilled shafts supporting cable barriers. Two levels are defined for ultimate loads as there is no consensus on the exact value of the deflection at which the cables serve satisfactorily. Author feels 0.5 in. is an acceptable criteria as this method result in larger and safer shafts. However such large shafts are not needed. Hence large deflection criterion of 1 in, is also considered. It should be noted that the final deflection criterion should be decided such this criterion can keep the cables from becoming slackened thereby maintaining the integrity of the cable barriers. Such systems will serve their roles in sustaining or absorbing any impact or weather induced loads without any damage. They will also protect the travelling public and mitigate the fatal accidents. However, lateral deflection at ground surface close to 1 in. can be applied in areas where non-expansive soils are encountered. Thus, in the present analysis, ultimate loads are established at both deflection criteria of 0.5 and 1.0 in., respectively.

The graphs or design charts developed for both criteria of 0.5 in. and 1 in. are shown in the next chapter. In addition, the charts with various undrained shear strengths of upper soil

strata are considered and included for designing the most suitable sizes of drilled shafts to support the ends of cable barrier system.

6.2.2.2 Lateral Capacity Models

For the models using in the analysis, many methods were used in the prediction, such as Broms' Method (1965), Characteristic Load Method (CLM) by Duncan, 1994, Strain Wedge Method by Ashour et al., 1998, and p-y Method (Com 624, FB-Pier, LPILE, etc.). However, in this study, Broms' Method, Characteristic Load Method, and the p-y Method using the LPILE program to find the best-fit trend leading to an appropriate design chart were considered. The Broms and Characteristic Load methods can provide the ultimate load values which correspond to 0.5 in. deflection criterion.

The load-deflection from the LPILE program can be compared through the ultimate load at various deflections and these results are primarily used for establishing ultimate loads at various deflection criteria. These deflections include 0.5 in. and 1 in. movements. In the LPILE analysis, the input parameters used are determined from the laboratory strength tests. The p-y curve model (soil type) is chosen such that it will match with the field soil conditions.

In this analysis, due to the top layer is thin when compared with all other soil layers and thus making the analysis simpler, both the first and second of soil layers were combined. The input parameters used are shown in Table 6.2. The results from the field tests and the models can be seen in Table 6.3 and a comparison between field test results and the models predictions is shown in Figure 6.1. The predictions from LPILE matches well with the measured results, similar to the observations recorded for Brom's method except that Brom's method has a slightly large scatter. The CLM on the other hand provided large scatter for the present shafts. It should be noted that the CLM method is preferred for long size drilled shafts and the present tested shafts are short and intermediate size.

The results from the LPILE program can be compared with the load-deflection curve from the field test results and these can be in Figure 6.2. For all the output from LPILE program,

176

the example of lateral movement, bending moment and shear force of 2 ft (0.6 m) diameter x 10

ft (3.0 m) depth drilled shaft are presented in Figure 6.3 – 6.5.

Table 6.2 Input Parameters for LPILE Analysis

Depth (ft)	p-y curve model	Effective Unit Weight (pci)	Undrained Cohesion (psi)	Strain Factor, E50
0 – 3	Soft Clay (Matock)	0.069	7.1	0.01
3 – 5	Stiff Clay w/o Free Water	0.072	11.25	0.0065
5 – 10	Stiff Clay w/o Free Water	0.080	17.45	0.005
10 - 12	Stiff Clay w/o Free Water	0.072	8.98	0.007

Table 6.3 Summary of Ultimate Lateral Results Compared with the Models at 0.5 in.

Shaft No.	Diameter (ft.)	Depth (ft.)	Field Test (kips)	Predictions of Lateral Load (kips)		
				Broms (1965)	CLM (1994)	LPILE
1	1	6	8.0	7.0	7.6	6.7
2	1	10	15.1	14.7	7.3	12.3
3	1	14	14.3	21.2	6.9	13.9
4	2	6	12.1	6.3	20.3	9.9
5[A]	2	10	-	18.4	19.5	19.2
6	2	10	25.8	18.4	19.5	19.2
7	2	14	41.6	31.6	18.5	31.7
8	3	6	14.1	5.7	39.2	12.0
9[B]	3	14	-	37.3	35.7	41.2
Average Ratio (Measured/Predicted)				1.50	1.28	1.21

Note: [A] denotes concrete material failure, and [B] denotes excessive channel section yielding
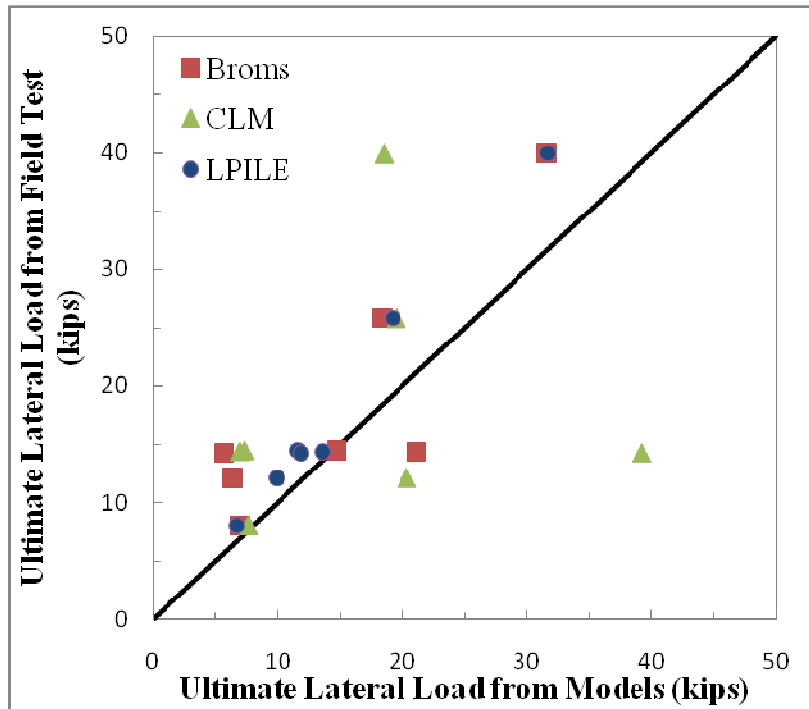
Figure 6.1 Comparisons between Ultimate Load of Field Results and Models
(Deflection – 0.5 in.)
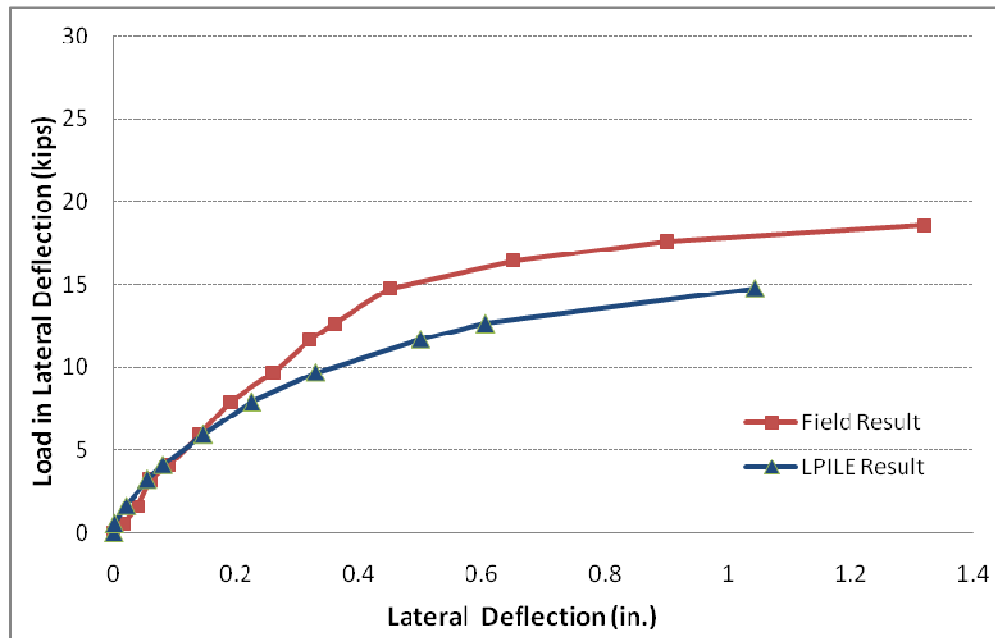
Figure 6.2 Comparison between Field Test Results and LPILE Model of the 1 ft (0.3 m)
Diameter x 10 ft (3.0 m) Depth
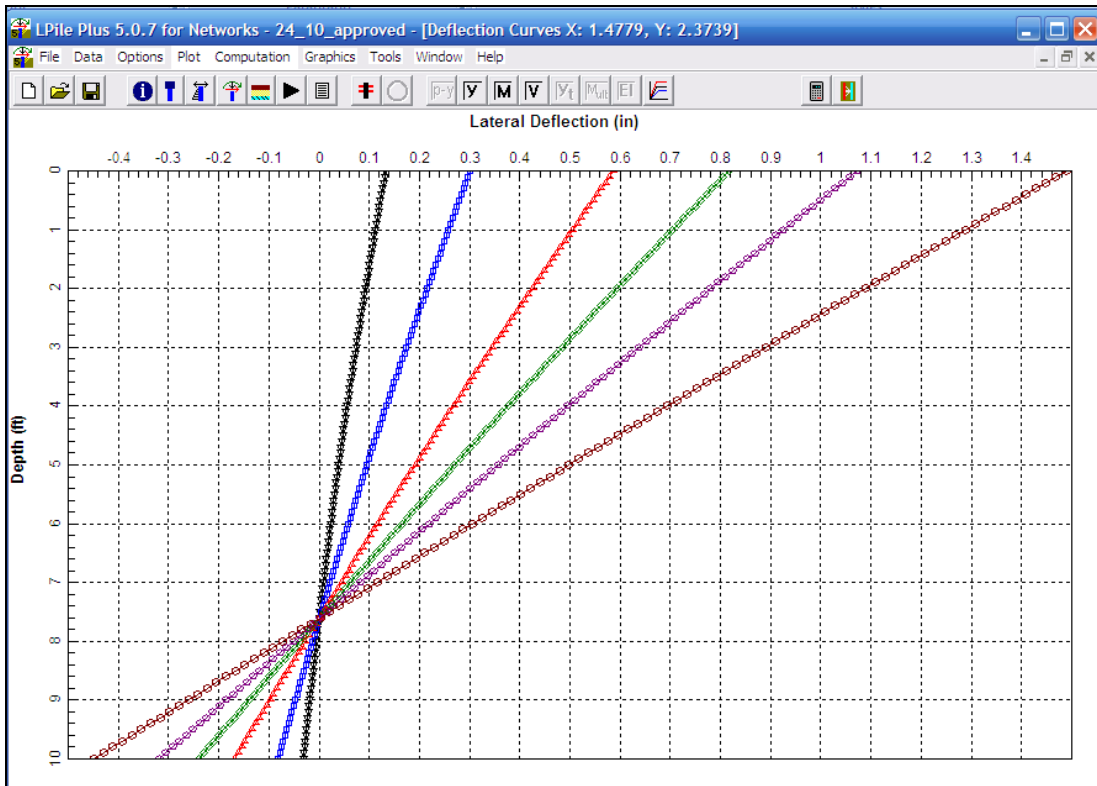
Figure 6.3 Lateral Movement Results from LPILE Program Under Given Load of the 2 ft (0.6 m) Diameter x 10 ft (3.0 m) Depth Test Shaft
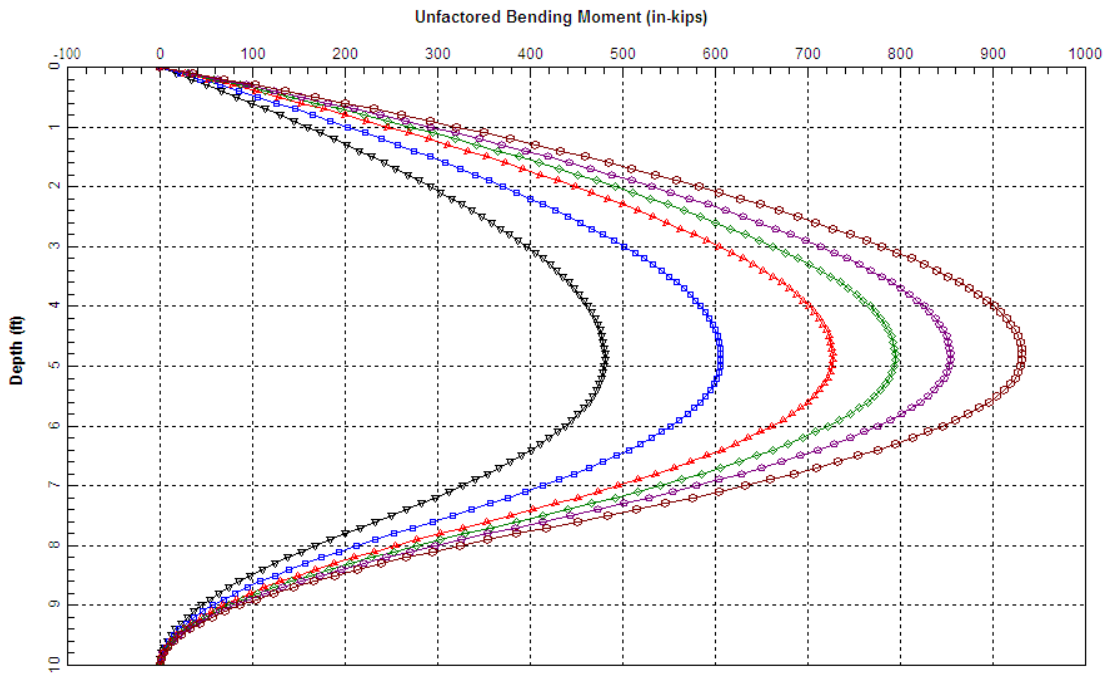
Figure 6.4 Bending Moment Results from LPILE Program Under Given Load of the 2 ft (0.6 m) Diameter x 10 ft (3.0 m) Depth Test Shaft
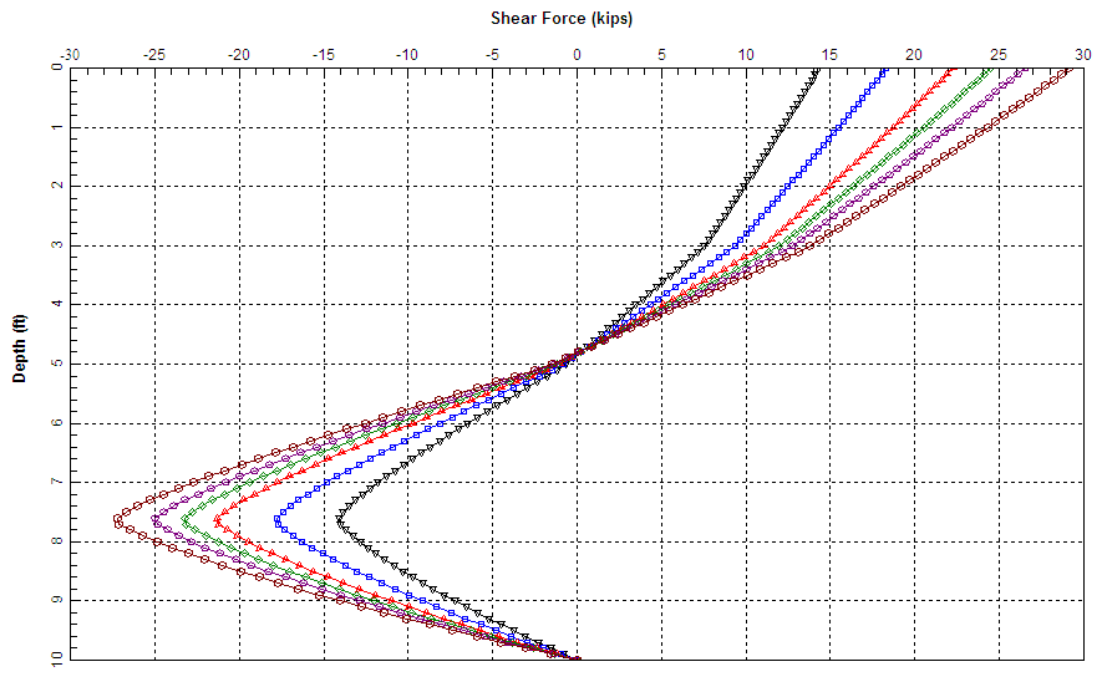
Figure 6.5 Bending Moment Results from LPILE Program Under Given Load of the 2 ft (0.6 m) Diameter x 10 ft (3.0 m) Depth Test Shaft

180

From Figure 6.1, the predicted results from LPILE show the trend close to the 1:1 line with the predicted results from the Broms and Characteristic Load Methods being more scattered. The reason that LPILE provided the results close to the field test results is a fundamental factor of this method developing the p-y curves representing the true behavior of soils by considering the non-linearity of the soil modulus. For the Broms' Method, the limitation is the soil along the depth of the drilled shaft being assumed as cohesive soil only. However, the undrained shear strength used in the calculations came from the average of the soil along with the depth.

The Characteristic Load Method has more limitations than the other methods. One limitation is that the shaft must be long enough so that the behavior is not affected to any significant degree by its' length. Another limitation is that the ultimate load could not be analyzed directly. However, in order to find the ultimate load at 0.5 in. (12.5 mm), a back calculation is required to be done. In short, the LPILE provides the predicted results closest to the actual field test results and the ratio between the actual lateral load results to the predicted load results is 1.21 and 1.20 for 0.5 and 1.0 in. respectively, which means the LPILE provided slightly lower load test results for present test shafts (Table 6.4). The reason for this is the use of undrained shear strength parameters close to saturated soil condition. Also, the loading approach in the field is not truly a lateral loading case and hence some variation should be expected.

Table 6.4 Calibration factor at different lateral deflection

Lateral Deflection Consideration	Calibration Factor (Ratio of Measured Load Results to LPILE Load Results)
at 0.50 in.	1.21
at 1.00 in.	1.20

6.3 Finite Element Modeling of Drilled Shaft Load Tests

In this chapter, finite element modeling (FEM) is performed by using ABAQUS program to simulate the drilled shaft under inclined load. Finite Element Method (FEM) have been successfully utilized to account for the effects of many practical conditions more realistically than theoretical solutions based on infinite slab and other idealized assumptions (Kuo and Huang, 2006). With the introduction of three-dimensional (3D) ABAQUS software and all the promising features, and results reported in the literature, several applications including in the areas of pavement engineering have been successfully modeled (Hammons. 1998; Kim and Hjelmstad, 2000).

Due to the complexity of the FEM modeling of complicated loading and structures, three dimensional finite-element analysis is not always easily implementable. The main objectives of this analysis are to study behavior of drilled shafts under inclined load, compare results with the field monitoring results and investigate force/stress distributions from shaft to surrounding soil. The following sections cover the analyses of these results.

6.3.1 Element Types and Bulit-in Model Used in the Analysis

In this present FEM analysis, material models used are two types, one is for concrete material model for simulating drilled shafts and the other is Mohr-Coulomb elasto-plastic soil model for surrounding soil. For soil and concrete modeling, the three dimensional 8-noded solid element, "C3D8R" is used. This element supports three translational degrees of freedom in the x, y and z directions and this means it will allow only displacements.

For the input parameters in this analysis, both elasticity and shear strength properties need to be inputted. Tables 6.5 and 6.6 present elasticity and strength properties used as input parameters for soil and concrete materials. For concrete material, only elasticity moduli properties are needed as input parameter. Soil around the shaft was divided into five layers with different thicknesses. Mohr Coulomb Plasticity model parameters were determined from the present laboratory triaxial tests on unsaturated soils close to field conditions.

182

Table 6.5 Elastic Properties of Material Models

Material	Density (pci)	Young's Modulus, E (psi)	Poisson's Ratio, μ
Soil Layer 1 (0 – 1 ft)	0.064	220	0.33
Soil Layer 2 (1 – 3 ft)	0.069	500	0.37
Soil Layer 3 (3 – 5 ft)	0.072	650	0.37
Soil Layer 4 (5 – 10 ft)	0.080	650	0.37
Soil Layer 5 (> 10 ft)	0.072	650	0.37
Concrete (Ultimate Strength 4.0 ksi)	0.087	3,605,000	0.20

Table 6.6. Shear Strength Properties for Mohr Coulomb Plasticity Model

Soil	Cohesion, c (psi)	Friction Angle	Dilation Angle
Layer 1	0	26.2	12
Layer 2	7.10	7.5	0.1
Layer 3	11.25	14.5	0.1
Layer 4	17.45	7.5	0.1
Layer 5	8.98	28.6	0.1

6.3.2 FEM Modeling Results

In the field, there are layers including silt at the top layer and clay at the bottom layer, which can affect the stress distributions in soil layers. Thus, two scenarios of FEM analyses are performed. The first one considers that the whole soil layer as a homogeneous clay layer and the second one treats the whole layer into five soil layers.

Overall, two drilled shafts, short and intermediate sized drilled shafts are simulated and analyzed here. Short shaft (1 ft diameter x 6 ft depth) and intermediate shaft (2 ft diameter x 14 ft depth) tested in winter conditions are considered for this simulation. Both shafts are modeled

with the properties mentioned in the previous section. The discretized models are presented in Figure 6.6 (short drilled shaft) and Figure 6.7 (intermediate size), respectively. In addition, the boundary conditions imparted during the analysis are shown in Figures 6.8 and 6.9. All external nodes have rollers and thus they allow lateral movements; loading as inclined similar to the field loads. In determining the horizontal and vertical deflections, the center of top drilled shaft is used as the reference point to evaluate the deflection due to loading applied. Figure 6.10 shows these results.

Overall, for the short drilled shaft simulation, a total of 3200 elements are used in the analysis, which can be separated into 216 elements for concrete drilled shaft and 2984 elements for soil around the shaft. In addition, there are 4026 nodes (323 nodes for concrete shaft and 3703 nodes for surrounding soil).

For the intermediate drilled shaft, there are 10604 elements in the analysis, which can be separated into 1088 elements for concrete drilled shaft and 9516 elements for surrounding soil. In addition, there are 12577 nodes which are 1435 nodes for concrete shaft and 11142 for surrounding soil).

The results from ABAQUS FEM computational analysis are shown in Figures 6.10 to 6.14 for short drilled shaft simulation and Figures 6.15 to 6.18 for intermediate drilled shaft simulation. In the set of the results presented here, first initial condition before analysis is presented followed by the force/stress distribution in and around drilled shaft and surrounding soil. For the complete loading analysis, the time for completing one set of analysis has taken 3 - 4 hours.
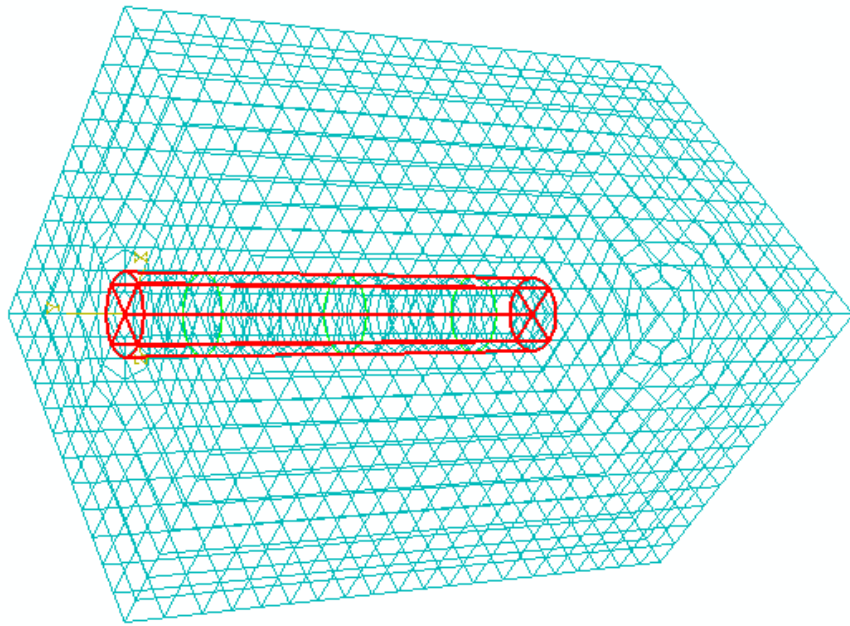
Figure 6.6 Model Developed for 1 ft diameter x 6 ft depth drilled shaft

185
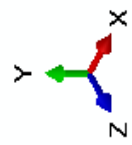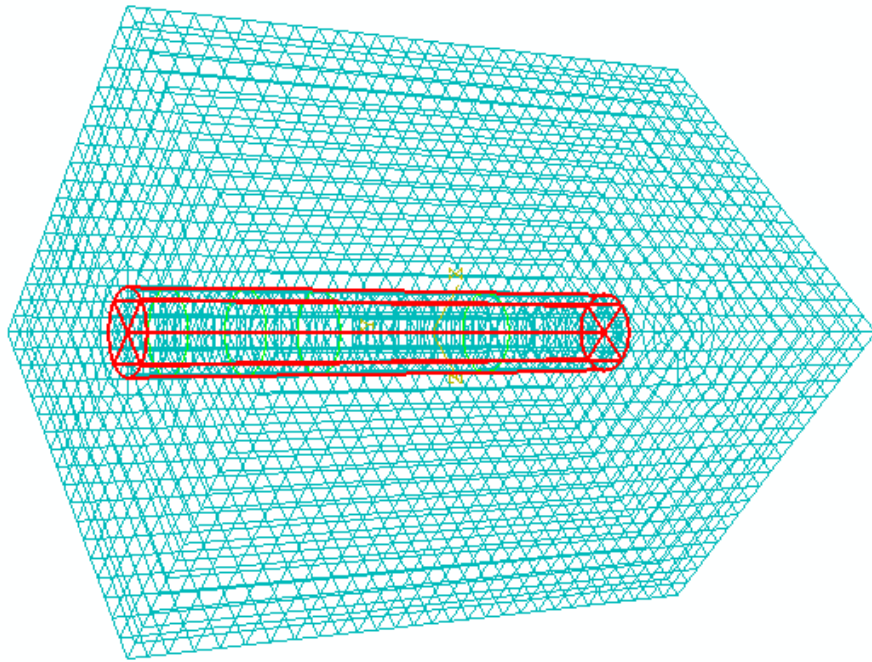
Figure 6.7 Model Developed for 2 ft diameter x 14 ft depth drilled shaft

186
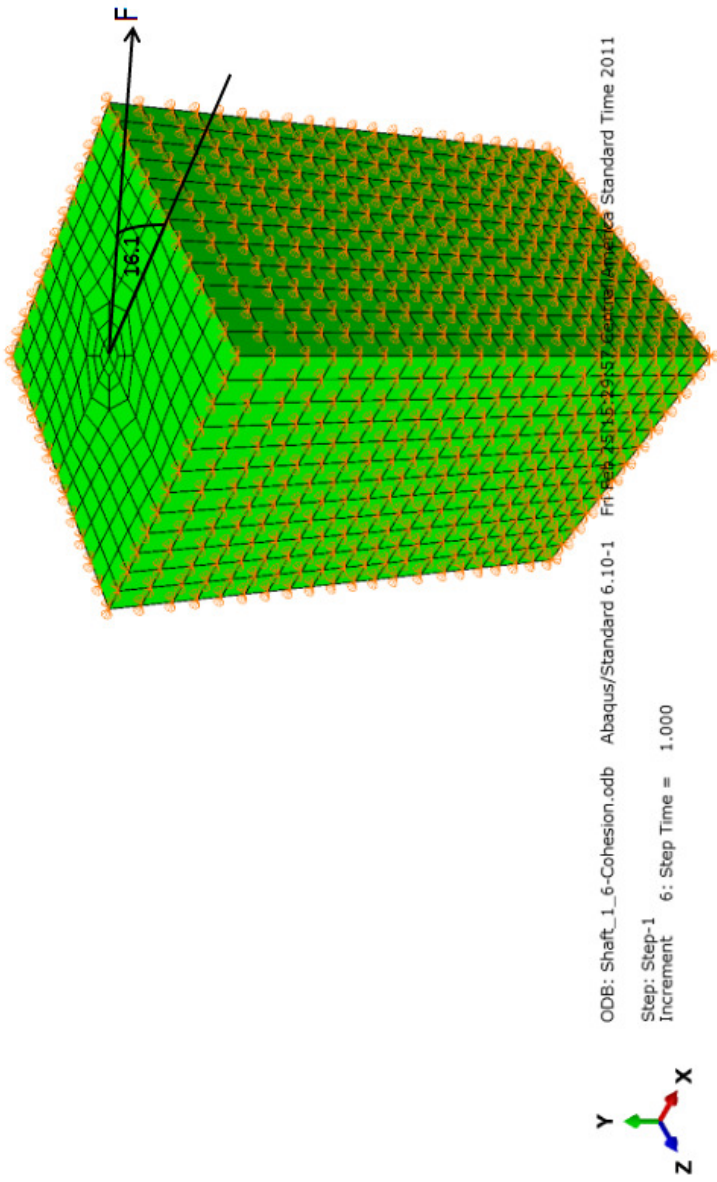
Figure 6.8 Boundary Condition for 1 ft diameter x 6 ft depth drilled shaft

187
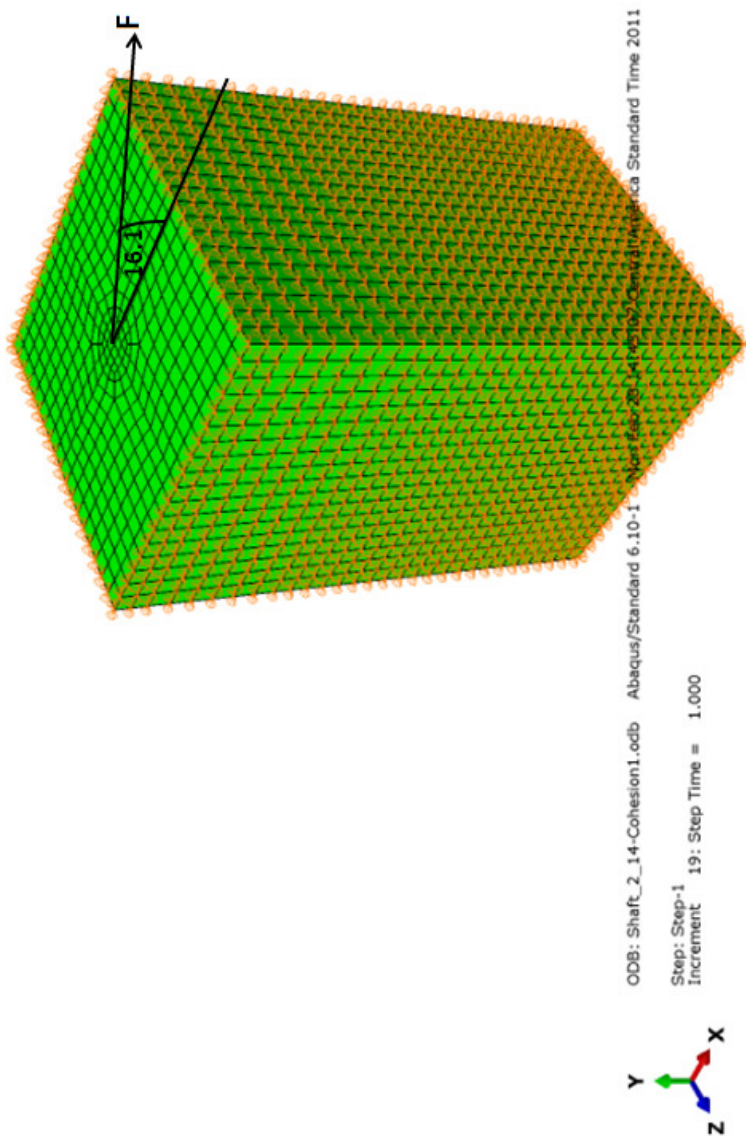
Figure 6.9 Boundary Condition for 2 ft diameter x 14 ft depth drilled shaft

188
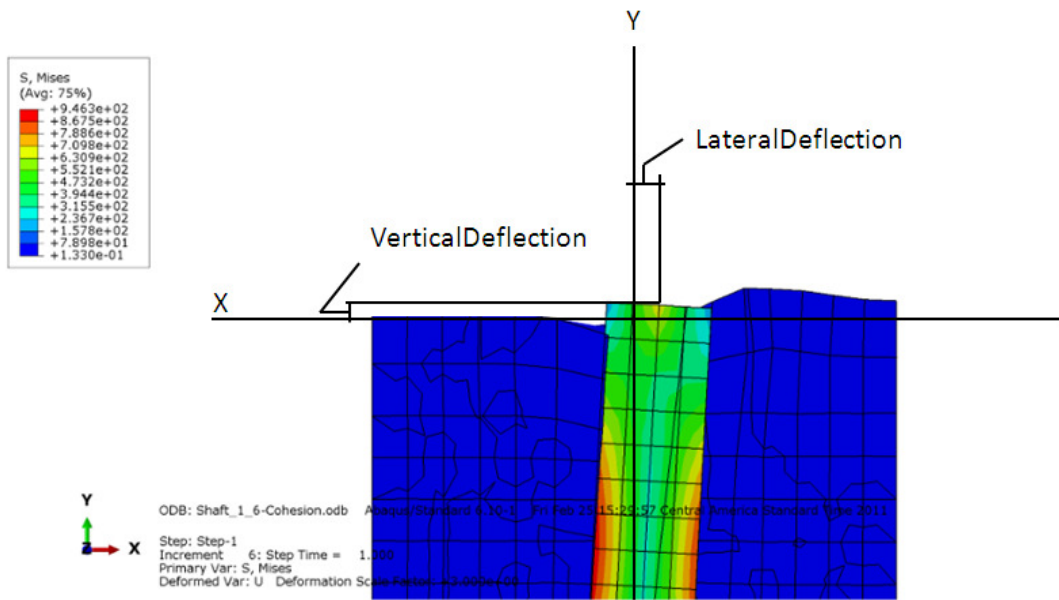
Figure 6.10 Example of Using the center of the top drilled shaft as the reference to measure deflection in horizontal and vertical direction
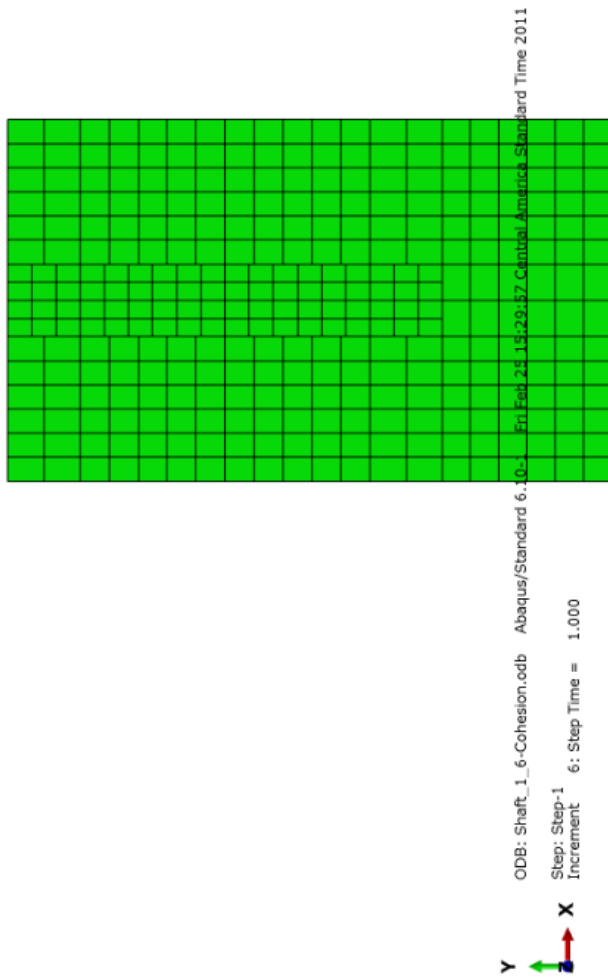
Figure 6.11 Initial Model of 1 ft diameter x 6 ft depth drilled shaft

190

S, Mises
(Avg: 75%)
+9.463e+02
+8.675e+02
+7.886e+02
+7.098e+02
+6.309e+02
+5.521e+02
+4.732e+02
+3.944e+02
+3.155e+02
+2.367e+02
+1.578e+02
+7.898e+01
+1.330e-01

ODB: Shaft_1_6-Cohesion.odb   Abaqus/Standard 6.10-1   Fri Feb 24 15:29:57 Central American Standard Time 2011

Step: Step-1
Increment   6: Step Time =   1.000
Primary Var: S, Mises
Deformed Var: U   Deformation Scale Factor: +4.000e+00
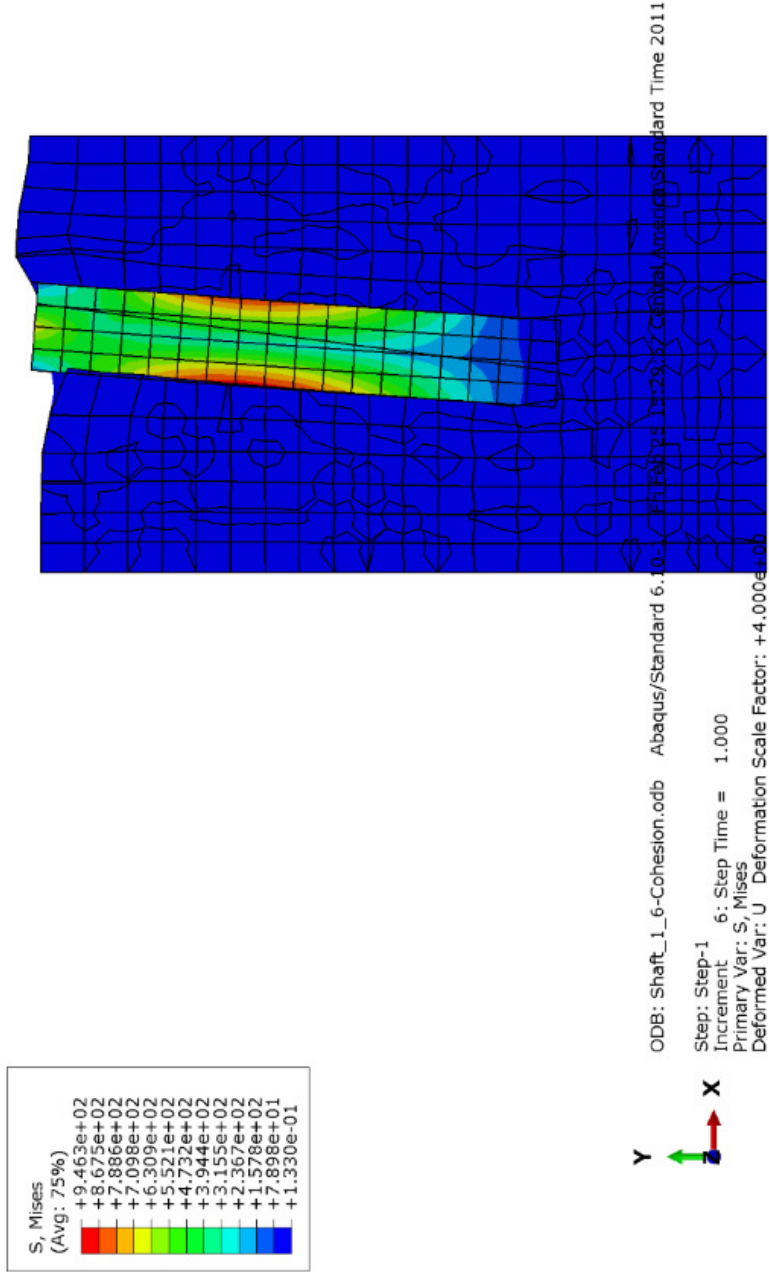
Figure 6.12 Stress Distribution in Drilled Shaft of 1 ft diameter x 6 ft depth drilled shaft

191

S, Mises
(Avg: 100%)
+7.975e+02
+1.757e+01
+1.612e+01
+1.466e+01
+1.321e+01
+1.175e+01
+1.030e+01
+8.840e+00
+7.385e+00
+5.930e+00
+4.476e+00
+3.021e+00
+1.566e+00
+1.107e-01

ODB: Shaft_1_6-Cohesion.odb   Abaqus/Standard 6.10-2   Fri Feb 25 12:33:40 Central America Standard Time 2011

Step: Step-1
Increment   9: Step Time =   1.000
Primary Var: S, Mises
Deformed Var: U   Deformation Scale Factor: +1.000e+00
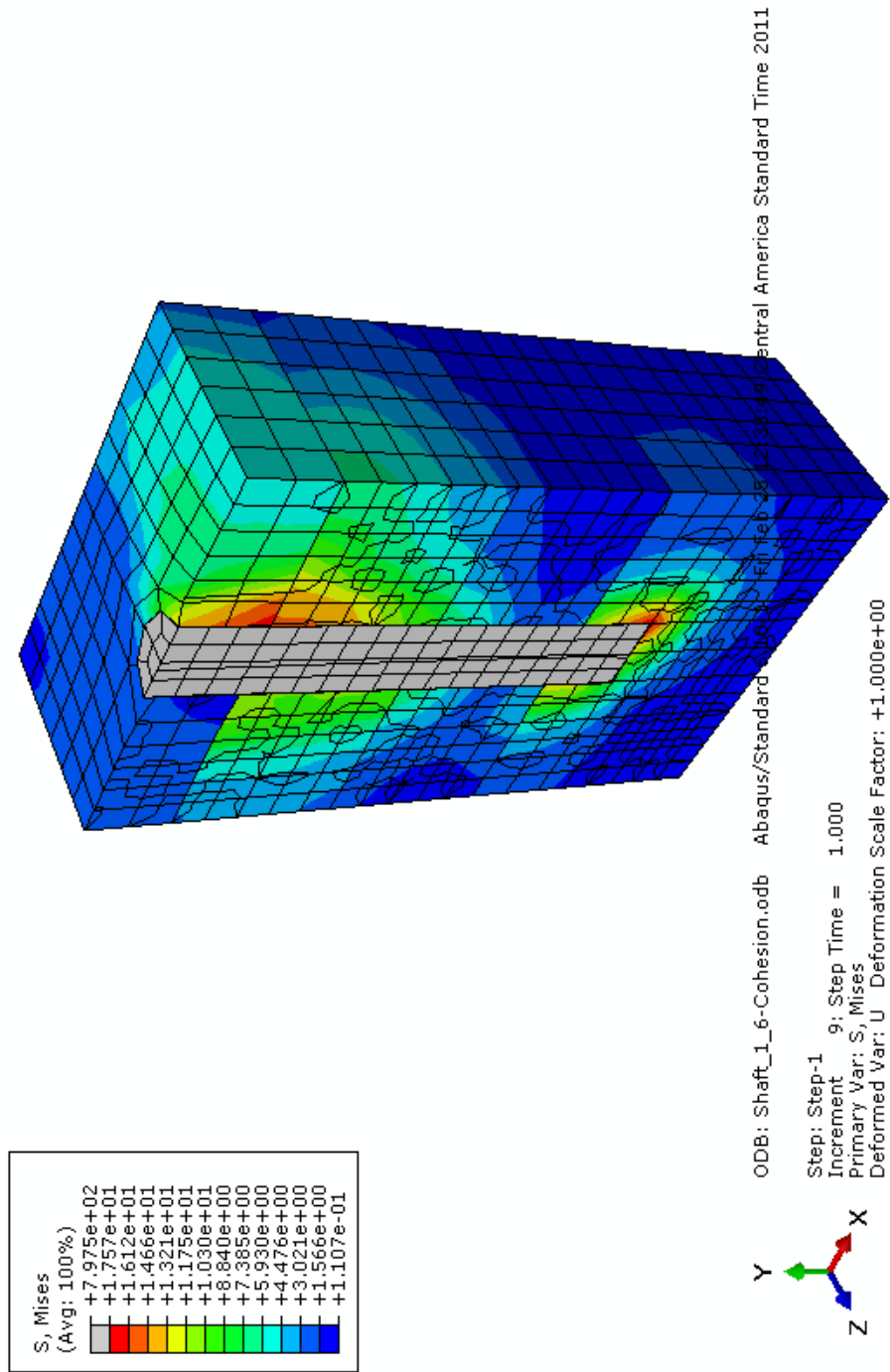
Figure 6.13 Increased Affected from 1 ft diameter x 6 ft depth drilled shaft

192

S, Mises
(Avg: 100%)
+1.757e+01
+1.757e+01
+1.612e+01
+1.466e+01
+1.321e+01
+1.175e+01
+1.030e+01
+8.840e+00
+7.385e+00
+5.930e+00
+4.476e+00
+3.021e+00
+1.566e+00
+1.107e-01

ODB: Shaft_1_6-Cohesion.odb   Abaqus/Standard 6.10-1   Fri Feb 25 12:33:49 Central America Standard Time 2011

Step: Step-1
Increment   9: Step Time =   1.000
Primary Var: S, Mises
Deformed Var: U   Deformation Scale Factor: +1.000e+00
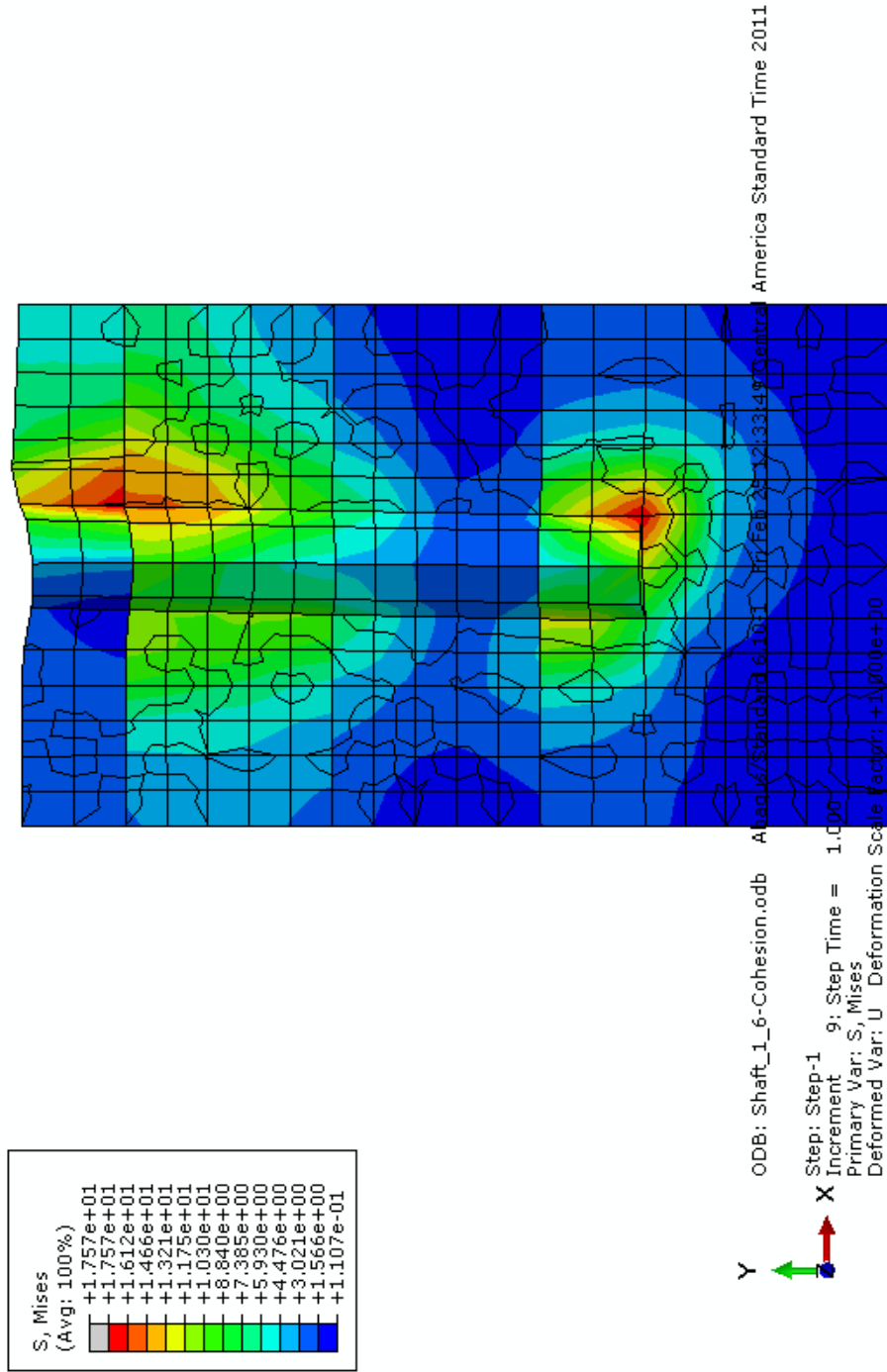
Figure 6.14 Stress Distribution in Surrounding Soil of 1 ft diameter x 6 ft depth drilled shaft

193

From the results shown in Figures 6.11 – 6.14, it can be summarized that when the shaft was subjected to a tensile load acting at angle of 16.1° with the horizontal plane, stresses at the top of the shaft are increased and then transferred to the adjacent soil nodes. The same was noted at the lower end of the drilled shaft. For the stress distribution in soil, it shows that surrounding soils are affected from this loading. In the second case that top soil layer is silt, the highest stress is shown in the clay soil layer (bottom layer) and then the stress is distributed as the first case as presented in Figure 6.14.

From the Figures 6.15 to 6.18, the result of intermediate size of drilled shaft shows that behavior of stress distribution for the multi layer case is similar to the short drilled shaft. The high stresses are recorded right side of the shaft at the top and left side of the shaft at the bottom, which indicates a rotation pattern. Comparisons between short and long shafts' stress distribution plots at ultimate load show similar pattern and it should be noted that these loads are different as ultimate load for short shaft is small when compared to longer shaft. Nevertheless the high stresses are recorded both near the top and bottom of the shafts. Such rotational induced stresses and soil movements can be expected for short to medium size shafts.

For each load applied on both shafts, the movement of top of shaft (reference point) is recorded. For various loads, both load and shaft lateral movements are computed and plotted in Figures 6.19 (short shaft) and 6.20 (Intermediate). The measured load-displacements are also included in the figure. All the results were separated into lateral and uplift components as shown in the Figure 6.19 and 6.21. Though there is some variation between comparisons, overall the FEM modeling showed reasonable match particularly smaller size shafts.
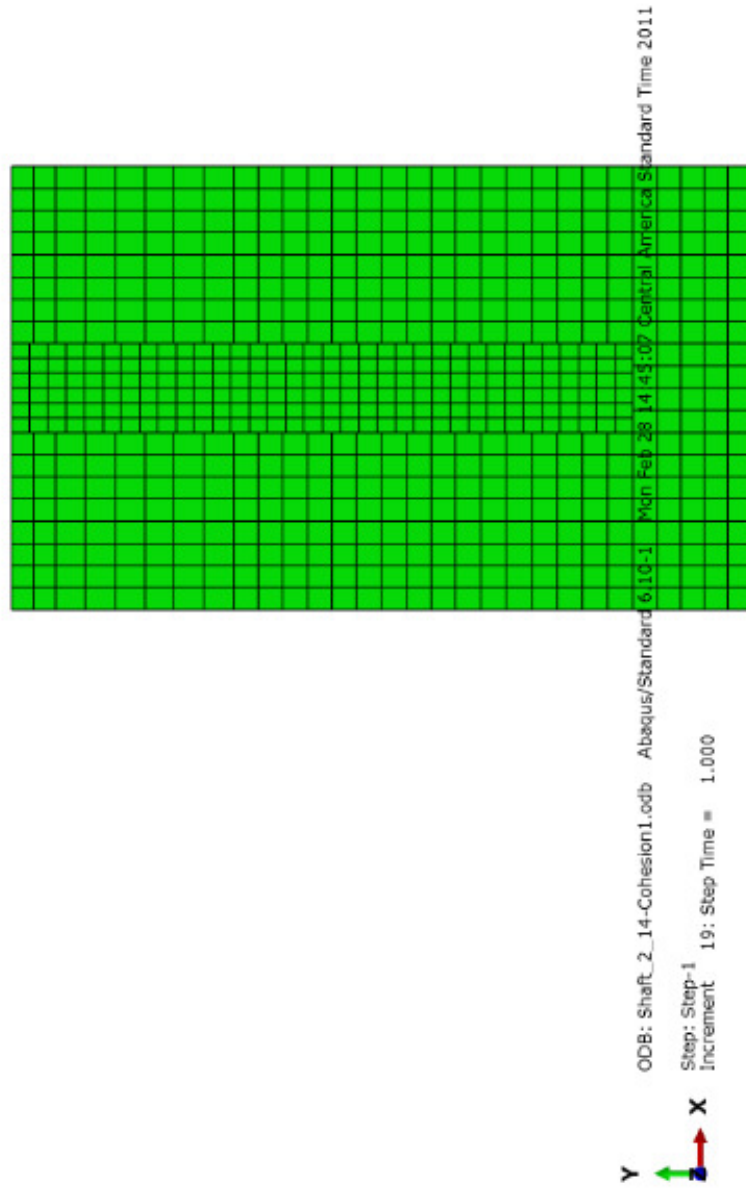
Figure 6.15 Initial Model of 2 ft diameter x 14 ft depth drilled shaft

195
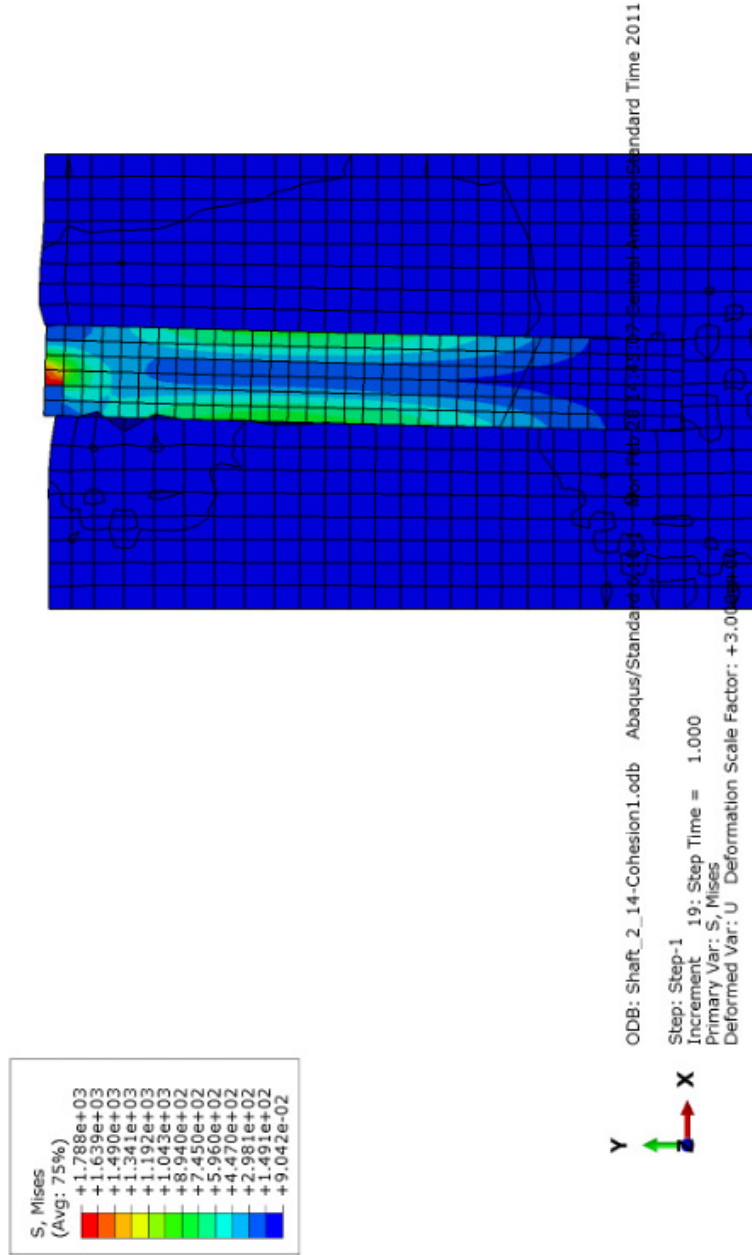
Figure 6.16 Stress Distribution in Drilled Shaft of 2 ft diameter x 14 ft depth drilled shaft

S, Mises
(Avg: 100%)
+1.612e+03
+1.521e+01
+1.395e+01
+1.269e+01
+1.143e+01
+1.017e+01
+8.912e+00
+7.652e+00
+6.391e+00
+5.131e+00
+3.871e+00
+2.611e+00
+1.351e+00
+9.042e-02

ODB: Shaft_2_14-Cohesion1.odb   Abaqus/Standard 6.10-1   (mon Feb 28 14:45:17 Central America Standard Time 2011

Step: Step-1
Increment   19: Step Time =   1.000
Primary Var: S, Mises
Deformed Var: U   Deformation Scale Factor: +1.000e+00
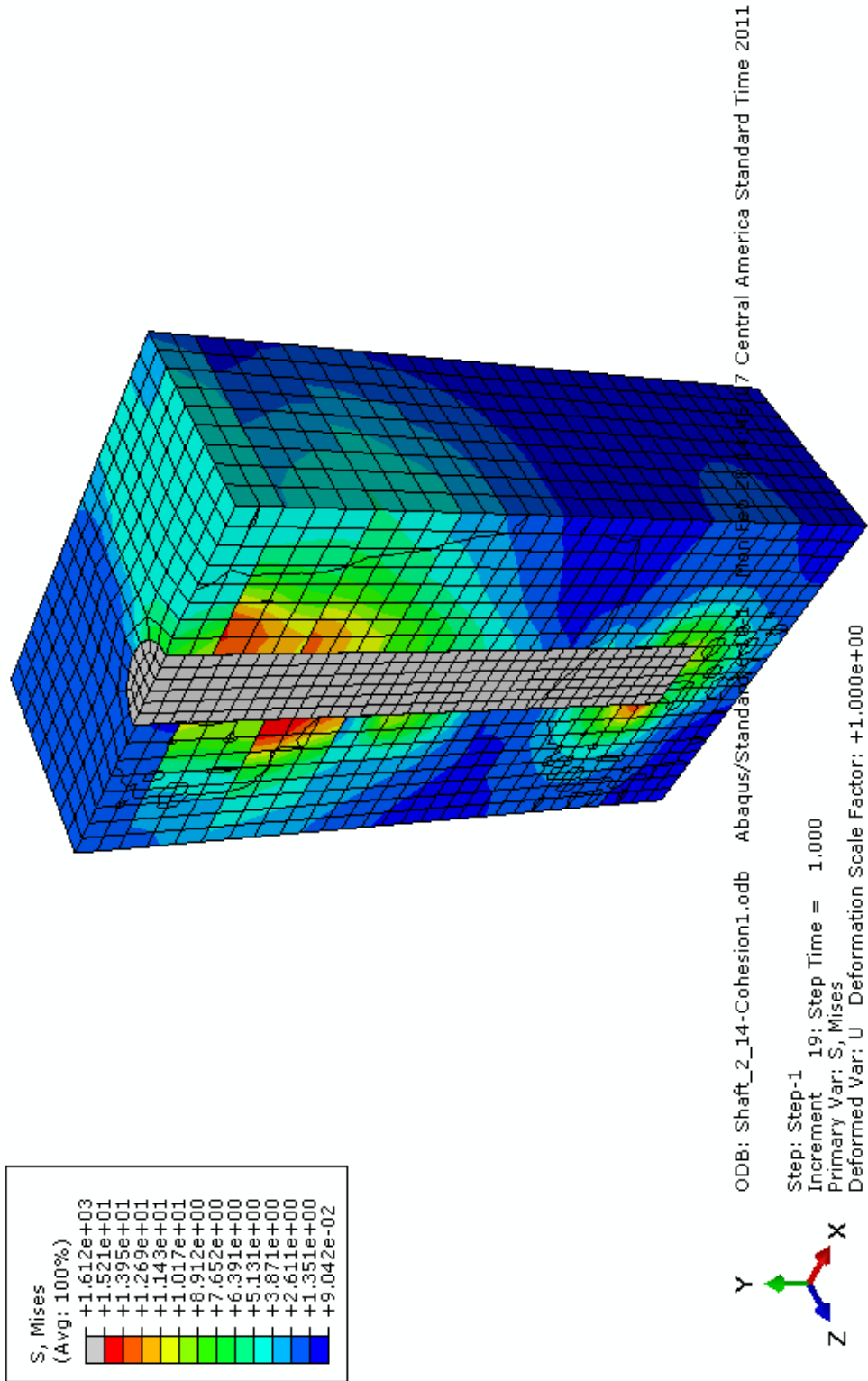
Figure 6.17 Stress Increased Affected from 2 ft Diameter x 14 ft Depth Drilled Shaft
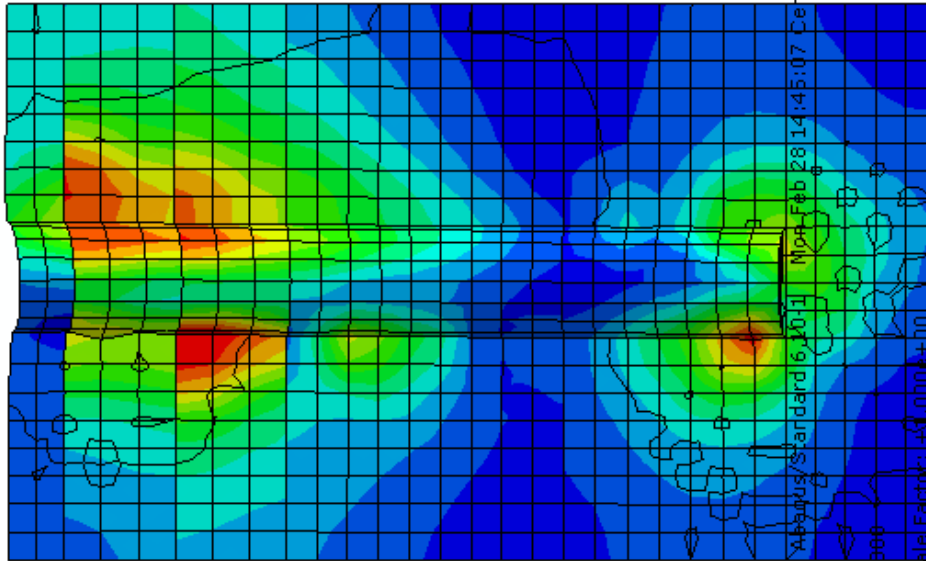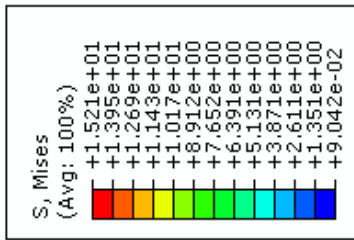
Figure 6.18 Stress Distribution in Surrounding Soil of 2 ft Diameter x 14 ft Depth Drilled Shaft
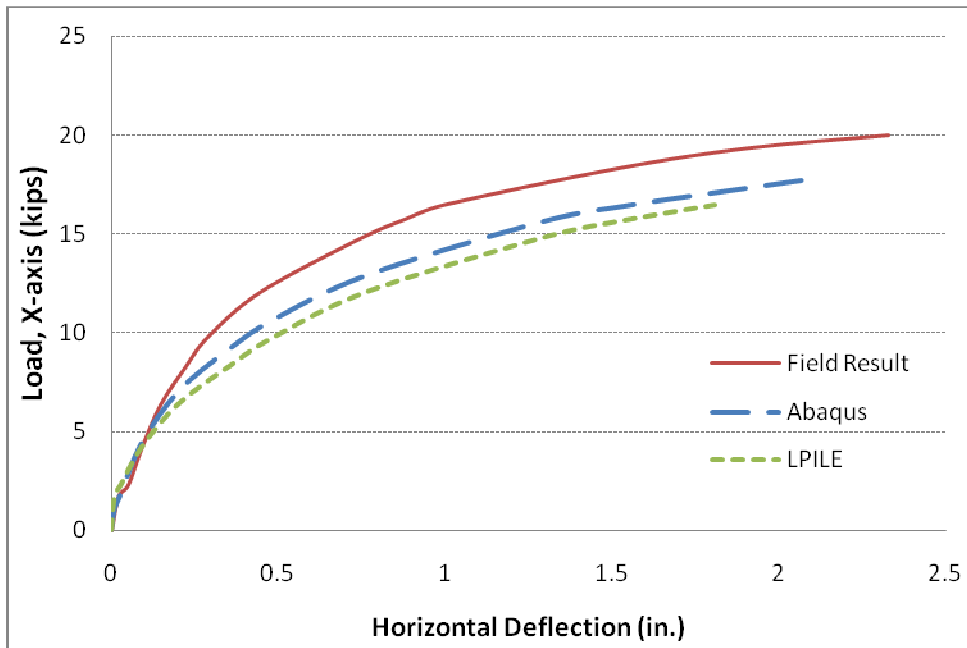
a)
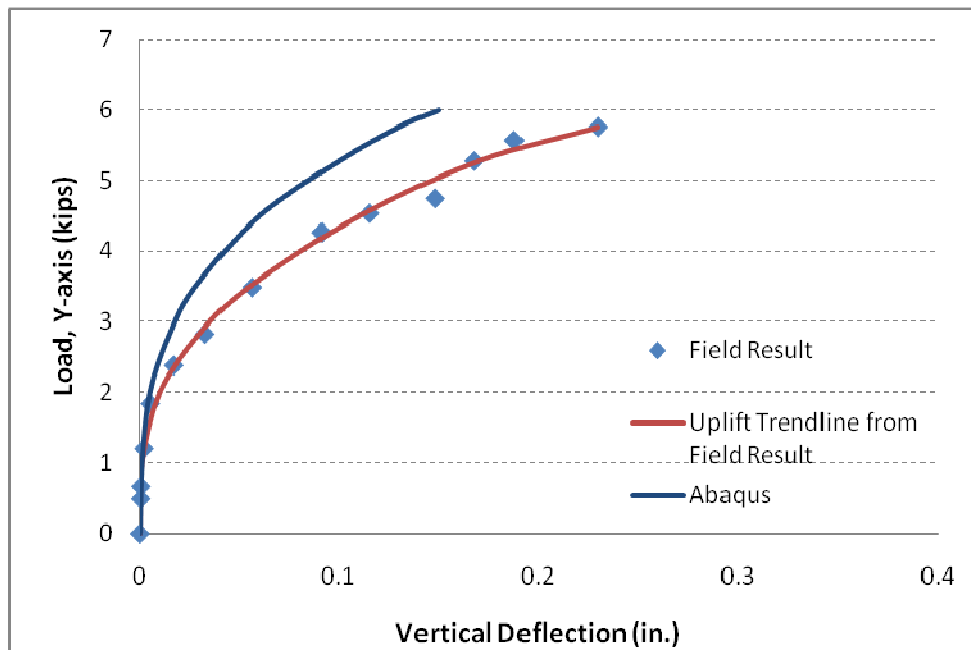
b)

Figure 6.19 Comparison between Field Test Result and FEM Model by Abaqus program of the 2 ft (0.6 m) Diameter x 6 ft (1.8 m) Depth: a) Lateral Load and b) Uplift Load
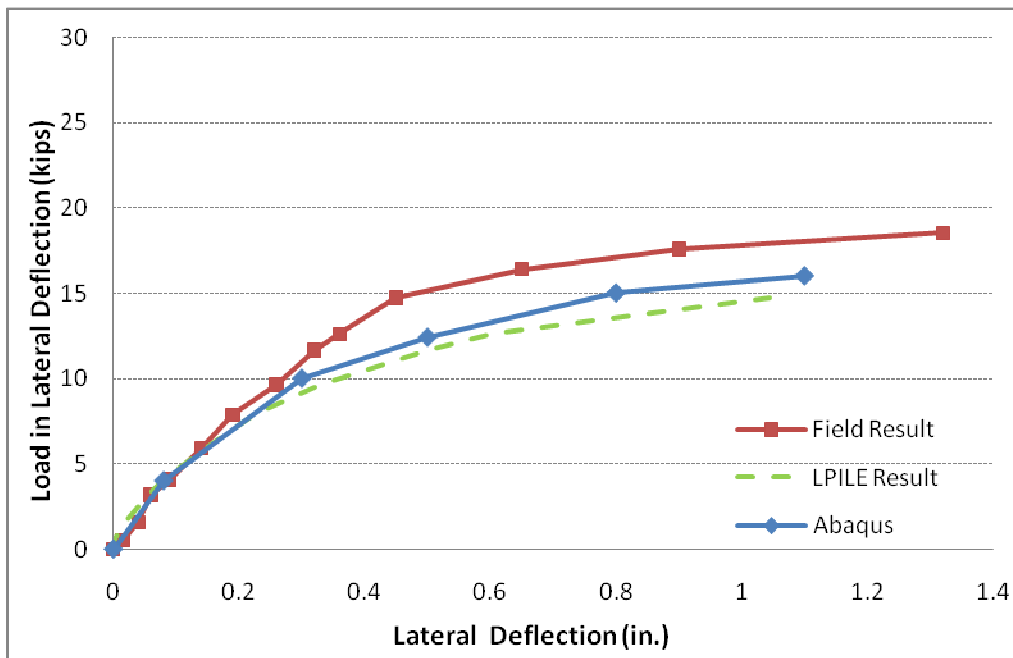
a)
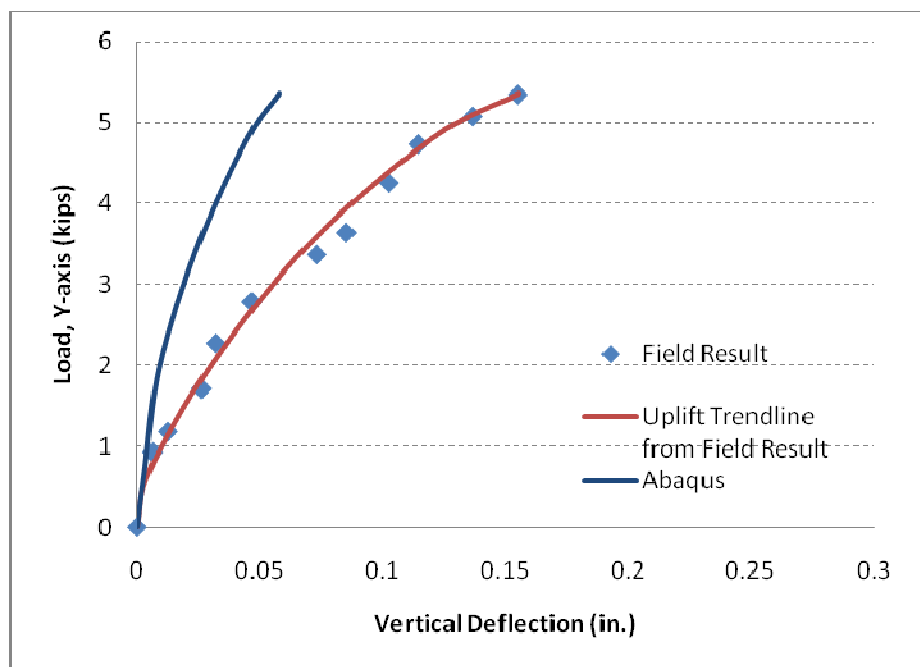
b)

Figure 6.20 Comparison among Field Test Result, FEM Model by Abaqus program and LPILE Model the 1 ft (0.3 m) Diameter x 10 ft (3 m) Depth: a) Lateral Load and b) Uplift Load

For vertical load component, the results indicate that for the same vertical deflection, the vertical load component from Abaqus (FEM) program is higher than the field measurement results. Similar result is recorded with the analytical model developed by Das and Seely (1982) for uplift capacity predictions. The most important factors controlling the vertical movement are vertical load component, skin friction induced around drilled shaft and the weight of drilled shaft.

The rest of the FEM analyses are attempted on other tested shafts in this research and these results are included in Table 6.7. Results in the table show that the average ratio of the measured ultimate load and FEM analyzed predicted load is 1.14, which indicates a decent comparison if not a complete agreement. When compared with the LPILE results of the previous section, it can be noticed that the FEM modeling results showed better comparisons than other analytical methods. Further comparison analysis shown in the next section.

Table 6.7 Summary of Ultimate Lateral Results Compared with the FEM Results at 0.5 in.

Shaft No.	Diameter (ft.)	Depth (ft.)	Field Test (kips)	FEM Results (kips)
1	1	6	8.0	7.4
2	1	10	15.1	12.4
3	1	14	14.3	14.5
4	2	6	12.1	10.5
5[A]	2	10	-	-
6	2	10	25.8	20.3
7	2	14	41.6	33.7
8	3	6	14.1	12.7
9[B]	3	14	-	-
Average Ratio (Measured/Predicted)				1.14

Note: [A] denotes concrete material failure, [B] denotes excessive channel section yielding

6.3.3 Comparison of Field Results, LPILE and FEM results

The FEM model results of ultimate lateral load are compared with the field results and results from finite difference based model, LPILE. Figure 6.21 presents all the comparisons.
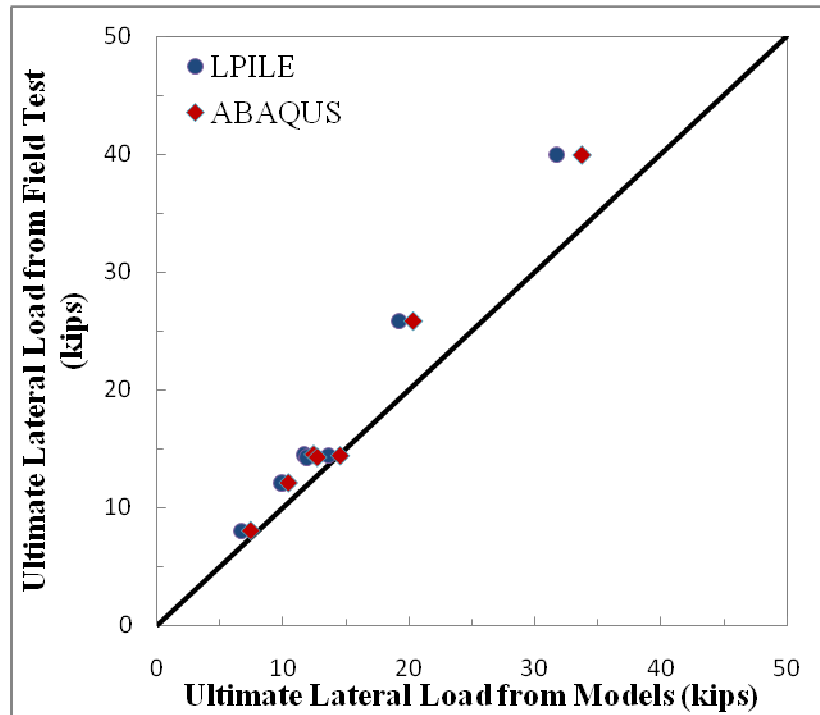
Figure 6.21 Comparisons among the Models Used in the Analysis and Field Results

The results show that both Abaqus (FEM) and LPILE (FDM) programs provided predictions that closely matched with the lateral load test measured. In addition, the results show that the Abaqus model provides closer matching with field load test results than LPILE.

In short, the FEM analysis has provided slightly better prediction than the LPILE model. However, the weak points of the FEM analysis are that the computational analysis is time-consuming and it requires more layer strength properties to simulate the field layer conditions. Hence, in the proposed design chart development which is covered in the next chapter, researcher has used the LPILE method for the analysis as this analysis requires the analyses for various hypothetical drilled shaft dimensions.

6.4 Summary

This chapter provides the comparisons of ultimate load predictions from analytical models, numerical models and field results. For uplift capacity, the model by Das and Seely provided reasonable results that matched with the trends of field measurements. For lateral capacity, the LPILE program can generate the load-deformation curve which is close to the field load test results. For numerical analysis, the results from Abaqus FEM program can be used to explain the behaviors of drilled shafts under inclined loading and stresses increased in and around the soil and possible stressing zones that contribute to the movements of drilled shafts. This information is difficult to interpret from simpler and analytical models. In the next chapter, the development of design chart is described.

CHAPTER 7

DEVELOPMENT OF DESIGN CHARTS / CONSTRUCTION GUIDELINE AND

RECOMMENDATION

7.1 Introduction

This chapter presents the development of design charts for drilled shafts to be supported in the cable median barrier systems for various subsoil conditions. The developed design charts can be used for different undrained shear strength properties of clayey soil encountered in the field. In addition, a flow chart is provided on how to choose the appropriate design chart for certain undrained shear strength of soils.

7.2 Development of Design Charts

From the previous chapter, both the lateral pile load analysis using LPILE method and numerical method based finite element modeling have shown potential to provide reasonable and realistic simulations of inclined loading behaviors of short to intermediate size drilled shafts. Though the FEM analysis provides slightly better predictions than the lateral and uplift load analyses as shown in the previous Chapter, still the later approach is followed for the design chart development for both simplicity and practical implementation of this approach.

The following assumptions are needed and used in the design chart development:

- All clayey soil layers are assumed to be saturated and hence only undrained shear strength properties are considered in the design chart development.

- Predominantly two types of soil layers with clay layer of high plasticity being underlained by another clay layer of mixed plasticity are considered. Undrained shear strength of upper clay layer is around 5.5 psi whereas the same of lower layer is 3.3 psi.

- Factors for correcting lateral and uplift loads developed from the present research are also assumed to be valid for other soil strata conditions.

These assumptions are needed as load tests on drilled shafts of other soil strata are difficult to perform with various hypothetical soil layer conditions. From the previous Chapter, the ultimate uplift force prediction model by Das and Seely and the ultimate lateral load prediction from LPILE software are used in the design chart development.

In the model validation analysis, the trends from the uplift force predictions are overestimated when compared to the uplift component of the field test results and hence the uplift predictions are reduced by using factors of 0.22 and 0.28 for lateral movements of 0.5 and 1.0 in. criteria, respectively. It should be noted here that Das and Seely method does not require the use of swell pressures of soil layers for uplift capacity analysis.

Also, the lateral load predictions are underestimated when compared to the lateral component of the field test results and hence another factor higher than 1 (1.21 and 1.20 for lateral deflections of 0.5 and 1.0 in. criteria, subsequently) is used to correct the LPILE predictions and these factors are summarized in Table 7.1.

Table 7.1 Summary of Correction Factor Used in Design Chart Development

	Correction Factor	
Axis / Deflection Criteria	0.5 in.	1.0 in.
Lateral (X) Analysis	1.21	1.20
Vertical (Y) Analysis	0.22	0.28

After corrections of the predicted load data, both uplift force and lateral loads are then combined to determine a resultant inclined load acting at 16.1 degrees with the horizontal. These details are given in Equation 7.1. Two clay layers with different depths are considered in the analysis. Design chart results for ultimate inclined loads of drilled shafts of various

diameters (1 – 3 ft or 0.3 – 0.9 m) and depths (6 – 14 ft or 1.8 - 4.2 m) are calculated and are

shown in Figures 7.1 and 7.2 for 0.5 and 1.0 in. deflection criteria.

$$\text{Inclined Load at } 16.1° = \sqrt{(U^2 + L^2)} \cos\left(\tan^{-1}\frac{U}{L} - 16.1°\right) \qquad 7.1$$

Where U = Uplift force and L = Lateral Force
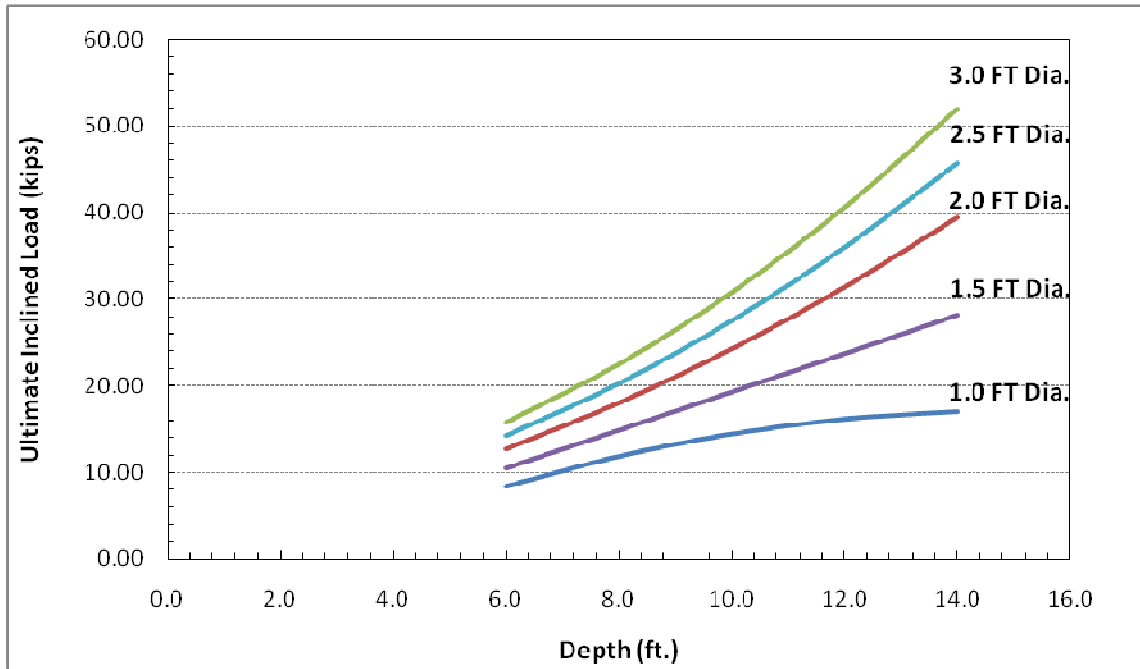
Figure 7.1 Preliminary Design Chart Based on Current Field Results for Finding the Appropriate
Size of Drilled Shaft Using 0.5 in. Lateral Deflection Criterion
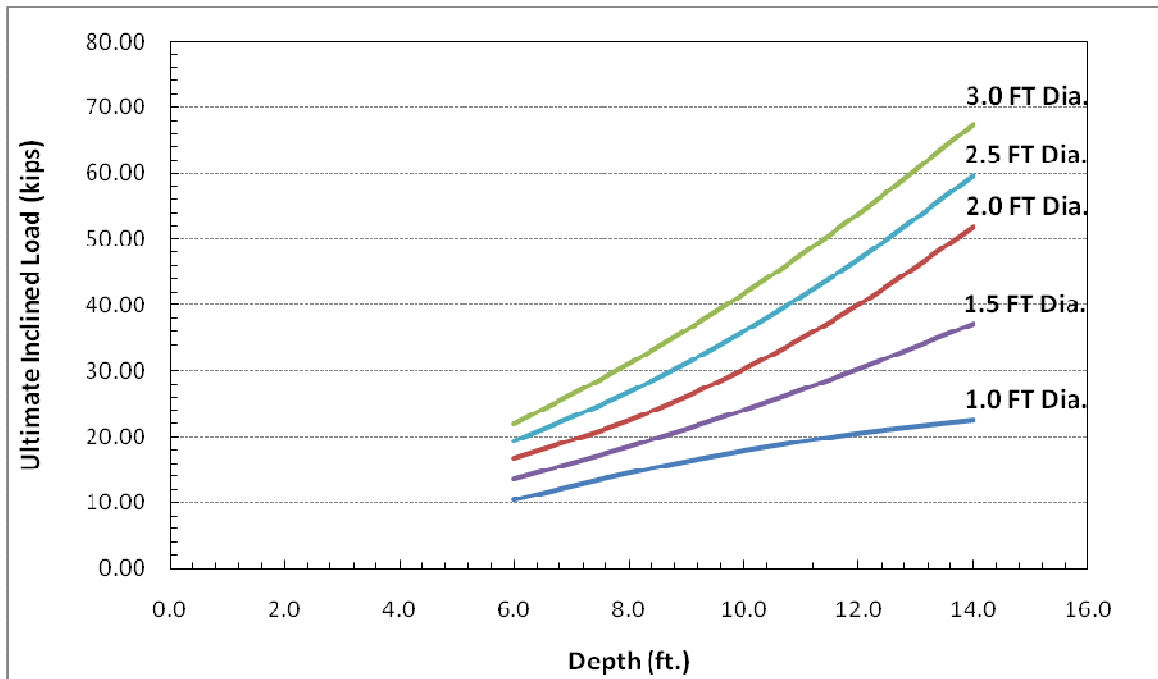
Figure 7.2 Preliminary Design Chart Based on Current Field Results for Finding the Appropriate Size of Drilled Shaft Using 1.0 in. Lateral Deflection Criterion

As shown in the previous figures, only one soil type is used here in these charts. However, in reality, there are more layers of soils with distinct undrained shear strengths that will prevail in the field. Hence, in order to provide the design charts that can be used for different soil conditions encountered in the field, further analyses were carried out by using three different soil layers and their properties.

For this analysis, the top 3 ft clay layer with different undrained shear strengths including 250 – 500 psf, 500 – 750 psf, 750 – 1000 psf, 1000 – 1500 psf and 1500 – 2000 psf is considered as a constant top layer for the entire analysis. The bottom two clay layers (between 3 and 15 ft depth zones) with different undrained shear strength properties (S_u) varying between 250 – 500 psf, 500 – 1000 psf, 1000 – 1500 psf and 1500 – 2000 psf, are considered and an average undrained shear strength of these two layers are then calculated and used as shear strength of the bottom layer.

Table 7.2 presents all these input parameters for LPILE software analysis. For effective unit weight, same soil unit weights (similar to the ones presented in Table 6.2) are considered and used as input for both layers. For this analysis, the appropriate soft and stiff clay model is considered and used in the LPILE analysis.

Table 7.2 Input parameters of various layer in LPILE analysis

Range of undrained Shear Strength (psf)	Soil type (p-y curve model)	Undrained Cohesion, c, (psi)	Strain Factor, E50
250 – 500	Soft Clay (Matlock)	1.735	0.02
500 – 750	Soft Clay (Matlock)	3.47	0.02
750 – 1000	Soft Clay (Matlock)	5.21	0.015
1000 – 1500	Soft Clay (Matlock)	6.94	0.01
1500 – 2000	Stiff clay w/o Free Water (Reese)	10.41	0.007

In choosing of the appropriate design chart, the magnitude of undrained shear strength of top 3 ft is required as the first step in the analysis. This is an important step since the top layer has considerable influence on the loading capabilities of the short drilled shafts used in the cable barrier systems. For example, the top layer of soil has an undrained shear strength of 600 psf which means that the soil has a range of undrained shear strength properties between 500 and 750 psf. Various other top layer's undrained shear strengths and their applicable chart details can also be found in Figure 7.3.
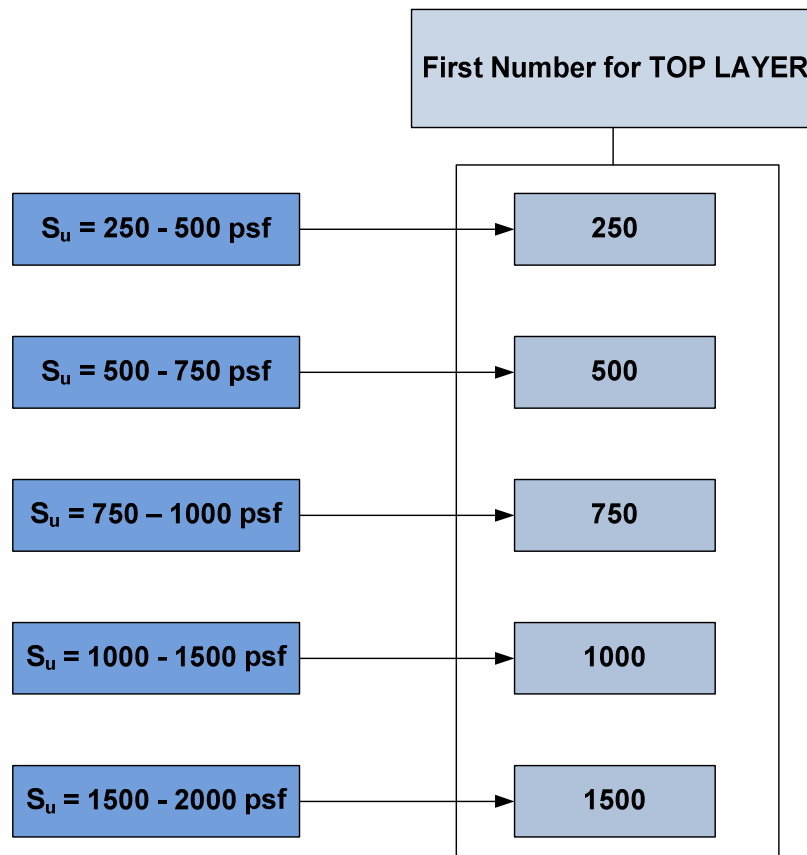
Figure 7.3 Flow Chart for Selection of Upper Soil Layer Strength

For the second step consideration, the average undrained shear strength of lower soil strata or layers is needed. These steps and details are presented in Figure 7.4 for choosing the appropriate design chart. From this step, one of the four design charts (A, B, C, or D) can be selected. For example, the design chart can be chosen in the second step based on the average undrained shear strength magnitudes of the layers below the top 3-ft layer. Once the design chart is selected, most appropriate design chart can be selected based on the upper layer strength. For example, if Design Chart A is selected from second step, and the top layer strength is 250 psf, then the 'Design Chart A_250' can be used for the design and analysis.

It should be noted here that the final selection of the design charts are based on several LPILE analyses with various soil strength properties for the bottom layer. Figure 7.5 presents the LPILE program results for various soil layers. For each range (ex: 250 - 500; 500 - 250 psf

209

and others), the lower bounds of the predicted capacities are considered here for conservative and safe designs of the shaft foundations. This will not only lead to safer design of drilled shafts, but will also simplify the use of design charts for practical implementation.

Overall, four design chart categories are introduced which are based on the average undrained shear strengths of the bottom layer. These charts are termed here as Design Charts A, B, C and D and they are valid for four ranges of average undrained shear strengths of bottom layers (between 3 and 15 ft, equal layer thickness) varying from 250 – 500 psf, 500 – 1000 psf, 1000 – 1500 psf and 1500 – 2000 psf, respectively (Figure 7.6). Soils which exhibit undrained shear strengths more than 2000 psf are not considered here as such soils considered strong and for those cases, the Design chart D will be recommended for usage.
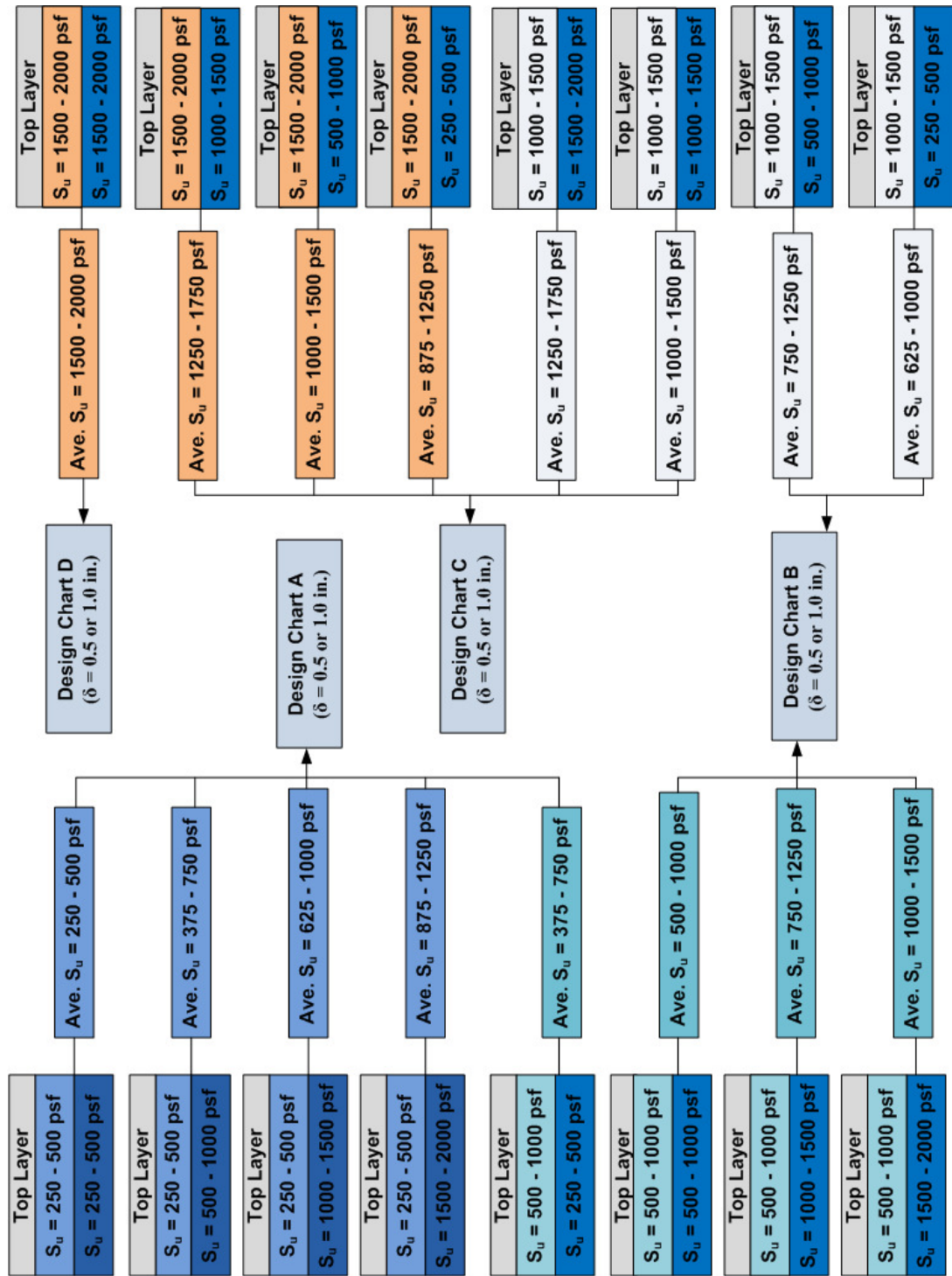
Figure 7.4 Flow Chart for the Design Selection for Bottom Layer Considreation
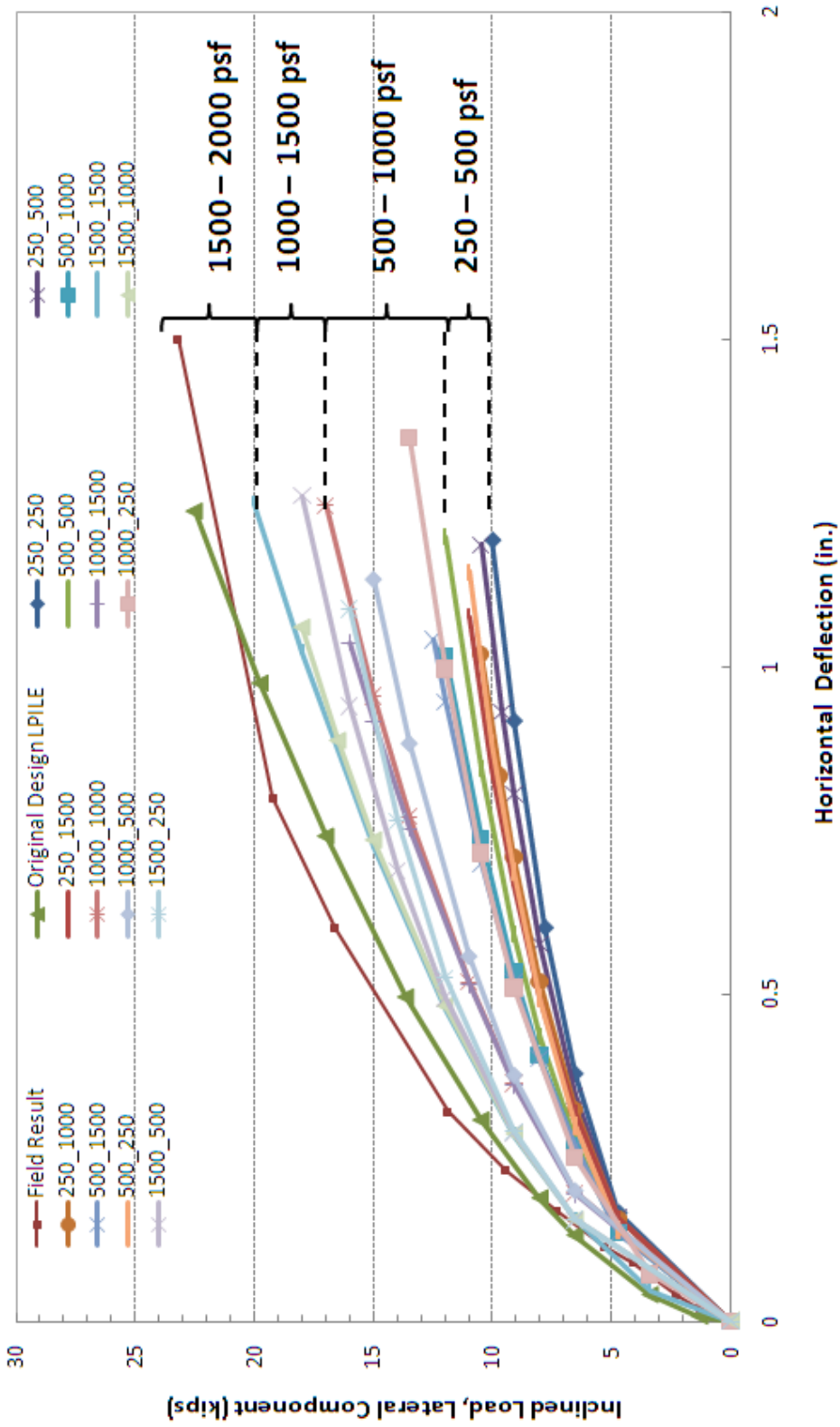
Figure 7.5 An Example of LPILE Results of 1 ft Diameter x 14 ft Depth under Different Undrained Shear Strengths
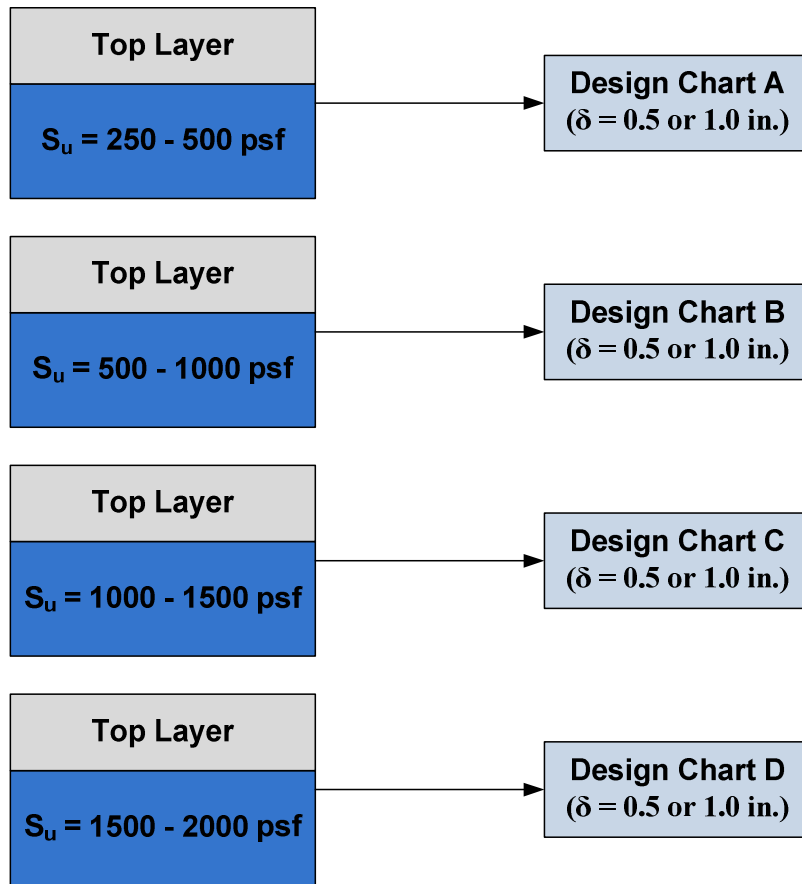
Figure 7.6 Flow Chart for the Design Chart Selection for Bottom Layer

Now, several design charts A, B, C, and D with varying undrained shear strengths for top layer and different bottom layer are developed and presented in the Figures 7.7 – 7.46. These charts are developed for both 0.5 in. and 1.0 in. deflection criteria. Overall, forty eight design chart scenarios of various soils layers are presented in the following pages.
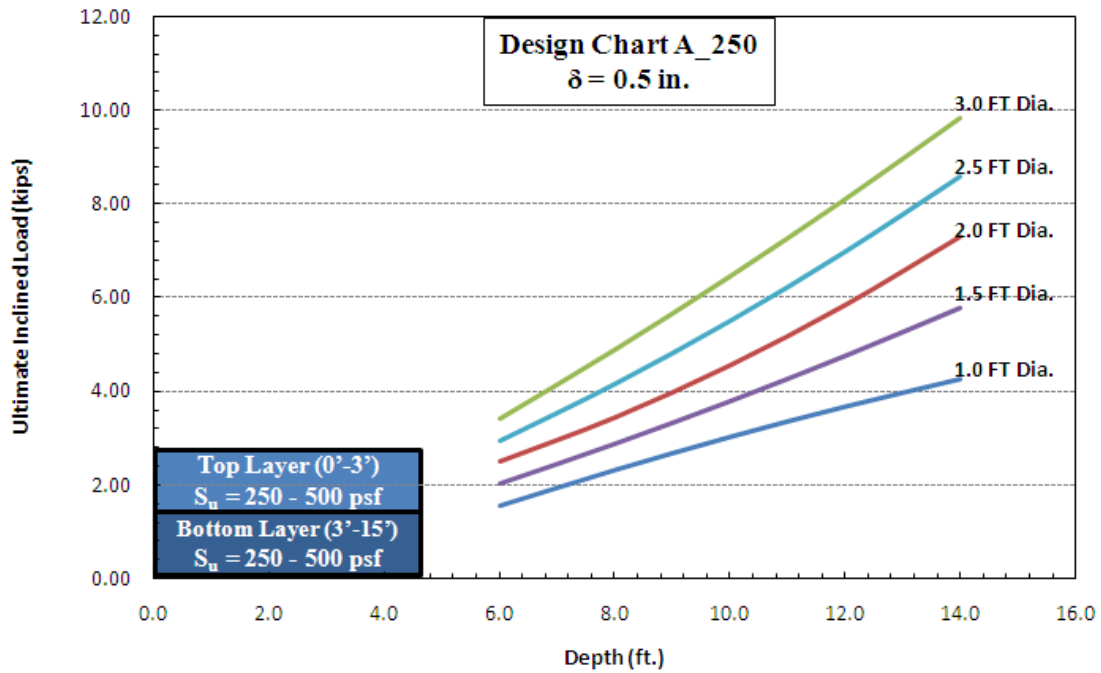
Figure 7.7 Design Chart A_250 for 0.5 in. Deflection Criteria (δ)
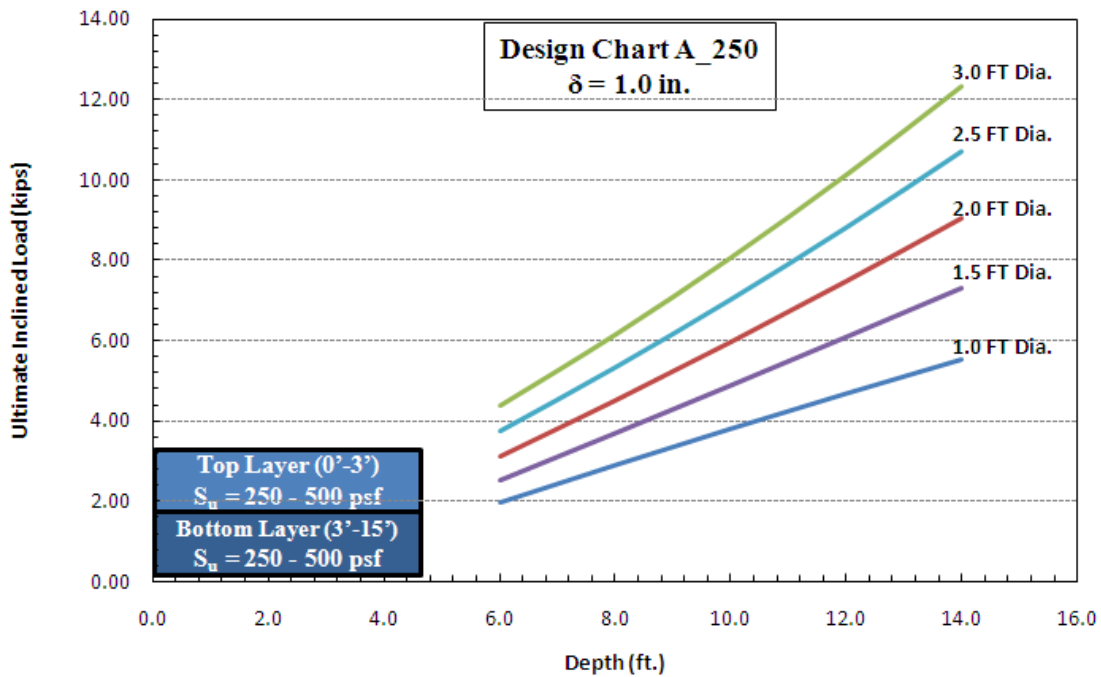
Figure 7.8 Design Chart A_250 with 1.0 in. Deflection Criteria (δ)

214
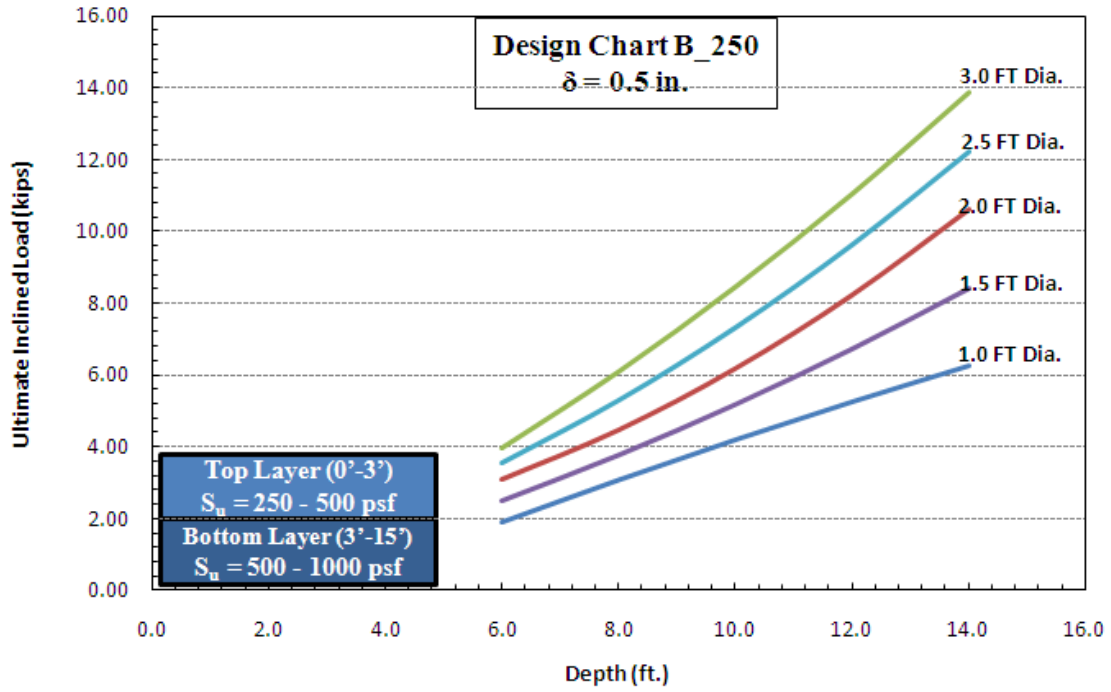
Figure 7.9 Design Chart B_250 with 0.5 in. Deflection Criteria (δ)
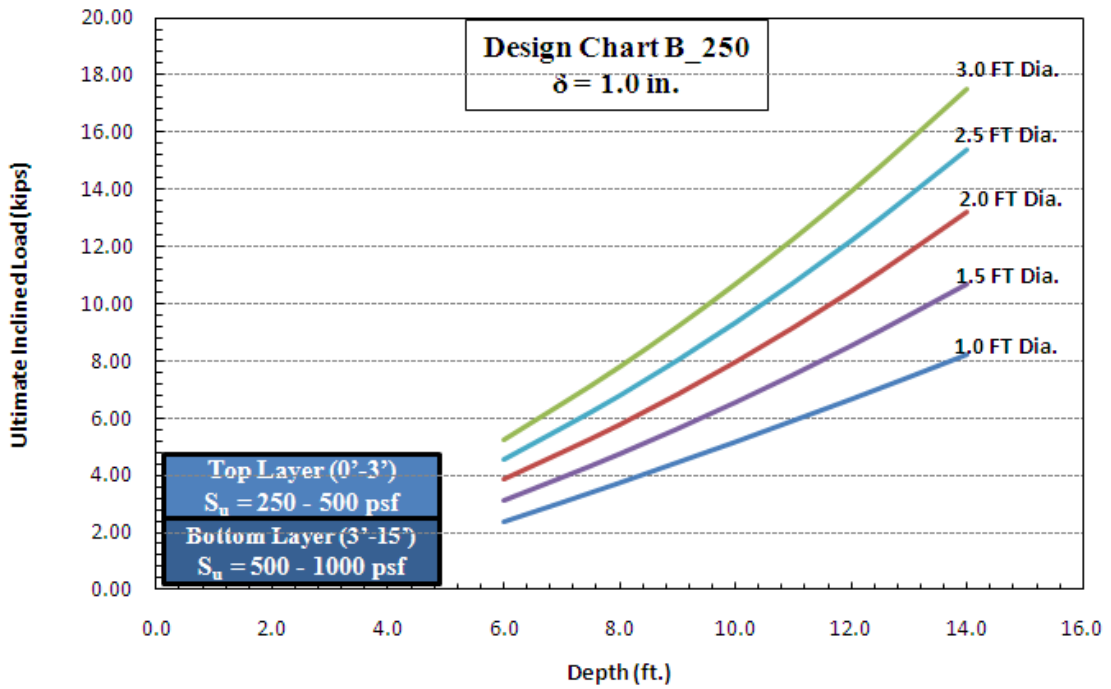
Figure 7.10 Design Chart B_250 with 1.0 in. Deflection Criteria (δ)

215
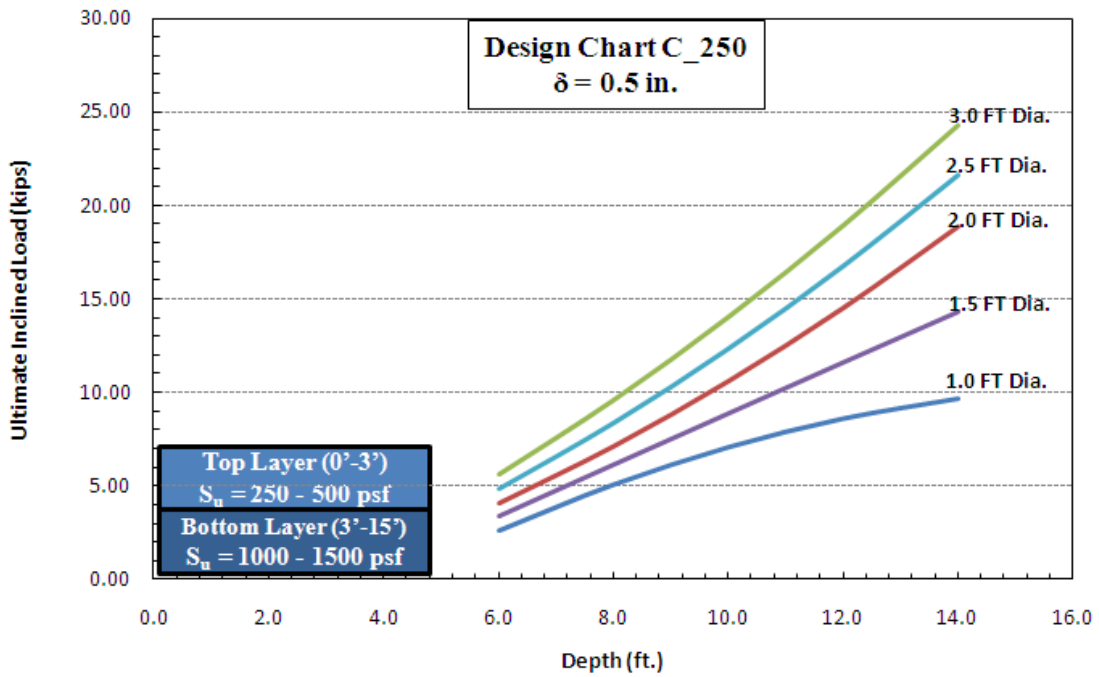
Figure 7.11 Design Chart C_250 with 0.5 in. Deflection Criteria (δ)
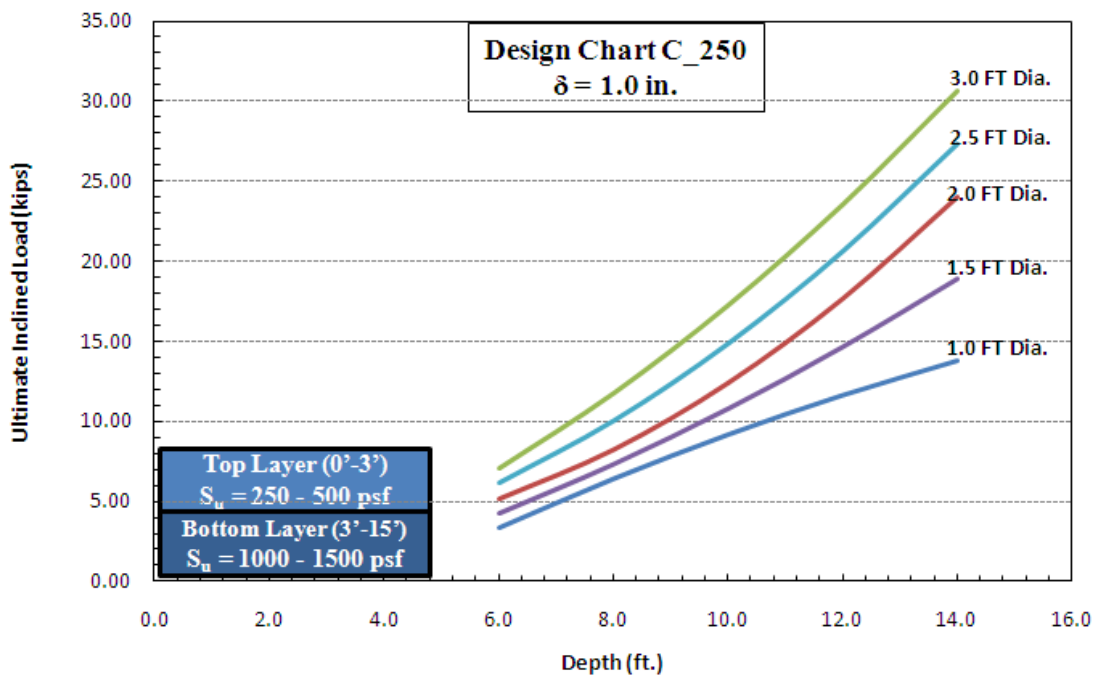
Figure 7.12 Design Chart C_250 with 1.0 in. Deflection Criteria (δ)

216
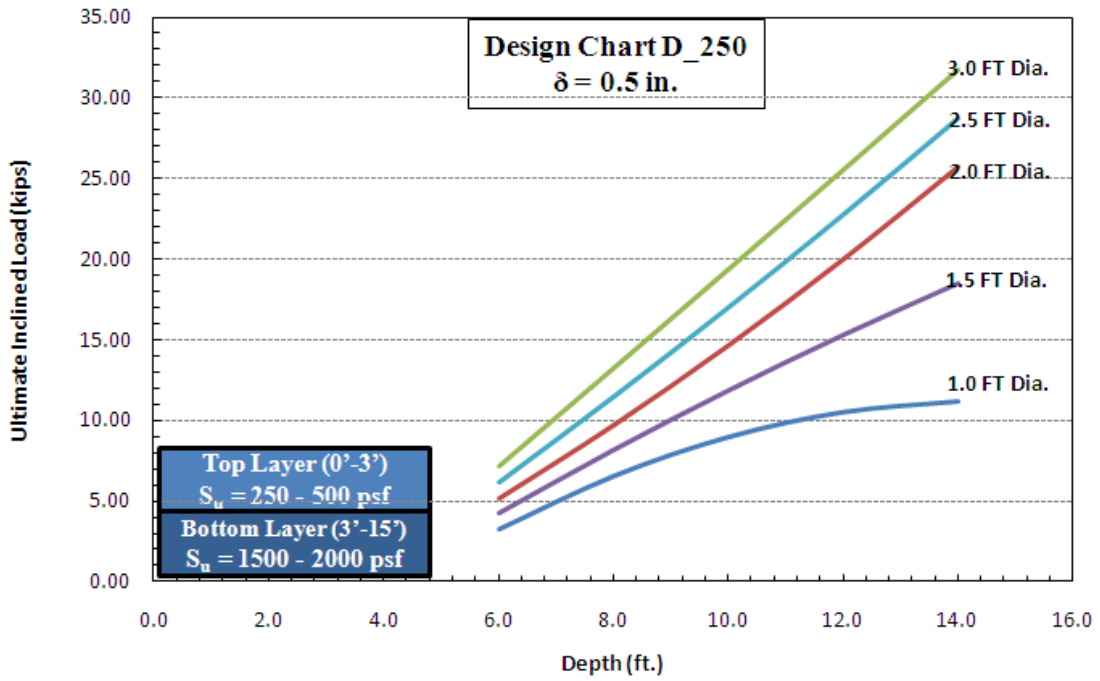
Figure 7.13 Design Chart D_250 with 0.5 in. Deflection Criteria (δ)
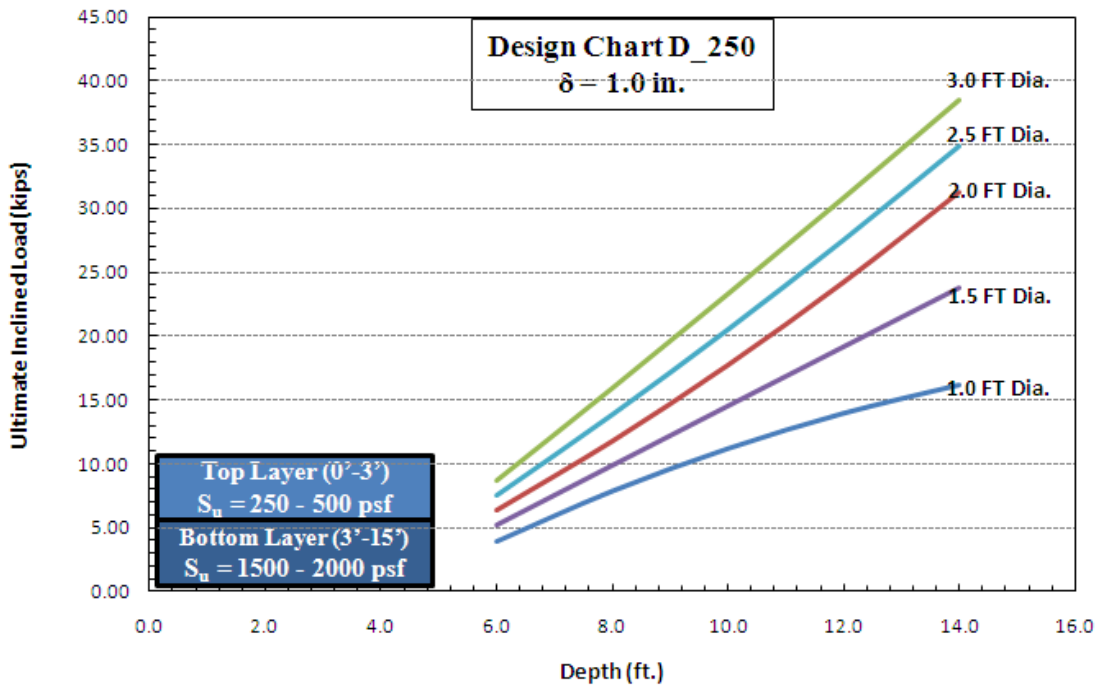
Figure 7.14 Design Chart D_250 with 1.0 in. Deflection Criteria (δ)

217
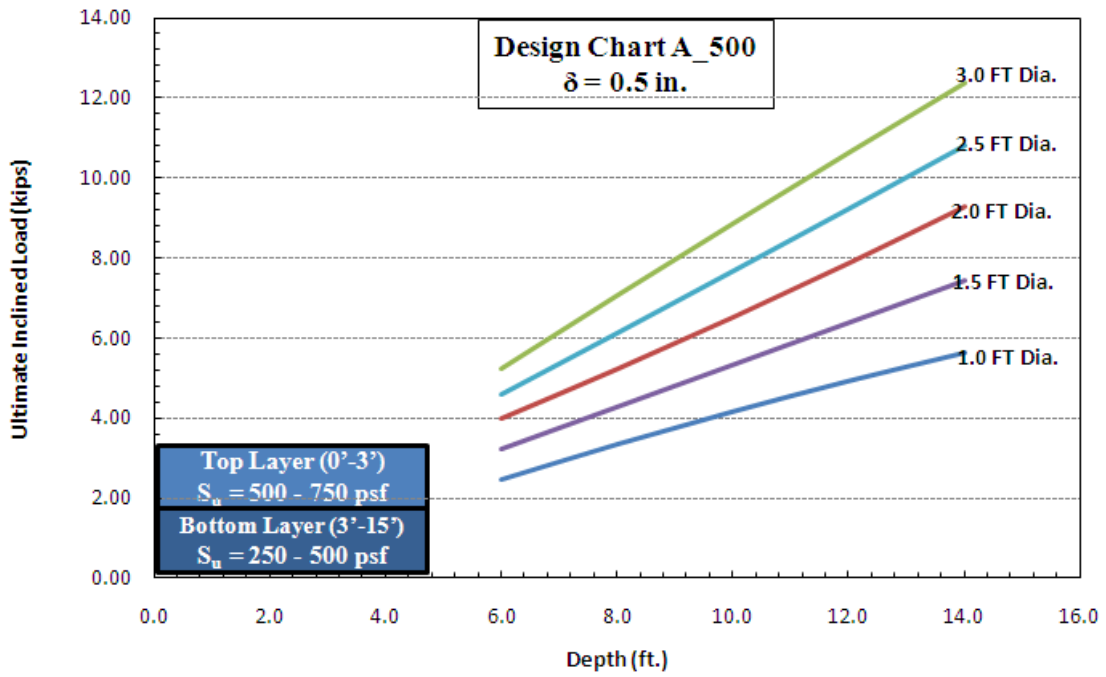
Figure 7.15 Design Chart A_500 with 0.5 in. Deflection Criteria (δ)
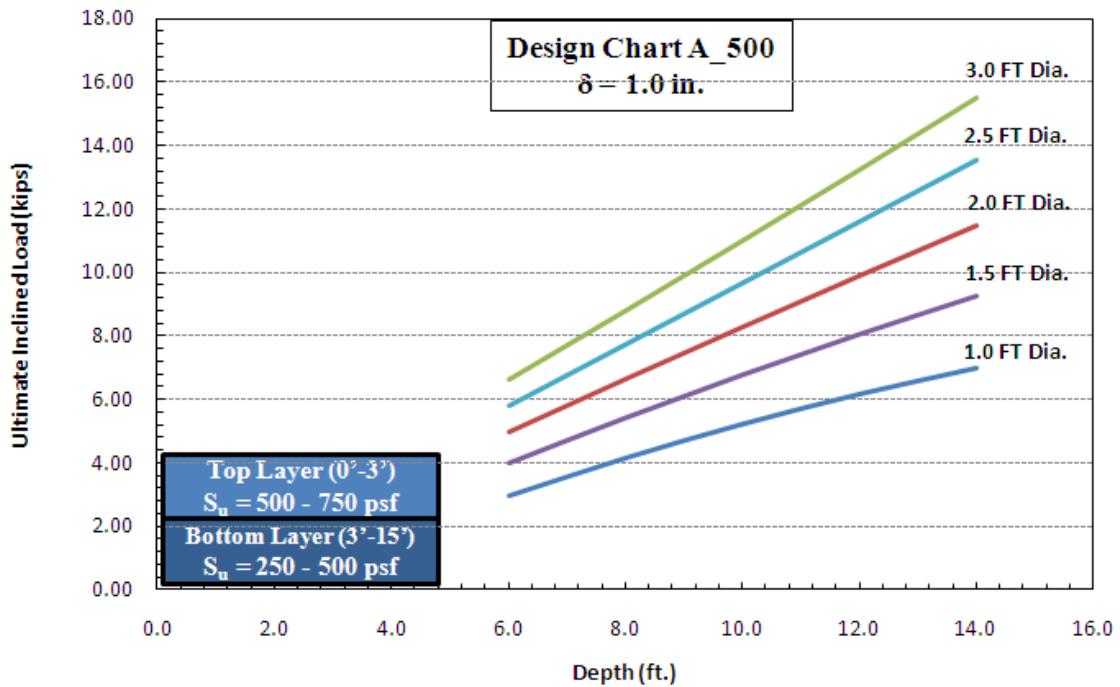
Figure 7.16 Design Chart A_500 with 1.0 in. Deflection Criteria (δ)

218
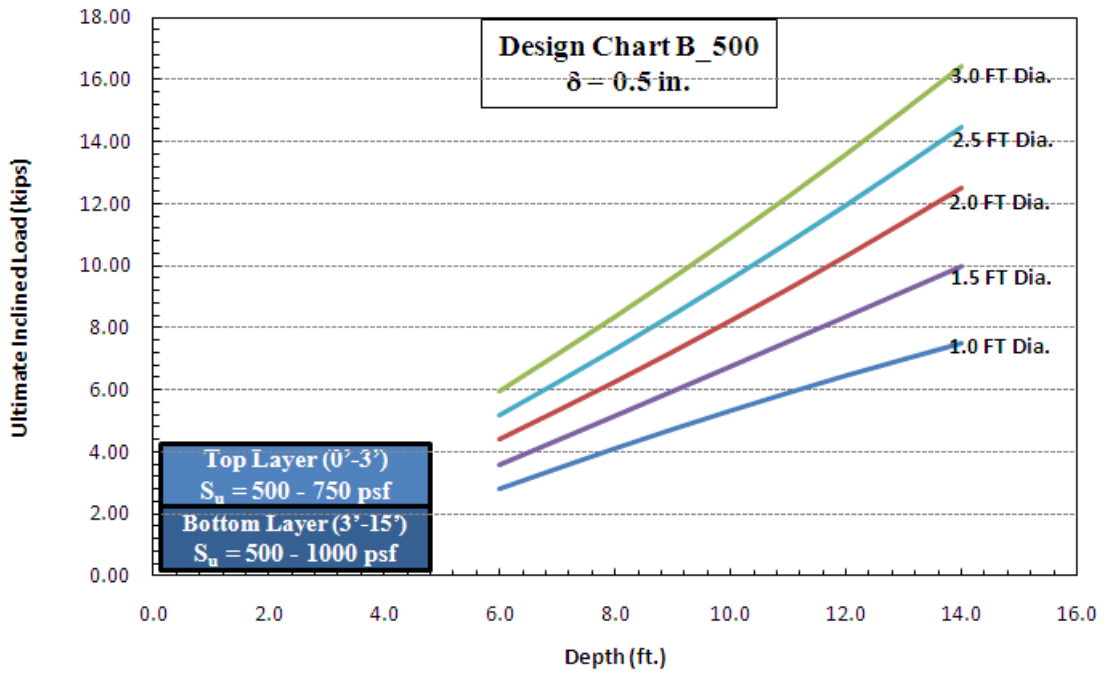
Figure 7.17 Design Chart B_500 with 0.5 in. Deflection Criteria (δ)
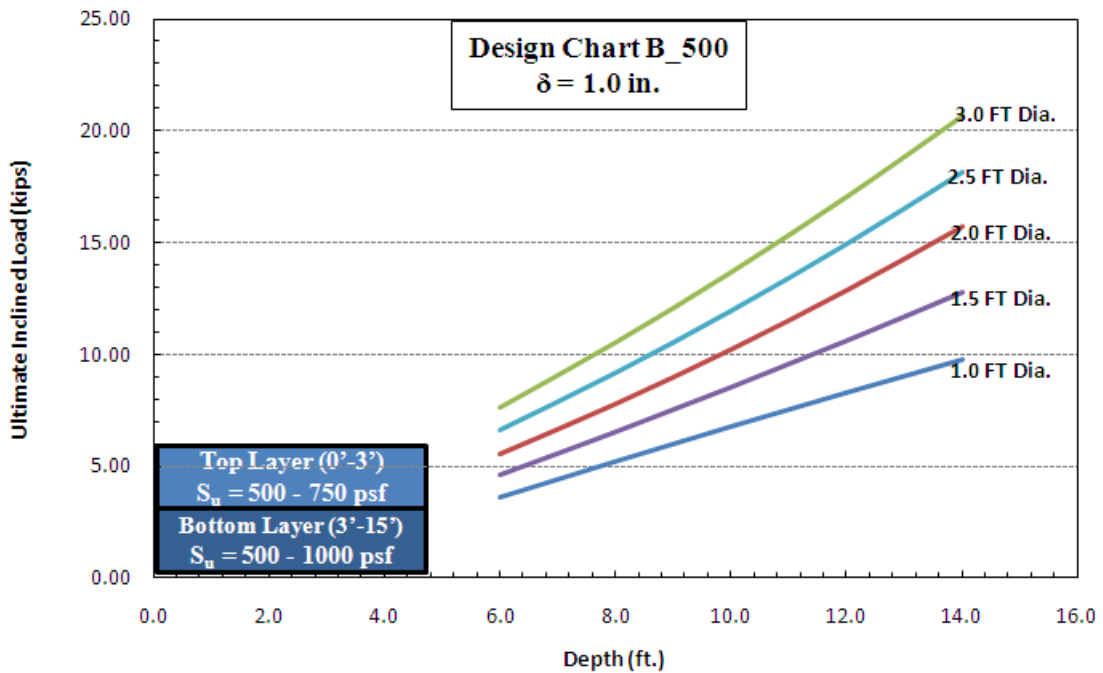
Figure 7.18 Design Chart B_500 with 1.0 in. Deflection Criteria (δ)

219
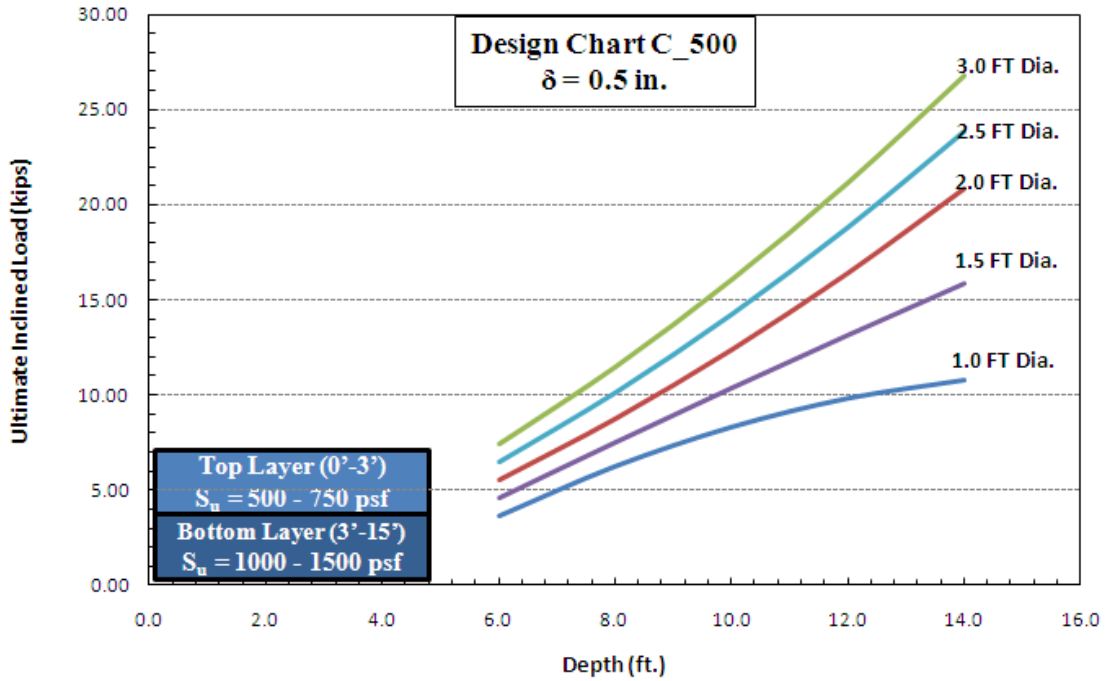
Figure 7.19 Design Chart C_500 with 0.5 in. Deflection Criteria (δ)
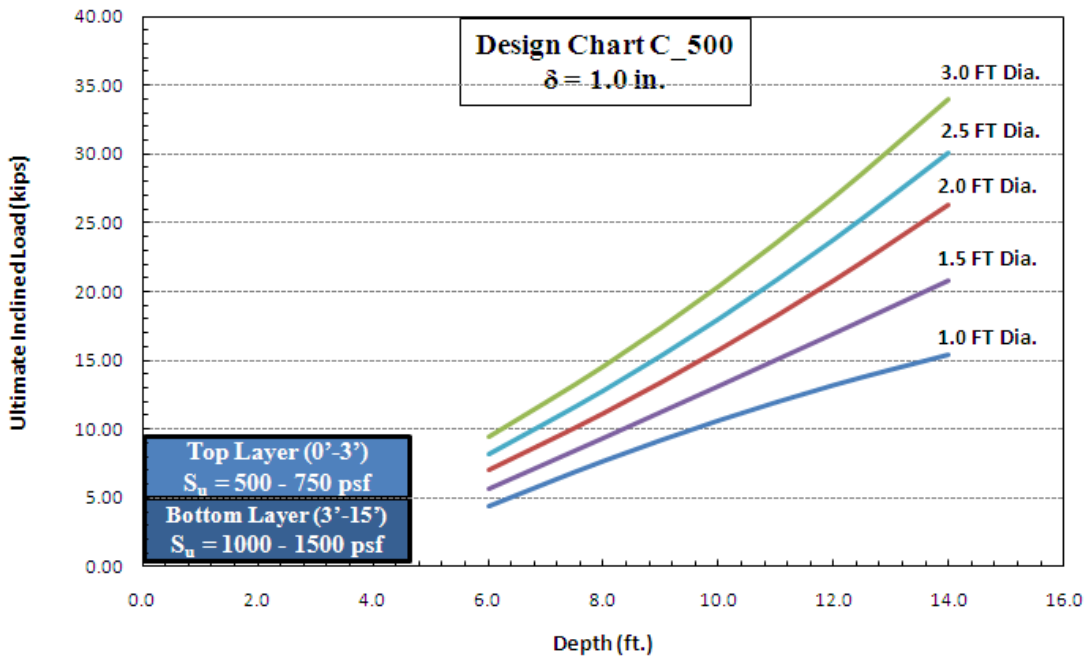
Figure 7.20 Design Chart C_500 with 1.0 in. Deflection Criteria (δ)
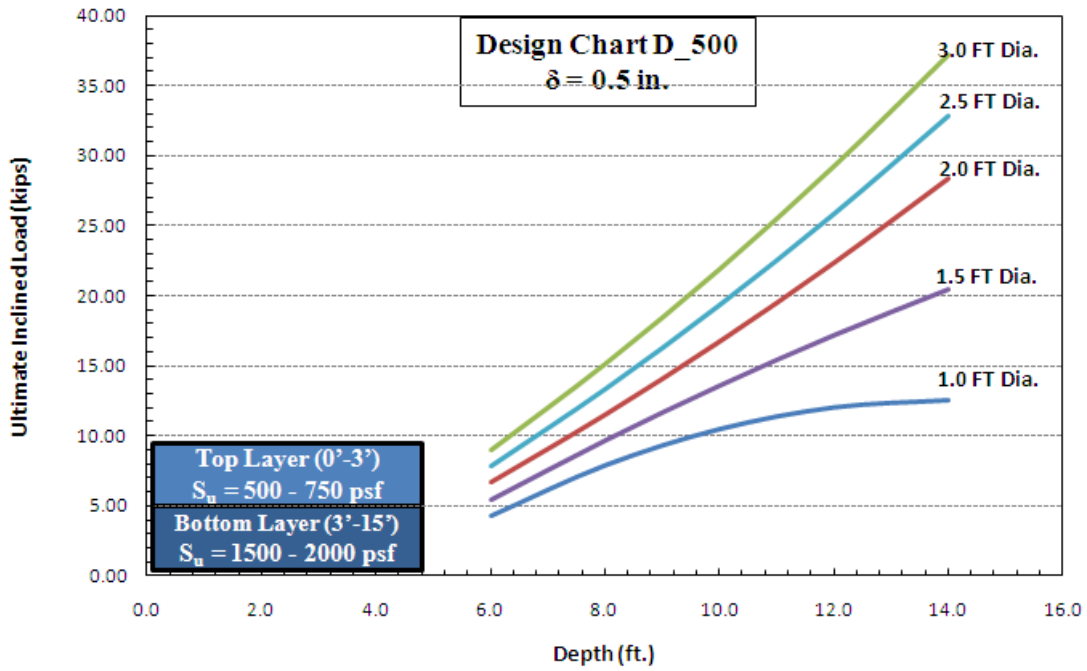
Figure 7.21 Design Chart D_500 with 0.5 in. Deflection Criteria (δ)
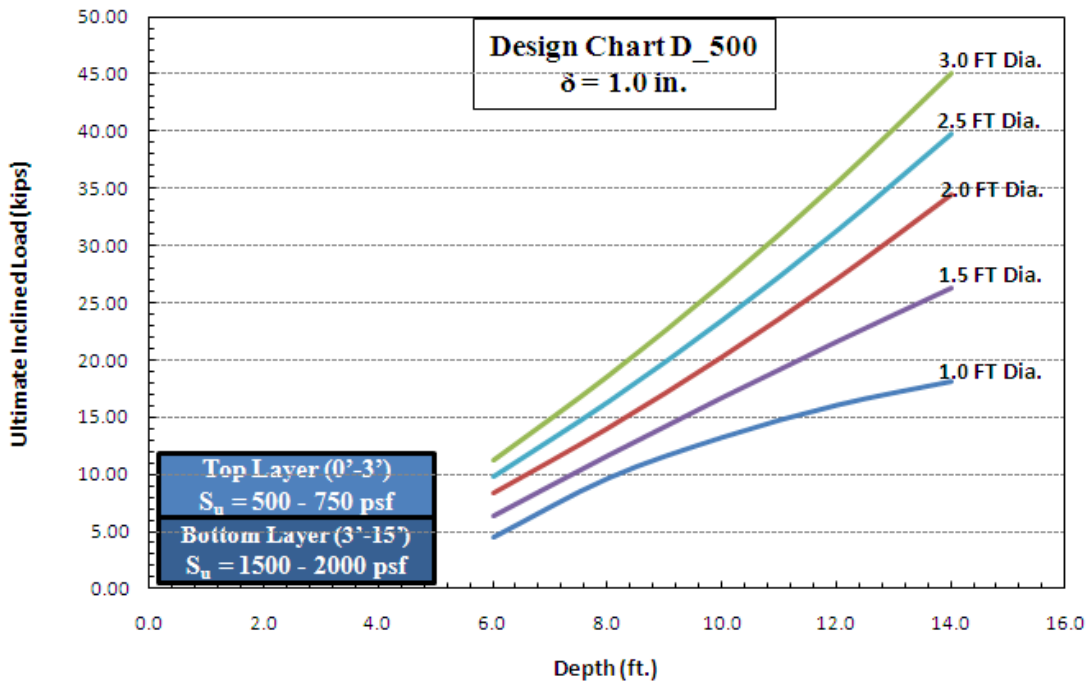
Figure 7.22 Design Chart D_500 with 1.0 in. Deflection Criteria (δ)

221
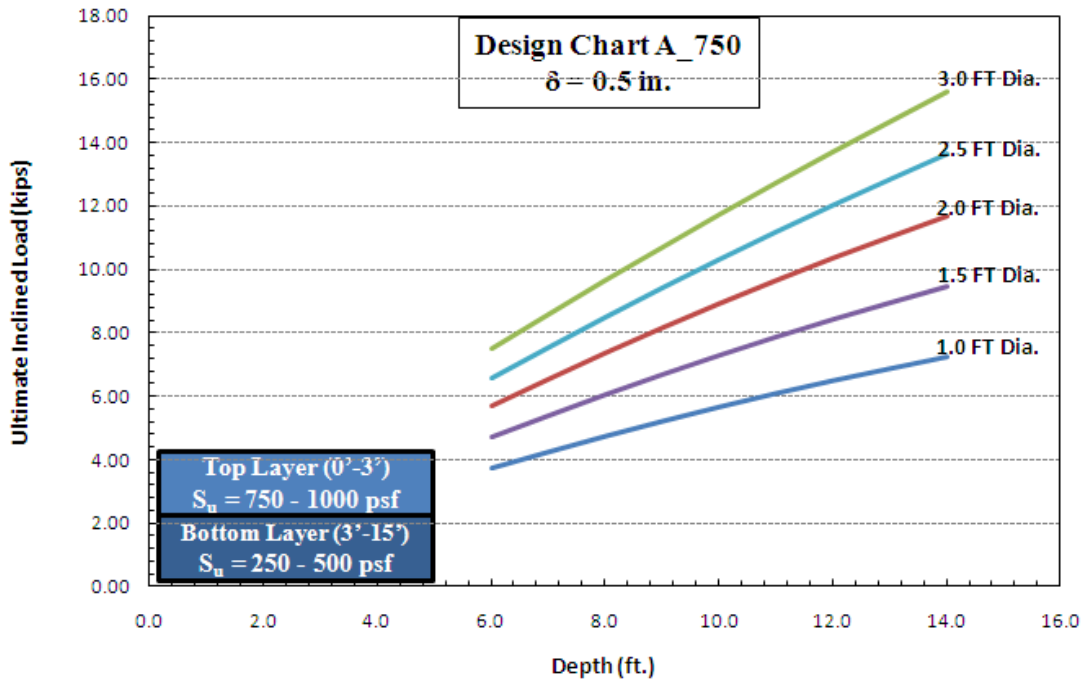
Figure 7.23 Design Chart A_750 with 0.5 in. Deflection Criteria (δ)
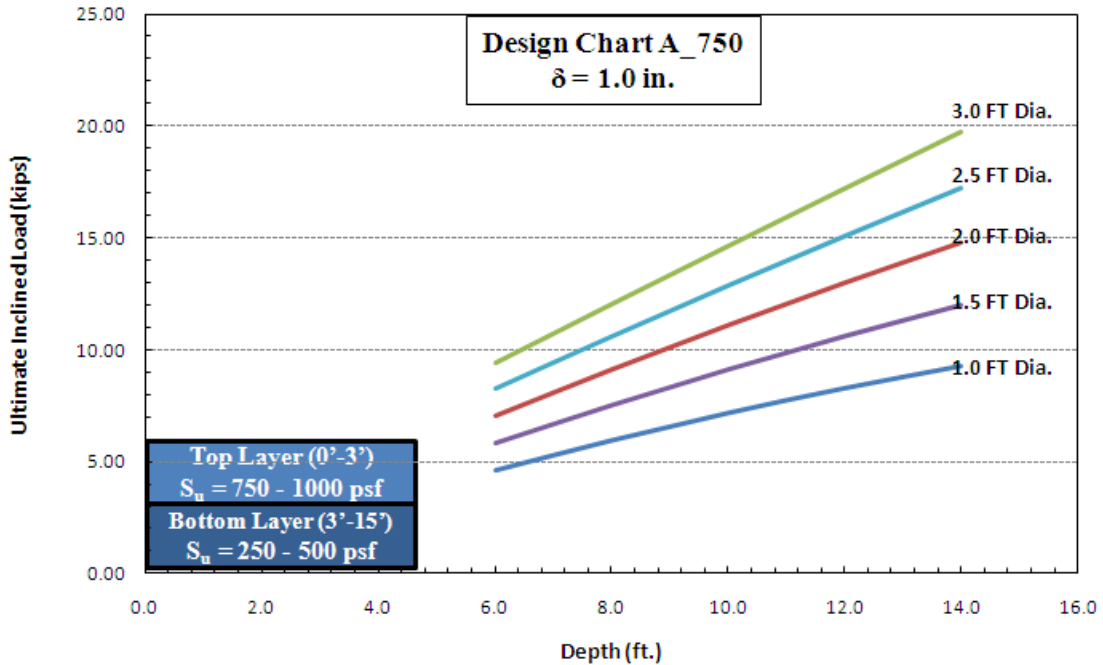
Figure 7.24 Design Chart A_750 with 1.0 in. Deflection Criteria (δ)

222
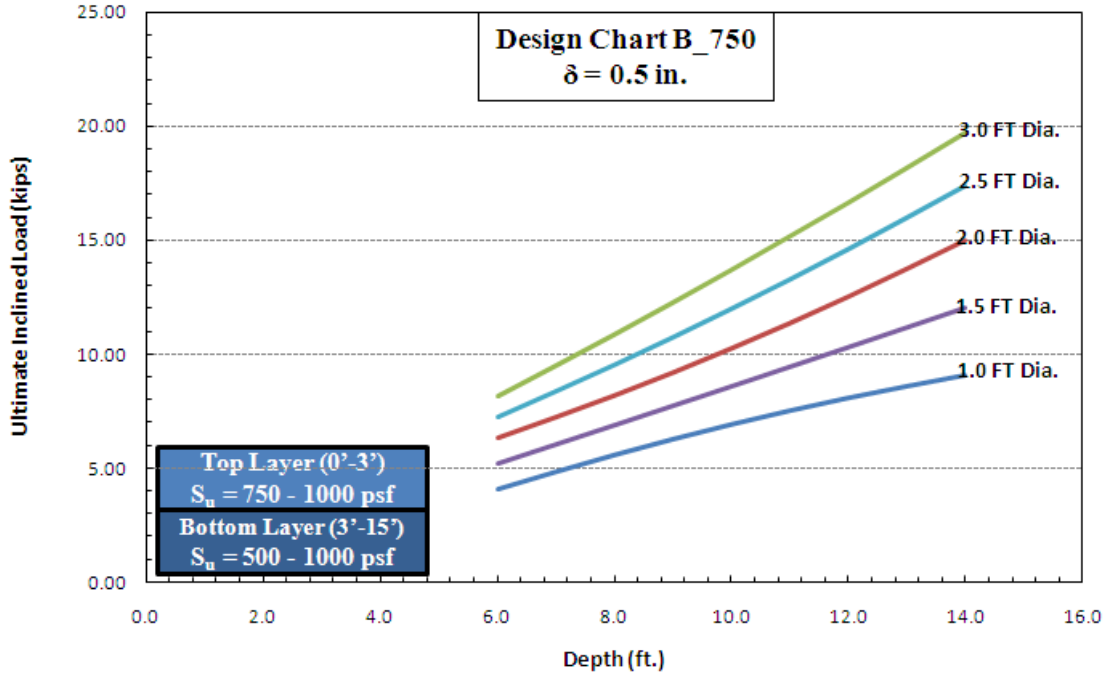
Figure 7.25 Design Chart B_750 with 0.5 in. Deflection Criteria (δ)
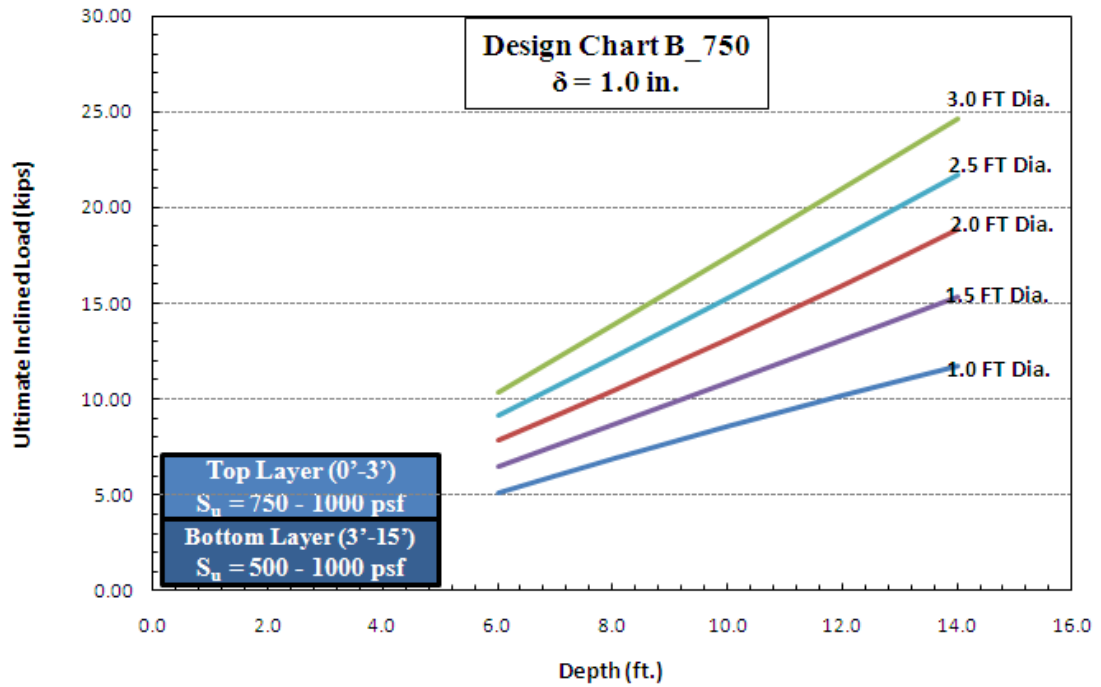
Figure 7.26 Design Chart B_750 with 1.0 in. Deflection Criteria (δ)
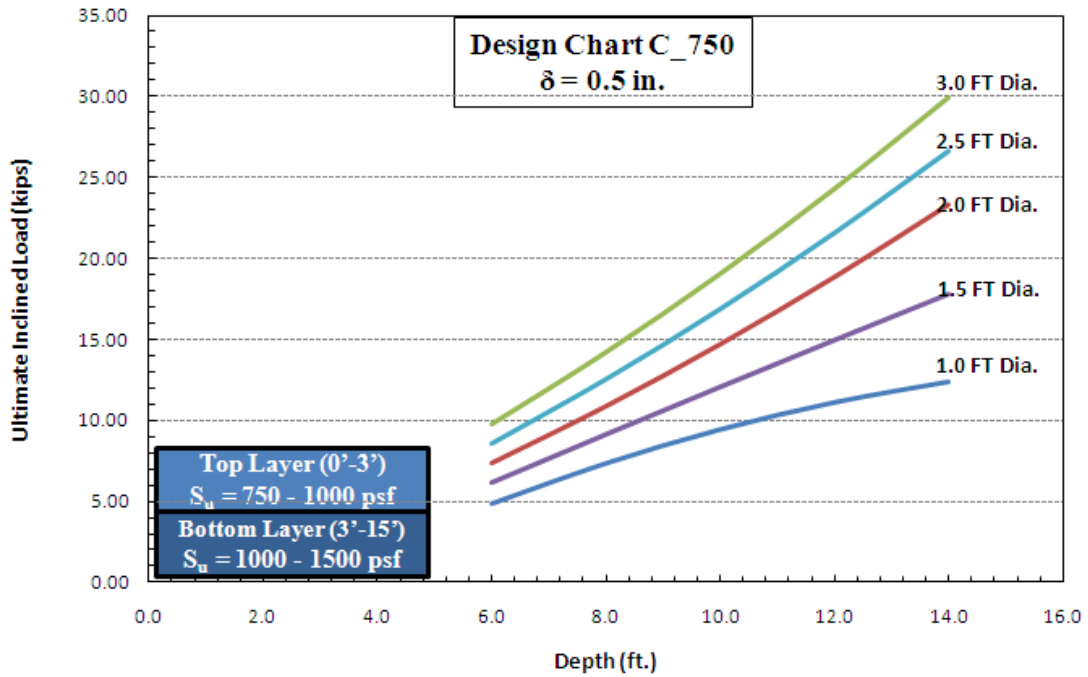
Figure 7.27 Design Chart C_750 with 0.5 in. Deflection Criteria (δ)
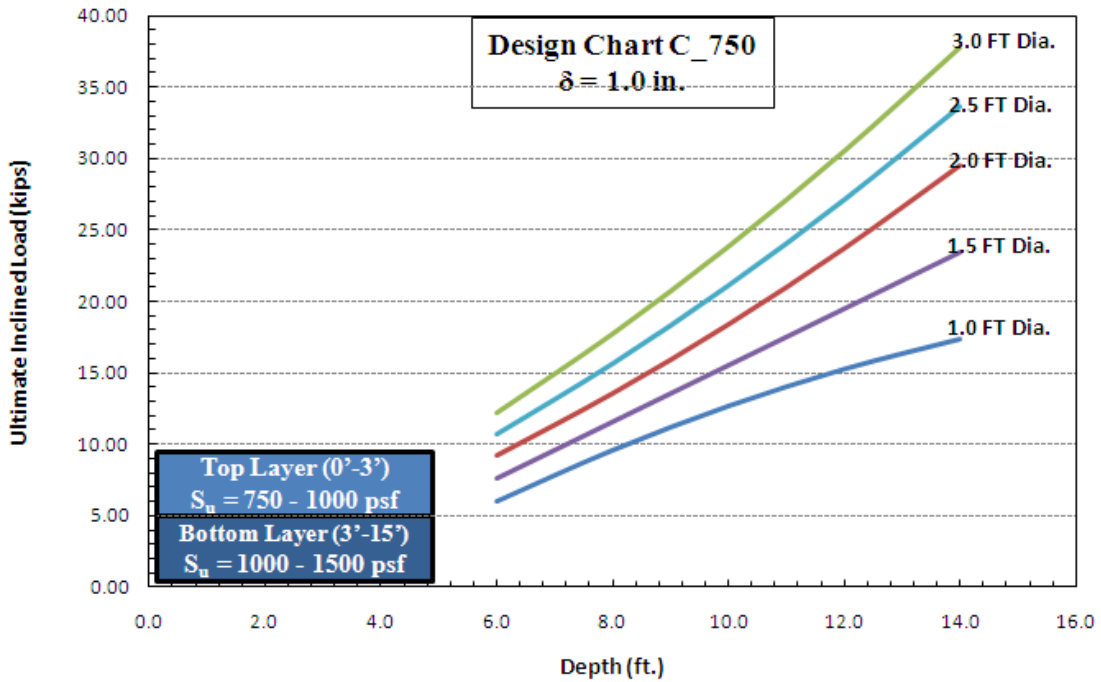
Figure 7.28 Design Chart C_750 with 1.0 in. Deflection Criteria (δ)
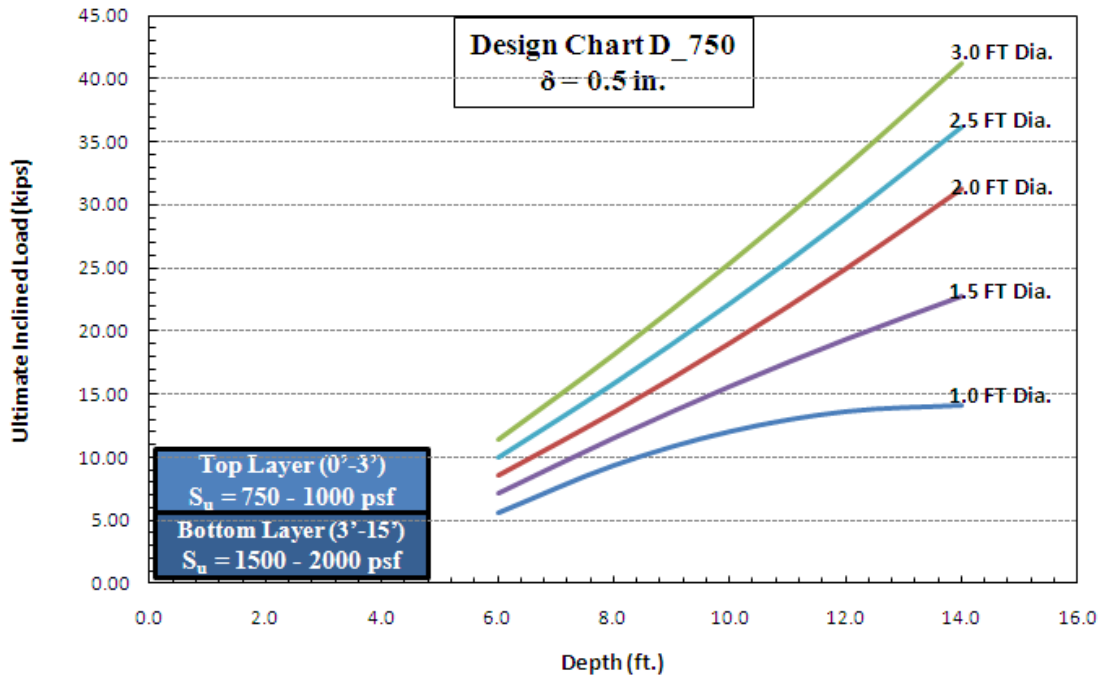
Figure 7.29 Design Chart D_750 with 0.5 in. Deflection Criteria (δ)
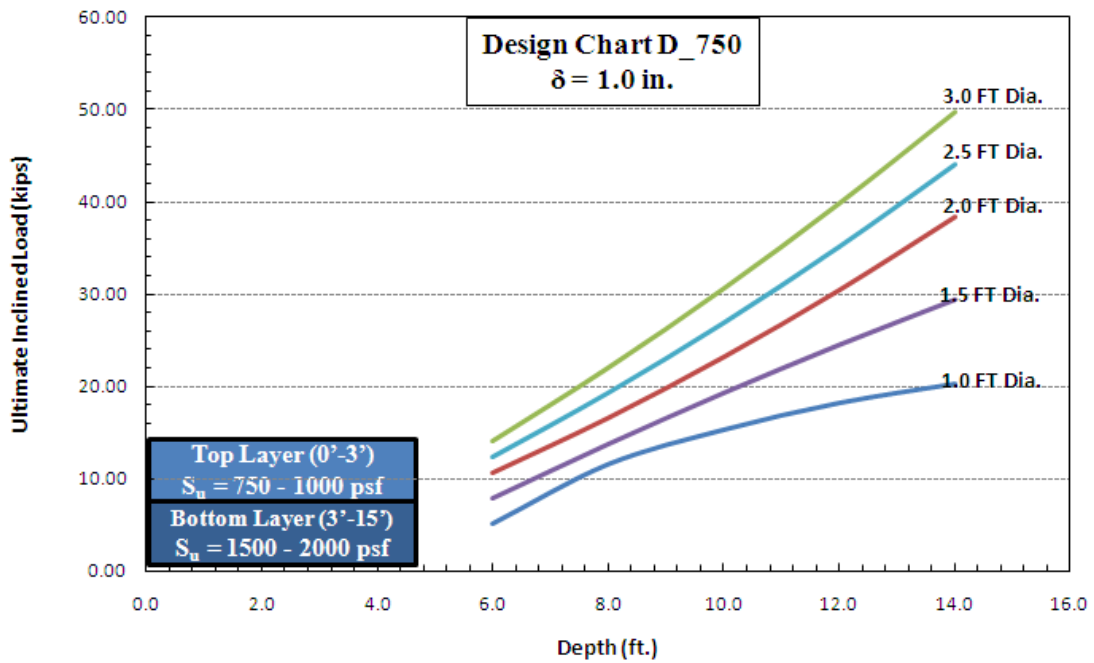
Figure 7.30 Design Chart D_750 with 1.0 in. Deflection Criteria (δ)

225
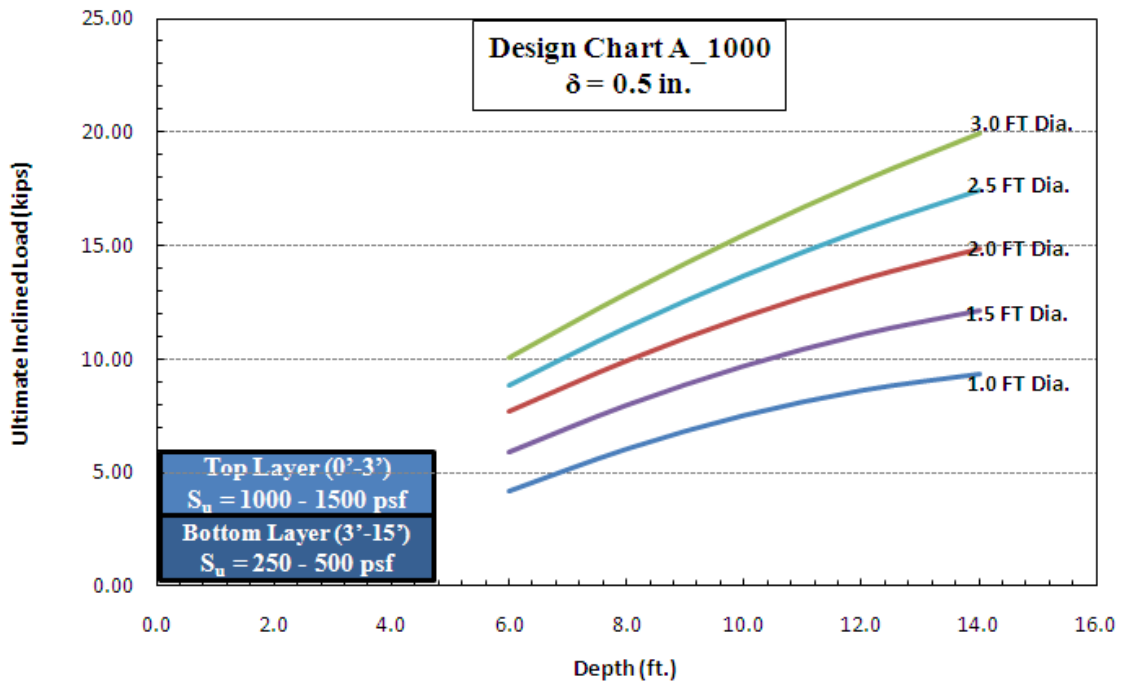
Figure 7.31 Design Chart A_1000 with 0.5 in. Deflection Criteria (δ)
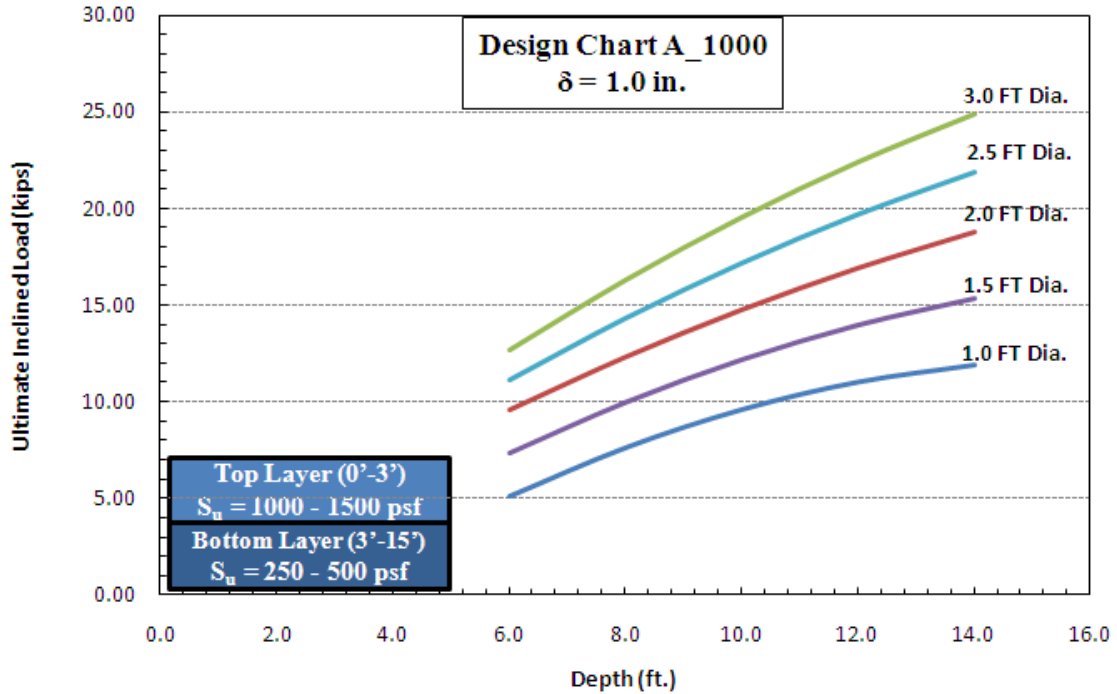
Figure 7.32 Design Chart A_1000 with 1.0 in. Deflection Criteria (δ)
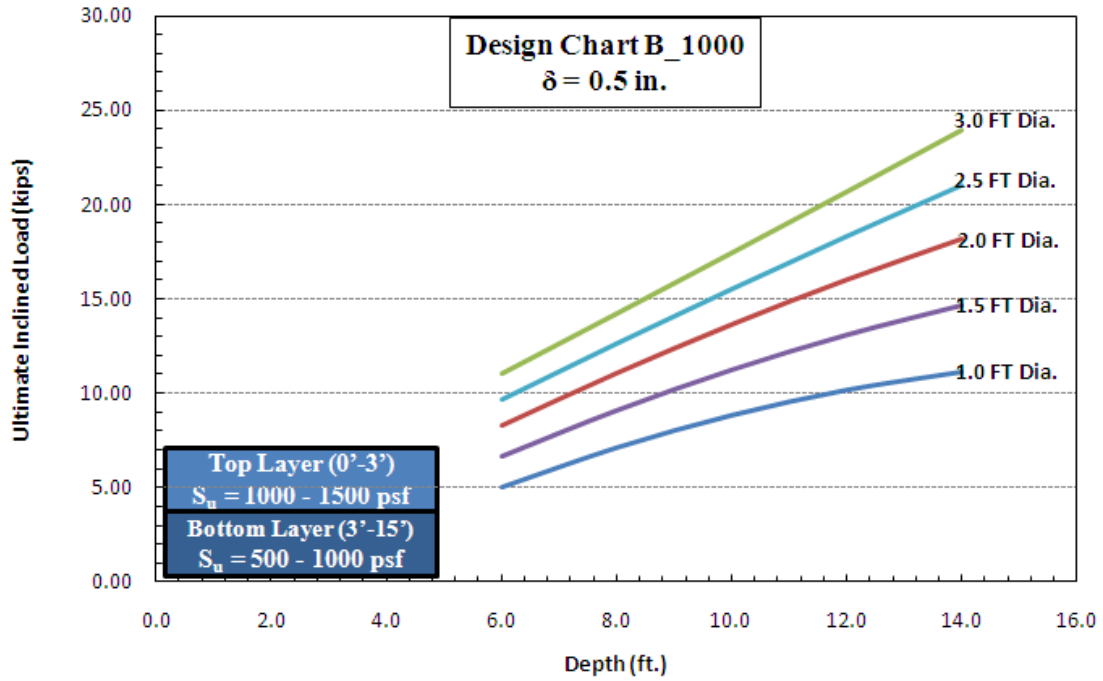
Figure 7.33 Design Chart B_1000 with 0.5 in. Deflection Criteria (δ)
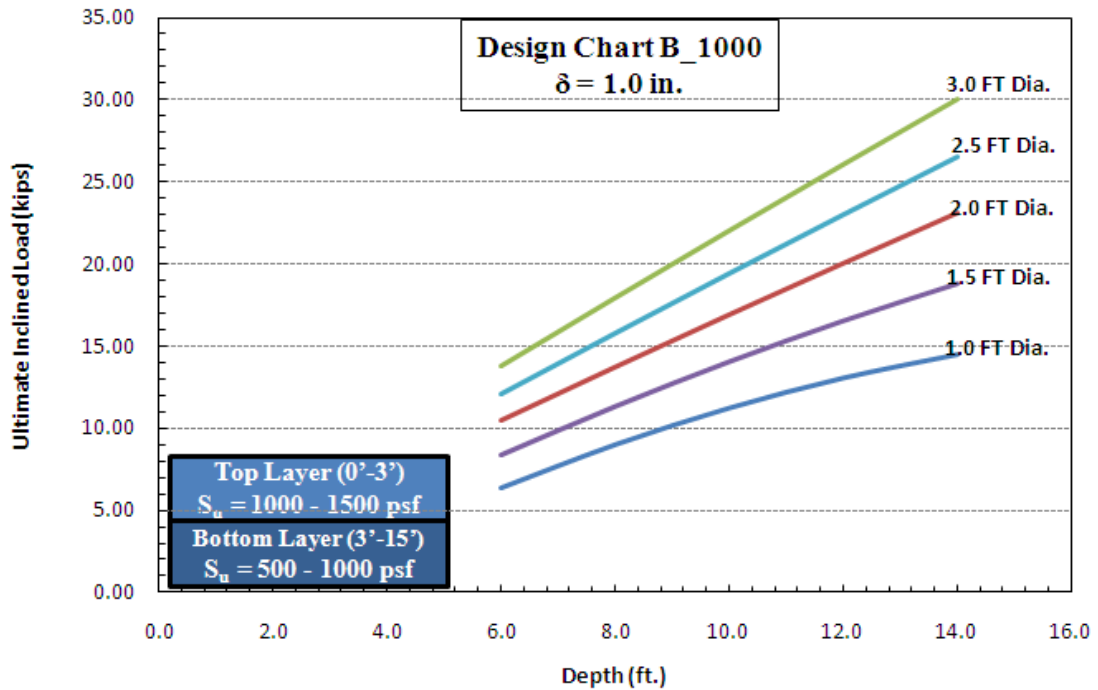
Figure 7.34 Design Chart B_1000 with 1.0 in. Deflection Criteria (δ)

227
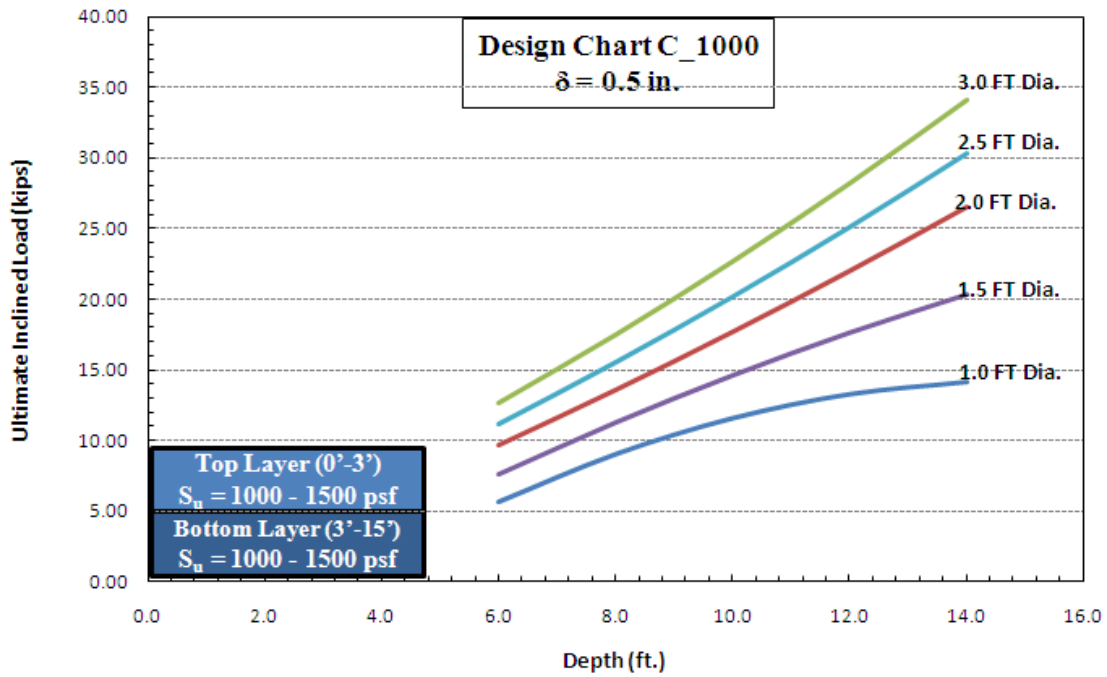
Figure 7.35 Design Chart C_1000 with 0.5 in. Deflection Criteria (δ)
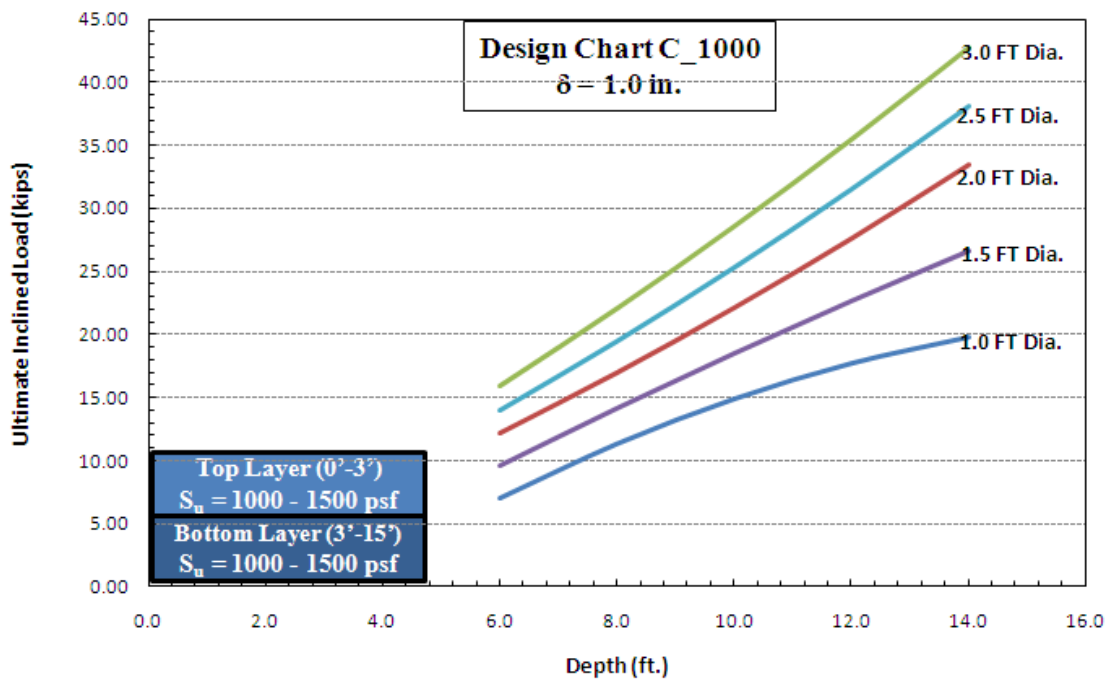
Figure 7.36 Design Chart C_1000 with 1.0 in. Deflection Criteria (δ)

228
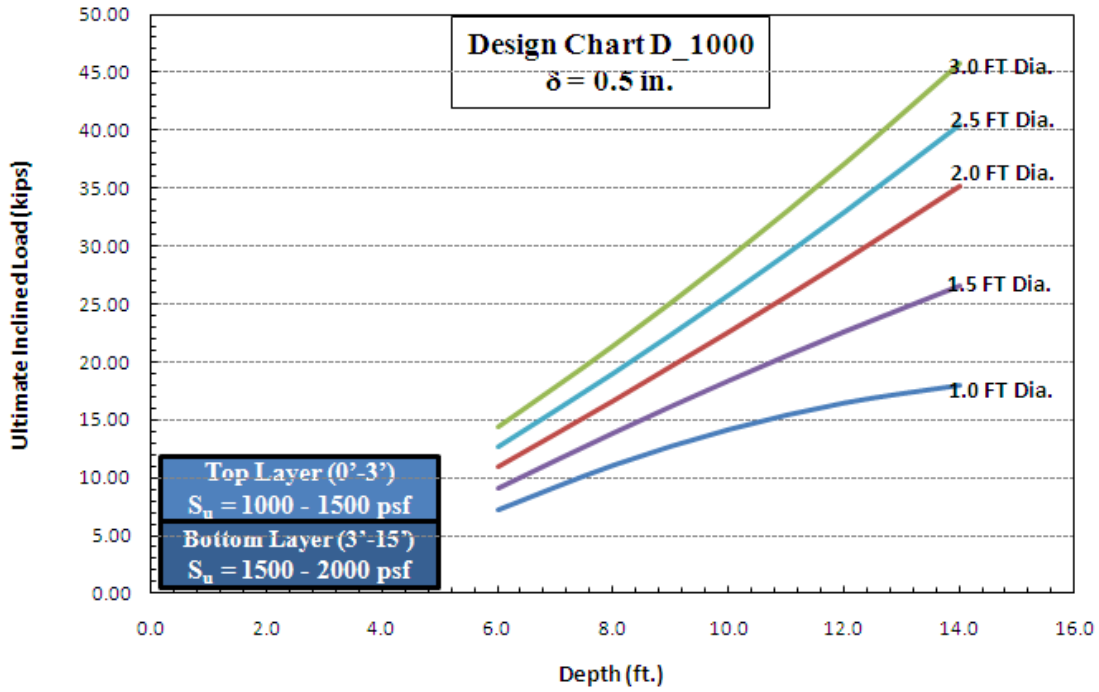
Figure 7.37 Design Chart D_1000 with 0.5 in. Deflection Criteria (δ)
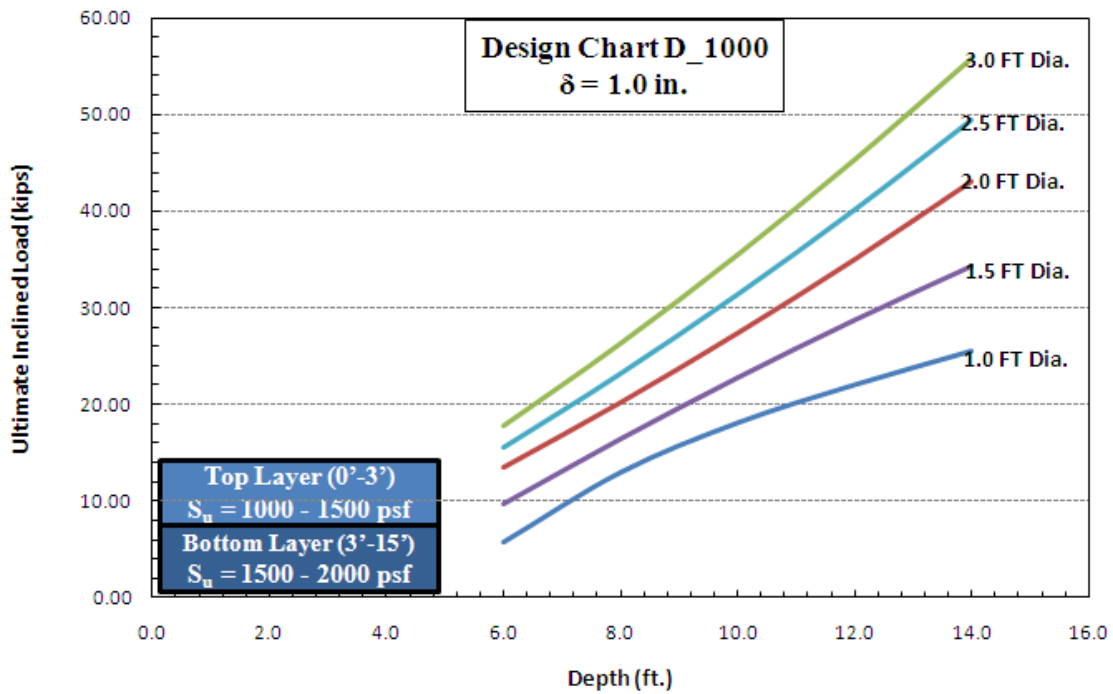
Figure 7.38 Design Chart D_1000 with 1.0 in. Deflection Criteria (δ)
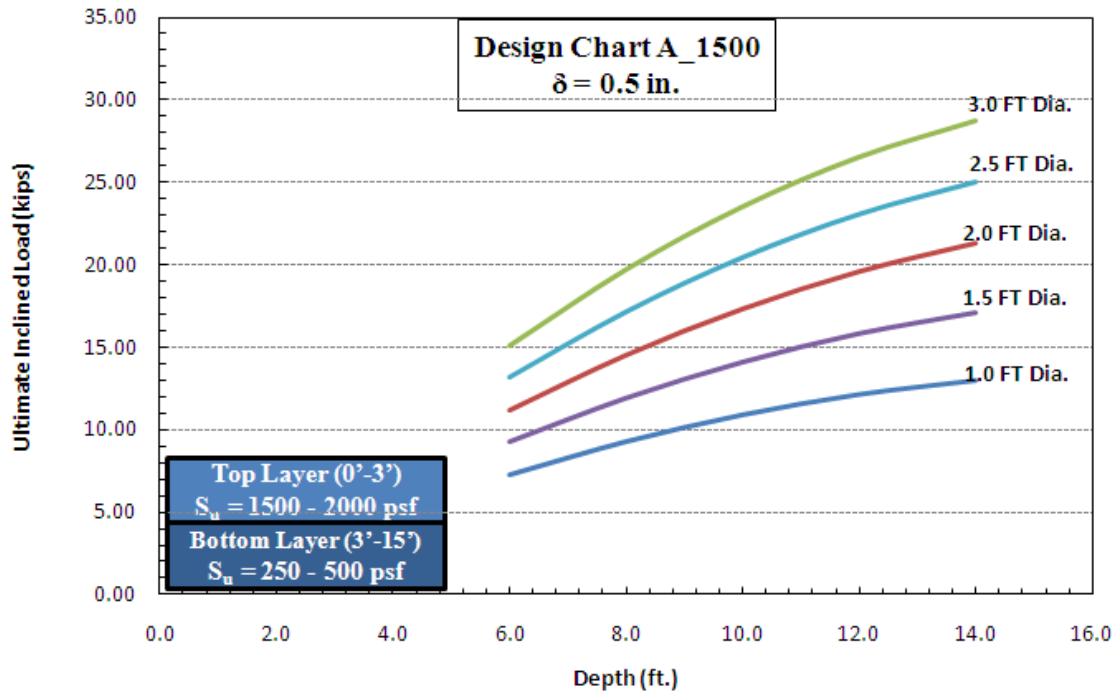
Figure 7.39 Design Chart A_1500 with 0.5 in. Deflection Criteria (δ)
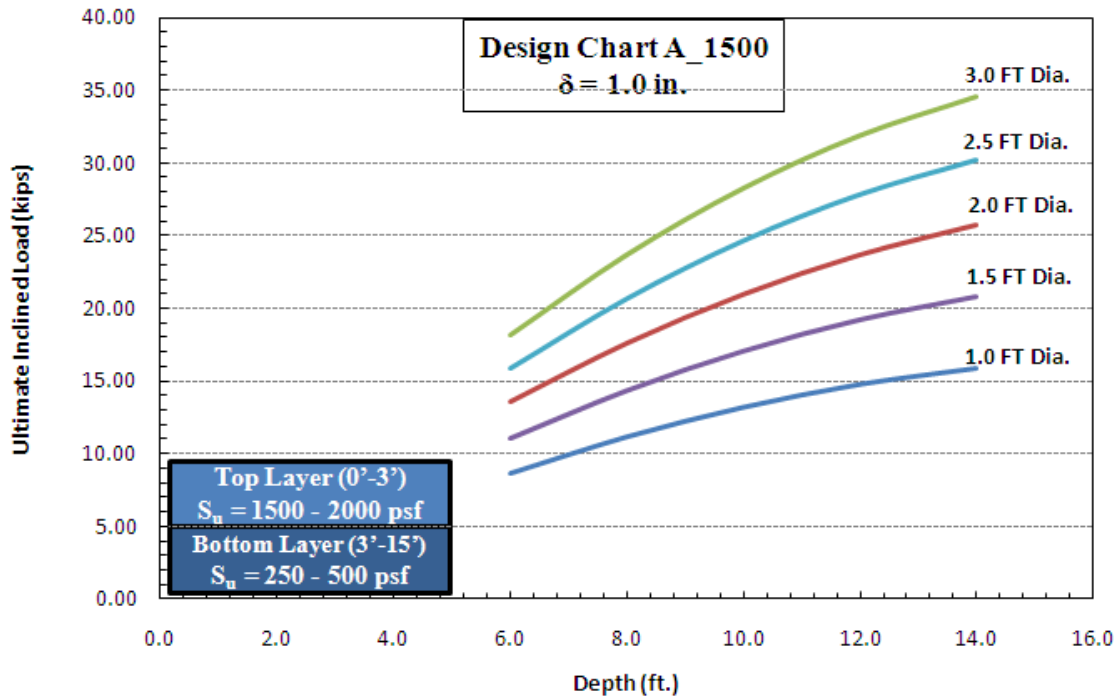
Figure 7.40 Design Chart A_1500 with 1.0 in. Deflection Criteria (δ)

230
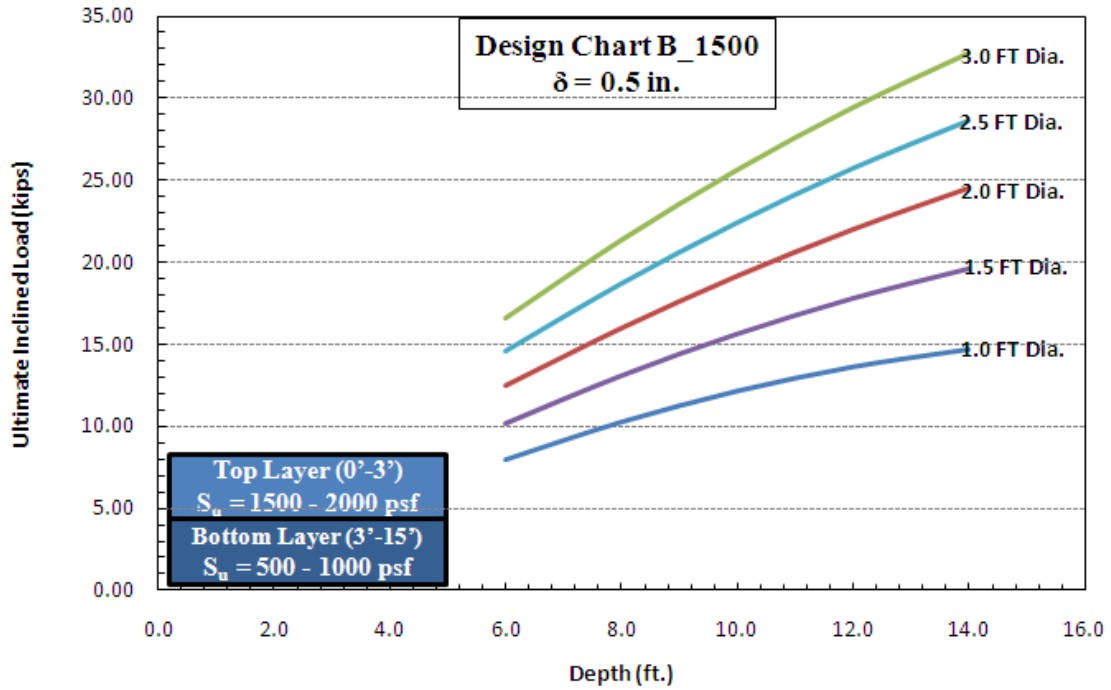
Figure 7.41 Design Chart B_1500 with 0.5 in. Deflection Criteria (δ)
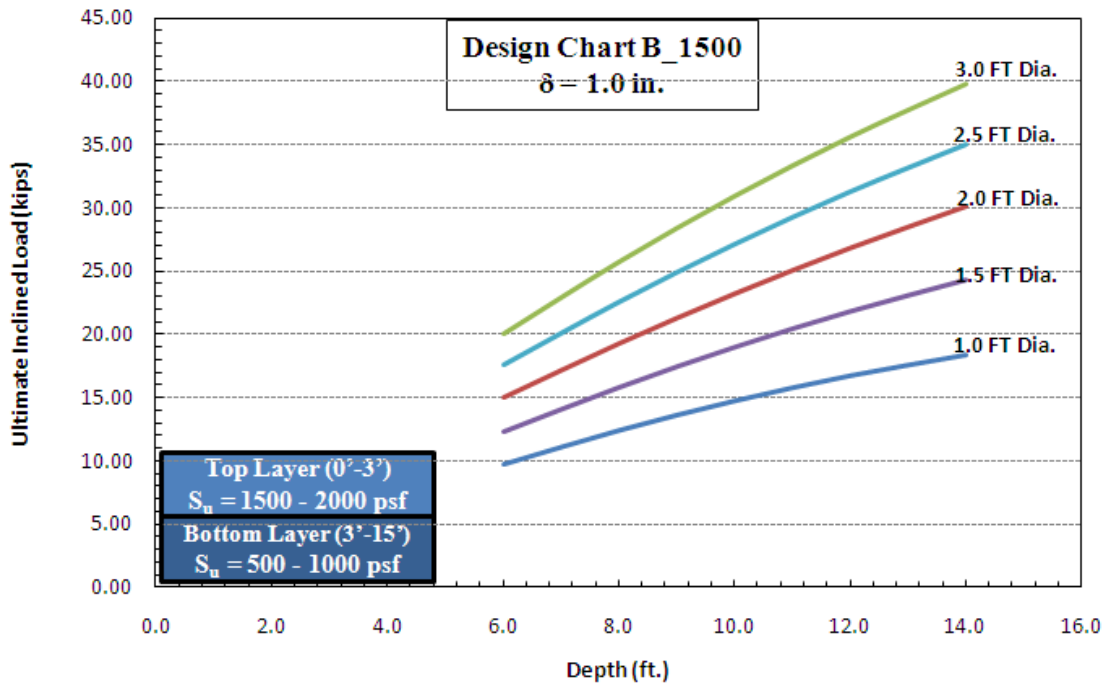
Figure 7.42 Design Chart B_1500 with 1.0 in. Deflection Criteria (δ)

231
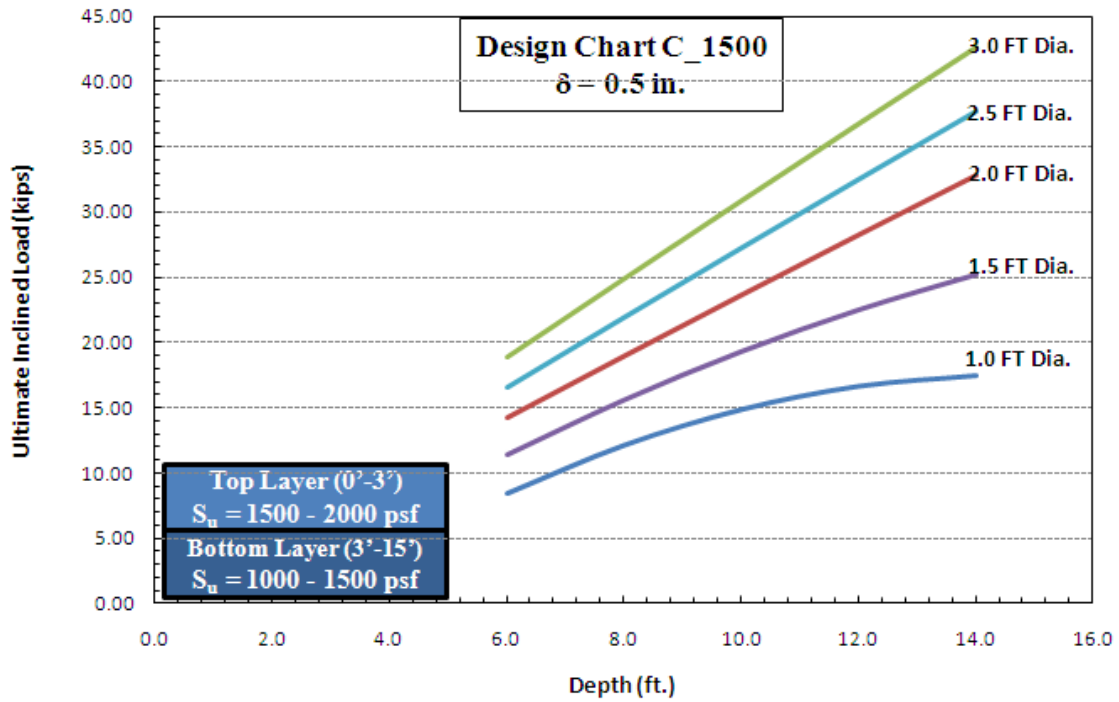
Figure 7.43 Design Chart C_1500 with 0.5 in. Deflection Criteria (δ)
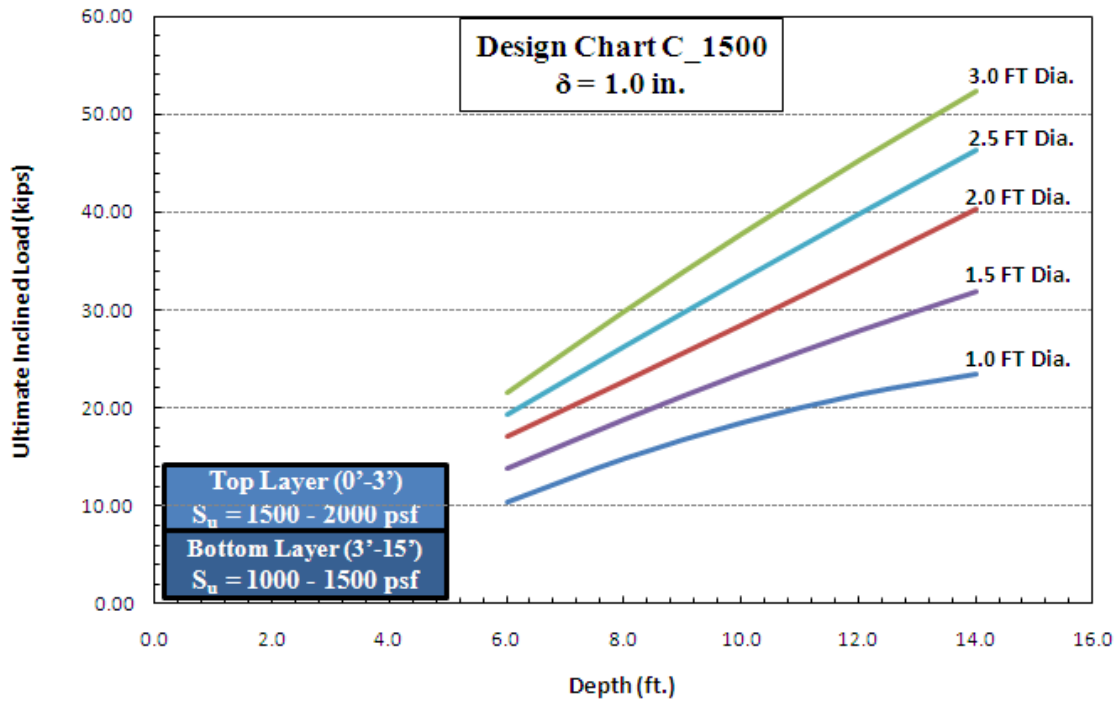
Figure 7.44 Design Chart C_1500 with 1.0 in. Deflection Criteria (δ)

232
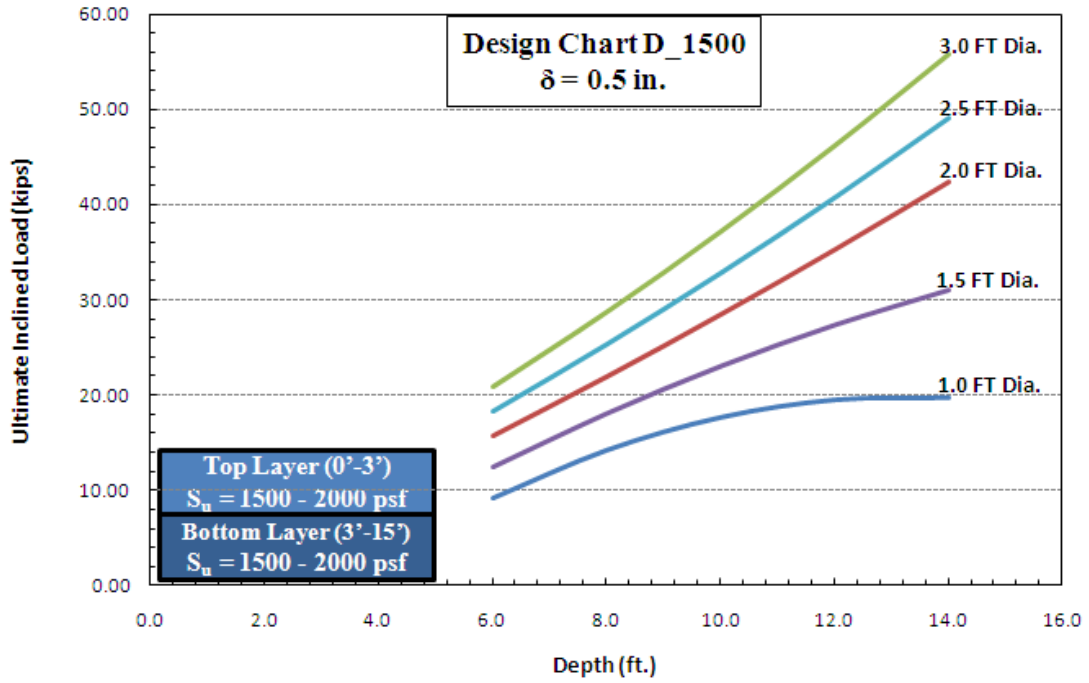
Figure 7.45 Design Chart D_1500 with 0.5 in. Deflection Criteria (δ)
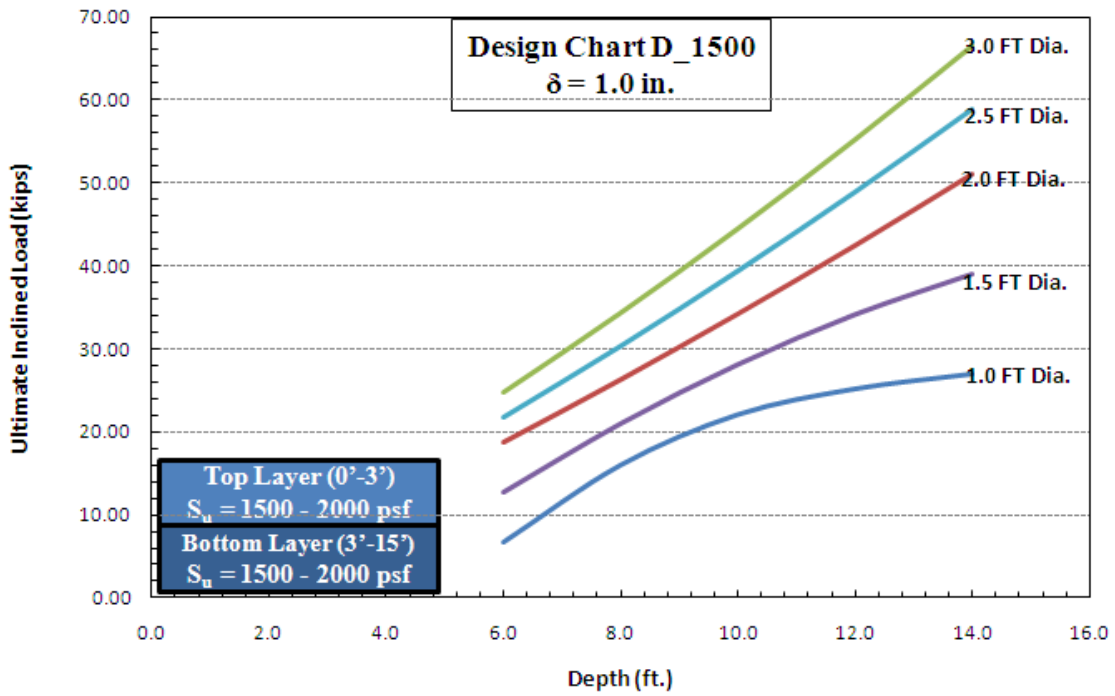
Figure 7.46 Design Chart D_1500 with 1.0 in. Deflection Criteria (δ)

233

In order to use a specific design chart, the undrained strengths of soils below the 3ft are needed. A simple arithmetic average of the shear strengths of layers between 3 and 15 ft is sufficient to select the appropriate design chart for designing drilled shaft. For cable tension consideration, the value will be based on ambient temperatures in the manufacturer's table and these details are given in Table 7.3. Typically the lowest temperature expected in the field is used for tensile load estimation. The next section describes the steps involved in the use of design chart for determining the sizes of the drilled shaft foundation.

The design tensile loads of the cables used in the cable barrier systems can vary between 3000 lbs for hot temperature conditions (around 100°F) to 8000 lbs for cold temperature conditions (below 0°F). Before selecting the number of cables from the present design charts, it is imperative to ensure that the tensile strength of the cables used can withstand the design tension that will be mobilized due to cold temperature conditions. If needed, more number of cables can be used such that no material failure will occur during the field operation conditions.

The present design charts are developed for three cable barrier system. However, in the case of two cable barrier system, users should check the cable material strength failure as an additional design step. In the case if the present design principles do not result in two or three cable barrier system due to deficiencies in material strength or extreme soil and environmental conditions, the researcher recommends the use of single shaft for each cable of the barrier system.

7.2.1 Example illustrating the use of the design chart for three Cable Barriers

When using the Design Chart to find the appropriate sizes of drilled shafts for supporting cable barriers, there are three main factors that need to be considered. The first one is determining the undrained soil strength properties in the region. The second one is to determine the tensile load generated in the cable based on the assumed coldest temperature

that the systems might experience. The last one is available space for the drilled shaft installation. From the manufacturer's design specifications, the load experienced by the cable at the ambient temperature condition is used to determine the tension generated in the cable barrier which is the required load to prevent cross-over collisions. An example design problem is given here:

First Step: Cable barrier system needs to be constructed in the area where the soil is clay. Site investigation shows the soil located is on clayey subsoil and the undrained shear strength of soil layers are given in the Table 7.3

Table 7.3 Undrained Shear Strengths of Soils for Design Chart Selection

Depth (ft.)	Undrained Shear Strength (S_u), psf
0 – 4	400
4 – 9	1000
9 – 15	750

Second Step: From the Flow Chart shown in Figure 7.3, the average undrained shear strength of top layer is in the range 250 – 500 psf, and hence 250 psf chart is selected. Then, from the Flow Chart of Figure 7.4, it can be identified that the best design chart suitable for the above soil condition is Design Chart B for 0.5 or 1.0 deflection criteria. Thus, the design chart needed here is the Design Chart B_250. For the 1.0 in. deflection criterion, the Design Chart B with 1.0 in deflection criterion is selected for the design of drilled shafts (Figure 7.10).

Third Step: In a 3-cable barrier system, the tension of each cable at 10° F (-12.2° C) from Table 7.3 should be 7200 lbs because cold temperature condition of 10° F (-12.2° C) is considered here as the worst case field temperature conditions. Since all three cables are anchored into one single drilled shaft, the ultimate load acting on the drilled shaft is 7,200 lbs X 3 cables = 21,600 lbs (21.6 kips).

Fourth Step: The factor of safety values against overturning (lateral failure) or pullout (uplift) failures of the drilled shaft are assumed to be 1.5 to 2.0. A value of 2 is assumed here for

conservative design purposes. Therefore, the ultimate load that the shaft needs to resist is 21,600 lbs x 2.0 = 43,200 lbs (43.2 kips).

Fifth Step: From Figure 6.13, at a load estimated from the previous step, it can be noticed that the load is beyond boundary provided in the graph. Hence, number of cable connected to drilled shaft should be changed to two cable connected to one drilled shaft plus another cable to a drilled shaft or three cable separated and connected to single drilled shaft each. Here, one cable connected to one drilled shaft is chosen.

Sixth Step: The ultimate load acting on one cable attached to one drilled shaft is recalculated as 7200 lbs x F.S. of 2 and this value is equivalent to 14,400 lbs (14.4 kips). Thus, from Figure 7.10, the appropriate sizes to withstand this load are 3.0 ft diameter x 12 ft depth and 2.5 diameter x 14 ft depth, respectively as shown in Figure 7.47. Final size of the shaft chosen from this group based on construction considerations.
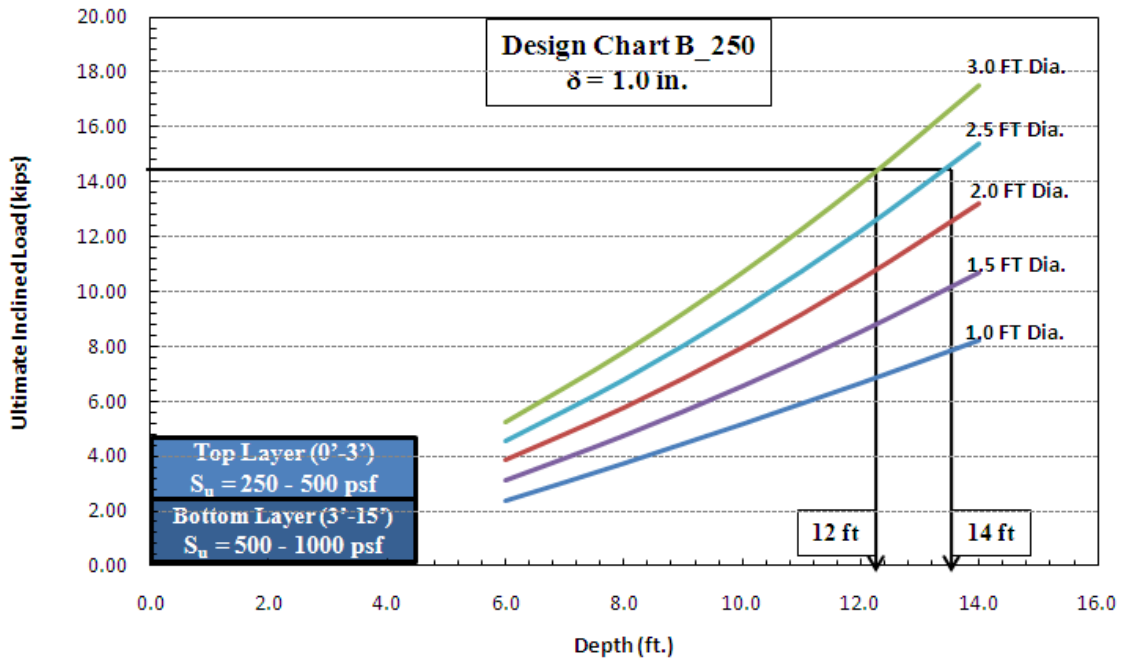
Figure 7.47 Example of using the Design Chart for three Cable Barriers

Another variable that influences the use of design charts is the assumed factor of safety value. Based on the limited number of field inclined load test data, currently the researchers

236

recommended the FS value of about 1.5 to 2.0, which is quite high, but this high value is needed as this design is related to safety issues involving human lives or to limit the number of crossover accidents. This FS value may be reduced in the future with the improved performance of these cables barriers with minimal distress.

<u>7.3 Construction Guideline and Recommendation</u>

Installation of the drilled shaft foundations for the cable barrier systems can be performed with general construction; however, there are a few additional recommendations for construction of shafts in high PI soils. During wet season, water is the main factor that can induce the swelling of expansive soils. Thus, drainage should be provided at the areas close to the ends of each cable barrier system.

Another consideration is after excavation is finished, the lateral expansion of the expansive soil underneath the ground should be visually examined to ensure that cross section of drilled shafts is consistent along the depth of drilled shaft. If there is some lateral soil expansion in the hole, necessary steps should be taken to ensure that the drilling is needed again to maintain the diameters of shafts.

Due to the potential of swelling and shrinkage of the soil, a concrete pad or mow strip (Figure 7.48) should be placed on the ground surface at the top of the end drilled shaft plus around the first post next to the drilled shaft in order to keep soils surrounding the shaft exposing to moisture movements. Also, this mow strip can prevent soil at the top shaft crack and lead to loss of contact between drilled shaft and soil in dry season. For the full detail of mow strip, it can be seen in the Appendix E. Current TxDOT contracts usually require a concrete pad poured as a mow strip continuously for the entire run of the cable system. It is recommended that this practice to continue with the additional requirement that the concrete be poured 1 – 2 ft (0.3 – 0.6 m) past the end shaft.
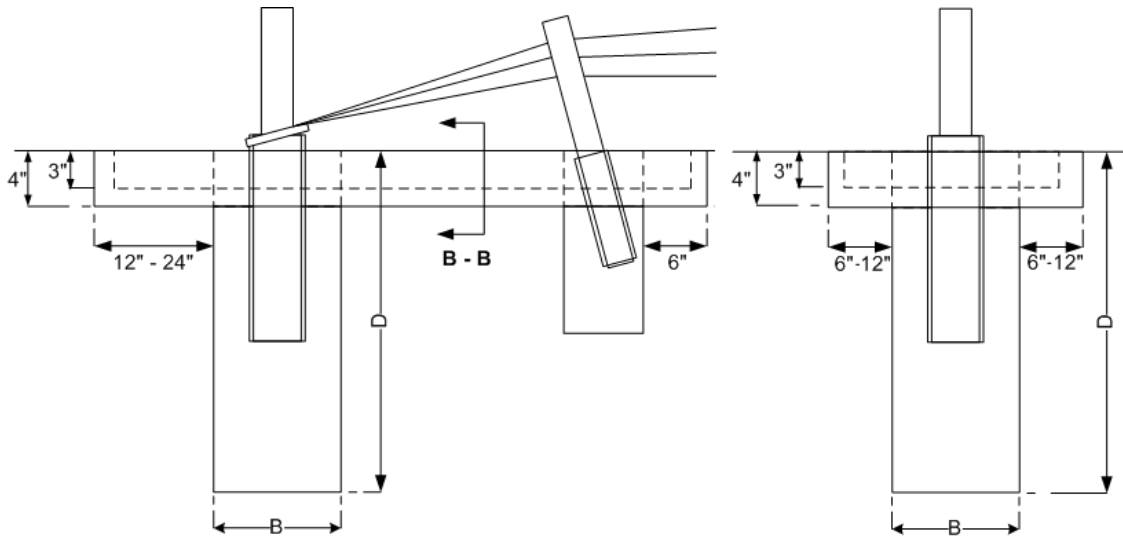
Figure 7.48 Details of Concrete Pad Placed on the Top of the Drilled Shaft at the End of Cable Barrier Systems

During a dry season, construction can be performed normally; however, curing of concrete above ground is needed to retain water in the mix to allow the hydration process as long as possible so that the concrete attains the highest strength.

Another recommendation for maintenance program is to perform monitoring and re-tensioning of cables. In each year, there are two major cycles of the weather changes, hot to cold conditions and cold to hot conditions, which induce major impacts including loss of tensile forces in the cables. Therefore, monitoring and re-tensioning of cables are necessary if the tension of the cable does not match with the tension design charts based on the current temperature conditions as per the manufacturers' specifications.

7.4 Summary

This chapter provides the details of design chart development including construction guidelines and recommendations. For the design chart development, the design charts for the field testing condition were originally developed. The charts are specific for certain shear strength values of top and bottom layers. Flow charts are provided here to help in the selection of the appropriate design chart.

In addition to the design, a modified concrete pad is recommended to be used with the foundation in order to help maintain the contact area between drilled shaft foundation and surrounding soil. A few recommendations are specified to maintain the tension in the cables remain constant which will protect the public from accidents.

CHAPTER 8

SUMMARY, CONCLUSIONS AND FUTURE RESEARCH

8.1 Introduction

Deep foundations including drilled shafts, piles and piers have a primary function to support axial compressive, uplift and lateral loads. When deep foundations are subjected to uplift and lateral loads in the same time, that foundation is necessary to be designed to support inclined load. The example of using the inclined load is the foundation that is connected with the cable to support transmission tower or cable median barrier systems.

In early 2007, the failure of foundation in cable barrier system occurred in the area south of Terrell in Kaufmann County, Texas, USA. This area had received an abundance of rain and experienced unusually cold weather for an extended period. It was hypothesized that soil expansion causing uplift and the tensile forces mobilized in the cables due to the colder weather might have caused the foundation failures. The main objective of this research is to develop an experimental plan to confirm or reject this hypothesis. In addition, the study of drilled shaft behavior under inclined loading was focused. This behavior is later used in the design chart development for cable barrier system.

This research effort mainly focused on site selection, site soil characterization, load test facility design and construction, discussion of the load test results, model comparisons and design chart development. The following describes some of the major findings and summary results presented in Chapters 3 to 7.

A test site was located on IH20 at Rose Hill Road, being near the site of the two previous failures, in an area that would readily accommodate the construction equipment, provide unrestricted access, and provide safety from the travelling public.

Preconstruction field investigation and laboratory testing yielded soil that was classified as silty sand, high-plasticity clay, and lean clay. The two clay soils were of significant interest to the researchers for this study. From these test results, it was deemed that the selected site was very satisfactory for the continuation of the installation of the design test sets in the field. Additionally, weather conditions during the past nine months from June 2009 to February 2010 allowed the researchers to perform load tests under summer- and winter-like conditions that contributed to the two actual cable barrier systems failures three years earlier.

In September 2009, field testing for the summer condition (dry and hot) occurred. This consisted of testing one test shaft from each of the three reaction shafts. As the hypothesis focused on soil expansion and cold weather, these three tests were only used for comparison purposes here. In February 2010, the additional nine shafts were subjected to load tests under ideal field winter conditions (totally saturated soil and cold temperatures). The area also unexpectedly received a record 24-hour snowfall of 12 in. (300 mm) adding to the continuance of the soil being totally saturated. Ice lenses were seen on the water that was ponded on the ground surface indicating freezing temperatures during the night. The 1 ft (0.3 m) and 2 ft (0.6 m) test shafts experienced large lateral and vertical displacements due to the load testing during this winter condition. Cracking of the concrete, both horizontally and vertically, was observed on few of the test shafts.

8.2 Conclusions

The present conclusions are categorized into three major areas, the first set of conclusions is based on the field load test setup design and load testing, the second set of conclusions is based on the load test results and analysis of them using analytical and numerical models. The last set is based on the design chart development. The following summarizes a few major conclusions arrived from each category:

Field Load Test Setup Design, Instrumentation Used and Load Tests:

1. Site selection and soil characterization showed that the upper strata contained soils that can be characterized as expansive in nature. The volumetric swell strains of soil layers 2 and 3 are 11.1% and 7.7% and the linear/volumetric shrinkage strains are 12.1/6.8% and 8.4/5.22%, respectively. These results indicate that the present soils are close to the surface are indeed expansive in nature.

2. The load test design includes the design of the reaction and the test shaft configurations and spacings between them. Preliminary LPILE analyses conducted on these reaction and test shafts using the hypothetical lateral loads estimated from design tensile loads in the cables showed that a spacing of 20 ft between each reaction and test shafts is required in order to have lesser influence of the reaction shaft movements on the test results during loading.

3. The load tests under the inclined load configuration were successfully performed and the field load testing went smoothly as per the design. Ultimate inclined loads were successfully obtained for the majority of the tests conducted. Though the channel section to which the high-tensioned steel bar (Dywidag bar) was connected had yielded in one test, this was quickly corrected with additional splicing of this section for other load tests. Subsequent tests on all of the other test shafts were conducted by providing the same additional splicing at each of the steel channel pieces. Overall, the inclined load tests were conducted successfully in these north Texas soil conditions.

4. The percent loss of the tensile loads applied at the reaction shafts and the loads experienced at the test shafts is less than 10%, indicating that there was no major friction loss during load testing of the test shafts. The recorded failures of all test shafts matched with the original distressed shafts visually observed in the Winter of

2006-2007. This indicated that the field inclined load testing was successful in simulating the loading mechanisms that transpired in the original distressed shafts.

5. The test drilled shafts were not influenced by the reaction movements which can be noticed from the soil movements within the influence zone. The inclinometer results at the center point between reaction shaft and test shaft showed a very small movement. In addition, the lateral movements recorded at the ground surface of both reaction shafts are well below 0.25 in. (6.35 mm) indicating that the load application on test drilled shafts are not influenced by the loading on the reaction shafts as massive reaction shafts have not yielded during loading.

6. The load-deformation patterns of test shafts were recorded by the MEMS-SAA probe, and these results showed very good agreement with those recorded with the inclinometer system embedded in the test shafts. The major advantage of the MEMS-SAA system was realized when it provided a complete load-displacement data collection process including the final inclined load and lateral displacement near failure conditions. This is possible due to the use of the in-place and flexible MEMS-SAA probe which was able to capture the complete loading profile at the same time allowing users to retrieve back the probe after the test.

Load Test Results and Analysis:

7. The drilled shafts tested in the summer and winter conditions showed major variations in their load versus displacement behaviors. The test shafts in the winter condition experienced larger lateral and vertical movements. The major contributor to differences in the summer (dry) and winter (wet) test conditions was the softening of soil response to loading due to moisture ingress in the shallow soil layers. Also, the nature of the high-plasticity clay in undergoing larger vertical movements in Winter due to soil expansion from the elevated moisture content levels. Overall, the load-lateral displacement pattern of drilled shafts in the winter condition showed

243

semi-brittle response (displacements reaching plateau conditions) whereas the same displacements of the test shafts in the summer condition is close to rigid brittle or abrupt failure pattern.

8. Models that were used in this study focused on uplift or vertical load component and lateral load component of the inclined load measured in the field. The ultimate uplift capacity was used for the vertical direction and the ultimate lateral load was used for the horizontal direction. From the comparisons between the field test results and the developed models, the uplift capacity model by Das and Seely provided reasonable results with an average ratio between the field test and the predicted results at 0.22 and 0.28 for 0.5 in. and 1.0 in. criteria.

9. O'Neill and Poormoayed (1980) model based on swell pressures to estimate uplift capacity has under predicted these values for the present tests and this variation is attributed to lack of swell induced uplift not occurring in the field. Overall the uplift forces induced by the inclined loading are due to mechanical loading occurring in tensile direction, not due to swell pressure inducement around the shaft.

10. The predictions from LPILE matches well with the measured results, same observation is valid for Brom's method except that Brom's method has a slightly large scatter. The CLM on the other hand provided large scatter for the present shafts. It should be noted that the CLM method is preferred for long size drilled shafts and the present tested shafts are short and intermediate size.

11. For the ultimate lateral load prediction, the p-y method using the LPILE program has provided the best-fit results against the field test results with over-predicted results at 1.21 and 1.20 for 0.5 in. and 1.0 in. deflection criteria, respectively.

12. Numerical modeling using 3-D Finite Element software (ABAQUS) was used to model the drilled shafts under inclined load and compare with the field results. The predictions by using this model showed a good match with measured load test

244

results. In addition, the behavior of stress distributions of soil-drilled shaft system can be clearly explained by using this finite element model. However, this FEM model was not used in design chart development because this program requires many input parameters for soil and also time-consuming due to computational analysis involved. Hence, the p-y curve based LPILE program was for design chart development.

Design Chart Development:

13. The Design Charts were initially developed based on the exact soils sampled and tested in the area. However, in reality, there are more layers of soils with distinct undrained shear strengths that will prevail in the field. Hence design charts for different strength properties are considered for the development. Thus, the top 3 ft clay layer with different undrained shear strengths including 250 – 500 psf, 500 – 750 psf, 750 – 1000 psf, 1000 – 1500 psf and 1500 – 2000 psf is considered as a constant top layer for the entire analysis. The bottom two clay layers with undrained shear strength properties (S_u) varying between 250 – 500 psf, 500 – 1000 psf, 1000 – 1500 psf and 1500 – 2000 psf, are considered and an average undrained shear strength of these two layers are then calculated and used as undrained shear strength of the bottom layer. Overall, 40 design charts are developed.

14. A construction guideline is provided in this research. A modified concrete pad is recommended to be used with the foundation in order to maintain the contact area between drilled shaft foundation and surrounding soil. A few recommendations are specified to maintain tension mobilized in the cables remain constant in both summer and winter conditions which will protect the public from accidents by preserving the integrity and tightness of the cables.

8.3 Future Research

1. More sites with various different environmental conditions are needed for further validation of the findings and a larger database development for better foundation design under inclined loading.

2. Performance of the drilled shafts under inclined loads on other soils is needed.

3. Different angles of the load acting on drilled shaft needs to be tested for further validation inclined loading analysis on the shafts.

4. Numerical modeling of drilled shafts under various soil types with new parameter considerations (ex. numerical modeling of unsaturated soil) that affect behavior of drilled shaft is needed to help in understand the behavior of short drilled shafts under different soil conditions.

APPENDIX A

FOUNDATION FAILURES IN EAST OF DALLAS

Figure A.1 Foundation Failures of 3-cable Median Barriers Built on
Expansive Soils at IH 20 Westbound Sta. 1338+57

Figure A.2 Foundation Failures of 3-cable Median Barriers Built on
Expansive Soils at IH 20 Westbound Sta. 1196+92

Figure A.3 Foundation Failures of 3-cable Median Barriers Built on
Expansive Soils at IH 20 Westbound Sta. 1071+00

Figure A.4 Foundation Failures of 3-cable Median Barriers Built on
Expansive Soils at IH 20 Westbound Sta. 1069+00

Figure A.5 Foundation Failures of 3-cable Median Barriers Built on
Expansive Soils at IH 20 Westbound Sta. 973+44

Figure A.6 Foundation Failures of 3-cable Median Barriers Built on
Expansive Soils at IH 20 Westbound Sta. 862+19

Figure A.7 Foundation Failures of 3-cable Median Barriers Built on
Expansive Soils at IH 20 Westbound Sta. 846+92

Figure A.8 Foundation Failures of 3-cable Median Barriers Built on
Expansive Soils at IH 20 Westbound Sta. 993+50

Figure A.9 Foundation Failures of 3-cable Median Barriers Built on
Expansive Soils at IH 20 Westbound Sta. 976+27

Figure A.10 Foundation Failures of 3-cable Median Barriers Built on
Expansive Soils at IH 20 Westbound Sta. 903+00

Figure A.11 Foundation Failures of 3-cable Median Barriers Built on
Expansive Soils at US 175 Eastbound

Figure A.12 Foundation Failures of 3-cable Median Barriers Built on
Expansive Soils at US 175 Eastbound Sta. 149+98

Figure A.13 Foundation Failures of 3-cable Median Barriers Built on
Expansive Soils at US 175 Eastbound Sta. 137+62

Figure A.14 Foundation Failures of 3-cable Median Barriers Built on
Expansive Soils at US 175 Eastbound Sta. 92+00

Figure A.15 Foundation Failures of 3-cable Median Barriers Built on
Expansive Soils at US 175 Eastbound Sta. 658+15

Figure A.16 Foundation Failures of 3-cable Median Barriers Built on
Expansive Soils at US 80 Eastbound Sta. 37+29

Figure A.17 Foundation Failures of 3-cable Median Barriers Built on
Expansive Soils at US 80 Westbound Sta. 37+58

Figure A.18 Foundation Failures of 3-cable Median Barriers Built on
Expansive Soils at US 80 Eastbound Sta. 46+68

Figure A.19 Foundation Failures of 3-cable Median Barriers Built on
Expansive Soils at US 80 Eastbound Sta. 64+28

Figure A.20 Foundation Failures of 3-cable Median Barriers Built on
Expansive Soils at US 80 Westbound Sta. 65+21

Figure A.21 Foundation Failures of 3-cable Median Barriers Built on
Expansive Soils at US 80 Eastbound Sta. 77+37

Figure A.22 Foundation Failures of 3-cable Median Barriers Built on
Expansive Soils at US 80 Westbound Sta. 77+07

Figure A.23 Foundation Failures of 3-cable Median Barriers Built on
Expansive Soils at US 80 Eastbound Sta. 81+50

Figure A.24 Foundation Failures of 3-cable Median Barriers Built on
Expansive Soils at US 80 Westbound Sta. 81+93

Figure A.25 Foundation Failures of 3-cable Median Barriers Built on
Expansive Soils at US 80 Eastbound Sta. 110+96

262

Figure A.26 Foundation Failures of 3-cable Median Barriers Built on
Expansive Soils at US 80 Westbound Sta. 111+27

Figure A.27 Foundation Failures of 3-cable Median Barriers Built on
Expansive Soils at US 80 Eastbound Sta. 113+79

Figure A.28 Foundation Failures of 3-cable Median Barriers Built on
Expansive Soils at US 80 Westbound Sta. 114+24

Figure A.29 Foundation Failures of 3-cable Median Barriers Built on
Expansive Soils at US 80 Westbound Sta. 120+90

Figure A.30 Foundation Failures of 3-cable Median Barriers Built on
Expansive Soils at US 80 Westbound Sta. 124+51

Figure A.31 Foundation Failures of 3-cable Median Barriers Built on
Expansive Soils at US 80 Eastbound Sta. 438+28

Figure A.32 Foundation Failures of 3-cable Median Barriers Built on
Expansive Soils at US 80 Eastbound Sta. 462+95
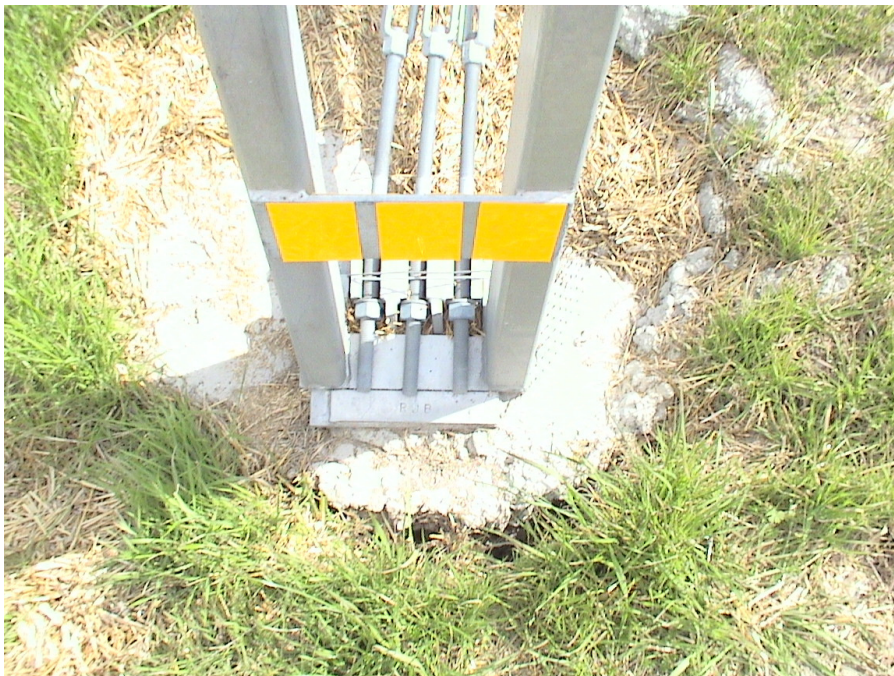
Figure A.33 Foundation Failures of 3-cable Median Barriers Built on
Expansive Soils at US 80 Eastbound Sta. 476+50

266

Figure A.34 Foundation Failures of 3-cable Median Barriers Built on
Expansive Soils at US 80 Eastbound Sta. 483+70

Figure A.35 Foundation Failures of 3-cable Median Barriers Built on
Expansive Soils at US 80 Eastbound Sta. 486+78

Figure A.36 Foundation Failures of 3-cable Median Barriers Built on
Expansive Soils at US 80 Eastbound Sta. 493+07

APPENDIX B

MANUFACTURER DESIGN PLAN SHEET

GENERAL NOTES

1. For additional information, contact Gibraltar, Inc. at 1-800-495-8957.

2. All concrete shall be class A.

3. All posts shall be socketed unless otherwise specified.

4. For additional information: See the manufacturer's product manual.

5. For payment see special specification "Cable Barrier System".

6. The GCBS system is designed for bi-directional traffic flows. See the manufacturer's product manual for placement adjacent to guardrail end treatments.

7. GCBS shall be installed on median shoulders or in depressed medians with slopes of 6:1 or flatter without obstructions, depressions, etc, that may significantly affect the stability of an errant vehicle.

8. GCBS may be installed on either side of the median.

9. See the Texas MUTCD for proper "Barrier" delineation.

10. Rock Clause: Where solid rock is encountered.

   a.) For socketed post, continue digging 12" dia, 15" deep into rock or the required plan depth, whichever comes first.

   b.) For driven post, core drill a 4" dia. hole 18" deep into rock or the required plan depth, whichever comes first.

   c.) For anchor post, continue digging 24" dia. hole 30" deep into rock or the required plan depth, whichever comes first.

CABLE TENSION CHART

F	Std.Cable
-10	8800
0	8400
10	8000
20	7600
30	7200
40	6800
50	6400
60	6000
70	5600
80	5200
90	4800
100	4400
110	4000

Allowable Deviation from Chart: 200 lbs/force.

GIBRALTAR (TL-4) CABLE BARRIER SYSTEM (Gibraltar Inc.)

ELEVATION VIEW

PLAN VIEW

C-SECTION POST

C-Section Post
ASTM A570 Gr 60
5.40 lbs/ft.
1.26 Section Modulus
75,600# Bend Moment
Galvanized In and Out
2.0 oz./sqft ASTM F1043 A

TURNBUCKLES

3/4" x 30" Anchor Terminal Fitting

3/4" x 24" 7/8 Cable Splice Fitting

BASE-PLATED POST

For Use On Concrete
5/8" Mechanical Anchor
Min. Pullout Strength 10,000 lbs.

24"Dia x 72" Deep Reinforced Foundation

3/4" Dia. Holes for 5/8" Dia. Anchors

(1) CABLE RELEASE POST

(2) WEAK TERMINAL POST

SOCKETED LINE POST OPTION (TYPE S POST)

DRIVEN LINE POST OPTION (TYPE D POST)

3 1/4" x 2 1/2" C-Section Post 4'-0" Long, Galv.

3/4" J-Bolts 6" Long

7/16"Dia x 33" (TL-4)Hairpin, Galvanized

Lock Plate
1/8" x 1 1/2" Flat Galv.

3 1/4" x 3 1/2" C-Section Post x 4'-9", Galv.

4"x 3" x 3/16" HSS Socket x 1'- 3"

(4)#4 Bars x 2'-8" Lg or (4)#4 1'- 8"Lg Bars welded to socket (Some at Terminal Post)

3/4" Wire Ropes

1 1/2" Dia Hole (Weak Post only)

* If a Mow Strip is used the socket foundation depth may be decreased to 2'- 6".

Anchor Terminal Fitting

(3) Anchor Terminal Fitting

(CMBS) Terminal Length 27'-6 (Each)

(2) Weak (4'-0") Terminal Post

(2)HSS 4 x 2 x 3/8

HSS 8 x 8 x 3/8 x 3'- 1"

(8)#6 Bars 5'-10" Long

(9)#4 18" Dia Rings

Top Cable to Center

Begin Length of Need for Cable Barrier System

Begin Pay Length for Cable Barrier System (FT)

20'-0" Typ (TL-4)

Line Post Typ. (Driven or Socketed)

(3) 3/4" 3 x7 Galvanized Standard Wire Rope Maximum 1000" between turnbuckle splices. (Turnbuckles may be staggered between line posts)

(2) (4'-9")Terminal Posts with J-Bolts (See the manufacturer's product manual)

Alternate posts for median barrier installation

Cable Reference Line

Ground Line

APPENDIX C

AS-BUILT DRAWING FOR LOAD TEST SETUP

Lateral Loads on Drilled Shafts
(AS-BUILT)

TX-DOT Project # 0-6146
Project Location located on I-20 & Rose Hill Rd.
Area ≈ 280,000 sq.ft.
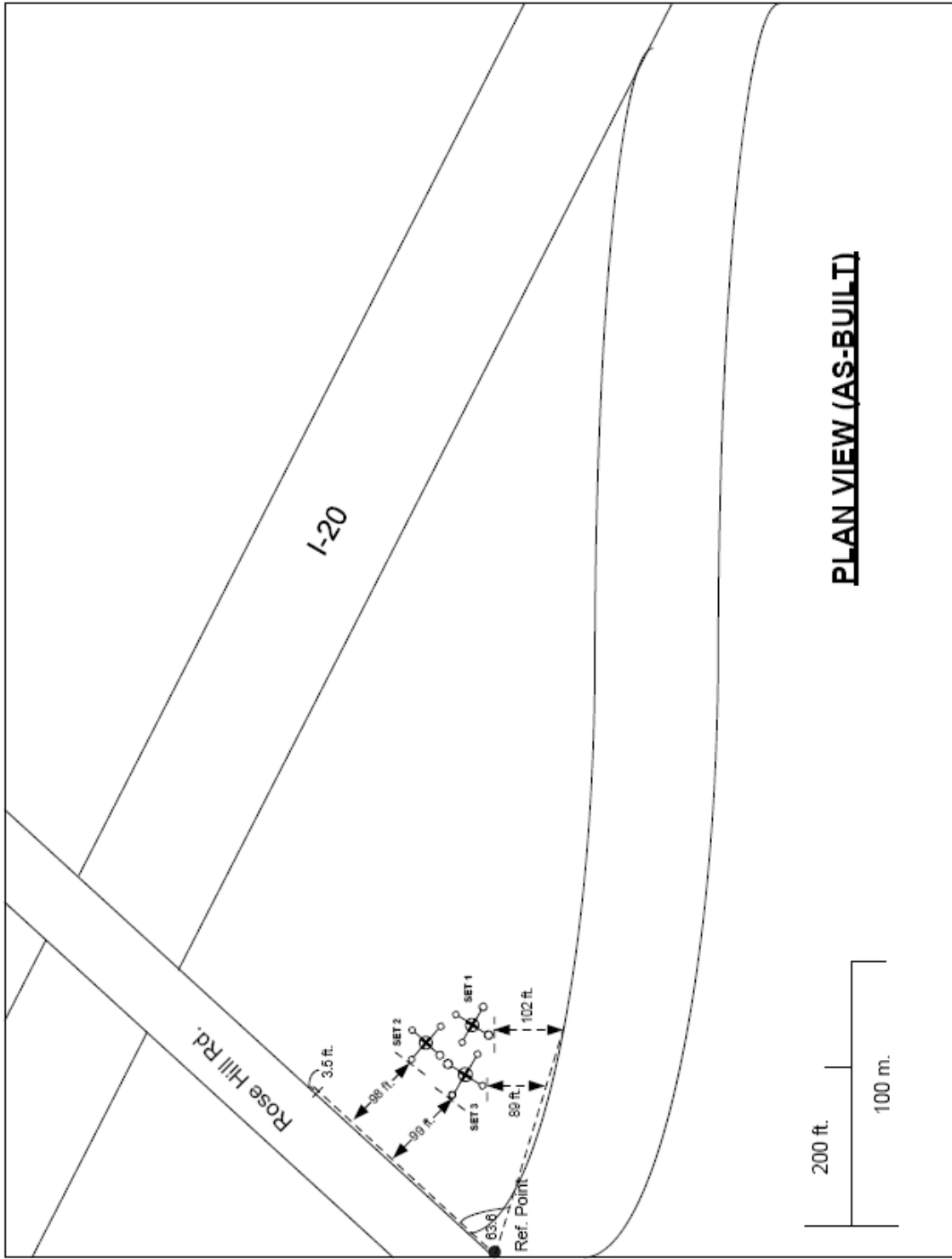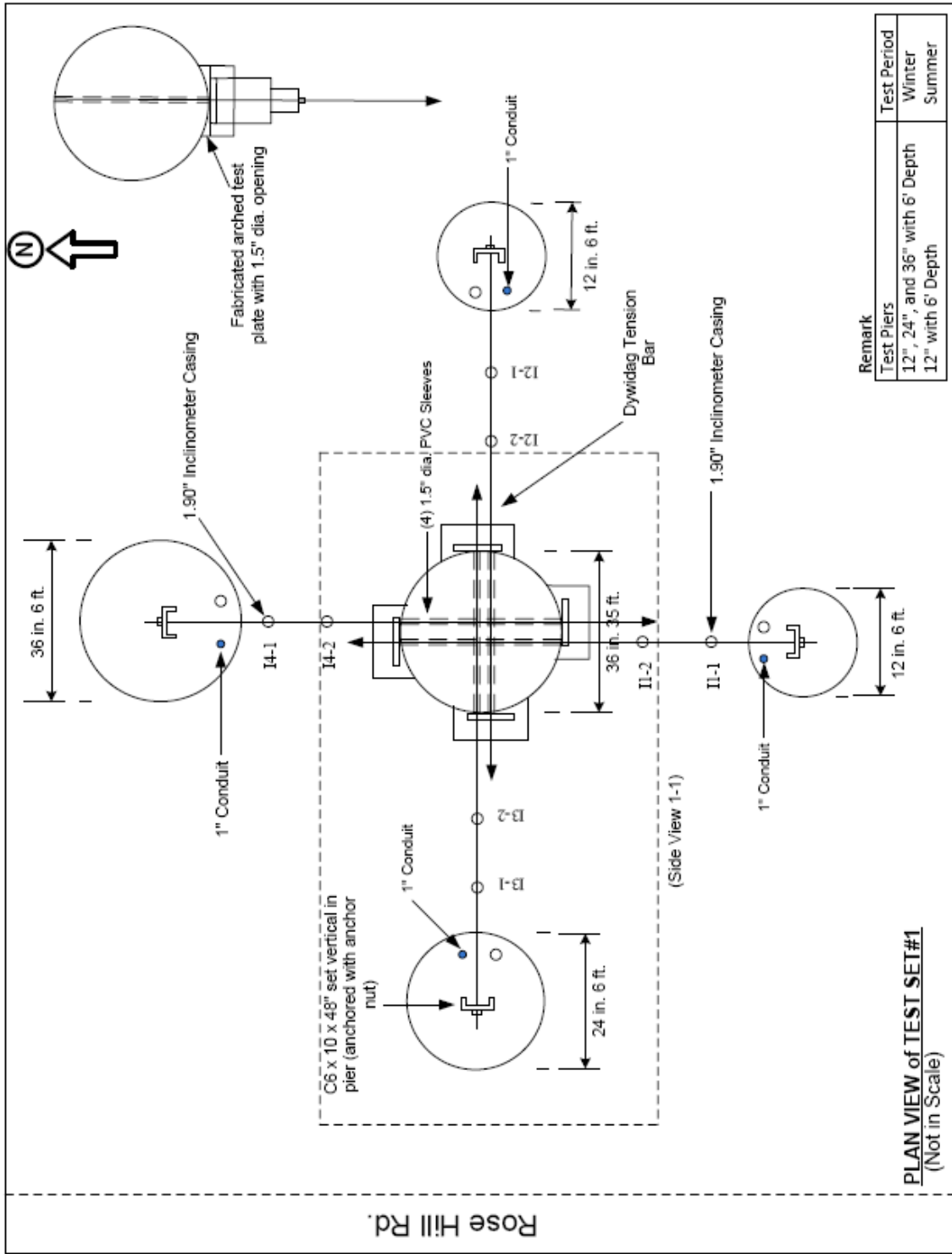
PLAN VIEW (AS-BUILT)

273

PLAN VIEW of TEST SET#1
(Not in Scale)

Fabricated arched test plate with 1.5" dia. opening

1" Conduit

1.90" Inclinometer Casing

Dywidag Tension Bar

1.90" Inclinometer Casing

(4) 1.5" dia. PVC Sleeves

12 in. 6 ft.

36 in. 6 ft.

12 in. 6 ft.

24 in. 6 ft.

36 in. 35 ft.

1" Conduit

1" Conduit

1" Conduit

C6 x 10 x 48" set vertical in pier (anchored with anchor nut)

(Side View 1-1)

I2-1

I2-2

I4-1

I4-2

I1-2

I1-1

I3-2

I3-1

N

Rose Hill Rd.

Remark		
Test Piers		Test Period
12", 24", and 36" with 6' Depth		Winter
12" with 6' Depth		Summer

274

PLAN VIEW of TEST SET#2
(Not in Scale)

N

Fabricated arched test plate
with 1.5" dia. opening

1.90" Inclinometer Casing

(4) 1.5" dia. PVC Sleeves

1" Conduit

Dywidag Tension Bar

1" Conduit

C6 x 10 x 48" set vertical
in pier (anchored with
anchor nut)

1" Conduit

1" Conduit

12 in. 10 ft.

24 in. 10 ft.

24 in. 10 ft.

24 in. 10 ft.

48 in. 35 ft.

(Side View 1-2)

I5

I6

I7

I8-1

I8-2

Rose Hill Rd.

Remark		Test Period
Test Piers	12" and (2)24"with 10' Depth	Winter
	24" with 10' Depth	Summer

275

PLAN VIEW of TEST SET#3
(Not in Scale)

Fabricated arched test plate
with 1.5" dia. opening

1.90" Inclinometer Casing

1" Conduit

C6 x 10 x 48" set vertical in pier
(anchored with anchor nut)

(4) 1.5" dia. PVC Sleeves

Dywidag Tension Bar

1" Conduit

1" Conduit

1" Conduit

12 in. 10 ft.

12 in. 10 ft.

24 in. 14 ft.

36 in. 14 ft.

48 in. 35 ft.

(Side View 1-2)

Rose Hill Rd.

Remark		Test Period	
Test Piers		Winter	Summer
12", 24", and 36" with 14' Depth			
12" with 10' Depth			

276

Side View 1-1

Hydraulic Ram

7.0 ft.

16.1°

35.0 ft. Depth

36 in.

(4) 1.5" dia. PVC Sleeves

1.90" x 6 ft. Depth Inclinometer Casing

10 ft

20 ft.

Dywidag Tension Bar

2.5D

12, 24, 36 in.

C6 x 10 x 48" set vertical in pier (anchored with anchor nut)

6 ft. Depth

1.90" x 6 ft. Depth Inclinometer Casing

1.0" x 6 ft. Depth Conduit for MEMs

277

Side View 1-2

Hydraulic Ram

7.5 ft.

35.0 ft. Depth

48 in.

16.1°

See Detail 1-1

(4) 1.5" dia. PVC Sleeves

1.90" x 10 & 14 ft. Depth Inclinometer Casing

10 ft.

20 ft.

Dywidag Tension Bar

See Detail 1-2

2.5D

12, 24, 36 in.

C6 x 10 x 48" set vertical in pier (anchored with anchor nut)

6, 10 and 14 ft. Depth

1.90" x 6 ft. Depth Inclinometer Casing

1.0" x 6 ft. Depth Conduit for MEMs

278

TEST SHAFT
REINFORCEMENT

(Not in Scale)

Notes

1. Rebar Grade 60

2. Minimum concrete
   strength is 4000 psi.

3. Covering 2 inches

Ground Surface

Notes
1. Rebar Grade 60
2. Minimum concrete strength is 4000 psi.
3. Covering 2 inches

(32) #7 Bar

Stirrup # 3 bar @ 5" spiral.

Stirrup # 3 bar @5" spiral.

(32) #7 Bar

Stirrup # 3 bar @ 5" spiral.

7.5 ft

35 ft. Length

48 inches

42 ft Length

(18) #7 Bar

Stirrup # 3 bar @ 5" spiral.

Stirrup # 3 bar @ 5" spiral.

(18) # 7 Bar

Stirrup # 3 bar @ 5" spiral.

7 ft

35 ft. Length

36 inches

42 ft Length

Ground Surface

REACTION SHAFT
REINFORCEMENT

280

0.5" thick arched plate cut out
of 36 and 48 inch diameter pipe

0.5" thick steel plate welded to
arched plate

0.5" thick plate welded at angle

Dywidag bar parallel to center
line of reaction Pier with 1.5-
2.0 inches distance

Cross Section

0.5" thick plate welded at 16.1°
with arched plate

Hydraulic Test Ram

0.5" thick plate welded at 16.1°

16.1°

16.1°

Reaction Pier

Side View

0.5" thick arched plate cut out
of 36 and 48 inch diameter pipe

1.5" Hole

0.5" thick plate welded at 16.1°

Front View

DETAIL 1-1

APPENDIX D

LOAD CELL CALIBRATION REPORT

CALIBRATION TEST CERTIFICATE

CON - TECH SYSTEMS
550 KING ST. W.
BROCKVILLE ONT.

LOAD TEST ON

S.N.   CTS-J-100-2

REFERENCE GAUGE ENERPAC DGB1 SN 468
CERTIFIED 06/2008 TRACEABLE TO NIST

REFERENCE	LOAD IN KIPS
1000 psi	18.46
2000 psi	35.94
3000 psi	54.80
4000 psi	73.06
5000 psi	91.13
6000 psi	109.98
7000 psi	129.43
8000 psi	146.90
9000 psi	164.39
10000 psi	181.28

AUTHORIZED SIGNATURE
DATE JUNE 1 2009
RECERTIFICATION DATE : JUNE 2010

CALIBRATION TEST CERTIFICATE

CON - TECH SYSTEMS
4502 HANNA DR.
ELIZABETH TOWN, ON.

LOAD TEST ON

S.N. CTS-J-100-2

REFERENCE GAUGE ENERPAC DGB1 SN 468
CERTIFIED 06/2008 TRACEABLE TO NIST

LOAD IN KIPS

PRESSURE ON GUAGE
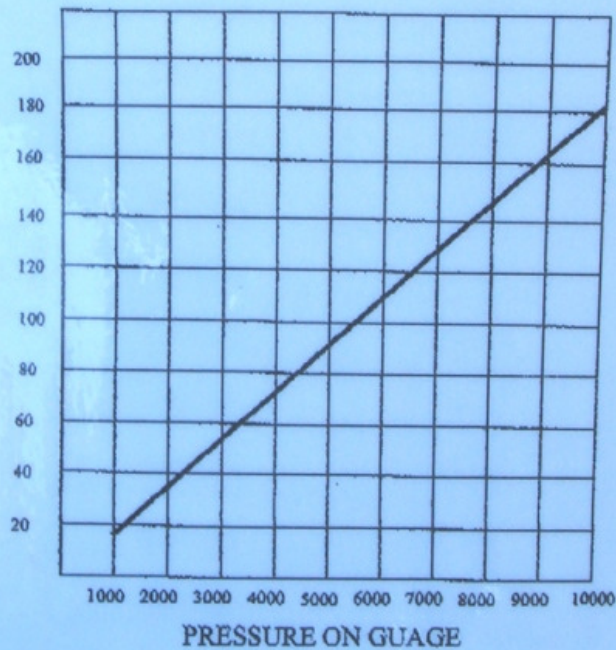
AUTHORIZED SIGNATURE
DATE JUNE 1 2009
RECERTIFICATION DATE : JUNE 2010

APPENDIX E

DETAIL OF RECOMMENDATION FOR CONCRETE PAD USED ON TOP OF DRILLED

SHAFTS AT THE END OF CABLE BARRIER SYSTEMS

Detail of Concrete Pad on the Top of
Drilled Shaft Used at the End of Cable
Barrier System
(Unit in Inches)

Note: Not In Scale

286
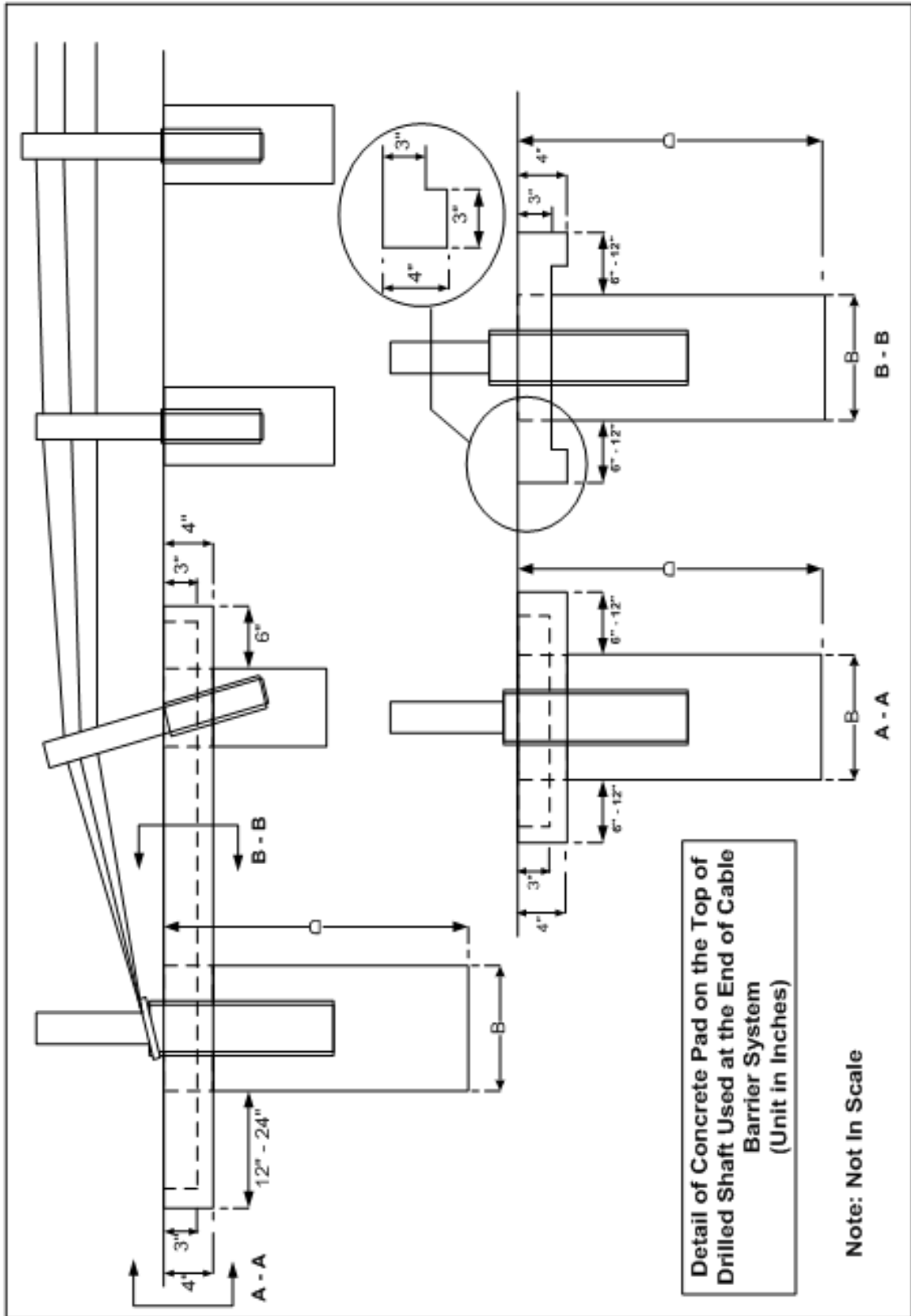
REFERENCES

1. Abendroth, R. E., Greimann, L. F., and Ebner, P. B. (1989). Abutment pile design for jointless bridges. *Journal of Structural Engineering, ASCE, 115*(11), 2914-2929.

2. Alberson, D. C. (2006). Update on guidelines for the selection of cable barrier systems. *NCHRP Project, 20-7(210)*.

3. Albin, R. B., Bullard D. L., Jr., and Menges, W. L. (2001). Washington State cable median barrier. *Transportation Research Record*, (1743), 71-79.

4. Al-Khafaf and Hanks, R. J. (1974). "Evaluation of the Filter Paper Method for Estimating Soil Water Potential." *Soil Sci.*, vol. 117, pp. 194 – 199.

5. Al–Saoudi, N. K. S. and Salim, H. M. (1998). "The behavior of groups of reinforced concrete model piles in expansive soil". *Proceedings of the 2nd International Conference on Unsaturated Soils, Beijing, August, Technical Committee of the 2nd International Conference on Unsaturated Soils Eds.*, Vol. 1, pp. 321 – 326.

6. Ashour, M., Norris, G., and Pilling, P. (1998). Lateral Loading of a Pile in Layered Soil Using the Strain Wedge Method, *Journal of Geotechnical and Geoenvironmental Engineering*, ASCE, Volume 124, No. 4, pp. 303-315.

7. Ashour, M., Norris, G. M., and Pilling, P., (2002). Strain Wedge Model Capability of Analyzing Behavior of Laterally Loaded Isolated Piles, Drilled Shafts, and Pile Groups, *Journal of Bridge Engineering,* Volume 7, No. 4, July 2002, pp. 245-254.

8. ASTM C31 / C31M – 09, (2009), "Standard Practice for Making and Curing Concrete Test Specimens in the Field." ASTM International, West Conshohocken, PA., 2009, DOI: 10.1520/C0031_C0031M-09, www.astm.org.

9.   ASTM C39 / C39M – 05e2, (2005), "Standard Test Method for Compressive Strength of Cylindrical Concrete Specimens." ASTM International, West Conshohocken, PA., 2005, DOI: 10.1520/C0039_C0039M-05E01, www.astm.org.

10.   ASTM C617 – 09a, (2009), "Standard Practice for Capping Cylindrical Concrete Specimens." ASTM International, West Conshohocken, PA., 2009, DOI: 10.1520/C0617-09A, www.astm.org.

11.   ASTM Standard D698-00a. (2003). "Standard Test Method for Laboratory Compaction Characteristics of Soil Using Standard Effort (12,400 ft-lbf/ft3(600 kN/m3))." *Annual Book of ASTM Standards,* Soil and Rock (I), 4(8), ASTM International,West Conshohocken, PA.

12.   ASTM Standard D2487-00. (2003). "Standard Classification of Soils for EngineeringPurposes (Unified Soil Classification System)." *Annual Book of ASTM Standards,* Soil and Rock (I), 4(8), ASTM International,West Conshohocken, PA.

13.   ASTM Standard D2850-95 (2003), "Standard Test Method for Unconsolidated-Undrained Triaxial Compression Test on Cohesive Soils." *Annual Book of ASTM Standards,* 4(8), ASTM International, West Conshohocken, PA.

14.   ASTM Standard D3080-98, (2003), "Standard Test Method for Direct Shear Test of Soils Under Consolidated Drained Conditions." *Annual Book of ASTM Standards,* 4(8), ASTM International, West Conshohocken, PA.

15.   ASTM Standard D 3966-90, (2003), "ASTM, Standard Test Method for Piles under Lateral Loads." *Annual Book of ASTM Standards,* 4(8), ASTM International, West Conshohocken, PA.

16. ASTM Standard D4318-05. (2003). "Standard Test Methods for Liquid Limit, Plastic Limit, and Plasticity Index of Soils." *Annual Book of ASTM Standards,* Soil and Rock (I), 4(8), ASTM International,West Conshohocken, PA.

17. ASTM Standard D4546-96, (2003), "Standard Test Methods for One-Dimensional Swell or Settlement Potential of Cohesive Soils," *Annual Book of ASTM Standards,* 4(8), ASTM International, West Conshohocken, PA.

18. ASTM Standard D5298-03, (2003), "Standard Test Method for Measurement of Soil Potential (Suction) Using Filter Paper," *Annual Book of ASTM Standards,* 4(8), ASTM International, West Conshohocken, PA.

19. Aung, K. K. Rahardjo, H. Leong, E. C. and Toll, D. G. (2001). "Relationship between porosimetry measurement and soil^water characteristic curve for an unsaturated residual soil." *Geotechnical and Geological Engineering*, 19, 401 – 416.

20. Bhushan, K., Haley, S.C., and Fong, P. T. (1979). Lateral Load Tests on Drilled Piers in Stiff Clays. *Journal of Geotechnical Engineering Division, ASCE, 105* (GT 8), 969 - 985.

21. Brinch Hansen, J. (1961). The ultimate resistance of rigid piles against transversal forces. *Geoteknisk Institutional Bulletin,* (12). Copenhagen, Denmark

22. Broms, B. B. (1964a). Lateral resistance of piles in cohesive soils. *Journal of the Soil Mechanics and Foundation Division, 90*(SM2), 27 - 63.

23. Broms, B. B. (1964b). Lateral resistance of piles in cohesionless soils. *Journal of the Soil Mechanics and Foundation Division, 90*(SM3), 123 - 157.

24. Broms, B. B. (1965). Design of Laterally Loaded Piles. *Journal of the Soil Mechanics and Foundation Division, 91*(SM3), 77 - 79.

25. Cameron, D. A. and Walsh, P. F. (1981). "Timber piles for residential foundations in expansive soil". *1st National Local Government Engineering Conference, Adelaide*, August. pp. 165 – 169.

289

26. Casagrande, A. (1932b). Discussion of "A New Theory of Frost Heaving" In A.C. Benkelman and F.R. Ohlmstead (Eds), *Proceedings of the Highway Research Board, 11* pp. 168 – 172.

27. Chapel, T. A. and Nelson, J.D. (1998). "Field investigation of helical and concrete piers in expansive soil". *Proceedings of the 2nd International Conference on Unsaturated Soils, Beijing, August, Technical Committee of the 2nd International Conference on Unsaturated Soils Eds.*, Vol. 1, pp. 206 – 211.

28. Chen, F. H. (1988). "*Foundations on expansive soils", 2nd Edition*. New York, USA: Elsevier Science Publications.

29. Chen, F. H. (2000). "*Soil Engineering: Testing, Design, and Remediation*", Florida, USA: CRC Press LLC.

30. Craig, R. R. (1999). "*Mechanics of Materials", 2nd edition*. New York, USA: John Wiley and Sons.

31. Czerniak, E. (1958), "Design Criteria for Embedment of Piers", Consulting Engineer, March.

32. Das, B. M., and Seeley, G. R. (1982). *"Uplift Capacity of Pipe Piles in Saturated Clay," Soils and Foundations*, The Japanese Society of Soil Mechanics and Foundation Engineering, Vol. 22, No. 1, pp. 91-94.

33. Davisson, M. T., and Robinson, K. E. (1965). Bending and buckling of partially embedded piles. *Proceedings, 6th International Conference on Soil Mechanics and Foundation Engineering, 2*, 243 - 246.

34. Day, R. W. (2006). *Foundation Engineering Handbook*. New York, NY: McGraw-Hill.

35. Duffy, D. and Charania, E. (1984). "Study of pile uplift characteristics in swelling clays using a newly developed test". *Proceedings of the 5th InternationalExpansive Soils Conference*, Adelaide, May, Vol. 1, pp. 75 – 79.

36. Duncan, J. M., Evans, L. T., Jr., and Ooi, P. S. K. (1994). Lateral load analysis of single piles and drilled shafts. *Journal of Geotechnical Engineering, ASCE, 120*(6), 1018 – 1033.

37. Dunnavant, T. W., and O'Neill, M. W. (1989). Experiment p-y Model for Submerged, Stiff Clay. *Journal of Geotechnical Engineering, ASCE, 115(1)*, 95 – 114.

38. Federal Highway Administration Publication No. FHWA-IP-84-11, "Handbook on Design And Construction of Drilled Shafts Under Lateral Load", 1984.

39. Fredlund, D.G. and Rahardjo (1993). *Soil Mechanics for Unsaturated Soils*, John Wiley & Sons, Inc., New York.

40. Fredlund, D.G., Xing, A., Huang, S. (1994). "Predicting the permeability function for unsaturated soils using the soil-water characteristic curve." *Canadian Geotechnical Journal*, v 31, n 4, Aug, 1994, p 533-546.

41. Greimann, L. F., Abendroth, R. E., Johnson, D. E., and Ebner, P. E. (1987). *Pile design and tests for integral abutment bridge, Final Report.* Ames, Iowa: Iowa DOT Project HR-273, ISU-ERI-Ames 88060.

42. Hammons, M. I. (1998). "Advanced pavement design: Finite element modeling for rigid pavement joints." Rep. No. II: Model Development, DOT/FAA/AR-97-7, Federal Aviation Administration, U.S. Dept. of Transportation.

43. Heady, J., TxDOT Dallas District, Personal Communication, March, 2008.

44. Hetenyi, M., (1946). *Beams on Elastic Foundations.* Ann Arbor: University of Michigan Press.

45. Hibbeler, R. C. (2008). *Mechanics of Materials 7th edition.* New Jersey, USA: Pearson Prentice Hall, Pearson Education.

46. Holtz, R. D., and Kovacs, W. D. (1981). *An Introduction to Geotechnical engineering.* Eaglewood Cliffs, NJ: Prentice Hall.

47. Houston, W. N., Walsh, K. D., Harraz, A.M., Perry, C.R, and Houston, S.L. (2004). Lateral Load Tests on Drilled Shafts in Cemented Soil. *GEOTECHNICAL SPECIAL PUBLICATION (Geo-Trans), ASCE, 126(2),* 1258-1269.

48. Hussein E. A. (2001). Viscoplastic Finite Element Model for Expansive Soils. *EJGE paper 2001-0122.*

49. *International Building Code. (2003). "Presumptive Load-Bearing Values"*, International Code Council (ICC).

50. Ivey, D. L. and Leon H. (1966), *"Signboard Footings to Resist Wind Loads", Civil Engineering, Dec, 1966.*

51. Johnson, L. D., and Stroman, W. R. (1976). Analysis of Behavior of Expansive Soil Foundations. *U.S. Army Engineer Waterways Experiment Station Technical Report S-76-8.*

52. Justo, J, Saura, J., Rodriguez, J, Delgado, A., Jaramillo, A. (1984). "A finite element method to design and calculate pier foundations in expansive collapsing soils". *Proceedings, 5th International Expansive Soils Conference, Adelaide* 1:119 – 123.

53. Jones, D. E., and Holtz, W. G. (1973). Expansive Soils - the Hidden Disaster. *Civil Engineering (ASCE), 43*(8), 49.

54. Kaplar, C. W. (1970). Pheonomenon and Mechanism of Frost Heaving. *Highway Research Record, 304,* 1 – 13.

55. Kim, J., and Hjelmstad, K. (2000). "Three-dimensional finite element analysis of multi-layered systems: Comprehensive nonlinear analysis of rigid airport pavement systems." Federal Aviation Administration DOT 95-C-001, COE Rep. No. 10, Univ. of Illinois at Urbana-Champaign, Urbana, Ill.

56. Kinney, E. E. (1959), "Correct Embedment for Pole Structures", *Wood Preserving News, Oct, 1959.*

292

57. Klaiber, F. W., White, D. J., Wipf, T. J., Phares, B. M., and Robbins, V. W. (2004). *Development of Abutment Design Standards for Local Bridge Designs.* Final Report for Iowa DOT TR-486: Volume 1 of 3, August 2004, 13 – 23.

58. Kuo, C.Huang, C. (2006). "Three-dimensional pavement analysis with nonlinear subgrade materials." Journal of Materials in Civil Engineering, v 18, n 4, August, 2006, p 537-544.

59. Lu, N. and Likos, W. J. (2004). *Unsaturated Soil Mechanics.* John Wiley & Sons, New York, 2004.

60. Matlock, H., and Ripperger, E. A. (1958). Measurement of soil pressure on a laterally loaded pile. *Proceedings, American Society for Testing and Materials, 58*, 1245 - 1259.

61. Matlock, H., and Reese, L. C. (1961). Foundation Analysis of Offshore Pile-Supported Structures. *Proceedings, Fifth International Conference, International Society of Soil Mechanics and Foundation Engineering, Paris, France, 2*, 91-97.

62. Matlock, H. (1970). Correlations for design of laterally loaded piles in soft clay. *Proceedings 2nd Offshore Technical Conference, 1*, 577 - 594.

63. Marinho, F. A. M., Oliveira, O. M. (2006). "The filter paper method revisited." *Geotechnical Testing Journal,* 29(3), 1 – 9.

64. McClelland, B., and Focht, J.A., Jr. (1958). Soil modulus for laterally loaded piles. *Journal of Soil Mechanics Foundation Division, ASCE, 123*, 1049-1086.

65. McClelland, M. (1996). *History of Drilled Shaft Construction in Texas.* Paper presented before the 75th Annual Meeting of the Transportation Research Board, Washington, D.C.

66. McVay, C. M., (2003). *Calibrating Resistance Factors for Load and Resistance Factor Design for Statnamic Load Testing, Final Report BC354-42*. Florida Department of Transportation.

67. Mitchell, J. K. (1976). *Fundamental of Soil Behavior*. NY: Wiley.

68. Meyerhof, G. G., and Adams, J. I**. (**1968). The ultimate uplift capacity of foundations. *Canada Geotechnical Journal, 5***,** 225-244.

69. Meyerhof, G. G. (1973a). The uplift capacity of foundations under oblique loads. *Canadian Geotechnical Journal, 10*, 64 – 70.

70. Meyerhof, G. G. (1973b). Uplift resistance of inclined anchors and piles. *Proceeding, 8th International Conference on Soil Mechanics and Foundation Engineering, Moscow, 2.1*, 167 – 172.

71. Meyerhof, G. G. (1980). The bearing capacity of rigid piles and pile groups under inclined loads in clay. *Canadian Geotechnical Journal, 18*, 297 – 300.

72. Mohamedzein, Y. E. A., Mohamed, M. G. and Shareif, A. M. (1999). "Finite element analysis of short piles in expansive soils". *Computers and Geotechnics*, Vol. 24, 231 – 243.

73. Nelson, J. D., and Miller, J. D. (1992). *Expansive Soils: Problems and Practice in Foundation and Pavement Engineering*. New York: Wiley.

74. Nuhfer E. B., Proctor R. J., and Moser N. (1993). *The Citizen's Guide to Geologic Hazards*. Arvada, CO: AIPG Press.

75. Nusairat, J., Liang, R. Y., Engel, R., Hanneman, D., Abu-Hejleh, N., and Yang, K. (2004). *"Drilled Shaft Design for Sound Barrier Walls, Signs, and Signals",* Final Report. Colorado Department of Transportation (CDOT). Report No. CDOT-DTD-R-2004-8.

76. O'Neill, M. W., and Poormoayed, N. (1980). *Methodology for Foundations on Expansive Clays. Journal of the Geotechnical Engineering Division,* ASCE, Vol. 106, No. GT12, December, 1980, 1345 – 1367.

294

77. O'Neill, M. W., Reese, L. C., and Cox, W. R. (1990). Soil behavior for piles under lateral loading. *22nd Annual Offshore Technology Conference, Houston, TX*, 279-287.

78. O'Neill, M. W., and Reese, L. C. (1999). Drilled shaft: Construction procedure and design methods. *Publication No. FHWA-IF-99-025, 2*, 1-21.

79. Penner, E., and Burn, K. N. (1970). Adfreezing and Frost Heaving of Foundations. *Canadian Building Digest,* National Research Council, Ottawa, Ontario: Institute for Research in Construction. *CBD-128*, 8*.*

80. Perez-Ruiz, D. D. (2009). *A Novel Servo-Controlled True Triaxial Apparatus for Modeling Unsaturated Soil Response under Suction-Controlled Stress Paths, Dissertation*. Texas, USA: University of Texas at Arlington.

81. Petry, T. M., and Armstrong, J. C. (1989). Stabilization of Expansive Soils. *Transportation Research Record*, (1219), 103-112.

82. Power, K. C., Vanapalli, S. K. and Garga, V. K. (2008). "A Revised Contact Filter Paper Method." *Geotechnical Testing Journal,* 31(6), 1 – 9.

83. Punthutaecha, K., Puppala, A. J., Vanapalli, S. K., and Inyang, H. (2006). "Volume change behaviors of expansive soils stabilized with recycled ashes and fibers." *J. Materials in Civil Engineering*, 18(2), 295-306.

84. Puppala, A. J., B. Katha, and L. R. Hoyos. (2004). Volumetric Shrinkage Strain Measurements in Expansive Soils Using Digital Imaging Technology. *ASTM Geotechnical Testing Journal*, Vol. 27, No. 6, 2004, pp. 547-556.

85. Reese, L. C., and Matlock, H. (1956). Non-dimensional solutions for laterally loaded piles with soil modulus assumed proportional to depth. *Proceedings, 8th Texas Conference on Soil Mechanics and Foundation Engineering*. The University of Texas, Austin, Texas: Bureau of Engineering Research.

86. Reese, L. C., Cox, W. R., and Koop, R. D. (1975). Field testing and analysis of laterally loaded piles in stiff clay. *Proceedings 7th Offshore Technical Conference, 2,* 473-483.

87. Reese, L. and Welch, R. (1975). Lateral Loading of Deep Foundations in Stiff Clay. *Journal of Geotechnical Engineering Division, ASCE, 101*(GT 7), 633 - 649.

88. Reese, L. C., and Allen, J. D. (1977). *Drilled shaft design and construction guidelines manual, Vol.2. Structural analysis and design for lateral loading*. U.S. Department of Transportation, FHWA, Office of Research and Development.

89. Reese, L. C. (1984) "Handbook on Design of Piles and Drilled Shafts Under Lateral Loads," Report No. FHWA-IP-84-11.

90. Reese, L. C. (1986) "Behavior of Piles and Pile Groups Under Lateral Loads," Report No. FHWA/RD-85/106 (NTIS PB86-238466).

91. Robinson, B., Suarez, V., Robalino, P., Kowalsky, M., and Gabr, M. (2006). Pile Bent Design Criteria. *NCDOT Research Project 2005-19*. In Final Revision.

92. Rollins, M., K., Weaver, T. J., and Peterson, K. T. (1997). *Statnamic lateral load testing of a full-scale fixed-head pile group*, Report. UDOT, FHWA.

93. Sinha, J. and Poulos, H. G. (1999). "Piled raft systems and free standing pile groups in expansive soils". *Proceedings, 8th Australia New Zealand Conference on Geomechanics*, Hobart, February, Vol. 1, pp. 207 – 212.

94. Soil Moisture Equipment Corp., 2003 Soil Moisture Equipment Corp., 2003. TRASE Operating Instruction.

95. Sridharan, A., Sreepada R. A., Sivapullaiah, P. V. (1986). "Swelling Clays." *Geotechnical Testing Journal*, v 9, n 1, Mar, 1986, p 24-33.

96. Terzaghi, K. (1955). Evaluation of coefficient of subgrade Reaction. *Geotechnique, 5,* 297 – 326.

97.   Tex-107-E, (2002). "Determination the Bar Linear Shrinkage of Soils." *Manual of Material Testing Procedure,* Texas Department of Transportation (TxDOT), Austin, Texas.

98.   Ubanyionwu, G. I., (1985). *Uplift Capacity of Rigid Piles in Clay under Inclined Pull, Thesis.* Texas, USA: The University of Texas at El Paso.

99.   Welch, R. C., and Reese, L. C. (1972). Laterally Loaded Behavior of Drilled Shafts. *Research Report* (89-10). The University of Texas at Austin: Center for Highway Research.

100. Westman, E. C. (1993). "*Evaluation of pier uplift in expansive so*ils". Master Thesis, Department of Civil Engineering, The University of Colorado at Denver.

101. Wilson, N. E. (1964), "Drilled-In Caissons Used to stabilize a moving Foundation," Proceedings, Congreso Sobre Cimientos Profundos, Sociedad Mexican de Mechanica de Suelos, Mexico City, pp. 311 - 326

102. Wiseman, G., Komornik, A., and Greenstein, J. (1985). Experience with Roads and Buildings on Expansive Clays. *Transportation Research Record, 103*, 60-67.

103. Yong, R. N., and Warkentin, B. P. (1975). *Soil Properties and Behavior.* New York, NY: Elsevier.

BIOGRAPHICAL INFORMATION

Thornchaya (Pomme) Wejrungsikul was born on July, 1982, in Bangkok, Thailand. He graduated a Bachelor's degree in Civil Engineering (B.Eng) from King Mongkut's University of Technology Thonburi, (KMUTT or Bangmod), Thailand in May, 2003. Thereafter, he worked as a civil engineer at International Project Administration Company (InterPac) about 2 years. As a site engineer at the construction site of Golden Jubilee Medical Center project at Mahidol University, he had obtained many experiences in several aspects such as design of structure, quality assurance and quality control, building and site layout surveys, on-site material testing, and cost estimating. He also had responsibilities to work in soil compaction and drilled shafts construction, which made him develop his interest in geotechnical engineering. In 2006, he decided to pursue masters degree in Geotechnical Engineering at University of Texas at Arlington (UTA), and received a Master of Engineering in Civil Engineering (M.Eng) in May, 2008. Soon after, he pursued the Doctoral degree in Geotechnical Engineering of Civil Engineering at UTA. He has performed his research studies under the guidance ofProfessor Anand J. Puppala at UTA since August, 2008. His research is focused on inclined load tests acting on drilled shafts. He also earned his EIT in 2008 after passing the Texas Board of Professional Engineers (TBPE) examination.